The University of Nottingham

UNITED KINGDOM • CHINA • MALAYSIA

School of Pharmacy

Molecular Therapeutics and Formulation

Cryomilling for Formulation

Rehab M. Elfakhri

BSc in Pharmacy & Pharmaceutical Science

Thesis Submitted to the University of Nottingham

for the degree of Doctor of Philosophy

September 2017

Abstract

The pharmaceutical industry has experienced an increase in the amount of development candidates with low aqueous solubility and accordingly poor bioavailability. In order for this problem to be solved, amorphisation is thought to be the most favourable solution.

The amorphous state is higher in free energy thus higher in solubility when compared to the crystalline form. Milling and specially cryomilling is a very unique technique for providing of the crystalline to amorphous transformation since there are no heat or solvents involved.

Phthalic acid, isophthalic acid and terephthalic acid, individual and pair mixtures, are crystalline organic non medicinal compounds, which have been used for the first time as model compounds to investigate whether cryogenic milling can induce crystal to amorphous transformation and if the preparation of pair mixtures could affect the recrystallization rate of the subjected materials or not. The materials were cryomilled and analysed by DSC, XRPD, and FTIR. It was found that only terephthalic acid become amorphous after cryomilling, and even after the cryomilled sample been stored for three weeks DSC thermogram still detects recrystallization exothermic along with the XRPD pattern, which shows a very broad peaks indicative of particle size reduction. Pair mixtures were also studied and analysed by DSC and XRPD. Phthalic acid/isophthalic acid, isophthalic

acid/terephthalic acid, phthalic acid/terephthalic acid were cryomilled together and mixed physically after been cryomilled separately. XRPD results show that unlike the cryomilled separately mixtures, phthalic acid/ isophthalic acid, isophthalic acid/terephthalic acid, terephthalic acid/phthalic acid cryomilled together samples produces a synergistic effect in which the Bragg peaks of both phthalic acid and isophthalic acid are suppressed. It appears that co-cryomilling of these pair mixtures together resulted in the production of a new material that could potentially either be two-component single phase (nano-sized co-crystal), or a new polymorphic form of either phthalic acid, isophthalic acid or terephthalic acid.

Single-component of aspirin (ASP), paracetamol (PCM) and caffeine (CAFF), along with multi-component systems of paracetamol/aspirin, paracetamol/caffeine and aspirin/caffeine were milled at room temperature and by a cryomill. The milled samples were analysed using DSC, XRPD and FTIR. It was noted that there are no clear indications of crystal to amorphous transformation in all three materials. When milling aspirin at room temperature a marked reduction in the melting point was observed. Generally, a reduction in the melting point is either attributed to particle size effects, polymorphism, impurities and decomposition. In this case, the decrease in the melting point was only noticed when aspirin was milled at room temperature, so it is possible that the heat generated during the milling process resulted in chemical decomposition of aspirin to salicylic acid. Anhydrous caffeine is acknowledged to have two polymorphic forms, Form II which is considered to be stable at room temperature until ~145 °C.

Form I is stable from ~145 °C to its melting point ~ 236 °C. This polymorphic transformation was detected by DSC, XRPD and hot stage microscope and it was noticed only with the as received and the room temperature milled samples. Cryomilled caffeine data showed only the presence of Form I. On the other hand, for the cryomilled multi-component systems DSC and hot stage microscope images confirmed the eutectic formation with a composition of 45:55% w/w (PCM:ASP), 50:50% (ASP:CAFF) AND 50:50% (PCM:CAFF). The obtained data were compared with room temperature milled and the theoretical values resulted from Van Laar equation.

Solid pharmaceuticals represent heterogeneous systems that typically consist of one or more active pharmaceutical ingredients (APIs) and a number of excipients. Multi-component systems from mixing aspirin, paracetamol and caffeine with different excipients, which included sucrose, lactose monohydrate, xylitol and trehalose dihydrate were prepared by the use of a cryomill and were analyesd by DSC and XRPD. It was found from the XRPD data that mixing both sucrose and lactose monohydrate respectively with ASP, PCM and CAFF would produce more of a synergistic effect than xylitol and trehalose dihydrate. Cryomilling caffeine/sucrose and caffeine/lactose resulted in a production of a new XRPD trace that cannot be described in terms of a linear combination of caffeine, sucrose and lactose monohydrate. A new material was therefore formed as a result of cryomilling which has not been reported before.

Acknowledgments

``my success can only come from Allah. In Him I trust, and unto Him I look``
(Holy Qur`an, Surat Hud, Chapter 11, Verse 88)

I would like to express my special appreciation and thanks to my supervisor Dr. Jonathan Burley for his patience, guidance, encouragement and advice he has provided throughout my time as his student. I have been extremely lucky to have a supervisor who cared so much about my work, and who responded to my questions and queries so promptly. Appreciations and thanks are extended to Prof. Dr. Clive Roberts, my second supervisor, for his help and guidance and his invaluable advice. Many thanks to Dr. Andrew Megarry for his support in the initial setting up of my project throughout my first year of study. I would like also to thank all members of the technical team at Boots science building who have given their time, knowledge and resources to help us students continuing our work.

A special thanks to all my family members. Words cannot express how grateful I am to my beloved husband and children for all of the sacrifices that they've made on my behalf.

To my brother and sisters especially Farah, thanks for all the things that you have done to me, your presence has made this experience more of a bearable journey.

My mother, I can't thank you enough for encouraging me throughout these years, your prayer was what sustained me this far.

My dear father, thank you for allowing me to realize my own potential. All the support, advice and guidance that you have provided me over the years was the greatest gift anyone has ever given me. You are my idol and my greatest inspirer and I will keep look up to you as long as I live.

Finally I thank God, my creator and sustainer, for letting me through all the difficulties. I have experienced your guidance day by day. You are the one who gave me the power to finish my degree. Thank you, Allah.

Table of Contents

Chapter 1 1
Introduction 1
1.1. Delivery of a drug in a solid oral dosage form 1
1.2. Biopharmaceutical Classification System (BCS) 2
1.3. Solid forms and formulation strategies 3
1.3.1. Amorphous Vs Crystalline materials 3
1.3.2. Glass transition temperature Tg 5
1.3.3. Stability against recrystalisation 6
1.3.4. Formulation strategies 9
1.4. Solubility and dissolution 17
1.5. Poor aqueous solubility 18
1.6. Reasons for the presence of poorly soluble drugs 21
1.7. Developability Classification System (DCS) 22
1.8. Current and potential strategies 23
1.8.1. Cryomilling 27
1.9. Aims and objectives 29

Chapter 2 30
2.1. Introduction 30
2.2. Materials and Methods 32
2.2.1. Materials 32
2.2.2. Preparation Methods 34
2.2.3. Characterization Methods 35
2.2.4. Stability Tests of Cryomilled mixtures 37
2.3. Results 38
2.3.1. One phase Systems 38
2.3.1.1. Phthalic acid 38
2.3.1.2. Isophthalic acid 45
2.3.1.3. Terephthalic acid 52

2.3.2. Two Phase systems 57
2.3.2.1. Phthalic and isophthalic acid 57
2.3.2.2. Isophthalic and terephthalic acid 62
2.3.2.3. Phthalic and terephthalic acid 65
2.4. Summary table 72
2.5. Summary discussion 77
2.6. Conclusion 78

Chapter 3 79
3.1. Introduction 79
3.2. Materials and Methods 81
3.2.1. Materials 81
i. Paracetamol 82
ii. Aspirin 82
iii. Caffeine 83
3.2.2. Methods 83
3.2.2.1. Preparation Methods 83
i. Cryomilling 83
ii. Room Temperature Milling (Ball Mill) 84
3.2.2.2. Characterisation Methods 84
i. DSC 84
ii. XRPD 84
iii. FTIR 84
iv. HSM 84
v. Solution NMR 85
3.3. Results 86
3.3.1. Single Component Systems 86
3.3.1.1. Paracetamol 86
3.3.1.2. Aspirin 89
3.3.1.3. Caffeine 94
3.3.2. Multi- Component Systems 98
3.3.2.1. Paracetamol and Aspirin (DSC) 98

3.3.2.2. Aspirin and Caffeine (DSC) 100
3.3.2.3. Paracetamol and Caffeine (DSC) 102
3.3.2.4. Hot stage microscopy results 104
3.4. Summary table 105
3.5. Discussion 108
3.5.1. Milling temperature 108
3.5.2. Melting point reduction 109
3.5.3. Summary discussion 113
3.5. Conclusion 115

Chapter 4 116
4.1. Introduction 116
4.2. Materials and Methods 118
4.2.1. Materials 118
4.2.1.1. Active Pharmaceutical ingredients APIs 118
4.2.1.2. Excipients 118
i. Sucrose 120
ii. Lactose 120
iii. Xylitol 121
iv. D-(+)-Trehalose dihydrate 121
4.2.2. Methods 122
4.2.2.1. Preparation method 122
i. Cryomilling: 122
4.2.2.2. Characterisation methods 122
i. DSC: 122
ii. XRPD: 122
iii. HSM: 122
4.3. Results 123
4.3.1. Xylitol 123
4.3.1.1. Xylitol and aspirin 123
4.3.1.2. Xylitol and paracetamol 127
4.3.1.3. Xylitol and caffeine 130

4.3.2. Lactose monohydrate 132
4.3.2.1. Lactose monohydrate and aspirin 132
4.3.2.2. Lactose and paracetamol 135
4.3.2.3. Lactose monohydrate and caffeine 138
4.3.3. Sucrose 142
4.3.3.1. Sucrose and aspirin 142
4.3.3.2. Sucrose and paracetamol 147
4.3.3.3. Sucrose and caffeine 149
4.3.4. D-(+)-Trehalose dihydrate 152
4.3.4.1. D-(+)-Trehalose dihydrate and aspirin 152
4.3.4.2. D-(+)-Trehalose dihydrate and paracetamol 155
4.3.4.3. D-(+)-Trehalose dihydrate and caffeine 157
4.4. Summary table 160
4.5. Discussion 165
4.5.1. Milling temperature 165
4.5.2. Melting point reduction 166
4.6. Conclusion 172

Chapter 5 173
Conclusions and future prospects 173
5.1. Conclusions 173
5.2. Future prospects 176
5.2.1. In situ-XRPD 176
5.2.2. Solid-State NMR 176
5.2.3. Accelerated stability studies 177
5.2.4. Implementation to real-world formulations 177

Appendix I 179

Bibliography 198

Table of Figures

Figure 1: Not to scale, schematic diagram showing the drug release profile from an oral dosage form 1
Figure 2: Biopharmaceutics classification system and formulation approaches for different classes of drugs (6). 3
Figure 3: Diagram showing the structure of the crystalline and amorphous states. 5
Figure 4: Phase diagram of binary mixture of component A and B, showing the temperature of the system as a function of % composition of the components. 14
Figure 5: In the developability classification system, the dotted line shows the change 23
Figure 6: DSC Thermogram of phthalic acid as received, immediately after cryomilling and after 3 weeks. 39
Figure 7: Tg region for phthalic acid immediately after cryomilling for 60 minutes. 40
Figure 8: XRPD pattern of phthalic acid as received, immediately after cryomilling and after 3 weeks 41
Figure 9: SEM scan at 10 kV of A. unmilled phthalic acid B. cryomilled phthalic acid for total period of 60 minutes 43
Figure 10: The FTIR spectra of phthalic acid before milling, freshly cryomillied phthalic acid and after storage for three weeks at 43% relative humidity. 44
Figure 11: DSC thermogram for as received isophthalic acid, immediately after milling and after storage for three weeks at 43% relative humidity. 46
Figure 12: A recrystallization exotherm in isophthalic acid immediately after cryomilling. 47
Figure 13: XRPD pattern of unmilled isophthalic acid, immediately after cryomilling and after three weeks of storage at 43% relative humidity .. 49
Figure 14: SEM images of as received isophthalic acid and after cryomilling for 60 minutes with a magnification of x400. 50
Figure 15: The FTIR spectra for unmilled isophthalic acid, immediately after cryomilling and after three weeks of storage at 43% relative humidity. 51
Figure 16: DSC thermogram of terephthalic acid before milling, immediately after milling and after storage for 1,2 and three weeks at 43% relative humidity. 52
Figure 17: XRPD pattern of terephthalic acid before milling, immediately after milling and after three weeks of storage at 43% humidity. 54
Figure 18: SEM images of unmilled and cryomilled terephthalic acid with a magnification of x 400 55
Figure 19: FTIR pattern of unmilled terephthalic acid, immediately after cryomilling and after storage for three weeks at 43% humidity. 56

Figure 20: DSC thermogram of cryomilled separately phthalic isophthalic mixture at zero weeks, after three weeks, cryomilled together at zero weeks and after three weeks. 58
Figure 21: XRPD pattern shows cryomilled phthalic, cryomilled isophthalic, cryomilled separately phthalic isophthalic mixture at zero weeks, after three weeks, cryomilled together at zero weeks and after three weeks.. 61
Figure 22: DSC thermogram of isopthalic terepthalic acid cryomilled separately mixture at zero weeks, after three weeks, cryomilled together at zero weeks and after three weeks. 62
Figure 23: XRPD pattern of cryomilled isophthalic acid and terephthalic acid pair mixtures milled separately at zero weeks, after three weeks, milled together at zero weeks and after three weeks. 64
Figure 24: DSC thermogram of phthalic acid before milling, unmilled terephthalic acid, pthalic terepthalic acid cryomilled separately mixture at zero weeks, after three weeks, cryomilled together at zero weeks and after three weeks. 66
Figure 25: Figure 20: XRPD pattern of cryomilled phthalic acid and terephthalic pair mixture milled separately at zero weeks, after three weeks, milled together at zero weeks and after three weeks 69
Figure 26: SEM images of different pair mixtures of phthaic acid, isophthalic acid and terephthalic acid. 71
Figure 27: Model compounds with range of physical properties (Table 12), used to study the effect of cryomilling on single component and binary mixtures. 81
Figure 28: DSC thermogram of unmilled paracetamol, room temperature milled and cryomilled paracetamol for 60 minutes. Data have been offset by 7 Wg^{-1} for presentational purposes. 87
Figure 29: XRPD pattern of unmilled and cryomilled paracetamol. The Data have been scaled and offset for clarity. 88
Figure 30: DSC thermogram of umilled, room temperature milled and cryomilled aspirin for 60 minutes. Data have been offset by 7 Wg^{-1} for presentational purposes. 90
Figure 31: FTIR spectra of aspirin as received, room temperature milled and cryomilled for 60 minutes. The data have been scaled and offset for clarity. 91
Figure 32: Solution proton NMR carried out in DMSO of unmilled, RT milled and cryomilled aspirin. 92
Figure 33: XRPD pattern of unmilled and cryomilled aspirin for 60 minutes. The Data have been scaled and offset for clarity 93
Figure 34: DSC thermogram of umilled, room temprature milled and cryomilled caffeine for 60 minutes. Data have been offset by 7 Wg^{-1} for presentational purposes 95
Figure 35: Hot stage microscope images of unmilled caffeine show transformation from form II to form I 96
Figure 36: XRPD pattern of unmilled and cryomilled caffeine for 60 minutes. The data have been scaled and offset for clarity. 97

Figure 37: DSC overlays for screening the eutectic composition of different ratios 98
Figure 38: DSC overlays for screening the eutectic composition of different ratios 99
Figure 39: DSC overlays for screening the eutectic composition of different ratios 101
Figure 40: DSC overlays for screening the eutectic composition of different ratios 102
Figure 41: DSC overlays for screening the eutectic composition of different ratios 103
Figure 42: DSC overlays for screening the eutectic composition of different ratios 104
Figure 43: Hot stage microscope images for three binary mixtures of cryomilled (CM)..... 105
Figure 44: Gibbs energy and chemical potential of a melting system….110
Figure 45: Calculated binary phase diagram of the system aspirin (ASP) - paracetamol (PCM) 111
Figure 46: Calculated binary phase diagram of the system aspirin (ASP) - caffeine (CAFF). 112
Figure 47: Calculated binary phase diagram of the system paracetamol (PCM) - caffeine (CAFF)..... 112
Figure 48: Model compounds with range of physical properties (Table 17), used to study the effect of cryomilling on binary mixtures of excipients and APIs..... 119
Figure 49: DSC thermograms of aspirin and xylitol before and immediately after cryomilling and a 50:50% w/w mixture of aspirin and xylitol cryomilled together for 60 minutes. Data have been offset by 10 Wg^{-1} for presentational purposes. 124
Figure 50: Hot-stage microscope images of cryomilled 50:50% w/w mixture of aspirin and xylitol..... 125
Figure 51: XRPD patterns collected at room temperature for aspirin, xylitol before and after cryomilling and a cryomilled 50:50% w/w mixture of aspirin and xylitol. The data have been scaled and offset for clarity. 126
Figure 52: DSC thermograms of paracetamol and xylitol before and immediately after cryomilling and a 50:50% w/w mixture of paracetamol and xylitol cryomilled together for 60 minutes. Data have been offset by 10 Wg^{-1} for presentational purposes. 128
Figure 53: XRPD patterns collected at room temperature for paracetamol, xylitol before and after cryomilling and a cryomilled 50:50% w/w mixture of paracetamol and xylitol. The data have been scaled and offset for clarity. 129
Figure 54: DSC thermograms of caffeine and xylitol before and immediately after cryomilling and a 50:50% w/w mixture of caffeine and xylitol cryomilled together for 60 minutes. The data have been offset by 10 Wg^{-1} for presentational purposes. 131
Figure 55: XRPD patterns collected at room temperature for caffeine, xylitol before and after cryomilling and a cryomilled 50:50% w/w mixture

of caffeine and xylitol. The data have been scaled and offset for clarity. 132
Figure 56: DSC thermograms of aspirin and lactose before and immediately after cryomilling and a 50:50% w/w mixture of aspirin and lactose cryomilled together for 60 minutes. Data have been offset by 7 Wg^{-1} for presentational purposes. 133
Figure 57: XRPD patterns collected at room temperature for aspirin, lactose before and after cryomilling and a cryomilled 50:50% w/w mixture of aspirin and lactose. The data have been scaled and offset for clarity. 134
Figure 58: DSC thermograms of paracetamol and lactose before and immediately after cryomilling and a 50:50% w/w mixture of paracetamol and lactose cryomilled together for 60 minutes. Data have been offset by 7 Wg^{-1} for presentational purposes. 136
Figure 59: Hot-stage microscope images of cryomilled 50:50% w/w mixture of paracetamol and lactose. 137
Figure 60: XRPD patterns collected at room temperature for paracetamol, lactose before and after cryomilling and a cryomilled 50:50% w/w mixture of paracetamol and lactose. The data have been scaled and offset for clarity. 138
Figure 61: DSC thermograms of caffeine and lactose before and immediately after cryomilling and a 50:50% w/w mixture of caffeine and lactose cryomilled together for 60 minutes. Data have been offset by 7 Wg^{-1} for presentational purposes. 140
Figure 62: Hot-stage microscope images of cryomilled 50:50% w/w mixture of caffeine and lactose. 140
Figure 63: XRPD patterns collected at room temperature for caffeine, lactose before and after cryomilling and a cryomilled 50:50% w/w mixture of caffeine and lactose. The data have been scaled and offset for clarity. 142
Figure 64: DSC thermograms of aspirin and sucrose before and immediately after cryomilling and a 50:50% w/w mixture of aspirin and sucrose cryomilled together for 60 minutes. Data have been offset by 10 Wg^{-1} for presentational purposes. 144
Figure 65: XRPD patterns collected at room temperature for aspirin, sucrose before and after cryomilling and a cryomilled 50:50% w/w mixture of aspirin and sucrose. The data have been scaled and offset for clarity. 145
Figure 66: The FTIR spectra of sucrose as received and immediately after cryomilling for 60 minutes. 146
Figure 67: Images of unmilled sucrose, after cryomilling and after melt-quenching. 147
Figure 68: DSC thermograms of paracetamol and sucrose before and immediately after cryomilling and a 50:50% w/w mixture of paracetamol and sucrose cryomilled together for 60 minutes. Data have been offset by 10 Wg^{-1} for presentational purposes. 148

Figure 69: XRPD patterns collected at room temperature for paracetamol, sucrose before and after cryomilling and a cryomilled 50:50% w/w mixture of paracetamol and sucrose. The data have been scaled and offset for clarity. 149
Figure 70: DSC thermograms of caffeine and sucrose before and immediately after cryomilling and a 50:50% w/w mixture of caffeine and sucrose cryomilled together for 60 minutes. Data have been offset by 10 Wg^{-1} for presentational purposes. 150
Figure 71: XRPD patterns collected at room temperature for caffeine, sucrose before and after cryomilling and a cryomilled 50:50% w/w mixture of caffeine and sucrose. The data have been scaled and offset for clarity. 151
Figure 72: DSC thermograms of aspirin and trehalose dihydrate before and immediately after cryomilling and a 50:50% w/w mixture of aspirin and trehalose dihydrate cryomilled together for 60 minutes. Data have been offset by 5 Wg^{-1} for presentational purposes. 153
Figure 73: XRPD patterns collected at room temperature for aspirin, trehalose dihydrate before and after cryomilling and a cryomilled 50:50% w/w mixture of aspirin and trehalose dihydrate. The data have been scaled and offset for clarity. 154
Figure 74: DSC thermograms of paracetamol and trehalose dihydrate before and immediately after cryomilling and a 50:50% w/w mixture of paracetamol and trehalose dihydrate cryomilled together for 60 minutes. Data have been offset by 5 Wg^{-1} for presentational purposes. 156
Figure 75: XRPD patterns collected at room temperature for paracetamol, trehalose dihydrate before and after cryomilling and a cryomilled 50:50% w/w mixture of paracetamol and trehalose dihydrate. The data have been scaled and offset for clarity. 157
Figure 76: DSC thermograms of caffeine and trehalose dihydrate before and immediately after cryomilling and a 50:50% w/w mixture of caffeine and trehalose dihydrate cryomilled together for 60 minutes. Data have been offset by 5 Wg^{-1} for presentational purposes. 158
Figure 77: XRPD patterns collected at room temperature for caffeine, trehalose dihydrate before and after cryomilling and a cryomilled 50:50% w/w mixture of caffeine and trehalose dihydrate. The data have been scaled and offset for clarity. 159
Figure 78: Phase diagrams of xylitol with a. aspirin, b. paracetamol and c. caffeine. 168
Figure 79: Phase diagrams of lactose monohydrate with a. aspirin, b. paracetamol and c. caffeine. 169
Figure 80: Phase diagrams of sucrose with a. aspirin, b. paracetamol and c. caffeine. 170
Figure 81: Phase diagrams of trehalose dihydrate with a. aspirin, b. paracetamol and c. caffeine. 171
Figure 82: SamplePrep 6870 Freezer/Mill (SPEX, Metuchen, NJ, United States). 180

Figure 83: Schematic diagram of electromagnetic impactor back, sample vial and end cap. 181
Figure 84: A. Stainless steel jars with two balls B. RETSCH ball mill (Mixer Mill MM400). 182
Figure 85: Sketched diagram showing the principle of power compensated DSC. 184
Figure 86: TA Q2000 Differential Scanning Calorimeter (TA Instruments, NewCastle, DE, USA). 187
Figure 87: Sketched diagram showing the principle of polarised thermoscopy. 189
Figure 88: PriorLux Pol advanced polarised light microscope (PriorLux Pol, Prior Scientific, Fulbourn, Cambridge, UK). 190
Figure 89: Diagram of Bragg diffraction from a set of crystal planes with a spacing of d. 192
Figure 90: the X'Pert PRO(PANalytical, Almelo, Netherlands). 194
Figure 91: Sketched diagram showing the principle of FTIR 195
Figure 92: Agilent/Cary630/FTIR, United States. 196
Figure 93: Sketched diagram showing the principle of attenuated total reflectance (ATR). 197

List of Tables

Table 1: Applications of eutectic mixtures in formulation development.. 17

Table 2: Solubility definition United States Pharmacopeia (USP); the percentage of IR drugs on the Great Britain (GB) and on the World Health Organization (WHO) lists Obtained from 20

Table 3: Advantages and disadvantages of different amorphisation techniques..... 25

Table 4: The difference between the potential amorphisation strategies in terms of, solubility, dissolution rate, heat and moisture..... 26

Table 5 : XRPD data of phthalic acid shows crystallite size reduction after 42

Table 6 : XRPD data of isophthalic acid shows crystallite size reduction after 49

Table 7: XRPD data of terephthalic acid shows particle size reduction after 54

Table 8: XRPD data of phthalic acid and isophthalic acid CM separately and CM together pair mixtures, shows crystallite size reduction after cryomilling and upon storage. 61

Table 9: XRPD data of isophthalic acid and terephthalic acid CM separately and CM together pair mixtures, shows particle size reduction after cryomilling and upon starage. 65

Table 10: XRPD data of phthalic acid and terephthalic acid CM separately and CM together pair mixtures, shows crystallite size reduction after cryomilling and upon starage. 70

Table 11: Summary table of research work in Chapter 2. 76

Table 12: Key physical properties of model compounds. 82

Table 13: XRPD data of paracetamol shows crystallite size reduction after cryomilling..... 88

Table 14: XRPD data of aspirin shows crystallite size reduction after cryomilling..... 93

Table 15: XRPD data of caffeine shows crystallite size reduction after cryomilling..... 97

Table 16: Summary table of research work in Chapter 3. 107

Table 17: Key physical properties of the selected excipients..... 120

Table 18: Summary table of research work in Chapter 4. 164

Chapter 1

Introduction

1.1. Delivery of a drug in a solid oral dosage form

In order for a drug to be delivered to the general blood circulation to produce its therapeutic effect, several routes of drug administration are available, such as oral, pulmonary, parental and topical. Solid oral dosage forms are well acknowledged to possess multiple advantages over liquid preparations for oral use due to their ease of administration and manufacturing costs and higher stability. The drug release from an oral dosage form to reach the general circulation goes through several stages which are shown in Figure 1.

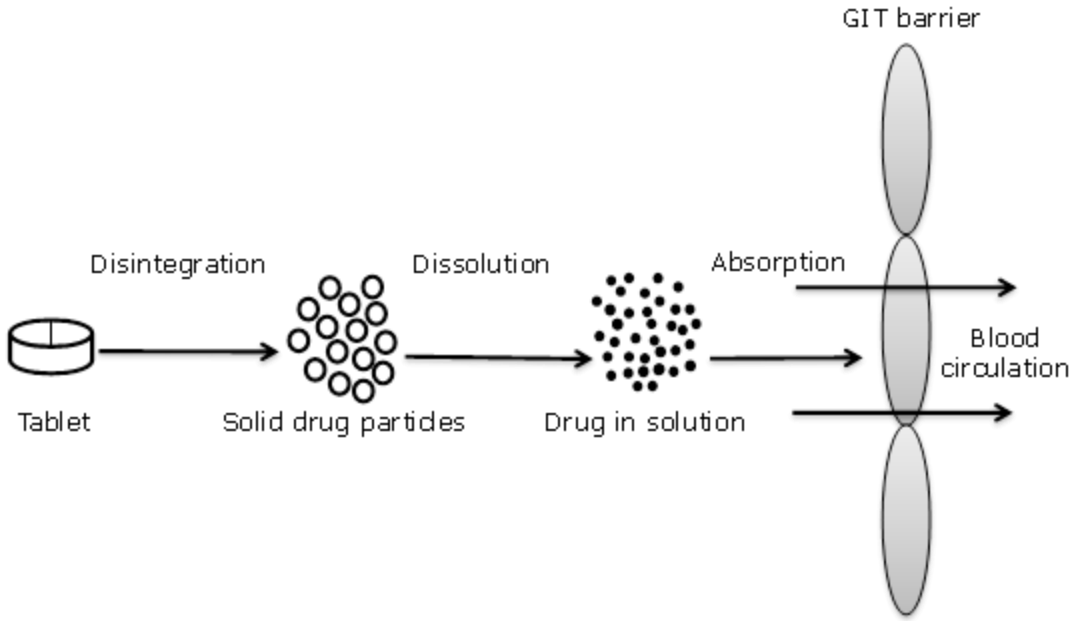


Figure 1: Not to scale, schematic diagram showing the drug release profile from an oral dosage form

1.2. Biopharmaceutical Classification System (BCS)

A better understanding of the physicochemical and biopharmaceutical characteristics of drugs would have a positive impact on developing pharmaceutical products. The biopharmaceutical classification system (BCS) is considered to be a beneficial tool for decision-making from a biopharmaceutical point of view in formulation development strategies for medicinal compounds through the early clinical stages (1-3). The BCS classifies substances into four different categories that depend on their solubility and intestinal cell membrane permeability characteristics (4). Figure 2 shows the BCS along with formulation approach recommendations based on this classification. A drug substance is described as highly permeable when 90% or more of the ingested dose is absorbed after administration in human (5). A drug is classified as highly soluble when the highest dose strength is soluble in 259 mL or less of aqueous media over pH range of 1-7.5 (5). Formulations for class I and III compounds can be easy to design without any major difficulty. These often are immediate release (IR) formulations, such as tablets and capsules (3). On the other hand, class II and IV formulation are more difficult to deal with, because they require careful formulation strategy depending on their physicochemical and biopharmaceutical characteristics (3).

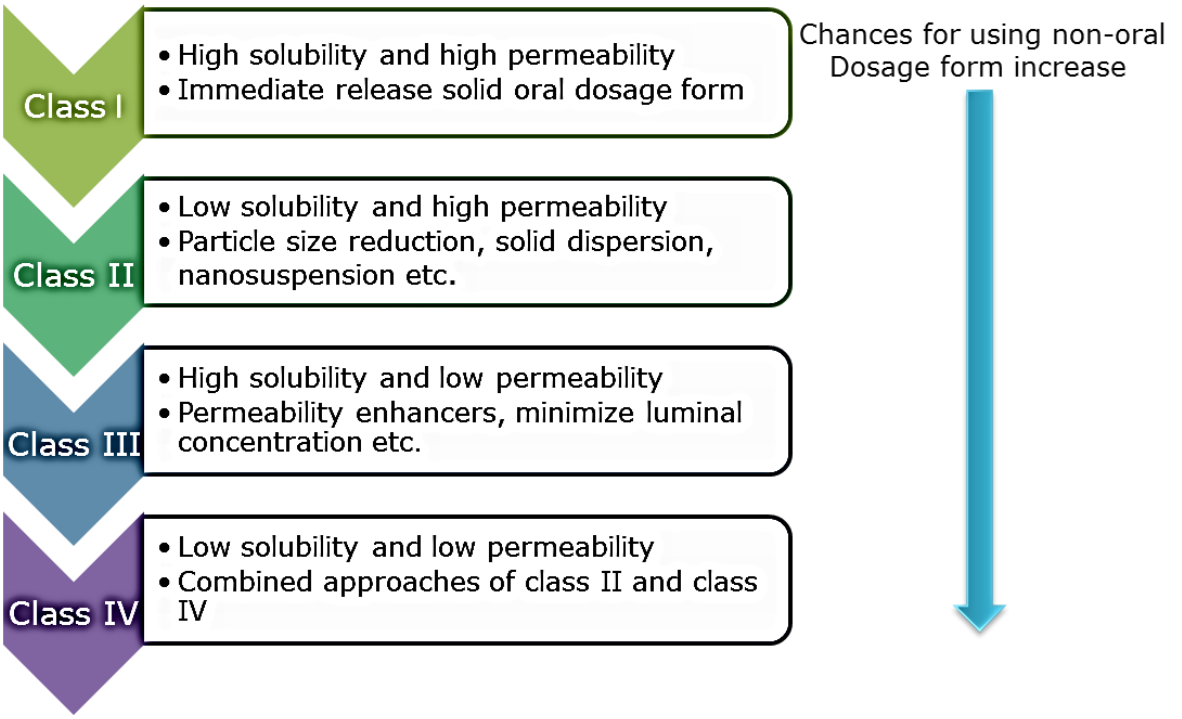


Figure 2: Biopharmaceutics classification system and formulation approaches for different classes of drugs (6).

1.3. Solid forms and formulation strategies

1.3.1. Amorphous Vs Crystalline materials

The majority of pharmaceutical substances are ingested in the form of tablets or capsules, and therefore solid state chemistry play an important role in giving medicines to patients. Studying the structure and properties of solid phase materials is considered to be a key stage before formulation.

Crystalline materials tend to be pure, very reproducible and stable, while on the other hand, amorphous materials can more readily accept impurities and they tend to be unstable. This can property would potentially lead to undesired transformations in formulated medicines. However, low stability of the amorphous form compared to the crystalline form is also an opportunity to enhance the apparent solubility and subsequently improving

the bioavailability. The crystalline state is characterised by long range translational order which mathematically corresponds to the crystalline lattice. The crystalline lattice is defined as the arrangement of points in space, which are organised in a specific pattern with high symmetry. The key properties of crystalline materials are that they exhibit reproducible melting points that tend to be known and they give sharp peaks in X-ray diffraction. Alternatively, materials can adopt an amorphous state and this is particularly the case with polymers, especially when they are melt-quenched. The amorphous state shows a lack of translational symmetry. A diagram comparing the structure of the crystalline and the amorphous phase is shown in Figure 3. The structure of the amorphous solids compared to crystals could be described as possessing a crystal like short range molecular arrangement, but lacking the long range order (7). Their random arrangements consequently lower their specific volume and mass, as a result of the free space between the molecules.

Amorphous material share most of the mechanical and thermodynamic properties of liquid with the key exception of flow (8). The amorphous form of pharmacologically active materials has received considerable attention (8-10) hence, compared to the crystalline form the amorphous form is usually the preferred form for poorly water soluble compounds due to their high energy as compared with the crystalline form. The crystal to amorphous transformation would provide the biggest advantages in terms of dissolution rate and bioavailability for class II BCS drugs. The amorphous form also shows several disadvantages, such as lower physical stability compared to the crystal form (8, 11). Moreover, differences in amorphous material properties were reported as a function of the preparation method (11, 12). For example, a difference was observed in the physical stability between simvastatin prepared by cryomilling, melting and quench-cooling, with the quench-cooled samples being more stable (13). There was a suggestion that the molecular mobility may differ in the same drug

according to the preparation method which play a significant role in the recrystalisation process (14). The key characterisation points when dealing with amorphous materials are that solid to liquid transitions are not characterised by sharp melting peaks and its associated enthalpy but is rather simply by the change in heat capacity which corresponds to a T_g.

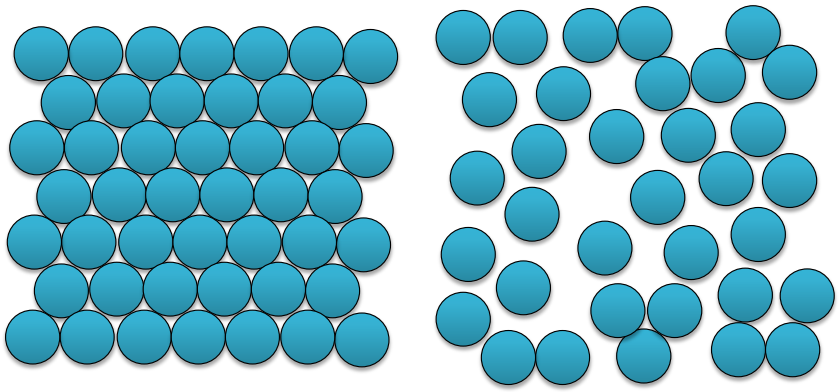


Figure 3: Diagram showing the structure of the crystalline and amorphous states.

Each circle represents an individual atom or molecule.

1.3.2. Glass transition temperature Tg

The glass transition temperature (T_g) is simply a solid to liquid transformation. It is a second order thermal transition involving only a change in heat capacity and not latent heat due to the absence of lattice energy found in crystalline state. It is usually detected by a reduction in heat capacity using a differential scanning calorimetry (DSC) (15).

The glass transition temperature is one of the important parameters to understand the thermodynamic stability of a particular amorphous formulation (16), although in some cases the crystallisation is possible below T_g value (17). The term glass is often used meaning an amorphous solid exhibit a glass transition (18). Below this temperature, supercooled

liquid is transferred into a metastable glassy phase (19). Heating the amorphous form of a material leads to recrystalisation. The recrystallisation typically appears between the T_g value and the melting point of the crystalline form of the initial material.

1.3.3. Stability against recrystalisation

The increase in the molecular mobility can have a negative effect on the physical and chemical stability of the amorphous materials. Physical stability refers to the capability of the amorphous solids to withstand crystallisation while chemical stability means the excessive degradation rates detected for amorphous materials. Recrystallisation can significantly affect the performance of the dosage form after administration and can lead to potentially harmful consequences for patients. Recrystallisation of amorphous materials is a difficult process to address since it depends on more than one factor.

Molecular mobility is identified as the diffusion or rearrangement of molecules either to form aggregates or molecules that contribute to the formation of a stable crystalline nucleus (14). It was reported that the degradation rate of amorphous β-lactam antibacterials occurred substantially faster than for their crystalline form (20). The chemical degradation of many pharmaceutical materials was attributed to the molecular motions accompanying the structural relaxation (21). The glass transition temperature T_g is usually used as an indicator of the molecular mobility and the differences between the glass transition temperature and the storage temperature is used as a signal indicating some kind of physical stability (22). For example, the physical stability of the two chemically similar calcium channel blockers felodipine (T_g 46.4 °C) and nifedipine (T_g 45.5 °C) is reported to be different (23). The difference in the

recrystallisation behaviour of both drugs was assigned to a higher thermodynamic driving force for crystallisation in nifedipene while felodipine shows lower activation energy towards nucleation. Furthermore, the preparation method assigned in the production of amorphous pharmaceuticals is thought to play a significant role on their physical stability and will be discussed in more detail in Section 1.9. The amorphous form can be prepared by several methods such as melt quenching, drying, precipitation from solution, mechanical disruption of the crystal lattice, condensation from the vapour state and supercooling of melt without inducing crystallisation. Differences in the thermal history which is low in freeze drying and high in spray drying and a variation in the mechanical stress both result in variances in the physical and chemical stability of the glass (24). No significant change in the dissolution profile of indomethacin was observed after melting and quench-cooling (using different cooling rates). However, the dissolution rate was reported to be improved for samples prepared by cryo-milling of indomethacin after exceeding a critical minimal milling time (⩾120 min) (25). The physical stability which was measured through relaxation time for different amorphisation methods for indomethacin was arranged according to the following order quench cool > cryomill α form > spray drying > ball mill α form > ball mill γ form = cryomill γ form (12).

Addition of excipients, such as surfactant, antiplasticisers and crystallisation inhibitor can affect crystallisation rates by several mechanisms including, H-bond formation, viscosity elevation, reduction in the thermodynamic barrier, adsorption at the interface. Surfactants were reported to enhance the nucleation rate through three different mechanisms, by lowering the interfacial energy, formation of the crystal core and reduction of the viscosity, therefore, reduce the kinetic barrier to crystallisation process. As the concentration of the surfactant increases or decreases then the crystallisation rate either increases or decreases (22).

Kaolin, hydrated aluminium silicate, can act as adsorbent that stabilises the amorphous material when milled together (26). Another example of an absorbent is magnesium aluminometasilicate (Neusilin) that stabilises amorphous drugs during storage and minimises their crystallisation (26). Mixing of two low molecular weight drugs can improve both the dissolution rate and the physical stability of the drug molecules, such as combining of simvastatin and glipizide (27) and a combination between poorly water soluble drug and certain type of amino acid (28). Moreover, the addition of polymer affects the intermolecular and intramolecular H-bonds that results in a significant influence on the relaxation time, consequently, altering the molecular mobility and the tendency of the molecule to crystallise (29).

Polymer addition stabilises the glass through increasing the energy of activation consequently resulting in the elevation of viscosity (24, 29, 30). Furthermore, it stabilises the amorphous state by increasing its T_g leading to the drug mobility minimisation by forming drug-polymer interactions (24, 30). Polymer addition can cause a reduction in the surface molecular mobility by the formation of H-bond and Van der Waals bonds which restrict both crystal growth and nucleation mechanisms (30, 31). Normally, a high number of the rotational bonds also plays a key role in slowing the recrystallization process by reducing the entropy of fusion (14). Combining of polymer such as polyvinylpyrrolidone (PVP) with a slightly soluble drug (acetaminophen) which has one strong acceptor H-bond or with polyacrylic acid (PAA) which has one strong donor H–bond can significantly inhibit the crystal growth. Moreover, a polymer such as hydroxypropyl methylcellulose (HPMC) was reported to have a strong impact on the nucleation rate by decreasing it without affecting crystal growth (30). To be effective inhibitors from nucleation and crystal growth, polymers must have either moderate level of hydrophobicity relative to the drug molecule and/or possess a functional group to prevent any intermolecular interaction with the drug (32). The higher the lipophilicity of the polymer, the more delay in crystal

growth or nucleation rate due to more effective adsorption at the crystal surface. Both the amount and the type of polymer contribute to the physical stability of the amorphous materials (29), for example as the concentration of Eudragit added to any mixture increases, the susceptibility to recrystallisation decreases. Furthermore, the addition of polymers was reported to show an effect on the dissolution rate of felodipine by improving the dissolution without changing the physical state of the material (33).

Temperature and humidity play a significant role in changing the structural relaxation or annealing of a compound resulting in the conversion of a glass into a crystal (34). Moreover, nucleation rate and crystal growth properties have a significant effect on the physical stability of the amorphous pharmaceuticals (35).

Furthermore, molecular weight determines the possibility of crystallisation of amorphous drug. In fact, as the molecular weight increases the glass transition temperature increases (36) and recrystallisation generally becomes less favoured kinetically.

1.3.4. Formulation strategies

There are several techniques used to increase the solubility of class II BCS drugs such as salt formation (37), complexation (38), prodrug formation (39), cocrystal formation (40, 41), particle size reduction (42), polymorphs (43) and solid dispersions (44). Each method has its advantages and disadvantages which can have an effect in the decision making process (pre-formulation) for selecting a specific method to be adopted in selected drug formulation. Salt formation is the most popular strategy to enhance the solubility of poorly water soluble drugs and the bioavailability of the liquid dosage form such as parenteral drugs. However, the reversion of the

salt dosage form might occur to get the free acid or base, subsequently, the bioavailability of the drug will reduce. Furthermore, the common ion effect happens which in turn causes a significant decrease in both solubility and bioavailability of a medicine. Most importantly, the selection of the drug to be prepared in the salt form should have specific physicochemical properties of the free base or acid to form the salt, which is considered to be the most challenging factor that limits the applicability of this strategy (45). Cyclodextrin complexation is another technique that has been used to enhance the solubility and dissolution rate of poorly water soluble drugs. Cyclodextrin is a water soluble cyclic oligosaccharide. It was reported that when cycoldextrin was combined with Ziprasodone mesylate (intramuscular dosage form aqueous solubility 0.89 mg/mL) that the aqueous solubility was improved significantly to 20-40 mg/mL (46).

Prodrug formation is an important method used in elevating both of solubility and dissolution rates of poorly water soluble drugs. A prodrug can be defined as "a chemical with little or no pharmacological activity, undergoing biotransformation to therapeutic active metabolite" (47). However, there are several challenges connected to this approach such as physicochemical, toxicological and extensive pharmacokinetic evaluation is required (39).

Cocrystals of pharmaceutical active ingredients have received a lot of attention over the last decade. Although, there is still a debate over finding a comprehensive definition for cocrystals (48, 49), one commonly used definition is that a cocrystal consists of multi-component crystals or molecular complex which are held together by non-covalent forces (50). As pharmaceutical cocrystal synthesis has been developed to improve the physicochemical properties of some APIs, it was reported that the stability of caffeine-dicarboxylic acid cocrystal shows better stability than anhydrous caffeine when was investigated in several relative humidity conditions (0%,

43%, 75% and 98%) (51). Cocrystals of triazole and 1,4-dicarboxylic acids were studied and showed to have a similar dissolution profile when compared to the amorphous form (52). However, sodium channel blocker and glutaric acid cocrystals were stated to have a significant increase in dissolution rate of the drug by 18 fold (53). Furthermore, saccharine was reported to enhance the dissolution rate when forming a cocrystal with indomethacin (54). It was reported to affect the pharmacokinetics when forms a cocrystal with carbamazepine. Carbamazepine-saccharine cocrystals exhibited higher C_{max} (Maximum Plasma Concentration) and T_{max} (Time to Maximum Plasma Concentration) (55).

According to the Noyes-Whitney equation (Equation 2), explained in more detail in Section 1.5, surface area is a key factor that has an effect on the dissolution rate of a material. Surface area is dependent on the particle size. Therefore, milling is a process of breaking up large particles to smaller size particles, which enhances the surface area surrounded by the dissolution media, consequently leading to increasing the dissolution rate. The effect of particle size reduction on the bioavailability of griseofulvin was studied and it was reported that the amount of drug in the blood was doubled as a result of reducing the particle size from 10 μm to 2.7 μm (56). Particle size reduction is believed to be a useful approach for drugs when dissolution is the rate limiting step.

Polymorphism is defined as the ability of a compound to exist in a physical state with different molecular arrangements or to crystallise as different crystal species despite the same chemical structure (57, 58). It is expected that many drugs which are capable of crystallising into different polymorphic forms will experience a change in their physicochemical properties (3). Usually the polymorph with the least energy and higher stability is considered to be a better choice during the drug development process. However, in case of ritonavir (HIV protease inhibitor)

polymorphism is considered to an undesirable property. This polymorphic transformation lead to the drugs withdrawal from the market (59). During storage an unexpected conversion of the less stable polymorph to a more stable yet less soluble (form II) occurred (60). A change in carbamazepine (form III) has been observed between different batches (55). Spironolactone was reported to exhibit an increase in dissolution rate by 12 folds as a result of polymorphic transformation (61). Where choosing the polymorphic forms with higher free energies may improve the dissolution rate and thus bioavailability, possible conversion of a metastable polymorph to a thermodynamically stable form during processing or storage, may lead to undesirable effect on bioavailability (62, 63).

A solid dispersion can be described as a dosage form characterised by a drug being dispersed in a biologically inert matrix (64, 65). Solid dispersions are one of the currently used strategies which is capable of enhancing the absorption, hence bioavailability of poorly soluble drugs. Solid dispersions are categorised into three groups, solid solutions (66, 67), glass solutions (66) and eutectic mixtures (66, 67). Eutectic mixtures been known for thousands of years. It is a phenomenon noticed when two crystalline materials mixed together in certain proportions. A melting point that is lower than the melting points of the individual pure materials is then achieved. Although it is not yet common in medicine, it has specific pharmaceutical applications such as EMLA Cream, an emulsion in which the oil phase is an eutectic mixture of lidocaine and prilocaine. Several more examples of pharmaceutical application of eutectic mixtures are going to be tabled in Section (1.4.4.2) (Table 1). In this thesis mixtures of several materials which have the potential of forming eutectic mixtures will be investigated.

1.3.4.1. Eutectic mixture

An obvious reduction in the melting points of APIs might be noticed as a result of the presence of impurities forming a mixture of two components that are completely miscible in the liquid state but immiscible in the solid state called an eutectic mixture (EM) (68). The melting point of the EM is lower than the melting point of either component (69). Thermodynamically, such systems can be considered as intimately blended physical mixtures (PM) (70, 71). Possible eutectic formation should be extracted from equilibrium phase diagram, which can be obtained experimentally or theoretically by the use of input thermodynamic data (72). Differential scanning calorimetry (DSC) is one of the appropriate techniques for the determination of equilibrium phase diagrams of binary systems comprising low-temperature melting organic substances (69, 73, 74). The liquidus curve of a phase diagram for binary systems is calculated based on the simplified Schroeder-van Laar equation (1) using the thermal data recorded by DSC (75). Furthermore observed connections between the melting point and eutectic composition and temperature for binary mixtures having one common component are shown to be applicable to a substantial number of systems (76, 77).

$$In\ x = \frac{\Delta H_i}{R}\left(\frac{1}{T_i} - \frac{1}{T}\right) \qquad (1)$$

Figure 4 shows a binary phase diagram of components A and B displaying melting points of the pure initial components. Both components are then mixed at different proportions, followed by increasing in the temperature to an extent that both components are completely melted (above the melting temperature of both individual material). The final melting

temperature is observed to be lower than the melting temperature of the individual components. In the binary phase diagram, these melting points are plotted against the corresponding composition of the component mixtures. The liquidus line or curve above which all the components are in liquid state and soluble in each other (L). The solidus line however, shows the temperatures below which both components are completely insoluble in each other and found in the solid phase. The eutectic point E is the point at which the dotted line passes through towards the composition at which eutectic mixture is formed. In the area starting from the eutectic point E until the maximum melting temperate either sample A or sample B passing through the eutectic temperature T_E, the mixture will contain a liquid phase enriched with a solid a solid phase of A or B depending on the mixture composition.

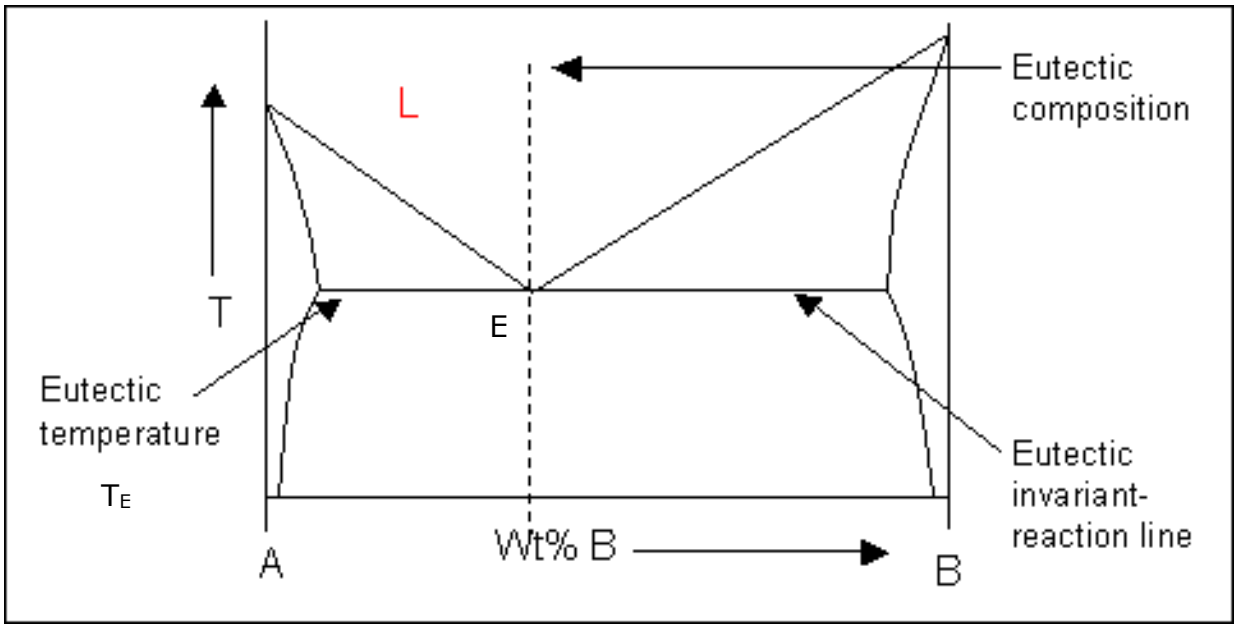


Figure 4: Phase diagram of binary mixture of component A and B, showing the temperature of the system as a function of % composition of the components.

1.3.4.2. Applications of Eutectic Mixtures in Pharmaceutical industry

During the pre-formulation stage, compatibility studies between APIs and excipient play a critical role in excipient selection. Testing for the probability of eutectic mixture formation can provide a helpful information regarding the expectation of possible physical incompatibility between drug and excipient molecules. Eutectic mixtures are sometime used in drug designing and delivery processes for various routes of administration (78). Table 1 lists few examples of eutectic mixtures and their application during manufacturing of pharmaceutical dosage form. It is extremely essential to predict the formation of eutectics and avoid manufacturing difficulties if present. For instance, during tablet compaction, the heat produced in the punch and die cavities may cause fusion or melting of tablet powder compacts resulting in manufacturing defects. Hence awareness of eutectic points of powder components may help avoid such problems. During the pharmaceutical analysis stage, understanding the concept of eutectic mixtures can be useful in the identification of compounds with similar melting points. Compounds having similar melting points, as a rule will have different eutectic point with a common other component (79). This information could be used to detect compounds like Ergotamine, Allobarbital and Imipramine HCl by their ability to form eutectic mixtures with Benzanilide (78).

Eutectic Components (a,b)	Ratio	Tm °C (a)	Tm °C (b)	Tm °C (e)	Challenges	Findings
Curcumin, Nicotinamide (80)	1:2	181.4	128.3	110.5	Oral route-Low solubility, poor oral bioavailbility	10-fold faster IDR* and 6-times higher AUC* compared to crystalline curcumin.
Ibuprofen, Thymol (81)	2:3	76.0	52.0 [6]	32.0	Transdermal Route- Limited ability to penetrate the skin	A flux of 150 mg/ cm / h, 5.9 times the flux from a saturated aqueous solution with thymol pretreated skin and 12.7 times the flux from a saturated aqueous solution across non-pretreated skin
Genistein, PEG* 460 (82)	1:24	305.0	2.0	0.2	Parentral Route- Low aqueous solubility, thus formulation difficulty.	Could help in solubilization of geinstein crystals for injection development .
Borneol, Menthol (Active 125I-cobrotoxin and eutectic mixture mixed) (83)	1:3	-	-	-	Nasal Route- Blood Brain Barrier	The eutectic mixture of Borneol Menthol, enhanced formulation and passage of active across the blood brain barrier.

Menthol and Poloxamer 188, Ibuprofen (Liquid-gel like Suppository) (84)	1:9	-	-	-	Rectal Route- Low bioavailability	Higher AUC as compared to a solid suppository.

Table 1: Applications of eutectic mixtures in formulation development (78).
IDR: Intrinsic Dissolution Rate; AUC: Area Under Curve; PEG: Poly Ethylene Glycol.

1.4. Solubility and dissolution

Solubility and dissolution are both considered to be key properties to obtain better bioavailability after oral drug ingestion. Solubility and dissolution rate are different concepts. Solubility is the capacity of a solid, liquid, or gaseous chemical substance called the solute to dissolve in a solid, liquid, or gaseous solvent at specified environmental conditions (an intrinsic property) and dissolution rate is the rate of solvation (an extrinsic property). Problems of solubility are considered as a major challenge for formulation scientist (85), which can be improved only by chemical modifications of the drug molecule, such as salt formation, structure alteration or prodrug formation (86), while there are several methods to produce an effect on dissolution rate, including particle size, solid state either amorphous or crystalline, polymorphism, salt formation, temperature, ionic strength, pH, addition of solubilising or dispersing agents, dissolution media, volume of dissolution media, thickness of boundary layer and diffusion coefficient of the solute in the dissolution media (87, 88). As a result, dissolution rate can be modified chemically or through formulation techniques.

The dissolution rate is expressed by the Noyes–Whitney equation or the Nernst and Brunner Equation (35, 47, 80) of the form:

$$\frac{dm}{dt} = \frac{DA(C_s - C)}{h} \qquad (2)$$

Where $\frac{dm}{dt}$ is rate of the drug dissolution, D is the diffusion coefficient, A is the surface area of the solid, Cs is the solute concentration in boundary layer, C is the concentration of the solute in the bulk solution solubility and h is the thickness of the boundary layer. From Equation 2, it can be seen that any change in the surface area, solubility, concentration or diffusion coefficient will all have a significant effect on the rate of dissolution.

1.5. Poor aqueous solubility

Aqueous solubility is one of the most substantial factors that has a direct effect on the substance bioavailability, because it controls both the dissolution rate and the maximum concentration in the gastrointestinal tract (GIT) (89). Poor water solubility of new drugs is thought to be one of the major problems in pharmaceutical formulation. Approximately 40% of the marketed immediate release drugs that are intended for oral administration are considered as nearly insoluble (less than 100 µg /mL) (3). According to the United States Pharmacopeia (USP), solubility is divided into seven classes as shown in Table 2 (90). These categories are ranging from very soluble (>1000 mg/mL; class I and III BCS) to practically insoluble (<0.1 mg/mL; class II and IV BCS). In order for the oral dosage form to produce the therapeutic effect after administration, it is important to reach what is known as the minimum necessary concentration in the general circulation, which is close to 0.1 mg/mL, below this value the problem of poor solubility develops (91, 92). A predominant percentage of

the drugs on each list (30-40%) were categorized as practically insoluble drugs (90). Recently, the percentage of poorly soluble drugs candidate has increased significantly to 70-90% (3, 93) due to the reasons mentioned in Section 1.6.

Descriptive term (solubility definition)	Parts of solvent required for 1 part of solute	Solubility range (mg/mL)	Solubility assigned (mg/ml)	Percentage of drugs on GB list	Percentage of drugs on WHO list
Very soluble	<1	≥1000	1000	3%	7%
Freely soluble	From 1 to 10	100-1000	100	8%	14%
Soluble	From 10 to 30	33-100	33	12%	10%
Sparingly soluble	From 30 to 100	10-33	10	14%	7%
Slightly soluble	From 100 to 1000	1-10	1	15%	18%
Very slightly soluble	From 1000 to 10000	0.1-1	0.1	6%	13%
Practically insoluble	≥10000	<0.1	0.01	39%	27%

Table 2: Solubility definition United States Pharmacopeia (USP); the percentage of IR drugs on the Great Britain (GB) and on the World Health Organization (WHO) lists Obtained from (90).

1.6. Reasons for the presence of poorly soluble drugs

One of the most highlighted reasons which led to the rapid increase in the number of poorly soluble compounds is the developments in combinatorial chemistry and high through-put screening (HTS) methods. These methods are known to be used frequently in drug discovery that cause millions of drug candidates to be screened (89). When in vitro studies are applied, the compounds should go through two stages, first dissolved in dimethyl sulphoxide (DMSO), which is acknowledged as a polar aprotic solvent that dissolves both polar and nonpolar compounds, and second dissolved in water. Misleading information will be provided about the compounds water solubility, which is thought to be resulted from that the apparent concentration of a compound in water is higher than the equilibrium concentration (92, 94, 95). In drug discovery the drug efficacy is predominantly optimized resulting in that HTS-based methodologies favouring the compounds with increased lipophilicity but decreased solubility (88, 96).

Lipinski's Rule is often applied by medicinal chemists in drug discovery field to address the oral bioavailability and overall drug-likeness of a compound (97), based on the following conditions: a lipophilicity (logP), the logarithm of the partition coefficient between water and 1-octanol, value below 5, molecular weight below 500, number of hydrogen bond donors, usually the sum of hydroxyl and amine groups in a drug molecule, less than 5 and the number of hydrogen bond acceptors, estimated by the sum of oxygen and nitrogen atoms, less than 10 (96, 98). This rule provides a standard as to which a molecular parameters are significant for a drug's absorption, distribution, metabolism and excretion (ADME) in the body. Any compound that disobeys more than two of these criteria is more expected to face

bioavailability challenges. However, recently Wang and Hou (89) reported that "drug-like" molecules which successfully pass the Lipinski's Rule of Five screening are twenty times less soluble than the "real drugs".

1.7. Developability Classification System (DCS)

A revised classification system based on BCS was introduced by Butler and Dressman (99), which is important in the evaluation of new drug candidates and is called developability classification system (DCS) to make it more useful in formulation development. DCS increases the volume for measuring solubility of a dosage form to 500 mL from 250 mL and uses a fasted-state simulated intestinal fluid as the medium (100). This classification depends on jejunal solubility which is affected by several factors such as, the pH alteration which is influenced by different factors such as food, age, disease and drug interaction.

This system divides drugs from Class II into dissolution rate limited and solubility limited as shown in Figure 5. The dissolution rate limited are controlled by two key factors which are particle size and intestinal solubility while the solubility limited are controlled by dose and solubility of the drug itself. Class IV is the permeability limited classification in which excipients may have an effect on the drug permeability, directly by affecting drug transit through GIT or indirectly through altering GIT residence time (99).

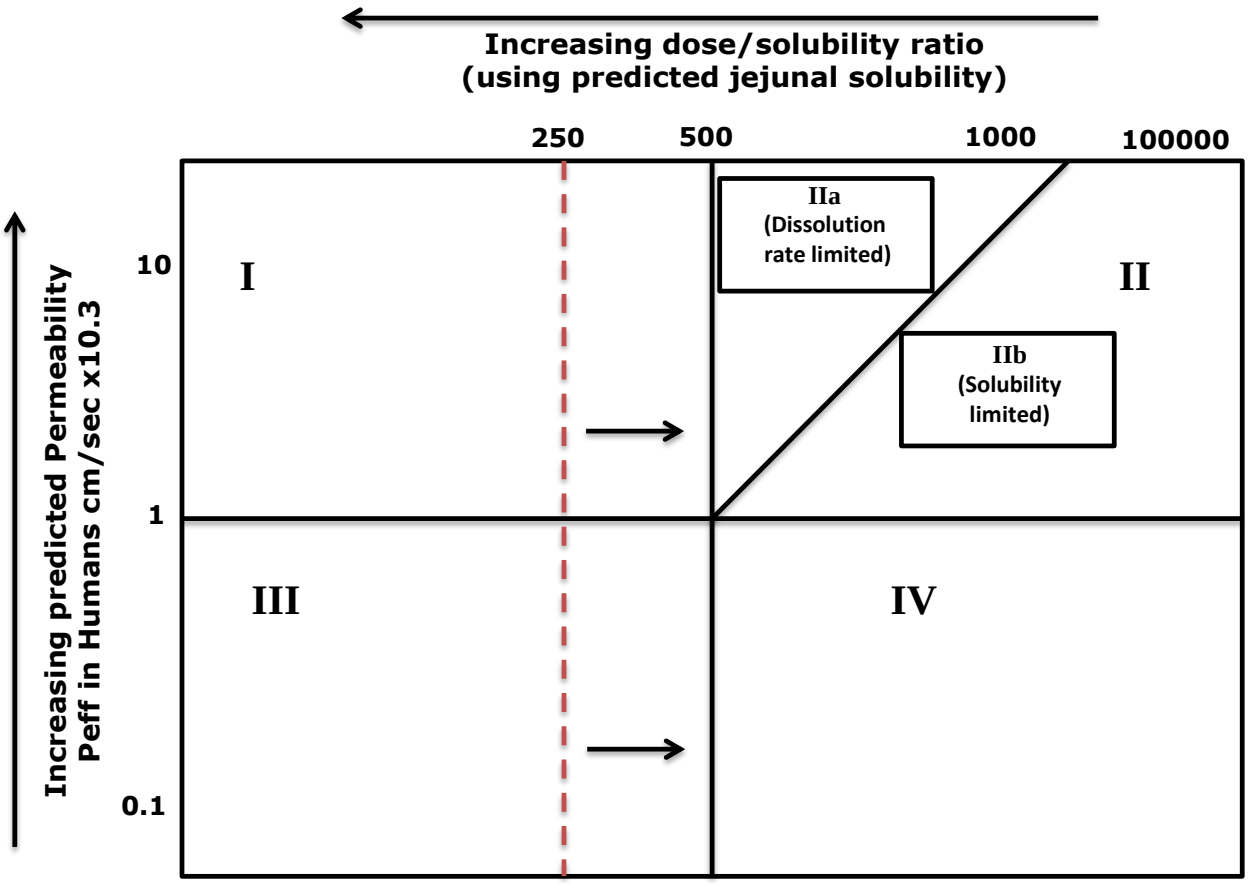


Figure 5: In the developability classification system, the dotted line shows the change in volume from the BCS. The diagonal line in class II divides it into class IIa, which is dissolution rate limited, and class IIb, which is solubility limited. Adapted from (99).

1.8. Current and potential strategies

Amorphisation can increase the drug solubility from 10 to 1600 fold (101). This is due to the enthalpy, entropy and free energy of the amorphous solid that is high in comparison with the crystalline form. This high energy causes rise in the dissolution rate of poorly water soluble drugs (29). There are several approaches that are used in amorphisation process, such as melt-quenching, solvent evaporation, spray drying, freeze drying, co-grinding (102).

Formulations of solid dispersions is an important amorphisation process in which the drug is dispersed in an inert matrix. The stability problem is the main drawback in this technique due to the recrystallization tendency which reduces the solubility and bioavailability of the slightly soluble drug (16). Freeze drying is a technique that enhances the dissolution profile of the drugs that are slightly soluble in water such as oxazepam (103).

Moreover, mechanical grinding of crystalline material which is either performed at room temperature by a ball mill and jet milling or by grinding at extremely low temperature provided by a cryogenic liquid (liquid nitrogen) this method is called cryomilling or cryogrinding which is going to be discussed later in Section (1.9.1). Excessive mechanical milling can cause changes in the structure of the grinded particles such as polymorphic transformation, crystal defects and partial or complete amorphisation. It was reported that a complete amorphisation was achieved when the milling occurs at a temperature lower than the glass transition temperature (35). Milling time is considered to be a very important parameter, since milling for short periods of time results in particle size reduction of the subjected sample without the formation of the amorphous form, therefore, this method requires longer period of time in order for the crystal to transform into the amorphous state (104). The advantages and disadvantages of different amorphisation methods are summarised in Table 3.

Process	Advantages	Disadvantages
Melting and quench cooling	Simple technique No need for solvent Eliminate the effect of humidity	Chemical degradation due to high temperature If cooling rate is too slow then crystallisation occurs Low compaction of the material
Spray drying	One step process Relatively low temperature	Difficulty for drug with low T_g to form stable amorphous product Product is too sticky Environmental safety due to organic solvent usage The difficulty in selection of suitable solvent for API and polymer High manufacturing cost
Freeze drying (lyophilisation)	Easy control of temperature	Recrystallisation might take place depending on the cooling rate
Dehydration of crystalline hydrate	Simple method	Low physicochemical stability Rarely applicable.
Milling	Simple	Change in morphology Polymorphism Chemical instability Energy consuming T_g control amorphisation process Static disorder Aggregation
Cryomilling	Mild method to produce amorphous material without using of solvent or melting Suitable for heat sensitive material and water liable method Less crystal deformation Reduction in recrystallisation tendency	Crystal defect Not well studied Emerging method not used in pharmaceutical formulation to date

Table 3: Advantages and disadvantages of different amorphisation techniques (49, 105-107)

Many of these above tabled methods are routinely used in industry but crystal to amorphous transformation is not always guaranteed. Regular milling process is considered difficult to control. However, with cryomilling in principle, the milling rate is easily controlled. Cryomilling also allows higher level of particle size reduction which is not necessarily achieved with

regular milling processes. Furthermore, with most of the above mentioned techniques solvent or heat are often used. This will negatively affect some heat labile drugs, such as aspirin. As a result of heat aspirin will decompose into salicylic acid. Table 4 shows the difference between amorphisation strategies in terms of, solubility, dissolution rate, heat and moisture.

Technique	Solubility	Dissolution rate	Heat	Moisture
Spray Drying	√ (108, 109)	√ (108, 109)	X (108)	X (110, 111)
Freeze Drying	√ (112)	√ (112, 113)	√ (87)	X (114)
Solvent evaporation	√ (86)	x	X (115)	X (115)
Dehydration	√	x	√	X (116)
Melt extrusion	√	x	X (117)	√ (117)
Milling	√	√ (118)	X	√
Cryomilling	√	√(107, 119)	√ (120)	√ (120)

Table 4: The difference between the potential amorphisation strategies in terms of, solubility, dissolution rate, heat and moisture.

A method of making materials amorphous without heat or solvent would potentially be useful. Cryomilling is an under used technique which is not currently used on an industrial level. Limited number of research papers

outlining the potential of the implantation of cryomilling a prospective formulation tool. Therefore, cryomilling is going to be looked at in more details in the next section.

1.8.1. Cryomilling

Various forms of milling are commonly used in pharmaceutical industry and indeed it is very popular technique applied in the wider fields of industry as well to reduce particle size. The large amount of mechanical perturbations generated during milling may result in significant changes in the structure of the grinded material, including polymorphic transformations, crystal defects and some degree of amorphization (121, 122). Complete transformation from crystal to amorphous state potentially occurs if the grinding process takes place at a temperature much lower than the glass transition temperature T_g (123). Grinding of various types of crystalline materials can be carried out using two options, the first one is milling at room temperature in a traditional ball mill or the second by using a cryogenic impact mill submerged in liquid nitrogen (cryogrinding, cryomilling), liquid nitrogen is classified as an inert gas which is liquefied by extensive cooling temperature or by compression under high pressure (124).

Recently, cryomilling of pharmaceuticals has attracted increasing intention (105, 125, 126). In cryomilling grinding takes place at extremely low temperature using liquid nitrogen, which facilitates the transformation of the crystalline form to amorphous form which is believed to be achieved in relatively short period of time compared to other types of milling such as ball milling at room temperature (123). Cryomilling, has been used in the production of nanostructured materials from a variety of systems (127),

including Al (128), Ni (129), Zn (130) and Fe (131). It has been indicated that the presence of liquid nitrogen during milling has several benefits, such as decreased oxygen contamination (132), enhanced deformation during milling (133) and for metals the formation of oxide and nitride particles that successfully stabilize the grain size (129, 134, 135). Furthermore, cryomilling has been used in food processing to enhance the digestion properties as a result of particles' size reduction (136). Cryomilling has successfully been reported to produce an amorphous telmisartan (137), which is used in the management of hypertension and it is classified as one of the poorly water-soluble compounds. Cryomilling is considered to be an efficient technique to deal with heat sensitive drugs, such as griseofulvin (138), because the milling process is performed under low temperature which potentially will prevent excessive heat generation during the grinding process therefore protecting the chemical structure and preventing any chemical decomposition. However, decomposition of furosemide when co-cryomilled with other materials was observed. Therefore, the process of selection of the appropriate method of amorphization and excipients is significant to avoid such a problem (123). Along with other parameter which would affect the end product of the cryomilling process milling time was reported to play an important role in improving the dissolution rate of indomethacin (25).

Cryomilling is particularly attractive for pharmaceutical processing for class II DCS dugs because it has the potential to improve dissolution rate due to decreasing the particle size as per Noyes–Whitney equation (Section 1.4 Equation 2), and also through potentially transforming drugs into amorphous form to improve their apparent solubility. Cryomilling has not been used in pharmaceutical industry to date and there is a gap in knowledge about making materials amorphous in an industrial setting. It can be seen from literature that cryomiling can be a promising technique to be used in order to improve dissolution rate and thus bioavailability of

poorly water soluble drugs. Therefore, the current work aims to approach the real world pharmaceutical formulations by milling a multi-component systems drug-drug and drug-excipients rather than cryomilling the drugs by themselves.

1.9. Aims and objectives

Aim:

To explore the potential of multi-component formulations via cryomilling as a mean to improve the physical properties of poorly water soluble drugs.

Objectives:

- Chapter 2: To study the effect of cryomilling on the physical behaviour of chemically near identical model compounds when treated individually and in pair mixtures. A stability study will then be performed to address the recrystallization behaviour of all mixtures.

- Chapter 3: More realistic medicinal substances will be used to study the potential of crystal to amorphous transformation of cryomilled and room temperature milled materials.

- Chapter 4: To address the ability of amorphous transformation of cryomilled pair mixtures of drugs and excipients by mimicking the real mixture of such materials in pharmaceutical formulations.

Chapter 2

The effect of cryomilling on single and multi-component isomers model systems

2.1. Introduction

Unfortunately, in many cases, formulation strategies for amorphous drugs are not further developed due to thermodynamic metastability of the amorphous system, which may easily undergo chemical decomposition as well as crystallize during storage (10). However, it is worth noting that amorphous active pharmaceutical ingredients often have greater ability to form tablets with respect to their crystalline counterparts (8). Moreover, differences in the properties of an amorphous material as a function of the preparation method should be expected (5, 87). It has been reported that the difference in the physical stability between simvastatin prepared by cryomilling and quench cooling, with the quench-cooled samples having higher stability (88). In the analysis of griseofulvin (85), and indomethacin (47) prepared by different techniques, differences in the thermal, structural and physical characteristics were observed. There was a suggestion that the molecular mobility may differ in the same drug according to the preparation method. This molecular mobility plays a significant role in the recrystallization process (139).

Milling is one of the most common mechanical processes which has been used regularly in the pharmaceutical industry in order to bring powders within the desired particle size (87, 93, 94, 100). The mechanical stress exerted during the milling process could play a significant role in the appearance of other several changes, such as particle fracture, polymorphic transformation and amorphization that have been reported for many pharmaceutical products, like gabapentin, famotidine, ranitidine

hydrochloride and fananserine (140). In contrast to conventional continuous milling (7), cryomilling seeks to operate at high energy at very low temperatures using cryogenic media such as liquid nitrogen (Cryogenic grinding).

Cryomilling represents an effective process of reducing the risk of chemical degradation as a result of thermal stress that occurs in other amorphisation strategies. Cryomilling has the potential of producing a table amorphous material if the molecular mobility is kept as low as possible consequently reducing the recrystallization ability of the cryomilled sample.

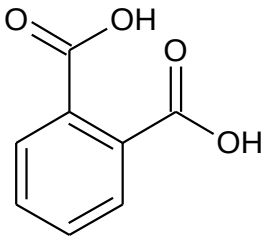
Before cryomilling can be evaluated as a potential formulation strategy for different active pharmaceutical ingredients and excipients, it is sensible to first study the properties and crystal transformation of different chemical models which are well known as crystalline isomers (that means have the same molecular mass and similar functional groups). In the present chapter phthalic, isophthalic and terephthalic acids were subjected to cryomilling and then characterised using DSC to detect their thermodynamic properties. XRPD was used to identify the crystalline structure of the three materials, detect the difference in XRD pattern between milled and unmilled sample, and calculate the particle size using the Scherrer equation with the use of silicon dioxide as a standard specimen in order to obtain the instrumental influence on XRPD peaks broadening. SEM was used to address the particle size reduction during cryomilling and finally FTIR to identify whether there is any evidence of chemical degradation.

2.2. Materials and Methods

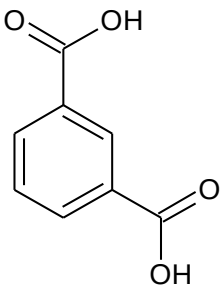
2.2.1. Materials

The materials which were chosen in this current study are crystalline organic compounds classified as aromatic dicarboxylic acid with a chemical formula $C_6H_4(CO_2H)_2$. They are isomers to each other with a molecular mass below 500 g/mol (around 166.14 g/mol), containing a benzene ring and a carbonyl group similar to APIs chosen to be worked with in the next chapters. Their melting points are considered to be on the higher regions which are going to be discussed later.

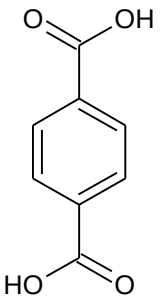
Sometimes the term "phthalic acids" is used to refer to this family of isomers, but in the singular, "phthalic acid", refers exclusively to the ortho-isomer.



a. Phthalic acid
o-Phthalic acid



b. Isophthalic acid
m-phthalic acid



c. Terephthalic acid
p-phthalic acid

a. Phthalic acid: Phthalic acid (A14450, batch no. - 10178989, +99%) was purchased from Alfa Aesar. In order for its purity to be detected, a DSC triple run was conducted with a heating rate of 10°C/minute. The melting point onset was measured using TA analysis software which as at 207.4 °C as mentioned on the manufacturer specification sheet.
b. Isophthalic acid: Isophthalic acid (A14445, batch no. - B25X004, +99%) was purchased from Alfa Aesar. The thermal properties of the as received material was characterised using DSC at 10°C/minute to measure its melting point which appeared as a sharp single endotherm at 344.5.0°C confirming with the its physical properties information on the manufacturer specification sheet.
c. Terephthalic acid: Terephthalic acid (A12527, batch no.-10180244, +98%) was purchased from Alfa Aesar. The as received sample was used to detect terephthalic acid melting point, which onset was not been detected using the DSC at heating at a rate of 10/minute.

d. Potassium carbonate: In order to prepare a 43% relative humidity atmosphere for the cryomilled samples to be kept in throughout the stability study, potassium carbonate (NFPA 704) was purchased from Minerals-Water Ltd.

2.2.2. Preparation Methods

2.2.2.1. Preparation of the cryomilled materials

- Phthalic acid (1 g), isophthalic acid (1 g) and terephthalic acid (1 g) were cryomilled individually for a total of time of 60 minutes.
- Physical pair mixtures of phthalic and isophthalic acid, isophthalic and terephthalic, phthalic with terephthalic acid were prepared by cryomilling each of the above material alone for 60 minutes followed by mixing similar proportion of 1:1 triturated by using mortar and pestle.
- The cryomilled together mixtures were prepared by weighing 500 mg of each individual material (which is considered to be a 1:1 molar ratio) as the molecular masses are the same, the mixture was then cryomilled for 60 minutes.

2.2.2.2. Cryomilling

Cryomilling the materials was achieved by using SamplePrep 6870 Freezer/Mill (SPEX, Metuchen, NJ, United States). It is supplied with an electromagnetic coil which can shuttle the impactor back and forward inside the sample vial in order to be grinded against the end cap. The liquid nitrogen submerges the coil and vial to keep sample temperature as low as possible. The cryomilling time was 60 minutes for all samples. The

instrument was set to pre-cool for 5 minutes then milling cycles starts for 2 minutes each at frequency of 15 cycles per second. Throughout the grinding process, there was a pause of 1 minute between cycles to prevent temperature rise. The cryomilled samples were then vacuum sealed inside a dry glove box in order to minimize moisture uptake, it is supplied with an argon cylinder to achieve minimum relative humidity.

2.2.3. Characterization Methods

i. DSC

A Q2000 Differential Scanning Calorimeter (DSC) (TA Instruments, New Castle, DE, USA) was used for thermal analysis with a constant purge of nitrogen gas of 50ml per minute. Tzero (TA Instruments, New Castle, DE, USA) aluminium hermetic pans and lids were used to contain the samples with a sample size of 5 mg. These pans were sealed in an argon purged dry-box and tapped lightly to spread out the sample evenly within the pans. The instrument was calibrated for temperature and enthalpy using indium. The standard or conventional DSC mode was adopted to measure Tg, melting points, recrystallization and enthalpy. Measurements were run from -40°C to specific temperatures above each component's melting temperature with specific heating rates except for terephthalic acid, the temperature was raised to around 380°C and no melting endotherm was detected. Analysis was carried out through the Universal Analysis Software

(TA Analysis) to estimate the enthalpy, onset and peak of thermal events such as the glass transition, melting and recrystallization. Experiment were carried out in triplicate (n=3).

ii. XRPD

The XRPD was measured by using flat-plate diffractometer, the X'Pert PRO (PANalytical, Almelo, Netherlands). Reflection mode was set up using Cu $K\alpha_1$ (λ = 1.54 Å) operating in Bragg-Brentano geometry. 0.0260 2 θ /° was used as a step size with a total collection time of 5 minutes. The voltage of the generator was set to 40 kV and the current to 40 mA. Brass was used as a holder for the samples. All the obtained data were analysed using the R statistical package.

iii. FTIR

The IR spectra of the samples were collected using Agilent/Cary630/FTIR, United States. Around 5-8 mg of the samples were applied to the Diamond ATR type II crystal plate, which is considered to have a strong resistance to chemical transformations. The signal reflection diamond has a 1 mm diameter sampling surface with 200 µm active area and provides approximately 2 µm depth of penetration for infrared energy at 1700 cm^{-1}. The resultant peaks were analysed by Agilent MicroLab PC software. The spectral range was taken between 4000-500 cm^{-1}.

iv. SEM

SEM images were captured using JSM – 6060LV (JEOL Ltd., Tokyo, Japan) variable pressure tungsten filament electron microscope. The samples were fixed on conductive carbon tape first and then sputter coated in gold. Images were collected at an accelerating potential of 10 kV.

2.2.4. Stability Tests of Cryomilled mixtures

Preparation of 43% Relative humidity

In order to study the stability of the cryomilled samples, a saturated solution of potassium carbonate was prepared and then kept in a gas-tight environment to achieve the required humidity of 43% at room temperature (141). Although the results that will be presented in this study was for the freshly cryomilled samples and for the samples after subjected to storage for three weeks, the samples were analysed regularly by XRPD, FTIR and DSC after 1, 2 and three weeks of storage.

2.3. Results

2.3.1. One phase Systems

2.3.1.1. Phthalic acid

DSC has the ability to address the thermal transitions of materials through which their properties can be characterised. The melting temperature, crystallisation temperature, or glass transition temperature can be revealed in any thermogram of a material subjected to heat.

The DSC thermogram for unmilled phthalic acid, immediately after cryomilling and after three weeks of storage at 43% relative humidity is shown in Figure 6. The melting onset value for phthalic acid as received was 207.4°C. After phthalic acid was cryomilled for 60 minutes, its thermogram displayed a T_g at 189.0°C which can be seen clearly in Figure 7, this indicates the formation of an amorphous product. It is followed by a melting peak with an onset of 207.4°C, which can clearly be seen a visual inspection that is similar to the melting onset of phthalic acid before milling. After the cryomilled phthalic acid has been stored in a relative humidity of 43% for a total period of three weeks, the DSC data shows no evidence of the presence of an amorphous material; only a melting peak was detected with an onset of 206.9°C.

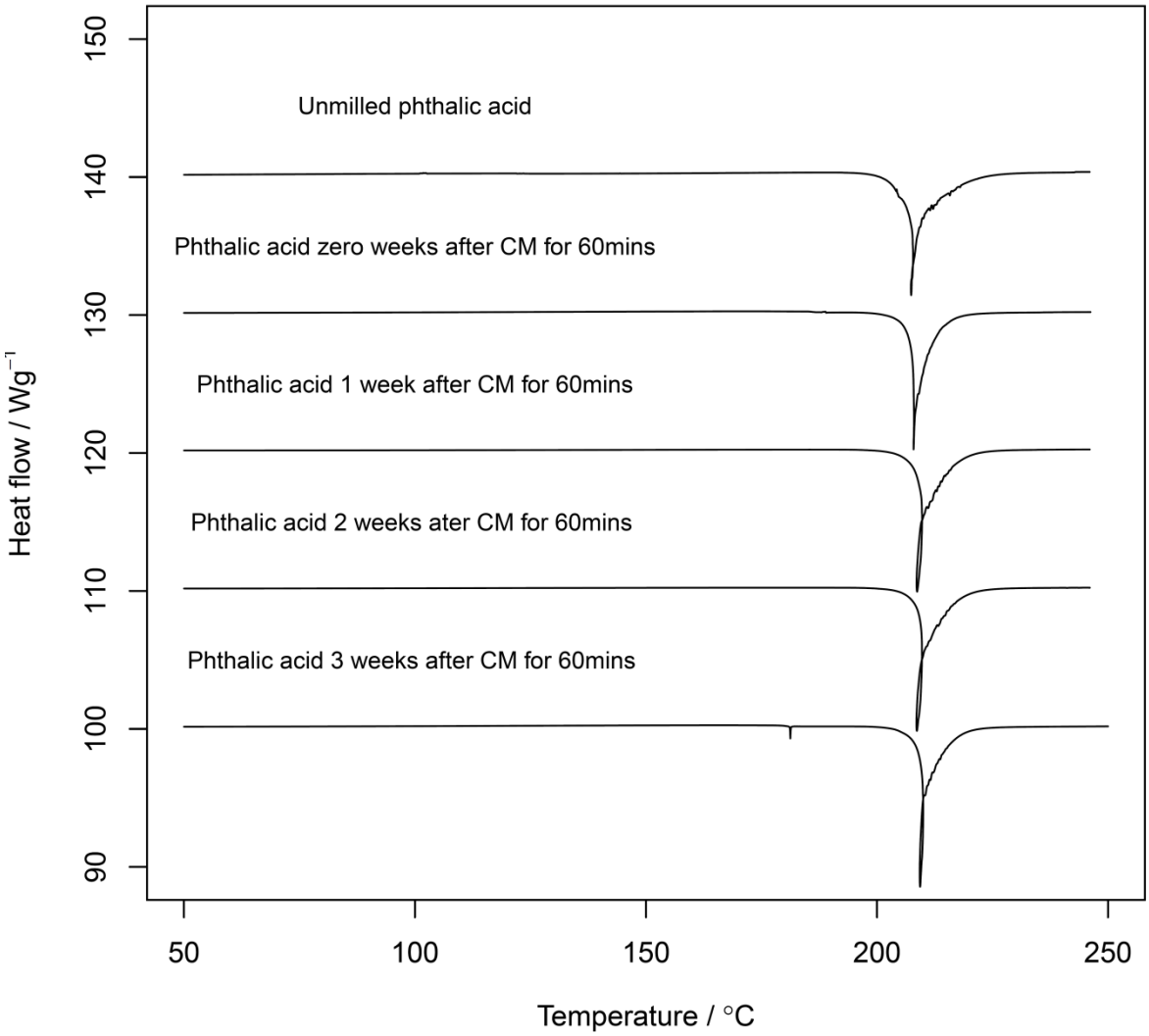


Figure 6: DSC Thermogram of phthalic acid as received, immediately after cryomilling and after 3 weeks.

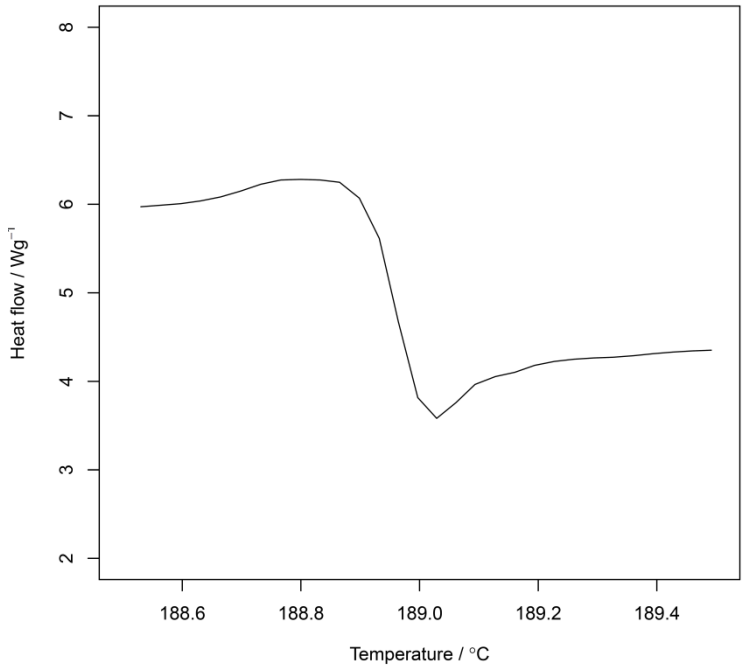


Figure 7: Tg region for phthalic acid immediately after cryomilling for 60 minutes.

Phthalic acid XRPD measurements are shown in Figure 8 for unmilled, cryomilled and for cryomilled sample after storage for three weeks. It is clear that the phthalic acid sample displays Bragg peaks, which differ slightly in width between the unmilled and cryomilled sample, which suggests some level of crystallinity was still existing. It was noted that the peaks for cryomilled phthalic acid are wider than those for the unmilled sample. The XRD patterns do not change markedly after three weeks. For example, the most intense expected peak for phthalic acid at (21.30°), which is detected in unmilled sample, is replaced by a broad peak in the cryomilled sample. After three weeks the same peak width started to decrease as shown in Table 5. Fityk software was used to measure the XRD peak intensity and width and then using the Scherrer equation to calculate the crystallite size at a constant wavelength of 1.54 Å. Brass measurements

were included since it was used as a sample holder, which explains the presence of a few background peaks.

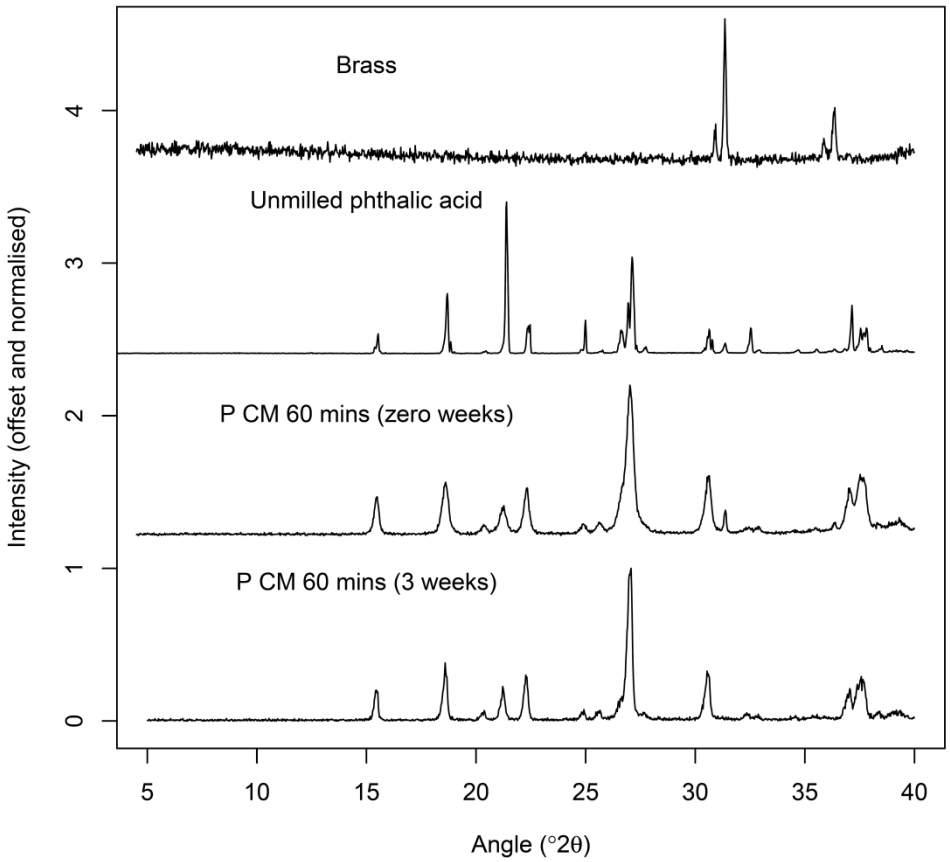


Figure 8: XRPD pattern of phthalic acid as received, immediately after cryomilling and after 3 weeks

Taken together, the data indicate that cryomilling of phthalic acid produces a direct effect on the crystallite size in which the Bragg peaks of phthalic acid sharpness is decreased. It should be noted that there is no clear indication of amorphous material (e.g. XRPD "halo") in our XRD data. However, the presence of a significant amount of amorphous material is not excluded, since the DSC data of cryomilled phthalic acid show an indication of amorphous transformation upon cryomilling as presented in Figure 7. It therefore appears that cryomilling of phthalic acid leads to an

obvious reduction in its crystallinity and reduces the crystallite size by half to ~ 20 nm. Cryomilling does not exhibit an obvious effect on the crystal structure of the material.

	Measured Peak Width (degrees)	Measured Peak Position (degrees)	Sherrer estimate of Crystallite Size (nm)
Unmilled phthalic acid	0.16	21.30	54
Cryomilled phthalic acid at zero weeks	0.42	21.25	20
Cryomilled phthalic acid after three weeks	0.23	21.22	38

Table 5 : XRPD data of phthalic acid shows crystallite size reduction after cryomilling and recrystallization upon storage.

SEM provides the most direct picture of nanoparticles, giving information about the size, shape and other general aspects. Particles with a size under 100 nm may be difficult to observe, depending on the microscope and the set up. Figure 9 show SEM images of unmilled and cryomilled phthalic acid. It is immediately apparent that cryomilling has a direct effect on particle size of phthalic acid, with an average particle dimension of approximately 120 nm for the cryomilled sample. Taken together, the observed SEM particle dimension is higher than the corresponding crystallite size which is estimated by sherrer equation of 20.16 nm. This discrepancy may be due

to the presence of aggregates in SEM grain consisting of several crystallites and/or poor crystallinity (78).

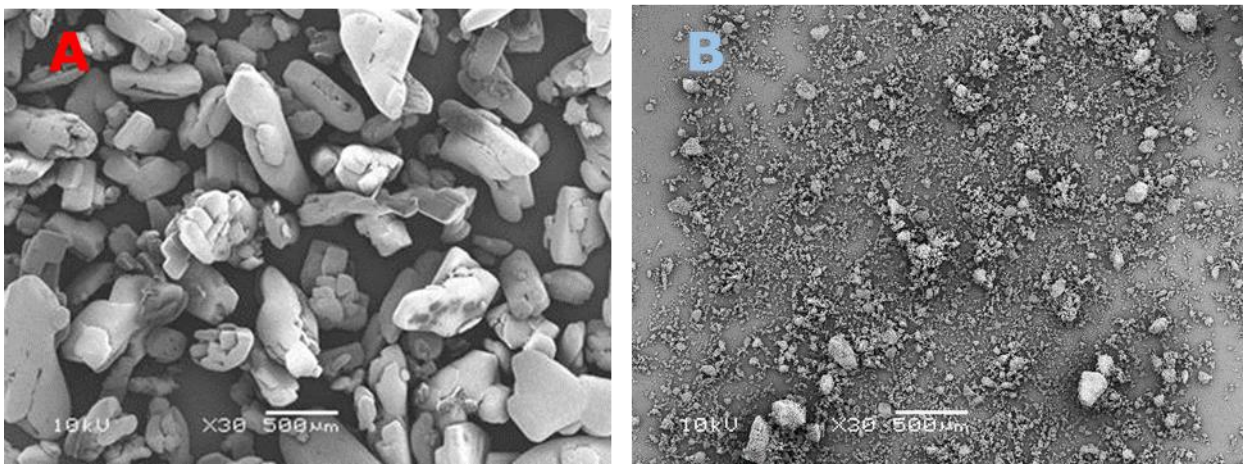


Figure 9: SEM scan at 10 kV of A. unmilled phthalic acid B. cryomilled phthalic acid for total period of 60 minutes

Moreover, the AT-FTIR results shown in Figure 10, the C=O peak after cryomilling of phthalic acid are found at relatively high wave numbers, 1666.29 cm^{-1} and 1666.97 cm^{-1} for freshly cryomilled phthalic acid and after keeping the cryomilled sample for 3 weeks respectively, compared to the unmilled sample which was detected at 1661.11 cm^{-1}.

In general this region for the carbonyl peak suggests a weakening of the hydrogen bond in the milled material since hydrogen bond formation reduces the carbonyl peak position (8, 9).

The carbon-oxygen single bond also has an absorption in the fingerprint region, varying between 1000 and 1300 cm^{-1}; it appeared at 1261.61 cm^{-1}

for the unmilled phthalic acid, there was a slight shift upwards by 5 cm^{-1} upon cryomilling. On the other hand, there was a significant change in the peak intensity; the peak sharpness was increased upon milling

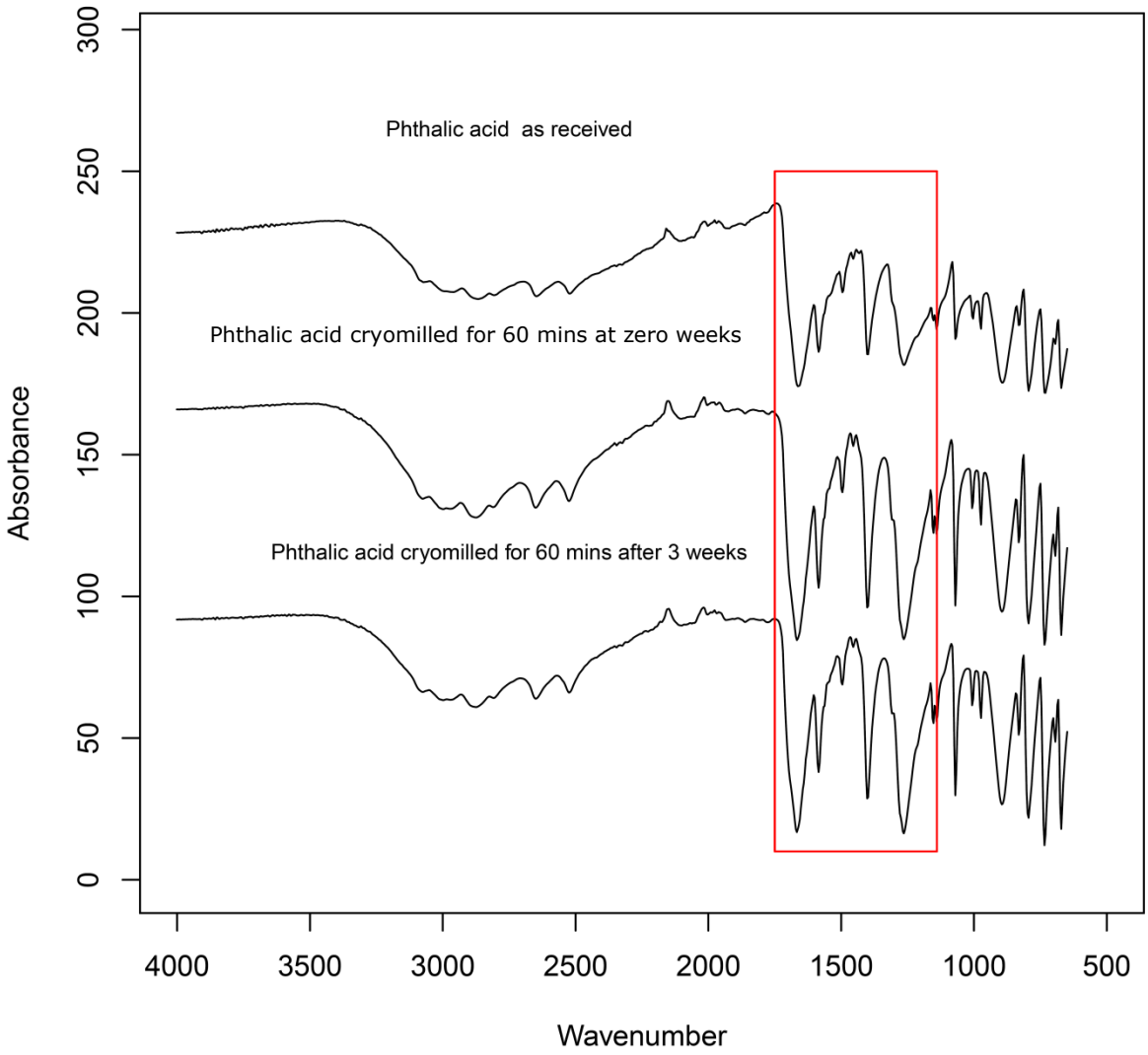


Figure 10: The FTIR spectra of phthalic acid before milling, freshly cryomillied phthalic acid and after storage for three weeks at 43% relative humidity.

2.3.1.2. Isophthalic acid

The DSC data for isophthalic acid as received, immediately after cryomilling for 60 minutes and after three weeks of storage are shown in Figure 11. In the the thermogram for unmilled isophthalic acid, a melt was seen with an onset at 344.1°C. After cryomilling there was a recrystallization exotherm detected with a peak maximum at 120.7°C show in Figure 12, confirming the presence of an amorphous material, followed by a melt with an onset of 344.2°C. On the other hand, the results obtained after the cryomilled sample was stored for three weeks, isophthalic DSC data show only a melt with an onset of 344.6°C.

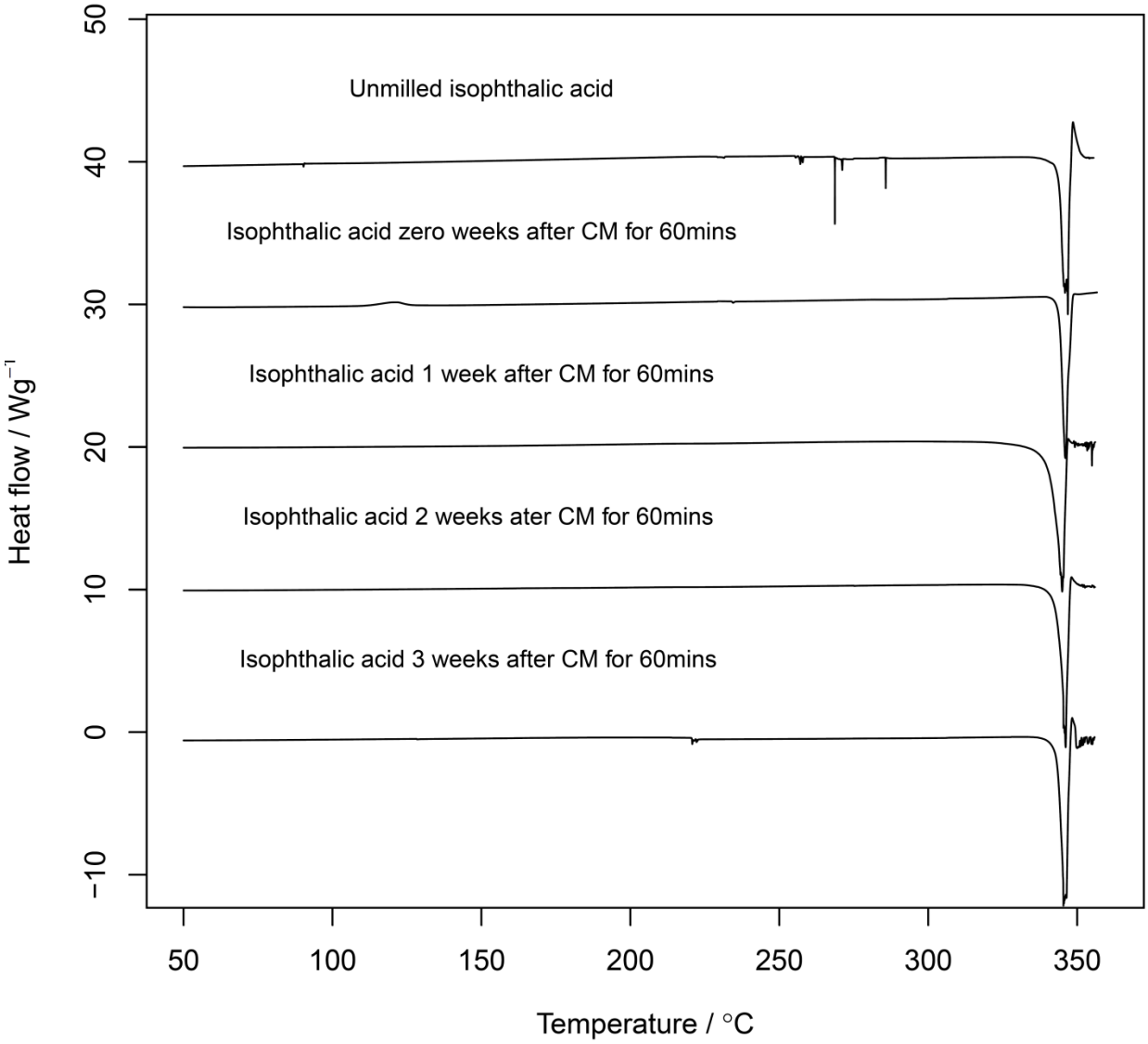


Figure 11: DSC thermogram for as received isophthalic acid, immediately after milling and after storage for three weeks at 43% relative humidity.

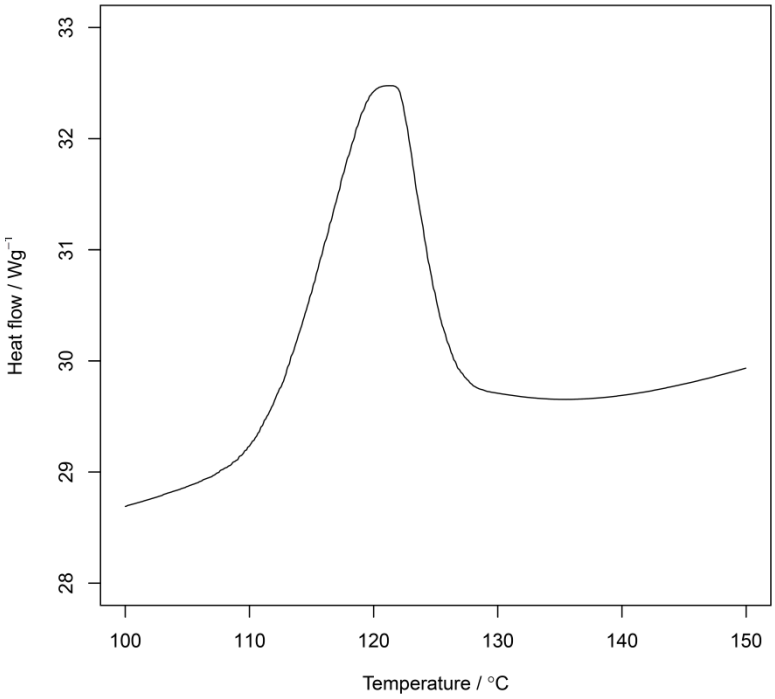


Figure 12: A recrystallization exotherm in isophthalic acid immediately after cryomilling.

Isophthalic acid XRPD measurements are presented in Figure 13 of unmilled, cryomilled and for cryomilled sample after been stored for three weeks. It shows a marked difference in peak appearance between the as received and the cryomilled isophthalic acid sample, the Bragg peaks of the cryomilled sample appear broader and slightly shifted to a lower angle compared with the unmilled isophthalic acid which exhibit somewhat sharp peaks. The two most intense expected peaks for isophthalic acid at (15.05° to 16.04°), which are detected in the unmilled sample, are replaced by a broad single peak in the cryomilled sample. After three weeks the same peaks are separated back into two individual relatively sharp peaks.

Taken together, the data indicate that crystallite size of isophthalic acid is strongly affected by cryomilling. The Bragg peaks of cryomilled isophthalic

acid are broad, which indicates particle size reduction. The DSC data of cryomilled isophthalic acid show a sign of amorphous transformation upon cryomilling as presented in Figure 12. It therefore appears that cryomilling of isophthalic acid leads to an obvious reduction in its crystallinity and the crystallite size from 60 nm to 6 nm as shown in Table 6. However, cryomilling of isophthalic acid does not exhibit an effect on the crystal structure of the material since the produced XRPD trace show no marked difference in peak position when comparing the unmilled with the cryomilled samples.

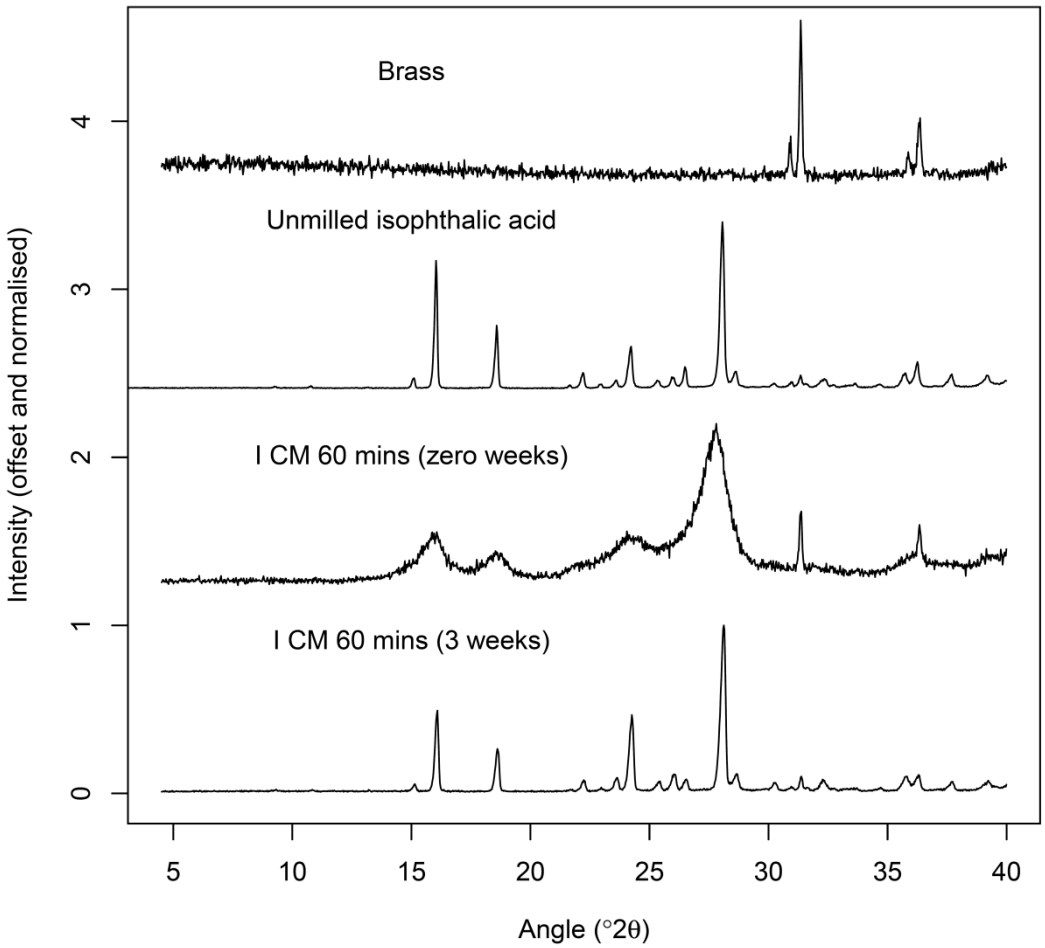


Figure 13: XRPD pattern of unmilled isophthalic acid, immediately after cryomilling and after three weeks of storage at 43% relative humidity

	Measured Peak Width (degrees)	**Measured Peak Position (degrees)**	**Sherrer Estimate of Crystallite Size (nm)**
Unmilled isophthalic acid	0.14	16.04	60
Cryomilled isophthalic acid at zero weeks	1.45	16.06	6
Cryomilled isophthalic acid after three weeks	0.21	16.09	43

Table 6 : XRPD data of isophthalic acid shows crystallite size reduction after cryomilling and recrystallization upon storage.

SEM images of unmilled and the cryomilled isophthalic acid are shown in Figure 14. It is clearly noticed that cryomilling has had a marked effect on particle size. Unlike the unmilled isophthalic acid sample, the SEM image containing the cryomilled sample show aggregates which are formed as a result of particle size reduction. The average particle dimensions of approximately 101 nm for the cryomilled sample which is expected to be different that the results obtained using Sherrer estimation as referred earlier with phthalic acid.

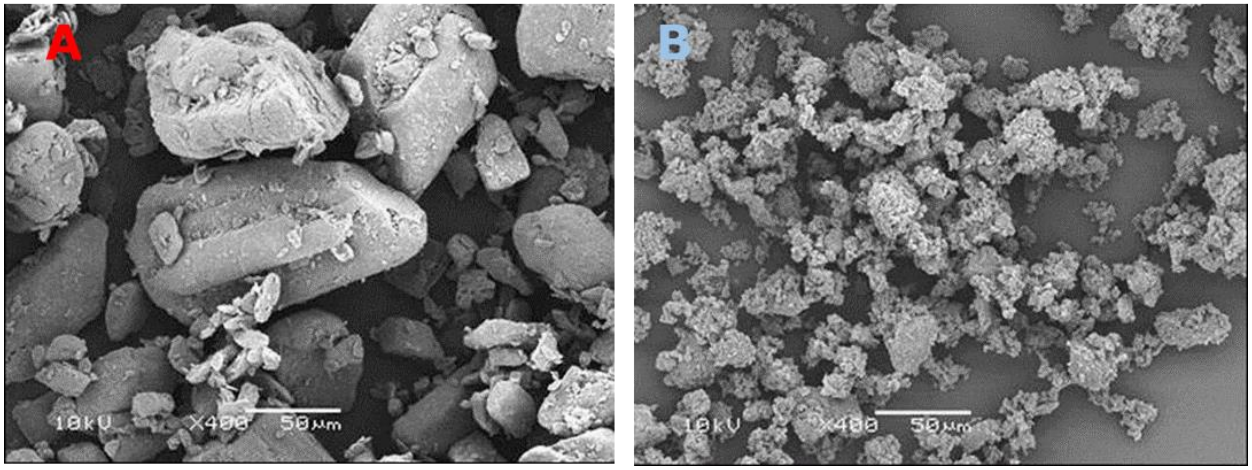


Figure 14: SEM images of as received isophthalic acid and after cryomilling for 60 minutes with a magnification of x400.

The FTIR results for isophthalic acid samples shown in Figure 15, indicate a slight change in the C=O stretching peak. Unmilled isophthalic acid shows a very sharp peak around 1682 cm^{-1}, after cryomilling there was a shift downwards by 10 cm^{-1} to 1672 cm^{-1} and remained on that position even after keeping the sample for three weeks. As a result the carbon-oxygen single bond has also experienced a shift to a lower region by 4 cm^{-1}, it was detected before milling at 1268 cm^{-1} and upon milling and storage it was

seen at 1264 cm^{-1}. There was no significant change when peak intensity is concerned.

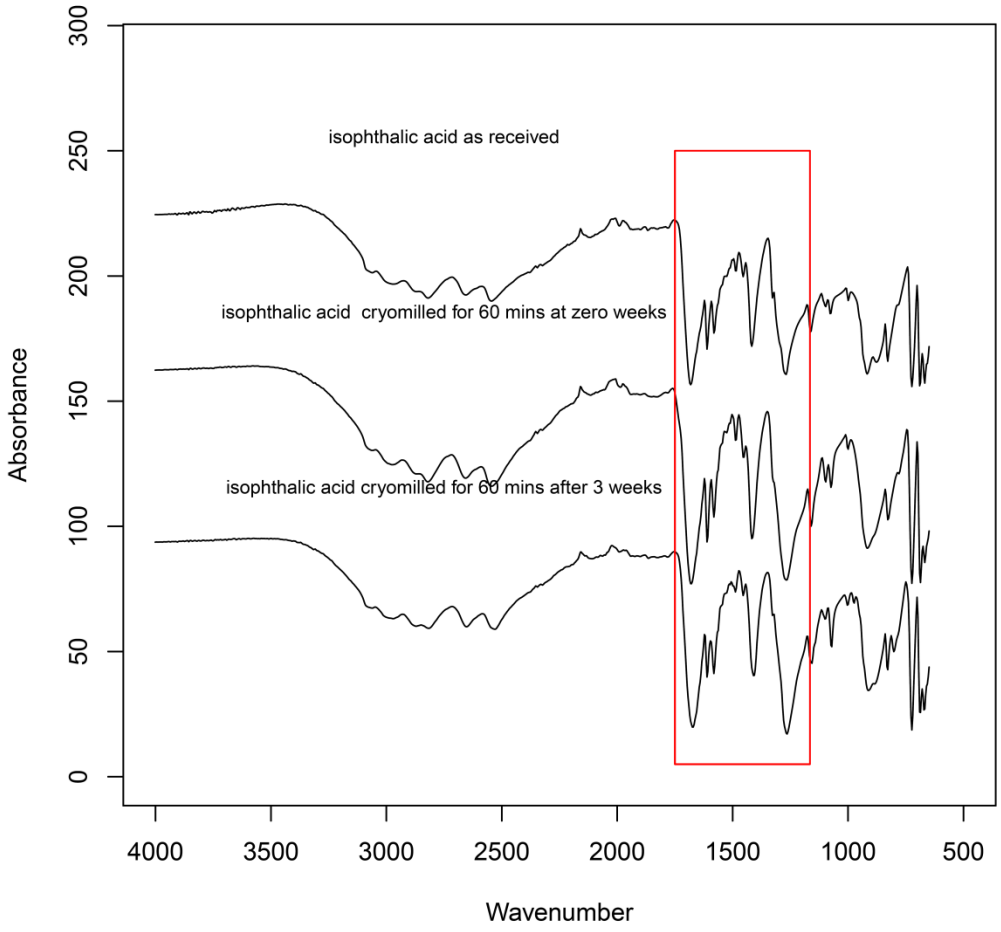


Figure 15: The FTIR spectra for unmilled isophthalic acid, immediately after cryomilling and after three weeks of storage at 43% relative humidity.

2.3.1.3. Terephthalic acid

As shown in Figure 16, representing the DSC data for terephthalic acid, a recrystallization peak could be detected which indicate the partial transformation from crystalline to amorphous caused by cryomilling for 60 minutes. Terephthalic acid thermogram shows a recrystallization with a peak maximum at 137.9°C. Terephthalic acid seems to retain its amorphous properties even after storage for three weeks a recrystallization was detected with a peak maximum at 118.2°C.

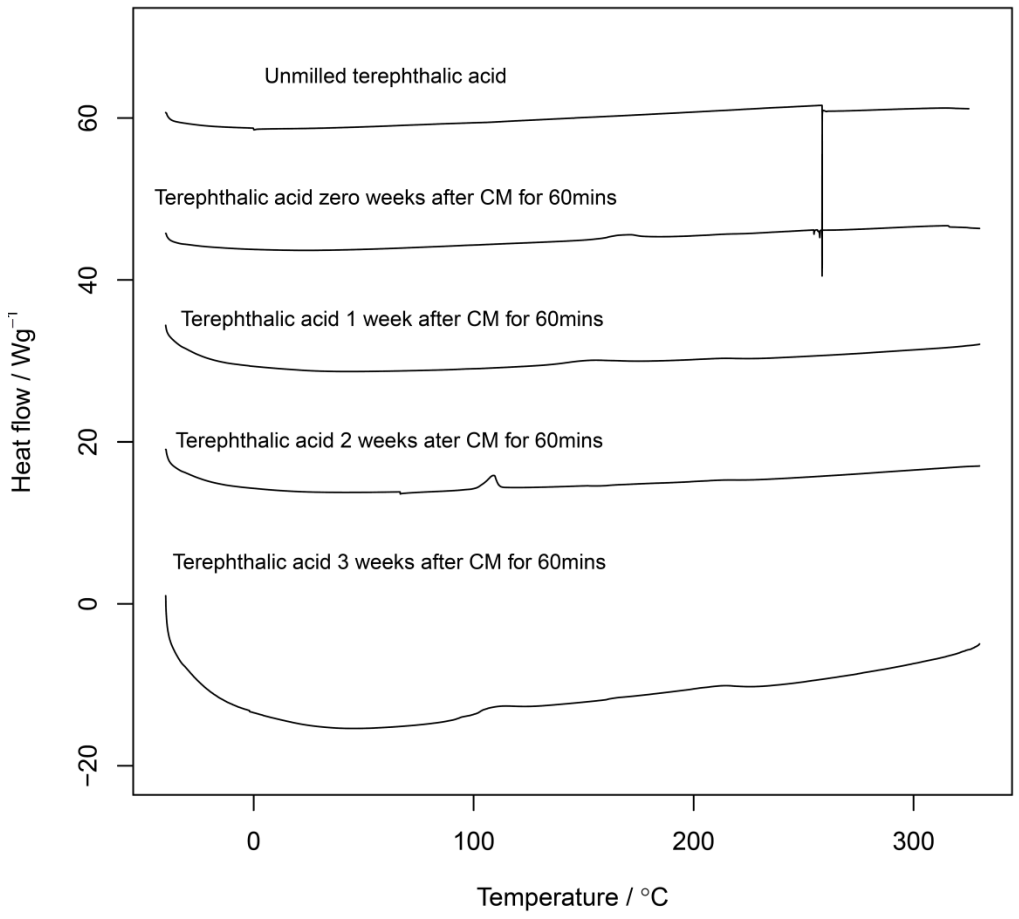


Figure 16: DSC thermogram of terephthalic acid before milling, immediately after milling and after storage for 1,2 and three weeks at 43% relative humidity.

The XRPD measurements shown in Figure 17 for unmilled, cryomilled and cryomilled sample which was stored for three weeks. There was a visual difference between the as received sample and after cryomilling in terms of peaks width. Unmilled terephthalic acid exhibits relatively sharp Bragg peaks which are transformed into broad peaks a result of cryomilling. These wide peaks seem to be stable after been measured at three weeks period.

The data indicate that cryomilling had affected terephthalic acid crystallinity, and broad Bragg peaks remain broad with time. Table 7 shows the most intense expected peak for terephthalic acid at 17.37° and from which the Sherrer crystallite size was estimated. Unlike phthalic acid and isophthalic acid, Terephthalic crystallite size seems to remain relatively small even after been stored for 3 weeks. There has been a slight increase in the crystallite size during the storage period but at the same time it is considered to be very small when compared with terephthalic acid's other isomers.

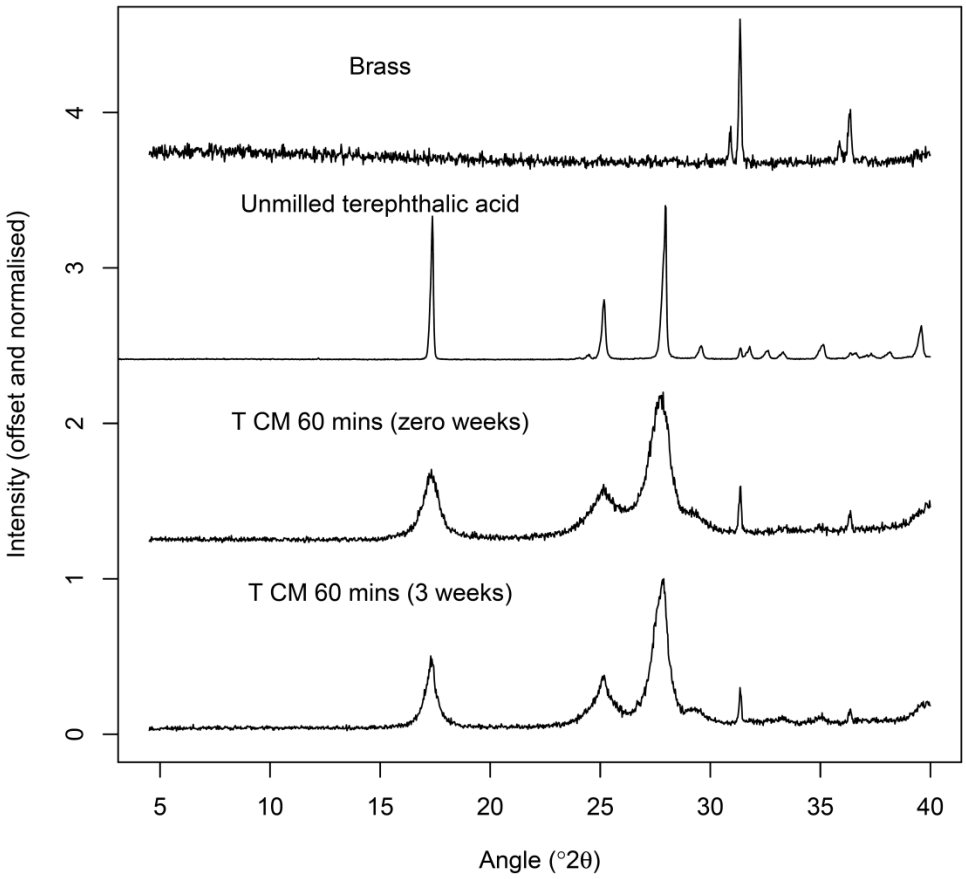


Figure 17: XRPD pattern of terephthalic acid before milling, immediately after milling and after three weeks of storage at 43% humidity.

	Peak Width (degrees)	Peak Position (degrees)	Crystallite Size (nm)
Unmilled terephthalic acid	0.14	17.37	60
Cryomilled terephthalic acid at zero weeks	1.02	17.32	9
Cryomilled terephthalic acid after three weeks	0.61	17.30	14

Table 7: XRPD data of terephthalic acid shows particle size reduction after cryomilling and upon storage.

SEM images of terephthalic acid before and after milling for 60 minutes are shown in Figure 18. As result of aggregates that seem to be formed in the SEM image for the cryomilled sample, it would be expected to negatively affect its flow properties.

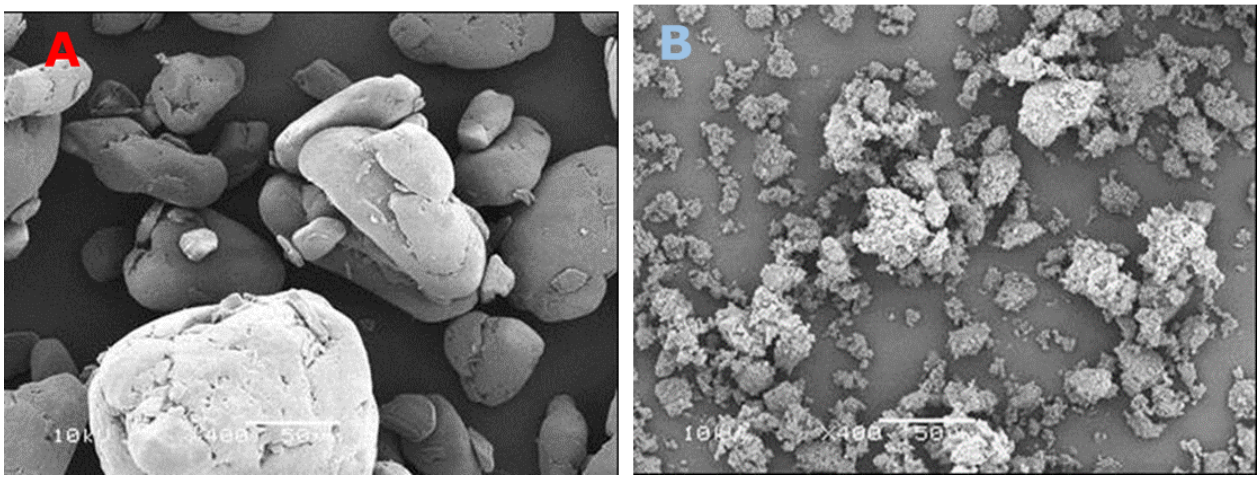


Figure 18: SEM images of unmilled and cryomilled terephthalic acid with a magnification of x 400.

The FTIR results for terephthalic acid samples are shown in Figure 19, and indicate no significant change in the C=O stretching peak position in all terephthalic acid samples. They were detected at 1673 cm^{-1}.The carbon-oxygen single bond has experienced a shift to a lower region by only 1 cm^{-1} from 1280 cm^{-1} to 1279 cm^{-1} for unmilled and cryomilled samples respectively.

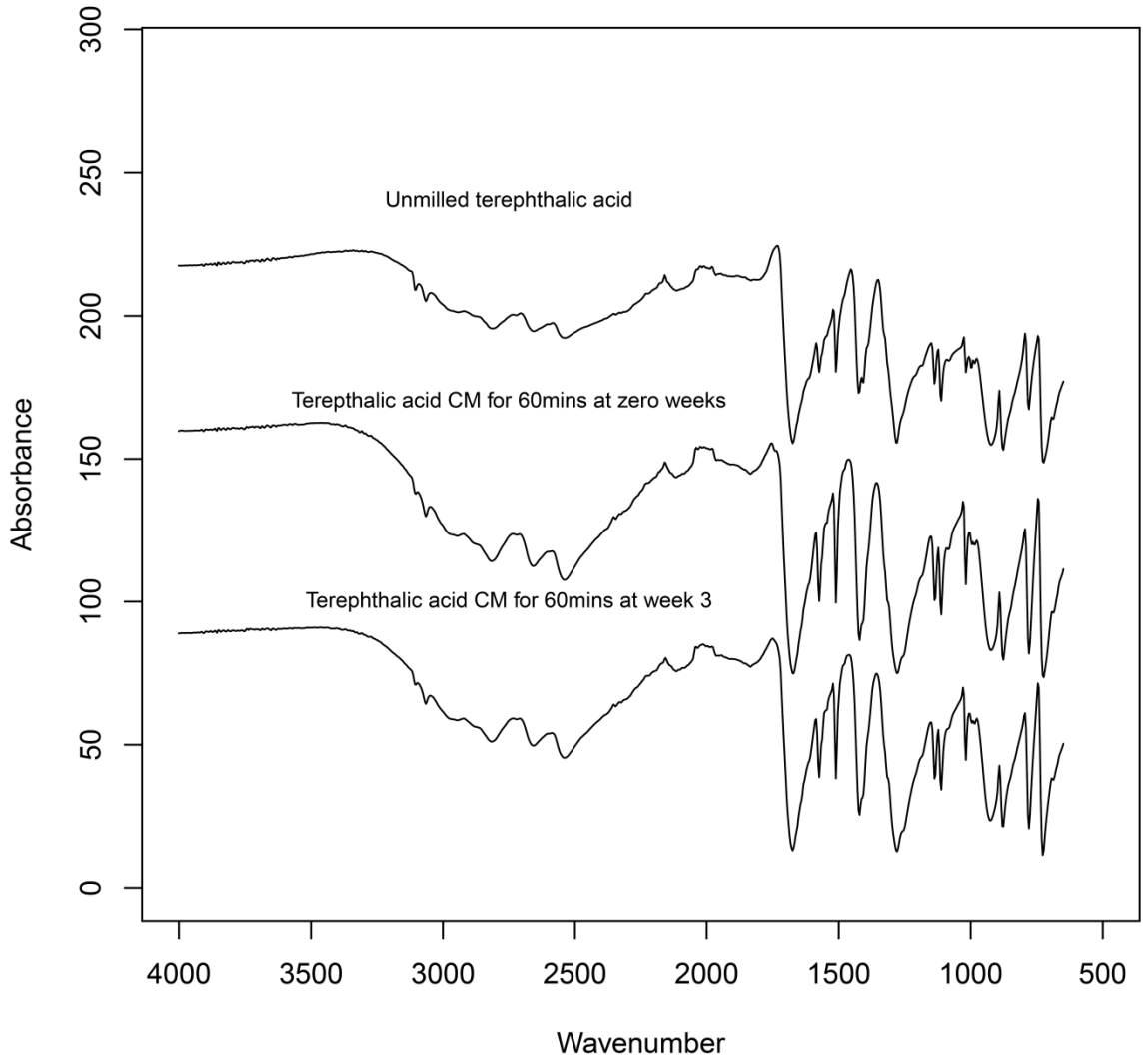


Figure 19: FTIR pattern of unmilled terephthalic acid, immediately after cryomilling and after storage for three weeks at 43% humidity.

2.3.2. Two Phase systems

2.3.2.1. Phthalic and isophthalic acid

DSC data of phthalic and isophthalic acid cryomilled together, cryomilled separately then physically mixed, immediately after milling and after storage for three weeks are shown in Figure 20. A recrystallisation at a 59.1°C followed by a melt with an onset of 208.4°C is detected in the DSC thermogram which represents the phthalic and isophthalic acid cryomilled together mixture immediately after milling, while after the sample been stored for three weeks its DSC thermogram shows only a melting peak with an onset of 207.3°C.

Moreover, the samples which were cryomilled separately at zero weeks exhibited a melting peak with an onset of 201.9°C, and after three weeks a melting endotherm with an onset of 200.4°C, which is considered to be lower than the onsets collected from the phthalic isophthalic acid mixture which was cryomilled separately. That obvious reduction in melting point might me a reason of particle size reduction, sample decomposition or colligative effect.

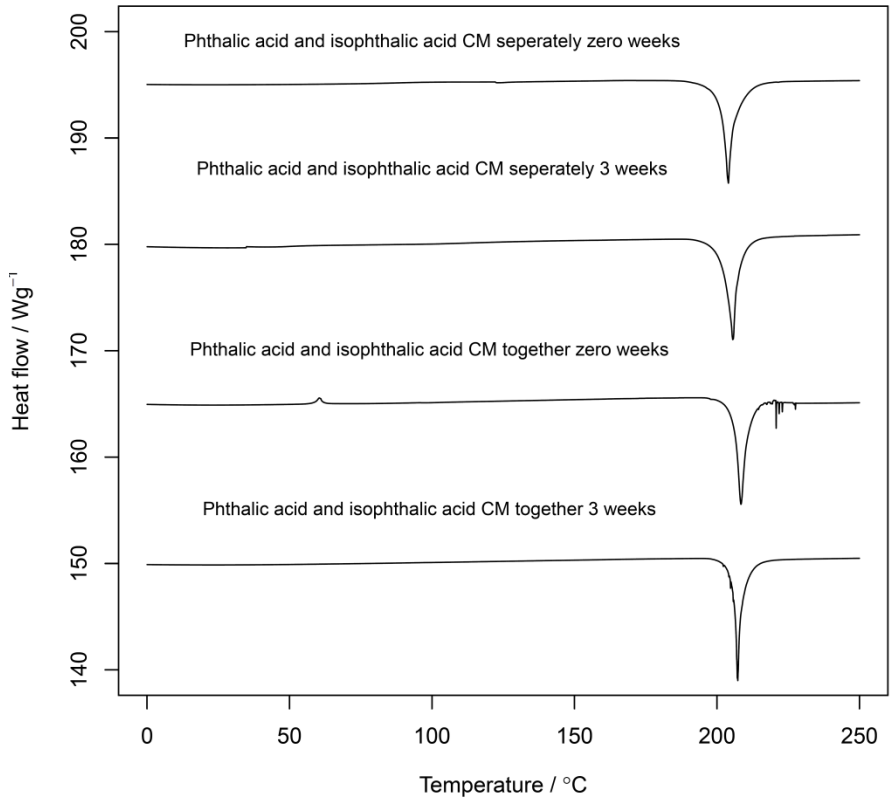


Figure 20: DSC thermogram of cryomilled separately phthalic isophthalic mixture at zero weeks, after three weeks, cryomilled together at zero weeks and after three weeks.

The XRPD measurements are shown in Figure 21 for phthalic acid and isophthalic acid cryomilled separately and cryomilled together mixtures. It is immediately apparent that all samples exhibit Bragg peaks, albeit which vary somewhat in width between samples, which suggests some level of crystallinity is present in all materials. As noted earlier in section 2.3.1.2, the peaks for cryomilled isophthalic acid are broader than those for cryomilled phthalic acid. This is noted in the physical mixture samples of separately cryomilled phthalic acid and isophthalic acid, in which phthalic acid exhibits moderately sharp peaks compared to isophthalic. The phthalic and isophthalic acid cryomilled separate patterns show the

presence of somewhat sharp peaks corresponding to phthalic acid, and a significant change after three weeks, isophthalic immediately noted sharp peaks reappears back. However, for the phthalic acid and isophthalic acid cryomilled together samples, phthalic acid sharp peaks not shown. Instead, several broad peaks are seen, fewer in number than for the cryomilled separate samples. For example, the two most intense expected peaks for phthalic acid and isophthalic acid in the range between (25° to 30°), which are observed in the cryomilled separate samples, are replaced by a single broad peak in the phthalic acid and isophthalic acid cryomilled together samples. The position of this peak corresponds with that of phthalic acid rather than isophthalic acid. After three weeks of the cryomilled together sample, the isophthalic acid peaks appear back albeit not as sharp as in the cryomilled separately mixture. Taken together, the data indicate that cryomilling phthalic acid and isophthalic acid together produces a synergistic effect in which the Bragg peaks of isophthalic acid are suppressed especially when characterized immediately after cryomilling. It can be noted note that while no clear indications of amorphous material are apparent in our XRPD data but when DSC data measures was concerned, which indicates an amorphous formation when phthalic acid and isophthalic acid were cryomilled together. It therefore appears that co-cryomilling phthalic acid and isophthalic acid leads to an obvious reduction in crystallinity for both reagents, as well as producing a new XRPD trace that cannot be described in terms of a linear combination of phthalic acid and isopthalic acid. A new material appears to

have been produced, albeit with very broad Bragg peaks. This new material could potentially a new polymorphic form of phthalic acid or with isophthalic becoming amorphous and dropping below detection limits, with time isophthalic acid appears to be detected back on the XRPD trace. As a result, co-cryomilling has produced a very significant effect on the crystal structure of phthalic acid and isophthalic acid mixture that cannot be achieved by separate cryomilling of the materials and that most intense peak in the XRPD is at a position which only tie in with pure phthalic acid since isophthalic acid peak was suppressed especially when co-cryomilled with phthalic acid.

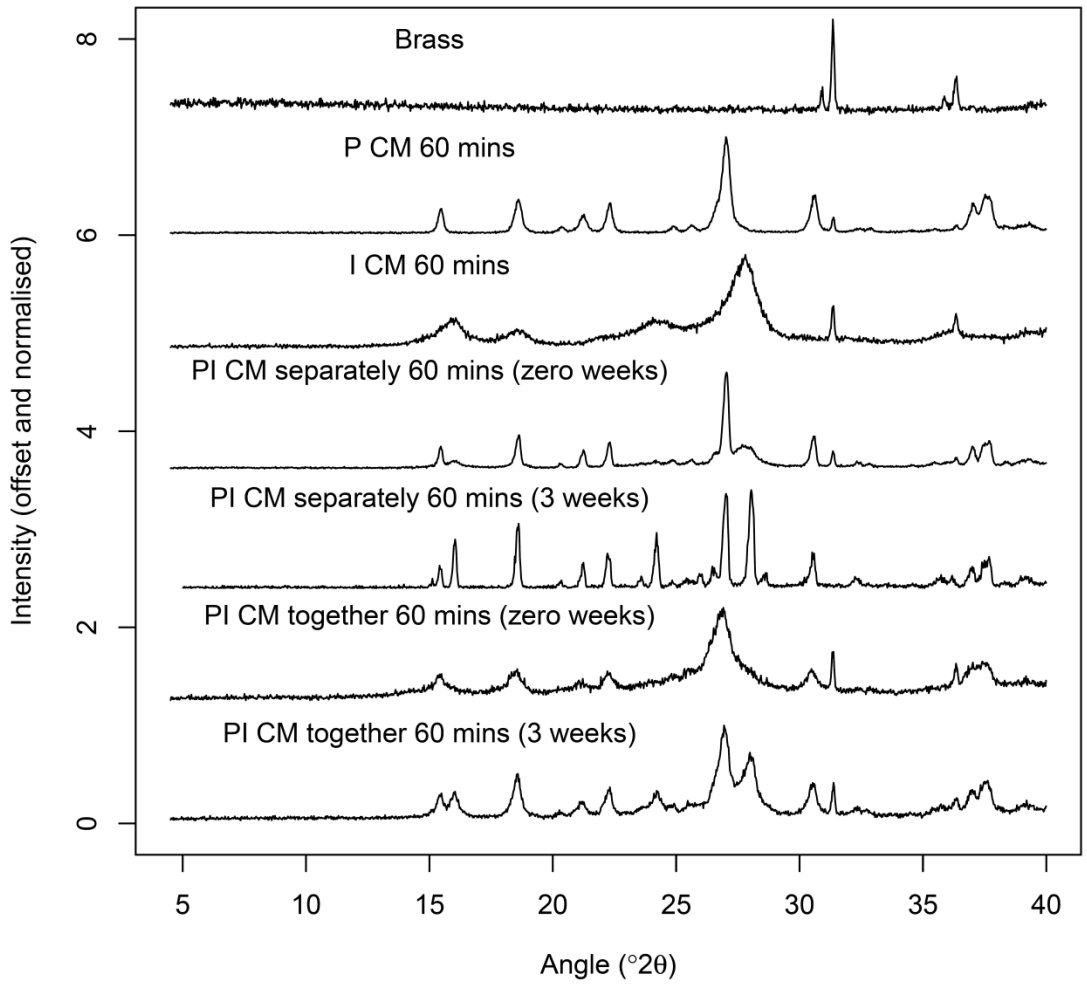


Figure 21: XRPD pattern shows cryomilled phthalic, cryomilled isophthalic, cryomilled separately phthalic isophthalic mixture at zero weeks, after three weeks, cryomilled together at zero weeks and after three weeks.

	Peak Width (degrees)	Peak Position (degrees)	Crystallite Size (nm)
PI CM separately Zero weeks	0.25	18.61	33
PI CM separately after three weeks	0.21	18.60	50
PI CM together Zero weeks	1.10	18.54	8
PI CM together After three weeks	0.50	18.55	17

Table 8: XRPD data of phthalic acid and isophthalic acid CM separately and CM together pair mixtures, shows crystallite size reduction after cryomilling and upon storage.

2.3.2.2. Isophthalic and terephthalic acid

The DSC results for the cryomilled isophthalic and terephthalic acid mixtures are shown in Figure 22. The separately cryomilled sample at zero weeks after milling shows a melting endotherm with an onset of 339.0°C, after a total period of 3 weeks a melting peak was detected with an onset of 340.0°C.

The same results were collected when measuring the sample with the cryomilled together materials; the only difference is that upon storing the mixture a reduction in melting onset have been detected, it was measured at 334.1°C with an increase in peak sharpness.

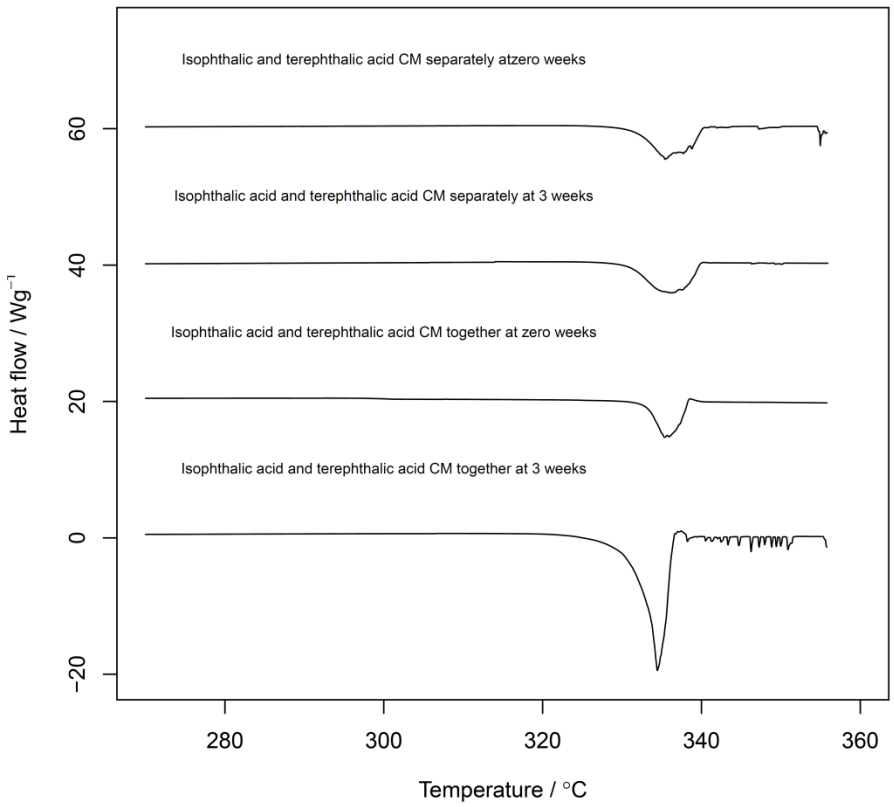


Figure 22: DSC thermogram of isopthalic terepthalic acid cryomilled separately mixture at zero weeks, after three weeks, cryomilled together at zero weeks and after three weeks.

XRPD measures presented in Figure 23 for isophthalic and terephthalic acid cryomilled separately and cryomilled together mixtures, seems to differ from the above shown DSC data. The XRPD pattern show clearly that all samples exhibit relatively broad Bragg peaks which vary in width in samples. It was noted earlier in sections 2.3.1.2 and 2.3.1.3 that both isophthalic acid and terephthalic acid produce broad peaks as a result of cryomilling. Unlike terephthalic acid, cryomilled isophthalic acid peaks after the sample been stored for three weeks was noted to produce somewhat sharp peaks. This is reflected in the physical mixture of separately cryomilled isophthalic and terephthalic acid in which after three weeks the XRPD pattern show sharp peaks which represent isophthalic acid. However, for the isophthalic acid and terephthalic acid cryomilled together samples, fewer number of broad peaks are seen, and after three weeks sharp peaks corresponding to isophthalic acid are not shown. Moreover, peak shift has been seen when these two materials are co-cryomilled together, see Table 9. Taken all together, cryomilling of isophthalic and terephthalic acid together leads to the production of a synergistic effect and this effect remains stable with time, since the Bragg peaks of the isophthalic acid were not detected even after the sample was kept for three weeks. It appears that co-cryomilling of isophthalic acid and terephthalic acid would to a clear reduction in isophthalic acid crystallinity, as well as the major reduction in peak postion would indicate the formation of a new material. This material could either be isophthalic acid and terephthalic acid nano-sized co-crystal,

or a polymorphic form of either isophthalic acid or terephthalic acid is produced with the other phase transformed amorphous. As a result, co-cryomilling of isophthalic acid and terephthalic acid has produced an effect on their crystal structure that cannot be accomplished by cryomilling the materials separately.

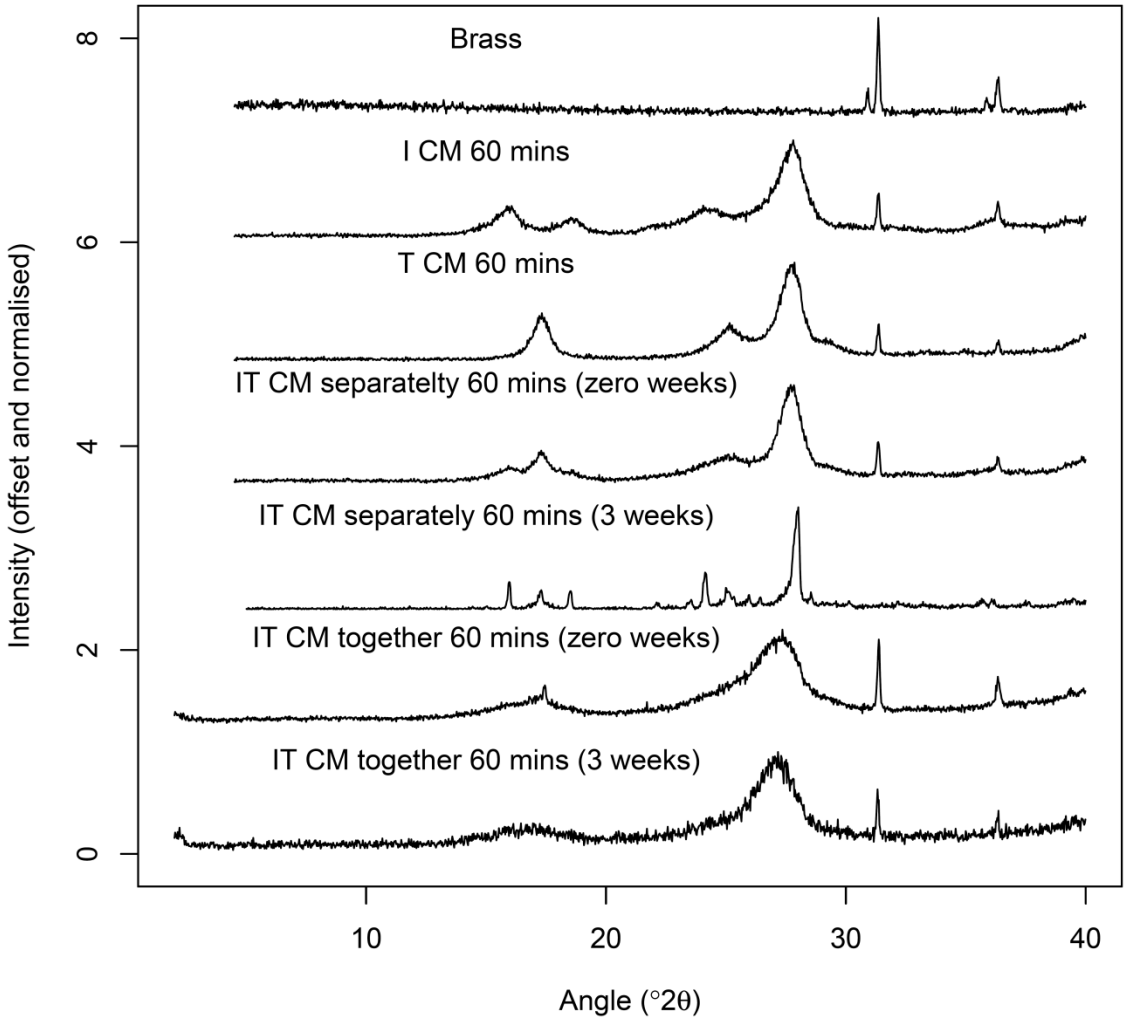


Figure 23: XRPD pattern of cryomilled isophthalic acid and terephthalic acid pair mixtures milled separately at zero weeks, after three weeks, milled together at zero weeks and after three weeks.

	Peak Width (degrees)	Peak Position (degrees)	Crystallite Size (nm)
IT CM separately Zero weeks	1.25	27.75	7
IT CM separately after three weeks	0.34	27.95	25
IT CM together Zero weeks	2.95	27.01	3
IT CM together After three weeks	2.40	27.02	3.5

Table 9: XRPD data of isophthalic acid and terephthalic acid CM separately and CM together pair mixtures, shows particle size reduction after cryomilling and upon starage**.**

2.3.2.3. Phthalic and terephthalic acid

DSC thermogram for phthalic and terephthalic acid cryomilled together, cryomilled separately then physically mixed, immediately after milling and after three weeks of storage at 43% relative humidity are shown in Figure 24. Two melting peaks with onsets of 204.6°C and 287°C were detected in the DSC data belong to the physically mixed mixture that were collected immediately after milling. The same melts were found after three weeks of storage with onsets of 205.0°C and 289.5°C with no sign of any T_g or recrystallization peak which exclude the formation of an amorphous product. The results collected immediately after milling of phthalic and

terephthalic acid together show single melt with an onset of 202.5°C and after and two melting peaks at 201.6°C and 306.16°C.

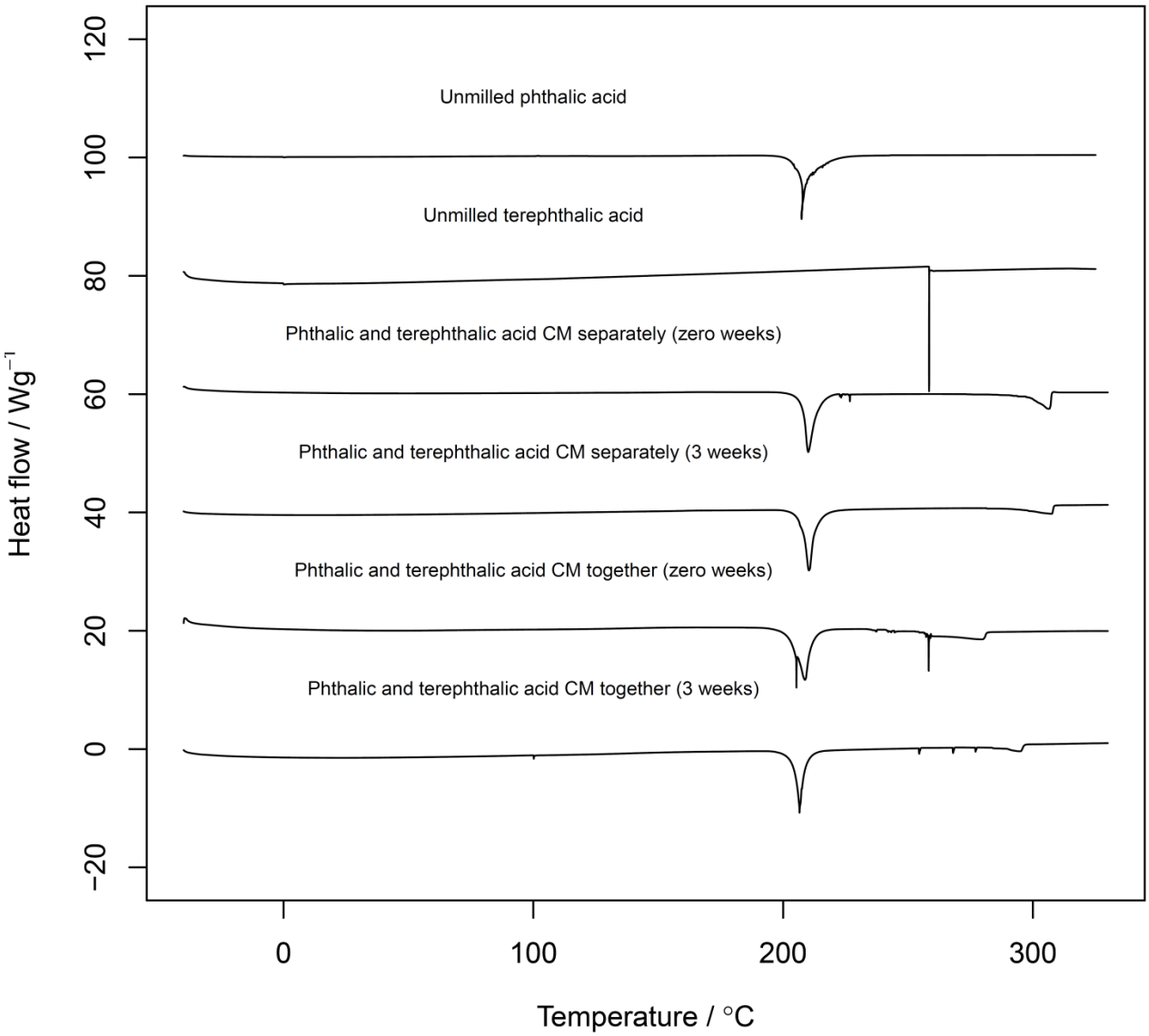


Figure 24: DSC thermogram of phthalic acid before milling, unmilled terephthalic acid, pthalic terepthalic acid cryomilled separately mixture at zero weeks, after three weeks, cryomilled together at zero weeks and after three weeks.

XRPD data shown in Figure 25 for physical mixure samples of cryomilled separately and cryomilled together isophthalic and terephthalic acid. It is immediately apparent that all samples exhibit Bragg peaks, albeit which vary somewhat in width between samples, which suggests some level of crystallinity is present in all materials. As noted earlier in Section 2.3.1.3, the peaks for cryomilled terephthalic acid are broader than those for cryomilled phthalic acid. This is mirrored in the physical mixture samples of separately cryomilled terephthalic acid and phthalic acid, in which phthaic acid exhibits relatively sharp peaks compared to terephthalic acid. The terephthalic acid and phthalic acid separate patterns do not change markedly after three weeks and can at both time points be approximated by a simple linear combination of the cryomilled separate terephthalic acid and phthalic acid traces. However for the cryomilled together samples, sharp peaks corresponding to phthalic acid are not shown. Instead, several broad peaks are seen, fewer in number than for the cryomilled separate samples. For example, the two most intense expected peaks for phthalic acid and terephthalic acid (25-30°), which are observed in the cryomilled separate samples, are replaced by a single broad peak in the terephthalic acid and phthalic acid cryomilled together samples. The position of this peak corresponds most closely to phthalic rather than terephthalic acid.

Taken together, the data indicate that cryomilling phthalic acid and terephthalic acid together produces a synergistic effect in which the Bragg

peaks of terephthalic are suppressed. While there were no clear indications of amorphous material (e.g. XRPD "halo") are apparent in our data, the limit of detection is likely to be quite high (20%) and that the presence of a significant amount of amorphous material is not ruled out. It appears that co-cryomilling terephthalic acid and phthalic acid leads to an obvious reduction in crystallinity for phthalic acid, as well as producing a new XRPD trace that cannot be described in terms of a linear combination of phthalic acid and terephthalic, acid see Table 10. A new material appears to have been produced, albeit with very broad Bragg peaks as noted earlier in Section 2.3.2.2 with isophthalic acid and terephthalic acid cryomilled together mixture. This new material could potentially either be two-component single phase (i.e. phthalic acid and terephthalic acid nano-sized co-crystal), or a new polymorphic form of either phthalic acid or terepthalic acid with the other phase becoming amorphous and dropping below detection limits. In either case, co-cryomilling has produced a very significant effect on the crystal structure of the phthalic acid and terephthalic acid mixture that cannot be achieved by separate cryomilling of the reagents.

The SEM images in Figure 26 show the cryomilled separately and the cryomilled together samples of the three mixtures. The formation aggregates is noted in all samples, it would be extremely difficult to exactly measure the particle size produced in each mixture.

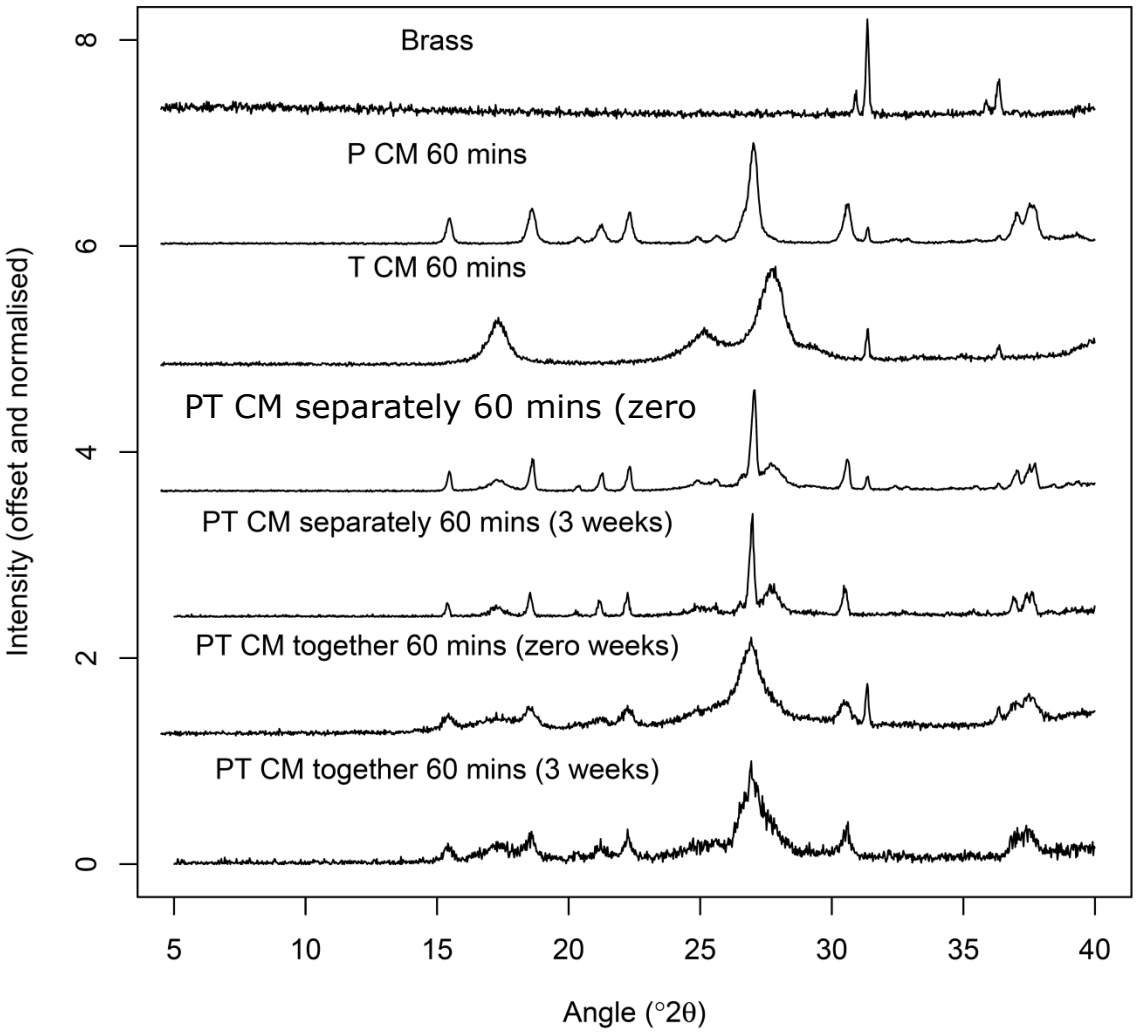


Figure 25: Figure 20: XRPD pattern of cryomilled phthalic acid and terephthalic pair mixture milled separately at zero weeks, after three weeks, milled together at zero weeks and after three weeks

	Measured Peak Width (degrees)	Measured Peak Position (degrees)	Shurrer Estimate of Crystallite Size (nm)
PT CM separately Zero weeks	0.98	27.69	9
PT CM separately after three weeks	0.81	27.68	10.5
PT CM together Zero weeks	1.26	26.89	7
PT CM together After three weeks	0.98	26.94	9

Table 10: XRPD data of phthalic acid and terephthalic acid CM separately and CM together pair mixtures, shows crystallite size reduction after cryomilling and upon starage.

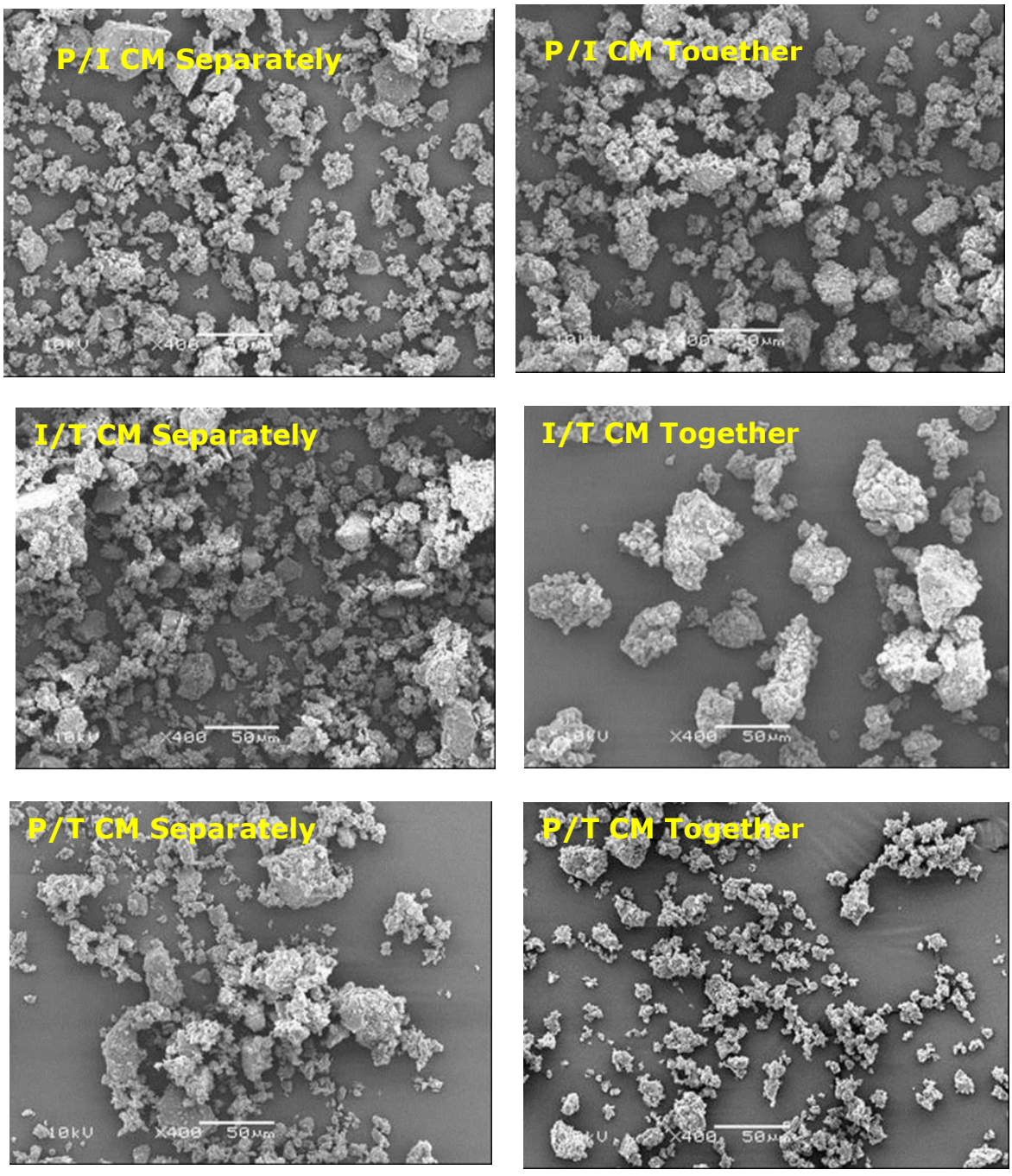
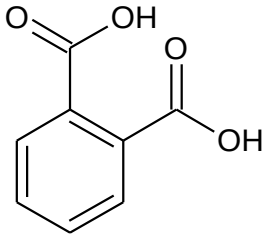
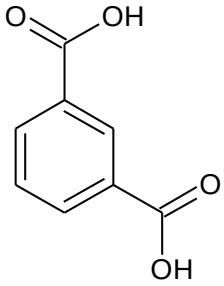
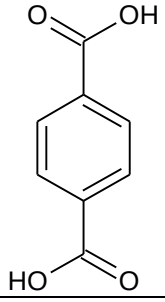


Figure 26: SEM images of different pair mixtures of phthaic acid, isophthalic acid and terephthalic acid.

2.4. Summary table

One component system	Phthalic acid	Isophthalic acid	Terephthalic acid
Chemical structure			
DSC	**Unmilled:** T_m 207 °C **CM Zero weeks:** T_g 189 °C T_m 207 °C **CM Three weeks:** T_m 207 °C	**Unmilled:** T_m 344 °C **CM Zero weeks:** T_c 120 °C T_m 344 °C **CM Three weeks:** T_m 344 °C	**Unmilled:** No melting endotherm was observed **CM Zero weeks:** T_c 137 °C **CM Three weeks:** T_c 118 °C
FTIR	**Unmilled:** C=O 1661 cm^{-1} C-O 1261 cm^{-1} **CM Zero weeks:** C=0 1666 cm^{-1} C-O 1265 cm^{-1}	**Unmilled:** C=O 1681 cm^{-1} C-O 1269 cm^{-1} **CM Zero weeks:** C=O 1672 cm^{-1} C-O 1264 cm^{-1}	**Unmilled:** C=O 1674 cm^{-1} C-O 1280 cm^{-1} **CM Zero weeks:** C=O 1672 cm^{-1} C-O 1277 cm^{-1}

	CM Three weeks: C=O 1666 cm^{-1} C-O 1265 cm^{-1} *Blue shift	**CM Three weeks:** C=O 1672 cm^{-1} C-O 1264 cm^{-1} *Red shift	**CM Three weeks:** C=O 1672 cm^{-1} C-O 1277 cm^{-1} ***Red shift
XRPD	**Unmilled:** Sharp peaks, peak width 0.1° at 21°(peak position) **CM Zero weeks:** Relatively sharp, peak width 0.4° at 21° (peak position) **CM Three weeks:** Peaks sharpness increase, peak width 0.2° at 21° (peak position)	**Unmilled:** Sharp peaks, peak width is 0.1° at 16° (peak position) **CM Zero weeks:** Few number of peaks, relatively smooth, peak width 1° at 16° (peak position) **CM Three weeks:** Peaks sharpness increase, peak width 0.2° at 21° (peak position)	**Unmilled:** Sharp peaks, peak width is 0.1° at 17° (peak position) **CM Zero weeks:** Few number of peaks, relatively smooth measured, peak width 1° at 17° (peak position) **CM Three weeks:** Smooth peaks remain showing on the XRP pattern, peak width 0.6° at 17° (peak position)
SEM estimate	**Unmilled:** ~1000 nm	**Unmilled:** ~600 nm	**Unmilled:** ~500 nm

	CM: ~100 nm	**CM:** ~100 nm	**CM:** ~80 nm
Sherrer estimate of crystallite size	**Unmilled:** ~45 nm **CM Zero Weeks:** ~20 nm **CM Three Weeks:** ~37 nm	**Unmilled:** ~60 nm **CM Zero Weeks:** ~ 5 nm **CM Three Weeks:** ~42 nm	**Unmilled:** ~60 nm **CM Zero Weeks:** ~8 nm **CM Three Weeks:** ~14 nm
Two component system	**Phthalic acid and Isophthalic acid**	**Isophthalic acid and Terephthalic acid**	**Terephthalic acid and Phthalic acid**
DSC	**CM Separately:** Zero weeks: Tm 201 °C Three weeks: Tm 200 °C **CM Together:** Zero weeks: T_c 59 °C T_m 208 °C Three weeks: T_m 207 °C	**CM Separately:** Zero weeks: T_m 339 °C Three weeks: T_m 340 °C **CM Together:** Zero weeks: T_m 339 °C Three weeks: T_m 334 °C	**CM Separately:** Zero weeks: T_m 204 °C and 287 °C Three weeks: T_m 205 °C and 289 °C **CM Together:** Zero weeks: T_m 202 °C Three weeks: T_m 201 °C

XRPD	**CM Separately:** Zero weeks: Relatively sharp peaks represent both P and I, peak width 0.2° at 18° (peak position) Three weeks: Peaks sharpness increase **CM Together:** Zero weeks: Relatively broad peaks, peak width is 1° at 18° (peak position) Three weeks: peak width 0.5° at 18° (peak position) * synergistic effect is produced with the CM together samples	**CM Separately:** Zero weeks: Relatively broad peaks represent both I and T, peak width 1° degrees at 27° (peak position) Three weeks: Peaks are intensely increased in sharpness **CM Together:** Zero weeks: New and broad peaks are produced, peak width is 2° at 27° (peak position) Three weeks: Peaks remain smooth with the same measured width at the same position * synergistic effect is produced with the CM together samples	**CM Separately:** Zero weeks: Relatively sharp peaks represent both T and P, peak width is 0.9° at 27° (peak position) Three weeks: Peaks sharpness increase **CM Together:** Zero weeks: New and broad peaks are produced, peak width is 1° at 26° (peak position) Three weeks: Peaks remain smooth with the same measured width at the same position * synergistic effect is produced with the CM together samples
SEM Particle size	**CM Separately:** ~160 nm **CM Together:** ~100 nm	**CM Separately:** ~140 nm **CM Together:** ~110 nm	**CM Separately:** ~230 nm **CM Together:** ~100 nm

Sherrer estimate of crystallite size **(XRPD)**	**CM Separately:** Zero weeks: ~ 33 nm Three weeks: ~50 nm **CM Together:** Zero weeks: ~7 nm Three weeks: ~16 nm	**CM Separately:** Zero weeks: ~6 nm Three weeks: ~25 nm **CM Together:** Zero weeks: ~3 nm Three weeks: ~3 nm	**CM Separately:** Zero weeks: ~8 nm Three weeks: ~10 nm **CM Together:** Zero weeks: ~6 nm Three weeks: ~8 nm

Table 11: Summary table of research work in Chapter 2.

2.5. Summary discussion

The outcomes obtained from this Chapter have not been reported to date for molecular materials subjected to cryomilling, typically the expected end result (in addition to particle size reduction) would be: amorphisation; polymorphic transformation or no change observed (142-144), with the key parameter being thought by other researchers to be temperature of milling with respect to T_g, that would be discussed at a later stage (Chapter 3, section 3.5). However the samples introduced in this Chapter seemed to form nanocrystals and possibly solid solutions or cocrystals, and that this is not typical for such processing. Reasons for such behaviour are not obvious at this stage. When comparing cryomilling to other processing methods, for example, noting that techniques like freeze drying would have to use an alkali as solvent so would produce salts (145), hot-melt extrusion has not been reported but would presumably be difficult due to the high melting points of the materials used, and that solvent-based processing would be difficult due to low solubilities (146). Making these samples amorphous using another technique would be difficult due to high melting points if melt-processing was used (also risk of chemical degradation), and again the use of solvent would be complicated due to low solubility. In conclusion this Chapter has outlined how cryomilling can be used to make new solid forms (nanocrystals and/or amorphous) of these otherwise intractable materials.

2.6. Conclusion

DSC, XRPD, FTIR and SEM have been used to study the formation of amorphous material by cryomilling in phthalic, isophthalic and tere-phthalic acid individual and pair mixtures. As far as single component system results were concerned, it has been found that all the subjected samples have experienced crystalline size reduction and amorphous transformation when characterized immediately after milling due to the appearance of a T_g in case of phthalic acid and a recrystallization exotherm in both cases of isophthalic acid and terepthalic acid. According to the DSC measures, after three weeks recrystallization peaks was observed in cryomilled terephthalic acid samples. With regards to two- component systems results, DSC results were not conclusive. Unlike DSC, XRPD measures show a significant difference between the samples which were cryomilled separately and the ones cryomilled together after three weeks of storage, and the mixtures which where cryomilled together seem to recrystallize at a slower rate, especially the ones containing terephthalic acid. Moreover, the results obtained from the SEM images show that cryomilled materials would have very poor flow properties due to aggregates formed the small milled particles.

Chapter 3

3.1. Introduction

In Chapter 2, the effect of cryomilling was studied on single and multiple component systems of three materials which are considered to be structurally similar and a new kind of nano-cocrystal material was noticed to be formed as a result of co-cryomilling of these materials together, therefore, in the current chapter, a more realistic types of drugs were selected to be the model compounds in order to investigate the effect of cryomilling on these materials individually and in the form of pair mixtures. Many brands of over-the-counter combination painkillers contain these three active ingredients, aspirin, paracetamol and caffeine. Anadin Extra tablets and soluble tablets, which are used for mild to moderate pain, for instance headache, migraine, toothache, sore throat, muscular and rheumatic pain, sprains and strains, nerve pain (neuralgia), sciatica, backache (lumbago) and period pain.

Solid pharmaceuticals represent heterogeneous systems typically consisting of one or more active pharmaceutical ingredients (APIs) and a number of excipients (147, 148). The knowledge of the different drugs behaviour towards temperature is considered essential for the manufacture of various forms of medication, such as tablets and capsules (72). Tablets are well known to offer numerous advantages over other dosage forms, including increased patient compliance, ease of packaging, shipping, storage, high content uniformity, and reproducible dissolution kinetics (87, 148). However, the three major factors leading to tablets being recalled by

manufacturers are failed content uniformity, dissolution and chemical stability.

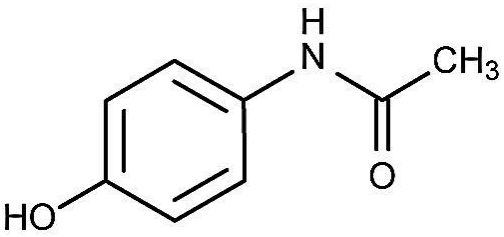
As a result of combining more than one API in the dosage form, interactions may take place producing, for example, low-temperature eutectic melts which can make certain stages in tablet production more complicated (148, 149), if it was produced accidentally, or stable chemical compounds (cocrystals) (72, 147) could be generated that would have an effect on the bioavailability of some drugs (150, 151) . Both cases are critical for drug development.

It is possible that an obvious reduction in the melting points of APIs arose from presence of impurities forming a mixture of two components that are completely miscible in the liquid state but immiscible in the solid state (68) called an eutectic mixture (see Chapter 1, Section 1.3.4.1). Differential scanning calorimetry (DSC) is one of the appropriate techniques for the determination of equilibrium phase diagrams of binary systems comprising low-temperature melting organic substances (69, 73, 74).
A lot of attention has been paid to the thermal stability and physicochemical properties of paracetamol (acetaminophen) (152-161), as it is considered one of the most frequently used antipyretic and analgesic drugs, as well as the binary systems comprising paracetamol using techniques other than cryomilling (148, 149, 159, 162, 163), mostly the solvent evaporation method (68, 147). Paracetamol was verified to be resistant to complete mechanical disordering and remained fully crystalline, even after 5 hours of cryomilling (4). Milling in general has received less attention in the literature compared to other amorphisation strategies. Therefore, the present work aims to study three binary systems, namely paracetamol-aspirin (PCM-ASP), aspirin-caffeine (ASP-CAFF) and paracetamol-caffeine

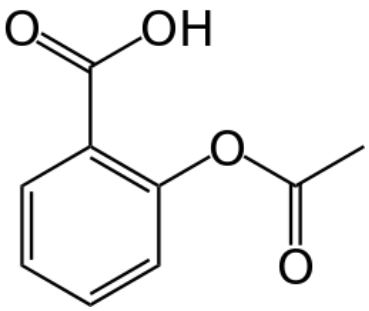
(PCM-CAFF) using DSC, FTIR and hot stage microscope on cryomilled and ball milled samples.

3.2. Materials and Methods

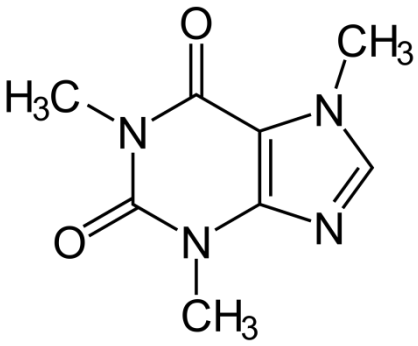
3.2.1. Materials



a. Paracetamol



b. Aspirin



c. Caffeine

Figure 27: Model compounds with range of physical properties (Table 12), used to study the effect of cryomilling on single component and binary mixtures.

Material	Molecular Mass (g/mol)	Water Solubility (mg/mL) (20◦C)	Melting Point (◦C)	Tg (◦C)
Paracetamol (form I)	151.17	~14 (164)	169 (156)	25 (165)
Aspirin	180.16	~3 (166, 167)	141 (4, 168)	-29°C (4)
Caffeine	194.19	~16 *(169)*	235 (170)	-

Table 12: Key physical properties of model compounds.

i. Paracetamol

Paracetamol (A7085, batch no.-20k0168,>99%), molecular structure shown in Figure 27, was purchase from Sigma. The purity of it is confirmed by DSC and XRPD. The melting onset was ~169 °C by DSC, which corresponds to literature (156), (heating rate of 10 °C / minute) and the XRPD was very similar to pattern from the crystal structure from the Cambridge Structural database and no extra peaks were detected (171).

ii. Aspirin

Acetylsalicylic acid (A5376, batch no.- 50782,>99%), molecular structure shown in Figure 27, was purchase from Sigma. The purity of this material was confirmed by XRPD and DSC. The melting point was by DSC is ~141 °C, in agreement with literature (4, 167), (using heating rate of 10 °C / minute) and the XRPD pattern was very similar the crystal structure from Cambridge Structure data base no extra peaks were detected (171).

iii. Caffeine

Caffeine (27600, batch no.- 1378801,>99%), molecular structure shown in Figure 27, was purchase from Fluka Analytical. The purity of this material was confirmed by XRPD and DSC. The melting point was by DSC is ~235 °C as reported in literature (170), (using heating rate of 10 °C / minute) and the XRPD pattern was very similar the crystal structure from Cambridge Structure data base no extra peaks were detected (171).

3.2.2. Methods

3.2.2.1. Preparation Methods

i. Cryomilling

Cryomilling the materials was achieved by using SamplePrep 6870 Freezer/Mill (SPEX, Metuchen, NJ, United States). 1 g was weighed for all the samples and placed in the vials. Cryomilling time was set to 60 minutes for all materials. Pre-cooling the instrument for 5 minutes then milling for 2 minutes at frequency 15 cycles per second. Throughout the grinding process, there was a pause of 1 minute between cycles to prevent temperature rise. The cryomilled samples were then hermetically sealed inside a dry glove box in order to minimize moisture uptake, which was supplied with argon cylinder to achieve a relative humidity about ~7%.

ii. Room Temperature Milling (Ball Mill)

A RETSCH Mixer Mill MM400 (Retsch GmbH, 42781 Haan, Rheinische Str.36, Germany), was used to mill the samples at room temperature. The grinding jars were filled with 200 mg of all the starting materials used, and sense the mixer mill is provided with two grinding stations, two samples were used at each run.

3.2.2.2. Characterisation Methods

i. DSC

As in Chapter 2, Section 2.2.3, Pages 35-36.

ii. XRPD

As in Chapter 2, Section 2.2.3, Page 36.

iii. FTIR

As in Chapter 2, Section 2.2.3, Page 36.

iv. HSM

The thermoscopic behaviour of pharmaceutical samples under study was investigated using PriorLux Pol advanced polarised light microscope (PriorLux Pol, Prior Scientific, Fulbourn, Cambridge, UK). The samples were placed on a 360 degree rotational mechanical stage and focused through several focusing eyepieces of 10x magnification and 20 mm view field. PriorLux Pol is equipped with free objectives of either 4x, 10x, 20x, 40x and 60x magnification. A halogen lamp was conducted with variable brightness

control to provide illumination to the subjected samples using 12 V and 30 V. CCD camera was attached to the microscope for basic image capture, or for more advanced imaging mode for moving pictures. There is an image capture software build within Linksys32 package that could be invested into video generation using different pictures captured at desired time intervals. The PriorLux Pol is supported with a Linkam dsc600 heating-freezing stage, which is controlled by T95-Linksys temperature programmer and Linksys32 software (Linkam Scientific Instruments Ltd., Tadworth, Surrey, UK). The latter is programmed to control the hot-stage temperature.

v. Solution NMR

Solution proton NMR was carried out using Avance 400 MHz (Bruker, Billerica, MA, United States). Samples were prepared by dissolving aspirin (15 mg) in DMSO.

3.3. Results

3.3.1. Single Component Systems

3.3.1.1. Paracetamol

Paracetamol, also known as acetaminophen or APAP, belongs to a group of medicines known as analgesics. It is classified according to the BCS as class III (low permeability, high solubility). Many brands of over-the-counter combination painkillers contain paracetamol, as do many cold and flu remedies. DSC thermogram for unmilled paracetamol, room temperature milled and after cryomilling for 60 minutes is shown in Figure 28. Both of the milled paracetamol samples used were noticed to be totally as white as the as received sample. Paracetamol DSC thermogram showed only endothermic peak for all three samples, neither a T_g nor an exothermic peak were detected. The melting onset value for paracetamol as received (form I) was observed at 169 °C with an enthalpy of fusion of 194 J/g. As a result of room temperature milling, the melting onset was observed at 168 °C with an enthalpy of fusion of 177 J/g. Unlike quench cooled paracetamol which has been reported to show a glass transition T_g at 25.2 °C, a single exothermic transition at 64.9 °C and an endotherm at 165.7 °C on heating rate of 10 °C/min (165), after cryomilling, DSC thermogram displays only a melting peak with an onset of 167 °C with an enthalpy of fusion of 184 J/g.

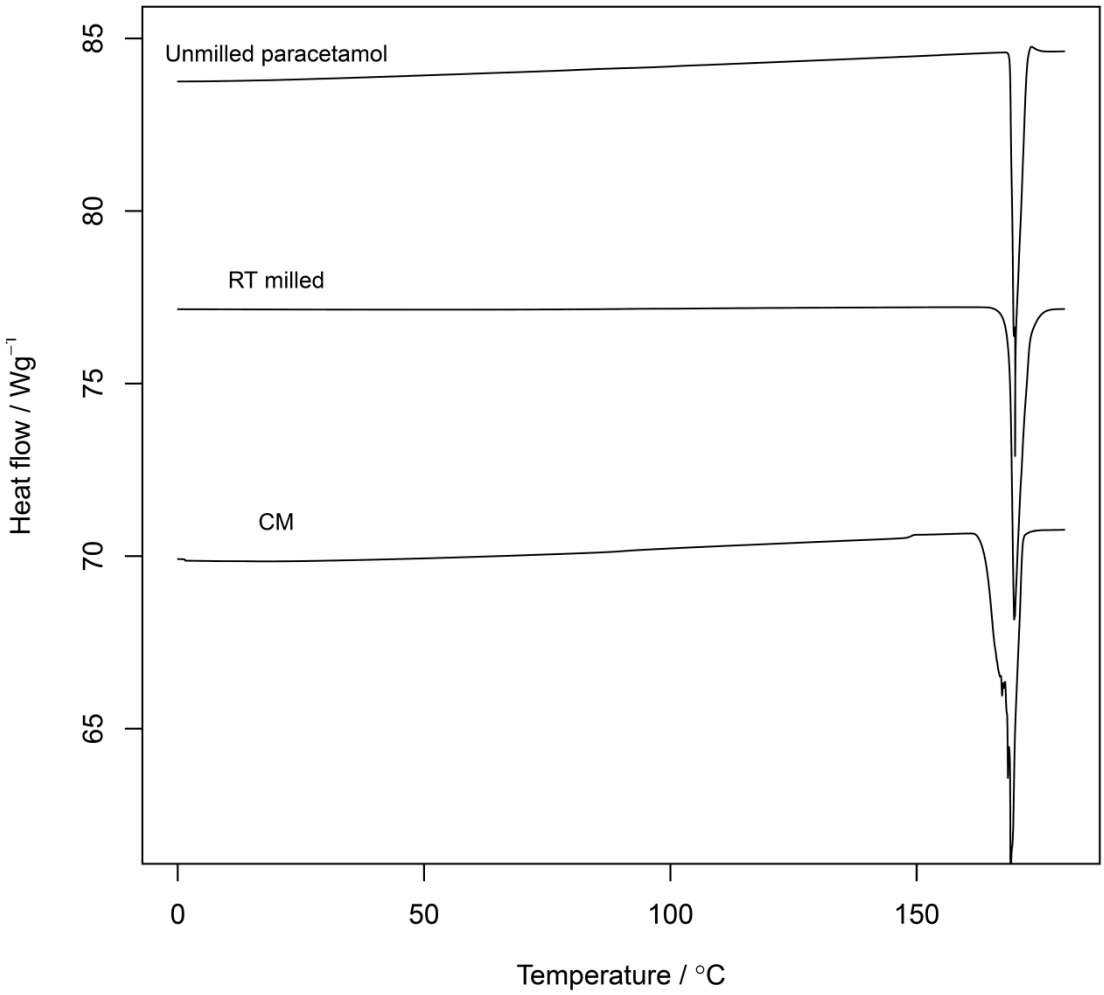


Figure 28: DSC thermogram of unmilled paracetamol, room temperature milled and cryomilled paracetamol for 60 minutes. Data have been offset by 7 Wg^{-1} for presentational purposes.

Paracetamol XRPD measurements are shown in Figure 29 for unmilled and cryomilled paracetamol. It was clear that both paracetamol samples display Bragg peaks, which suggests some level of crystallinity in both samples. It was noted that the peaks for cryomilled paracetamol are wider than those for the unmilled sample. One of the intense expected peaks for paracetamol at (~15°), which is detected in unmilled sample, was replaced by a broad peak in the cryomilled. That peak was used to estimate the crystallite size of paracetamol before and after milling using the scherrer equation as shown in Table 13.

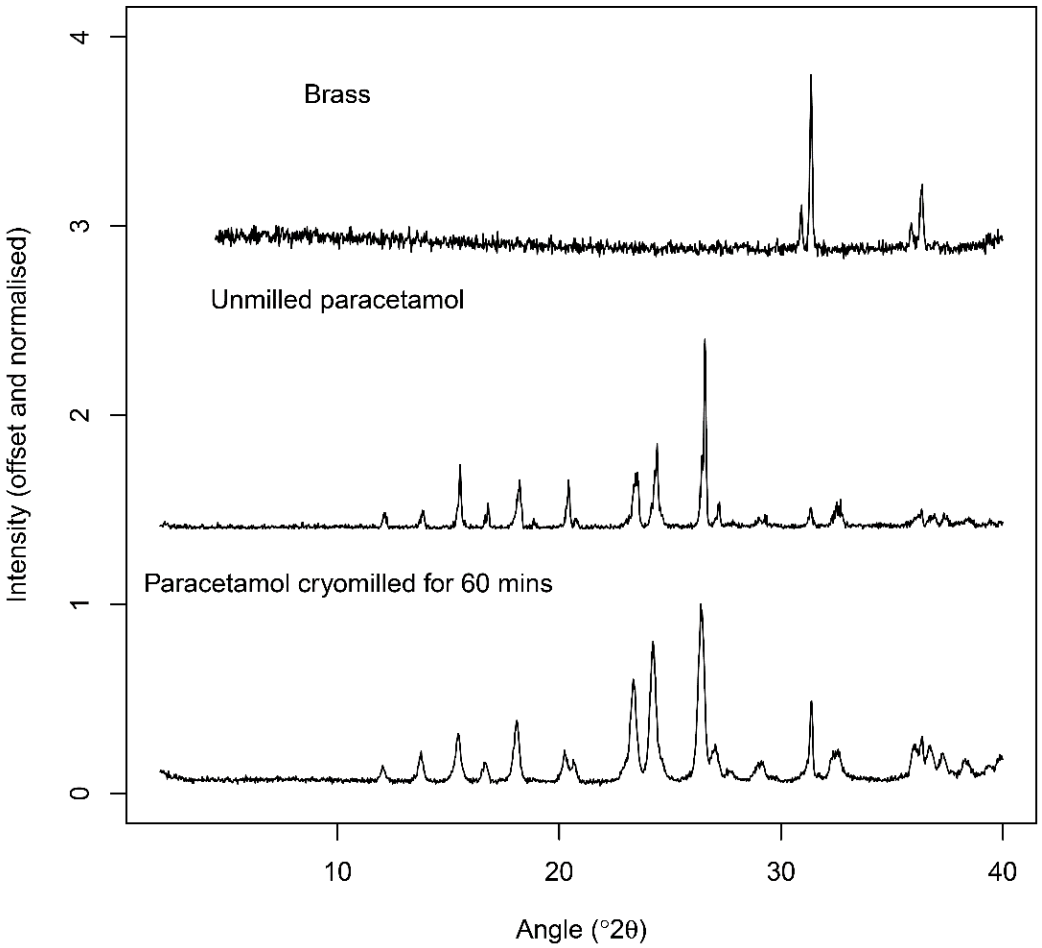


Figure 29: XRPD pattern of unmilled and cryomilled paracetamol. The Data have been scaled and offset for clarity.

	Measured Peak Position (degrees)	**Measured Peak Width (degrees)**	**Sherrer estimate of Crystallite Size (nm)**
Unmilled Paracetamol	15.52	0.13	80
Cryomilled Paracetamol	15.43	0.27	33

Table 13: XRPD data of paracetamol shows crystallite size reduction after cryomilling.

3.3.1.2. Aspirin

Aspirin, also known as acetylsalicylic acid (ASA), is a BCS class III (low permeability, high solubility) pharmaceutical substance and is used to treat pain, fever, and inflammation. Aspirin is also used long-term to help prevent heart attacks, strokes, and blood clots in people at high risk. Aspirin was reported to resist complete mechanical disordering and retain its crystalline properties even after 5 hours milling (4). Two different milling techniques were used to address any difference in the milled product produced by milling at room temperature and the other resulted from cryomiling.

DSC thermograms for aspirin before and immediately after room temperature milling and cryomilling are shown in Figure 30. From visual inspection it can clearly be seen that there is a difference between the unmilled, cryomilled and the room temperature milled thermograms in terms of the melting onsets. Unmilled aspirin DSC thermogram show an endotherm with an onset of 141 ◦C and an enthalpy of fusion of 167 J/g, these results are in complete agreement with previous literature (4). After cryomilling of aspirin for 60 minutes, there was clearly no T_g observed in the DSC thermogram only a melting peak with an onset of 142 °C and enthalpy of fusion of 160 J/g. On the other hand, the room temperature milled shows a melting onset at 132 °C, which is a reduction in melting point by 11 °C and an enthalpy of fusion of 165 J/g. In general, depression in melting point could possibly be caused by particle size reduction or decomposition, in aspirin case it was only observed as a result of milling at room temperature and not on the cryomilled sample this suggests that

some kind of sample decomposition have took place and it was most probably resulted from the heat generated from milling process.

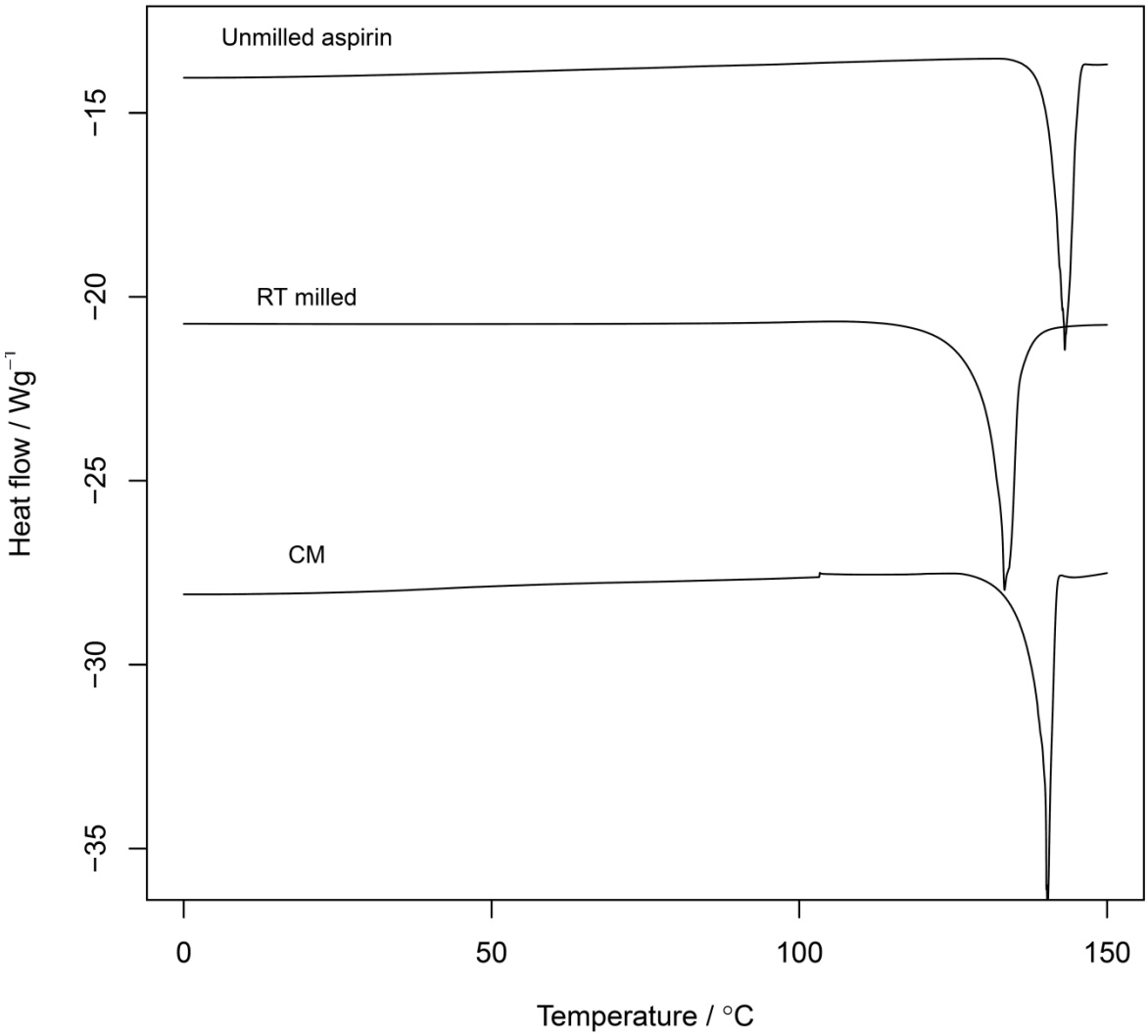


Figure 30: DSC thermogram of umilled, room temperature milled and cryomilled aspirin for 60 minutes. Data have been offset by 7 Wg^{-1} for presentational purposes.

The reduced melting point of the milled aspirin at room temperature might have resulted from several reasons, of which chemical degradation was the most reasonable cause. Solid-state IR was employed to investigate the possibility of sample chemical degradation caused by milling at room temperature. The FTIR spectra of aspirin as received, room temperature milled and cryomilled for 60 minutes are shown in Figure 31. From the FTIR spectra of the analysed samples it can be noticed that milled samples spectra are rather similar to the unmilled aspirin spectrum. The

characteristic bands of the C=O vibration from the vinyl ester group in the 1750-1730 cm^{-1} region, C=O group of the aromatic acid appears around 1690 cm^{-1} (172), can both be observed in all aspirin spectra. Solution proton NMR was employed to further investigate the possibility of sample degradation as a result of milling at room temperature. As shown in Figure 32 all spectra are identical and no sign of sample decomposition was detected.

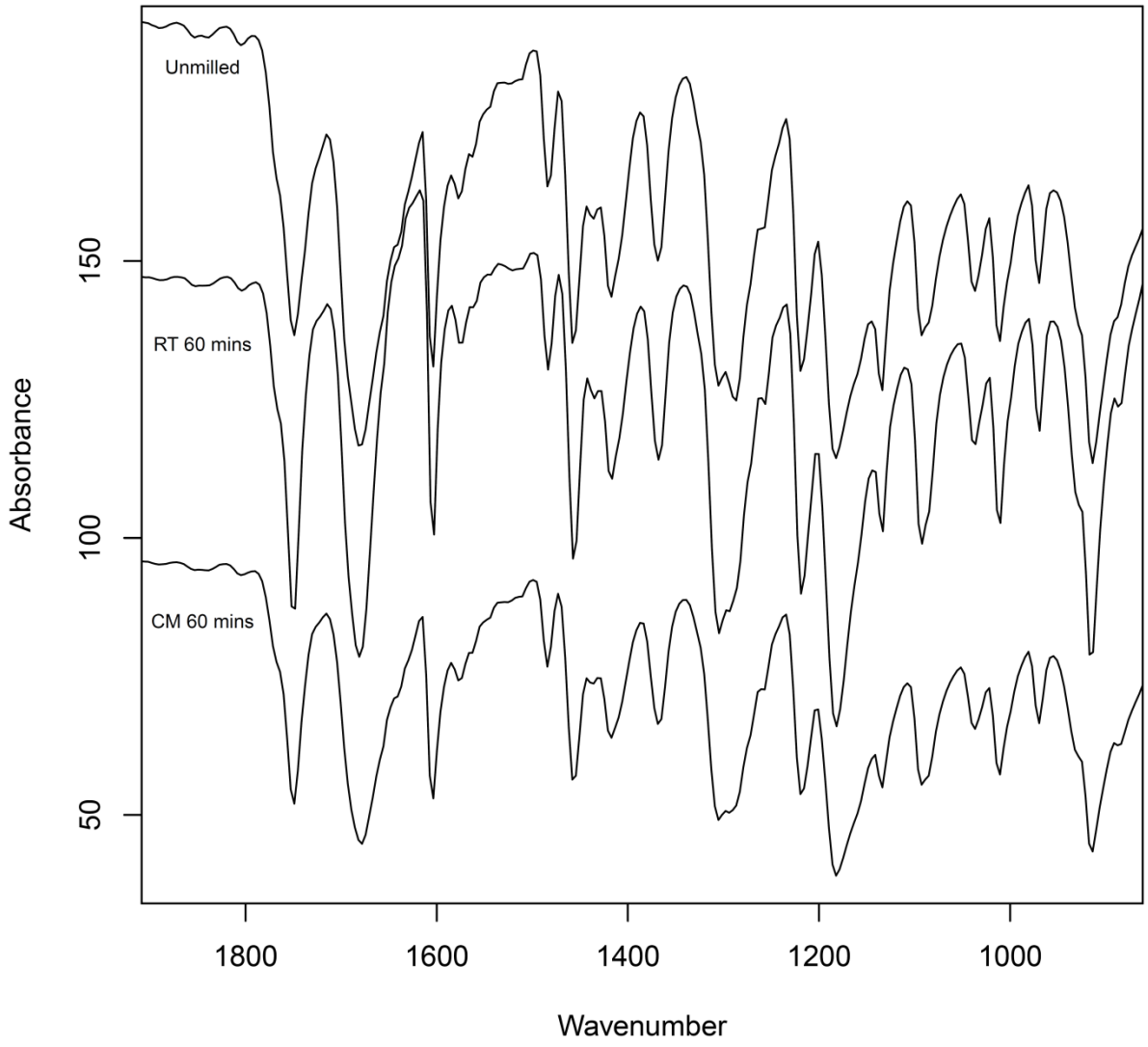


Figure 31: FTIR spectra of aspirin as received, room temperature milled and cryomilled for 60 minutes. The data have been scaled and offset for clarity.

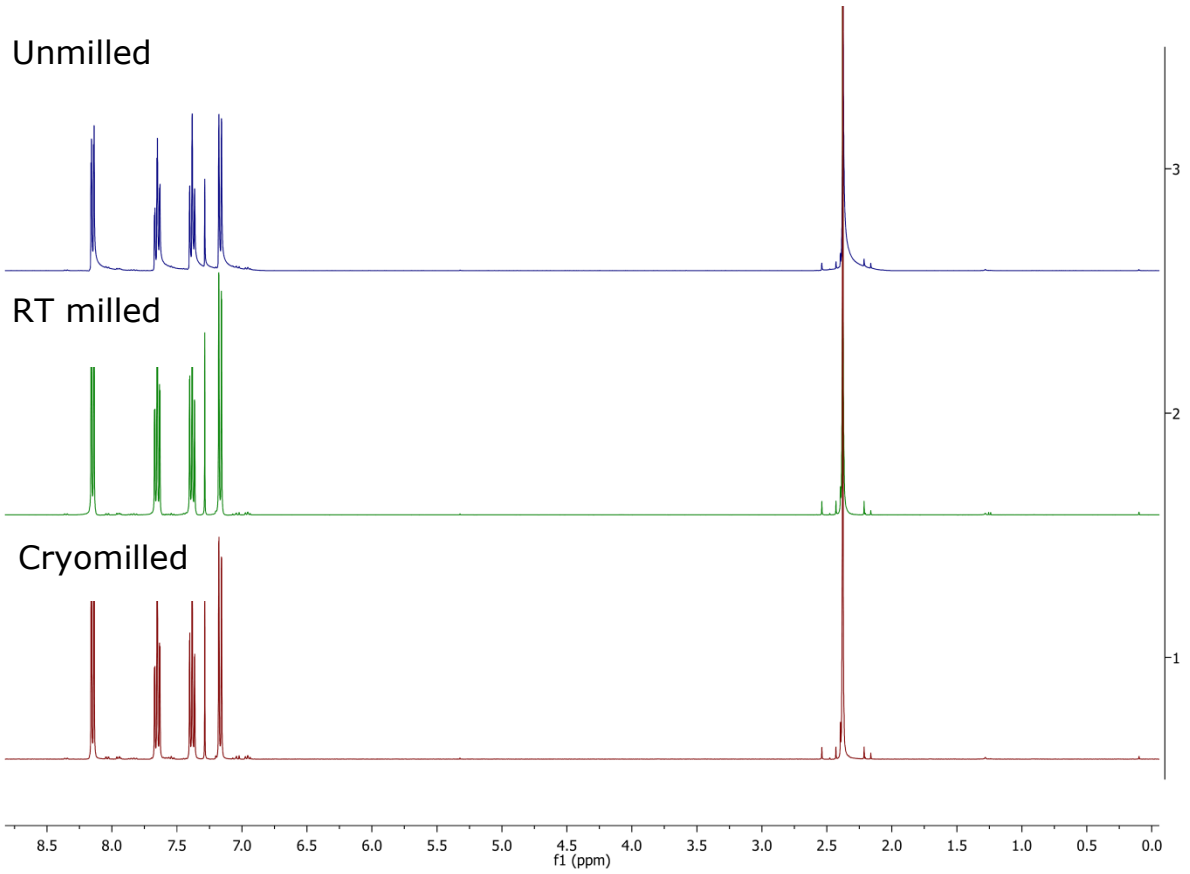


Figure 32: Solution proton NMR carried out in DMSO of unmilled, RT milled and cryomilled aspirin.

XRPD measurements are presented in Figure 33 of unmilled and cryomilled aspirin for 60 minutes. Multiple Bragg peaks were noticed in both traces which show different shapes and widths. A marked change in the relative peak intensities was noticed. The peaks of the cryomilled sample appear broader compared with the unmilled aspirin which exhibit somewhat sharp peaks. One of the most noticeable peaks was detected at (~15°) which was chosen to estimate the crystallite size of aspirin before and after milling using the Scherrer equation as shown in Table 14.

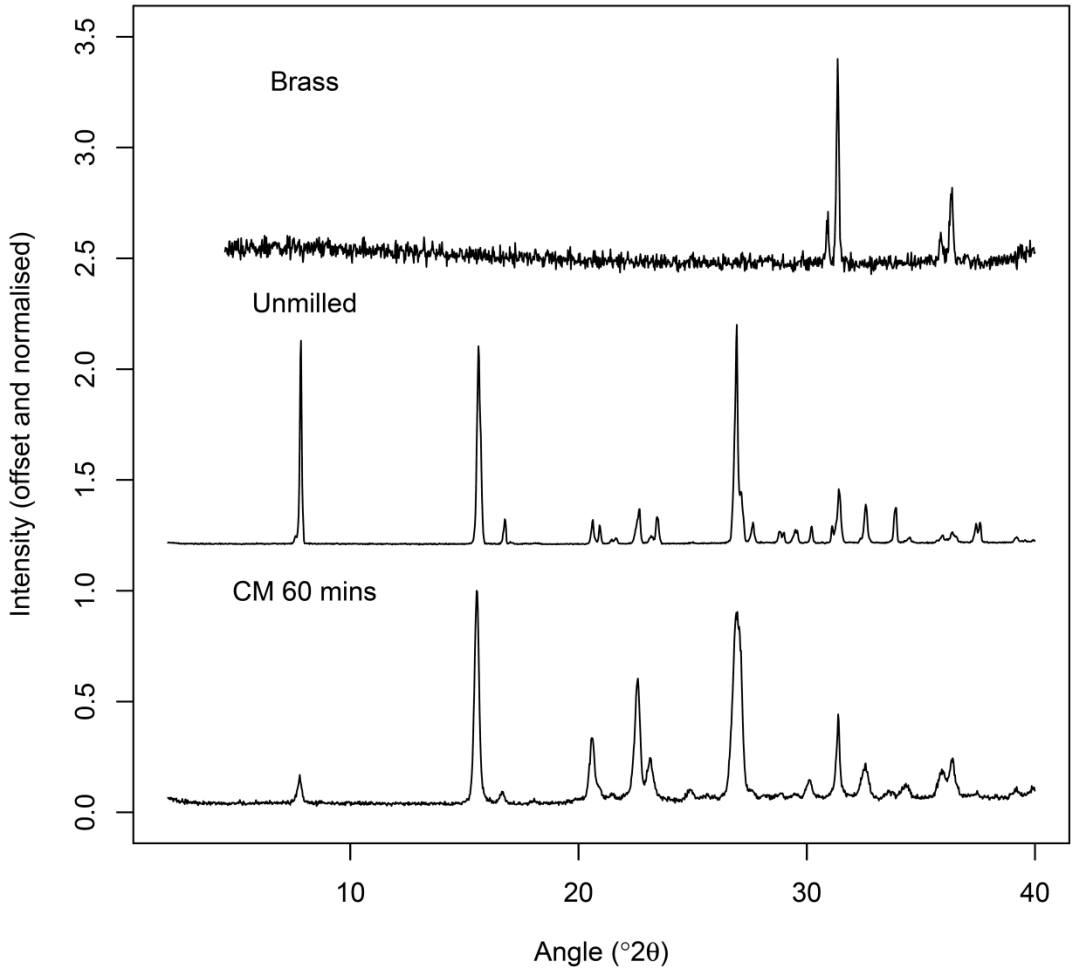


Figure 33: XRPD pattern of unmilled and cryomilled aspirin for 60 minutes. The Data have been scaled and offset for clarity

	Measured Peak Position (degrees)	Measured Peak Width (degrees)	Sherrer estimate of Crystallite Size (nm)
Unmilled Aspirin	15.6	0.18	50
Cryomilled Aspirin	15.5	0.28	39

Table 14: XRPD data of aspirin shows crystallite size reduction after cryomilling.

3.3.1.3. Caffeine

Caffeine is a central nervous system (CNS) stimulant of the methylxanthine class (173). It is the world's most widely consumed psychoactive drug with stimulant properties. Caffeine is an important ingredient of coffee and tea, which is produced in large quantities as a by-product of the technical decaffeination of raw coffee beans. Caffeine is also used as an ingredient in a variety of pharmaceutical drug preparations. Many painkillers contain caffeine because caffeine increases their effectiveness. It is also added to many medications that cause drowsiness in order to counteract this side effect. Both the thermodynamics and the phase behaviour of anhydrous caffeine are well studied (174). Anhydrous caffeine is a well-known model API for polymorphism studies (175). Anhydrous caffeine is acknowledged to have two polymorphic forms and called, Form II which is considered to be stable at room temperature until ~145 °C. Form I is stable from ~145 °C to its melting point ~ 236 °C (176).

DSC thermograms for unmilled, room temperature milled and cryomilled caffeine for 60 minutes is shown in Figure 34. Caffeine DSC theromgram for form II referred to the unmilled caffeine showed two melting peaks, the first one with an onset of 147 °C, while the second endothermic peak which represents form I was detected at 235 °C with an enthalpy of fusion of 110 J/g. After milling at room temperature, the first melting peak was shifted to a lower region with an onset of 124 °C and an enthalpy of fusion of 8 J/g and the second peak was found on relatively the same region as the unmilled sample, with an onset of 234 °C and an enthalpy of fusion of 109 J/g. On the other hand, as a result of cryomilling only one melting endotherm was noticed with an onset of 235 °C and an enthalpy of fusion of 102 J/g. Taken together, the data indicate that cryomilling produce a direct effect on the crystalline lattice of caffeine which is known as one of

the phase induced transformations (PITs) (177). These transformations are mainly produced as a result of stress or a modification of temperature and pressure (178).

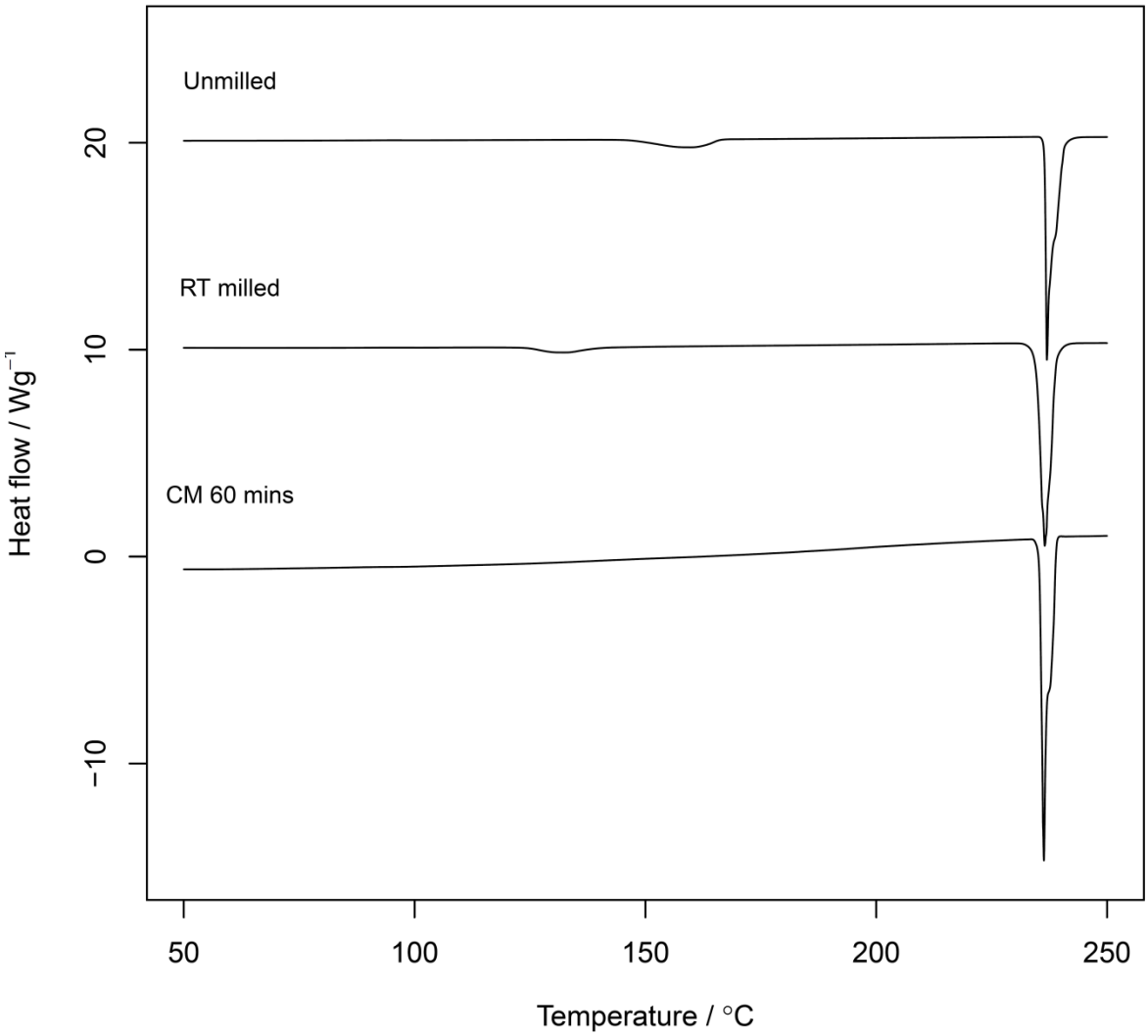


Figure 34: DSC thermogram of umilled, room temprature milled and cryomilled caffeine for 60 minutes. Data have been offset by 7 Wg^{-1} for presentational purposes

Caffeine polymorphic transformation was visually confirmed through capturing hot stage microscope images while the temperature was rising. Needle like shaped crystals was found to be formed at 147 °C suggesting the formation of a new polymorphic form of caffeine as a result of temperature increase as shown in Figure 35.

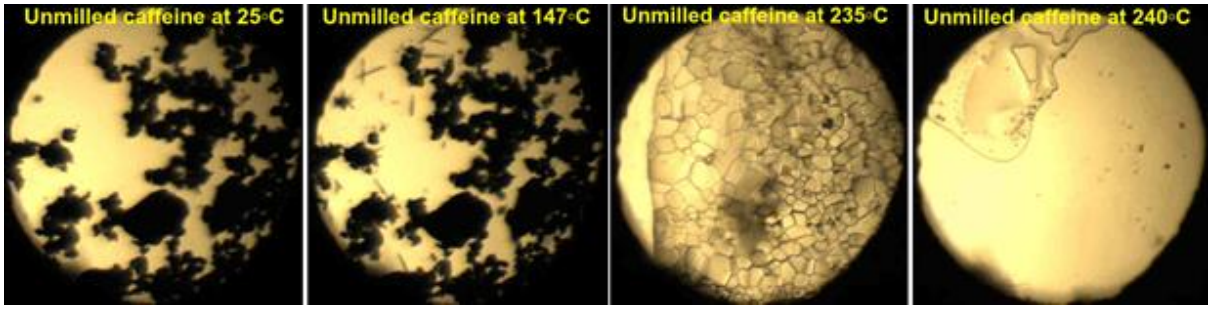


Figure 35: Hot stage microscope images of unmilled caffeine show transformation from form II to form I

When dealing with polymorphic forms of the same solid material, X-ray diffraction is considered to be a practical technique to detect these kind of transformations (179). XRPD measurement was performed at room temperature for both unmilled and cryomilled caffeine, see Figure 36. There is an obvious difference in the XRPD pattern between the unmilled and the cryomilled samples in terms of peaks number and width. Unmilled caffeine exhibits relatively sharp Bragg peaks and two peaks were detected at the position of ~ 26◦ which are transformed into a single broad peak at the same position as a result of cryomilling.

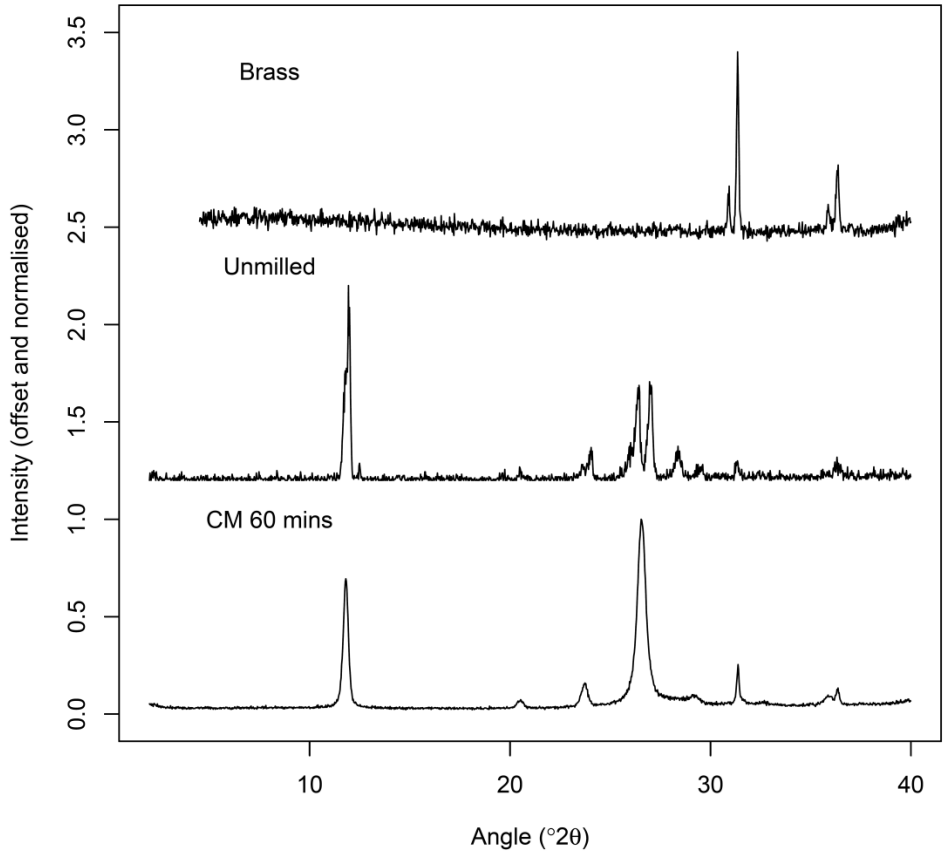


Figure 36: XRPD pattern of unmilled and cryomilled caffeine for 60 minutes. The data have been scaled and offset for clarity.

One of the most noticeable peaks appeared on the XRPD pattern was used to estimate the crystallite size of caffeine before (Form II) and after milling (Form I) using the Scherrer equation as shown in Table 15.

	Measured Peak Position (degrees)	Measured Peak Width (degrees)	Sherrer estimate of Crystallite Size (nm)
Unmilled Caffeine	11.85	0.30	29
Cryomilled Caffeine	11.80	0.41	21

Table 15: XRPD data of caffeine shows crystallite size reduction after cryomilling.

3.3.2. Multi- Component Systems

3.3.2.1. Paracetamol and Aspirin (DSC)

All mixtures of cryomilled ASP and PCM containing 5–53% w/w ASP showed two endothermic events as shown in Figure 37. A single endothermic event was observed at 112.70 °C when the ASP concentration reached 55% w/w, above 55% w/w ASP, two endothermic events were again observed. Therefore, it can be concluded that the eutectic system was formed at a concentration ratio of 55:45% w/w of ASP and PCM, respectively. The results obtained were in fair agreement with previous reports, which confirmed an eutectic mixture formation was observed at 53:47% w/w (68, 180).

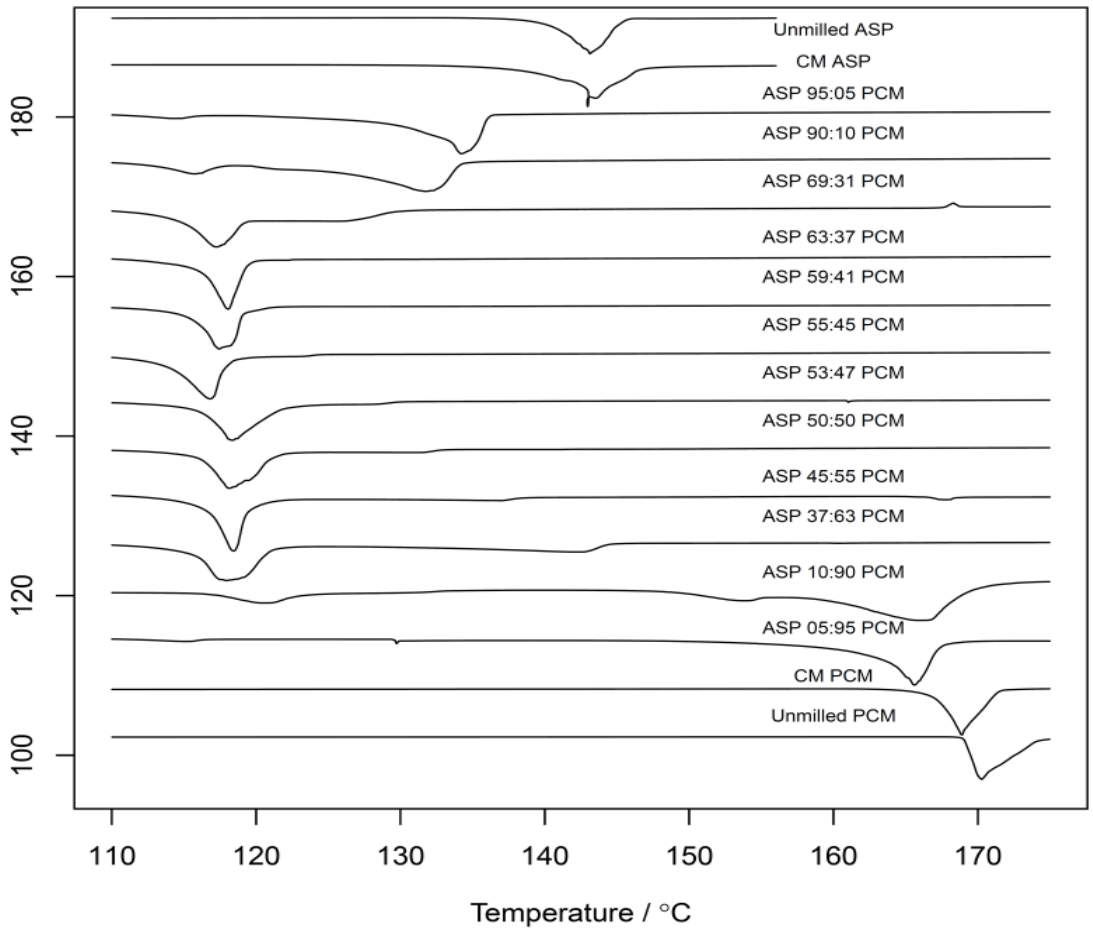


Figure 37: DSC overlays for screening the eutectic composition of different ratios of cryomilled (CM) aspirin : paracetamol (ASP:PCM %, w/w).

On the other hand, all mixtures milled at room temperature containing 50–59% w/w ASP showed two endothermic events as shown in Figure 38. A single endothermic event was noticed at a higher aspirin concentration when compared with the cryomilled samples, a single melt was observed at 120.73 °C when the ASP concentration reached 65% w/w.

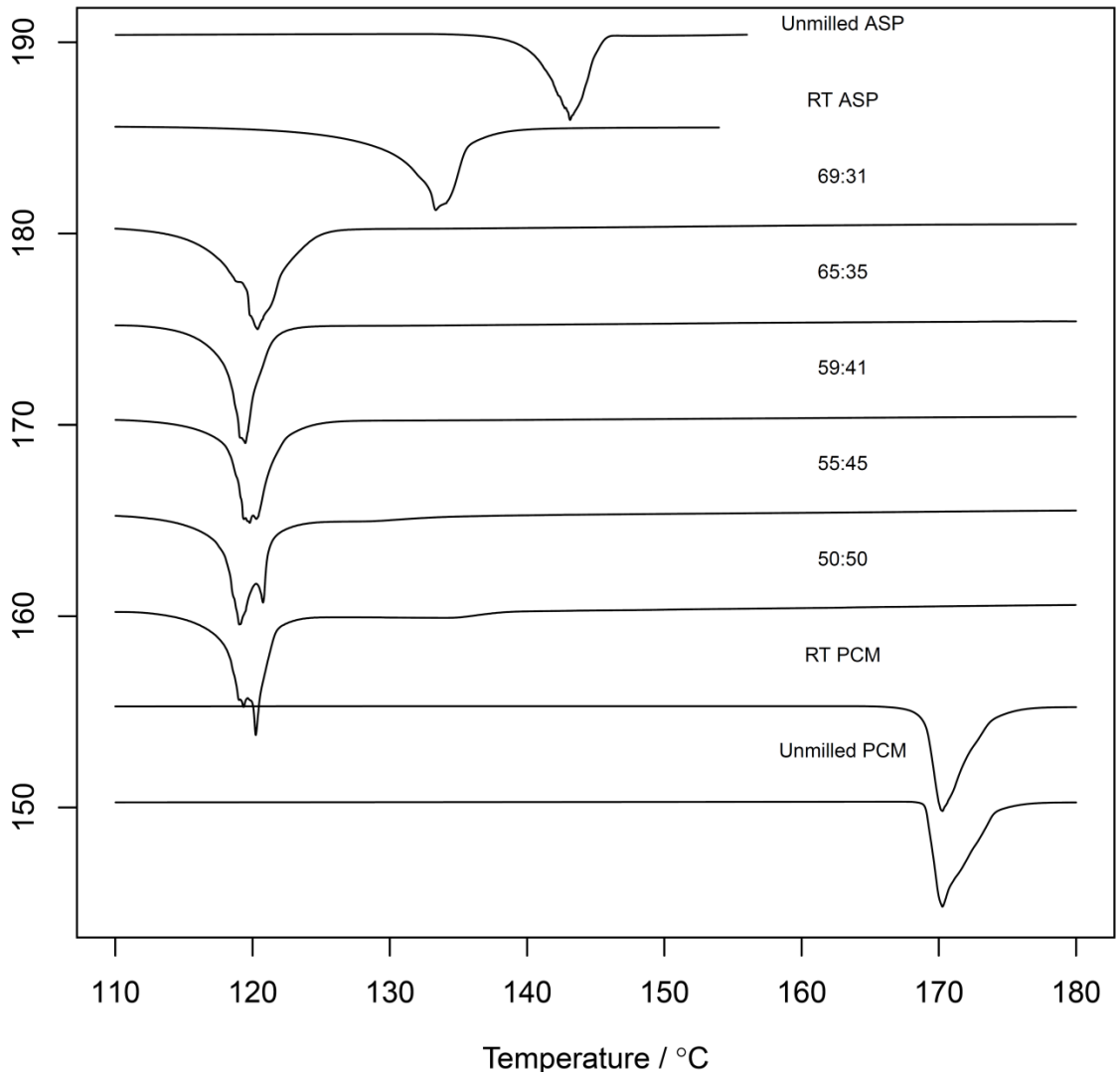


Figure 38: DSC overlays for screening the eutectic composition of different ratios of room temperature milled (RT) aspirin : paracetamol (ASP:PCM %, w/w).

3.3.2.2. Aspirin and Caffeine (DSC)

The DSC results for ASP and CAFF cryomilled pair mixtures are shown in Figure 39. More than one endothermic event was observed in all mixtures containing 5-37 % w/w CAFF. A single melting endotherm was detected at 105.67 °C when the concentration of CAFF reached 49% w/w. At higher caffeine concentrations, two endothermic peaks were starting to reappear representing ASP and caffeine. Therefore, it can be concluded that the eutectic system was formed at a concentration ratio of 51:49% w/w of ASP and PCM, respectively.

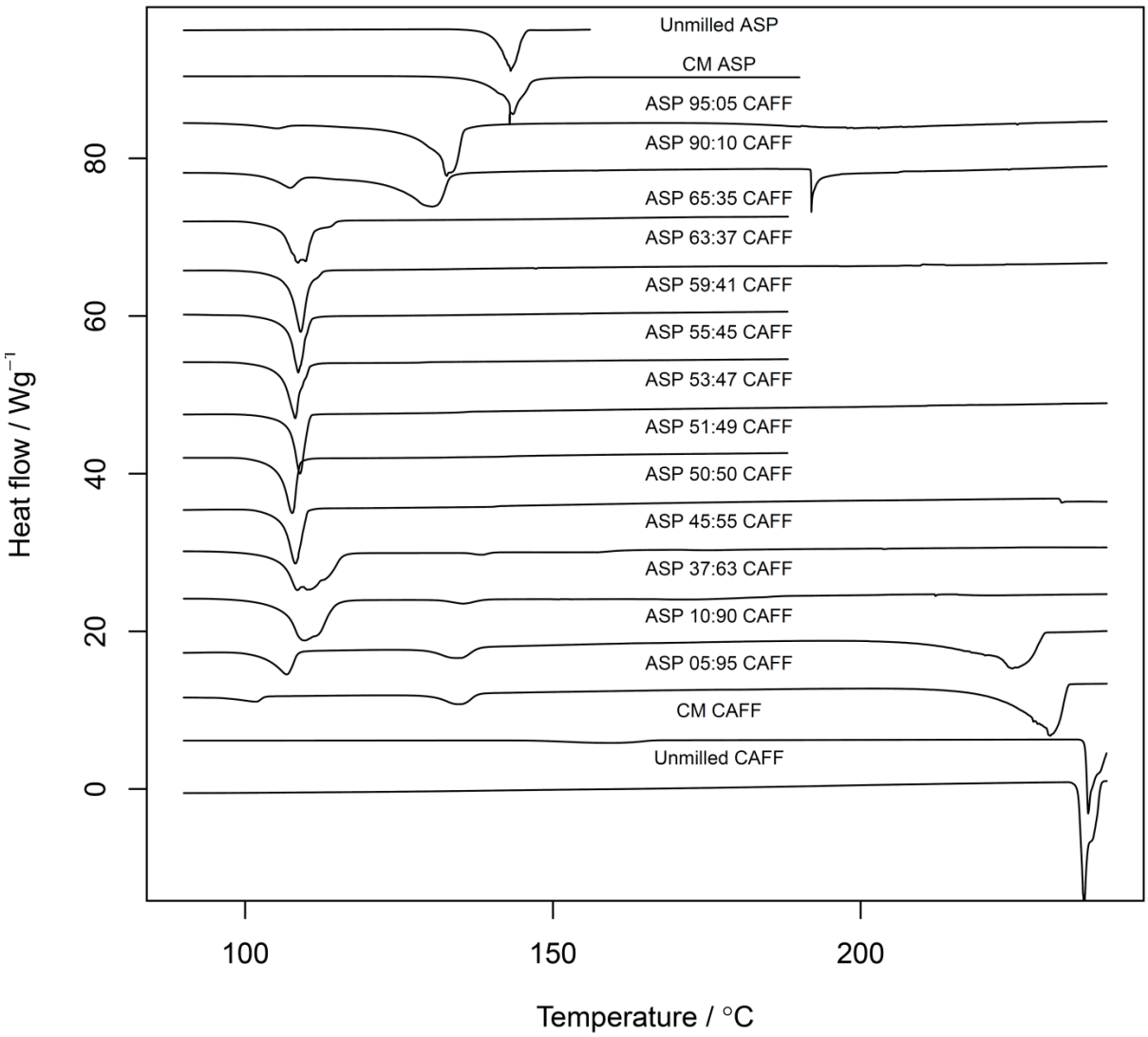


Figure 39: DSC overlays for screening the eutectic composition of different ratios of cryomilled (CM) aspirin : caffeine (ASP:CAFF %, w/w).

Furthermore, as a result of milling at room temperature of all ASP and CAFF mixtures, a single melting endotherm was noticed at lower region containing 45% w/w CAFF as shown in Figure 40.

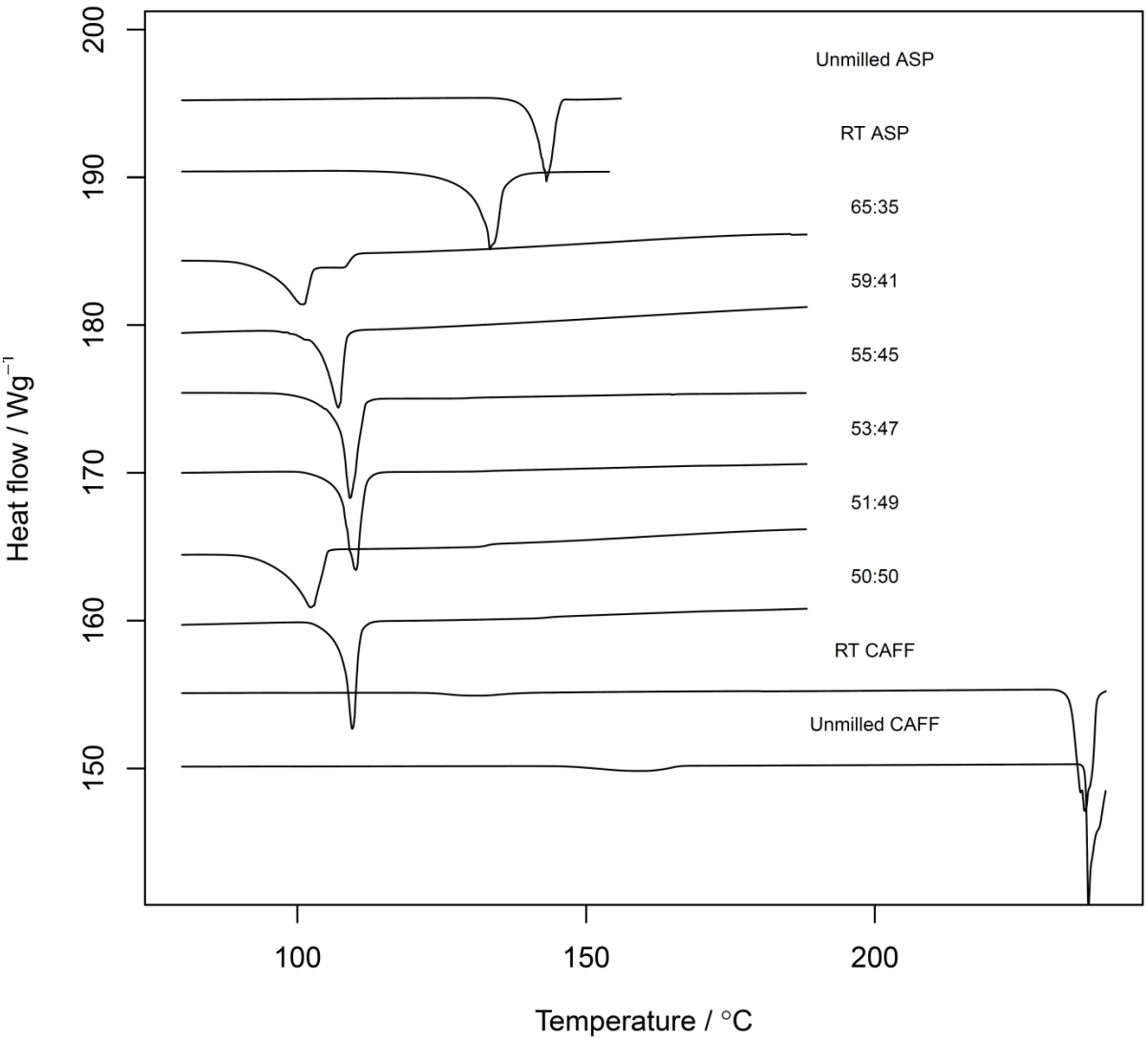


Figure 40: DSC overlays for screening the eutectic composition of different ratios of room temperature milled (RT) aspirin : caffeine (ASP:CAFF %, w/w).

3.3.2.3. Paracetamol and Caffeine (DSC)

DSC thermograms of the binary system of PCM with CAFF at different ratios are given in Figure 41. The major endotherms at 167.3 °C and 236.2 °C represent the melting point of pure PCM and CAFF, respectively. The

eutectic melting point was found to be noticed at 123.8 °C with the system containing 50:50% w/w of PCM and CAFF respectively.

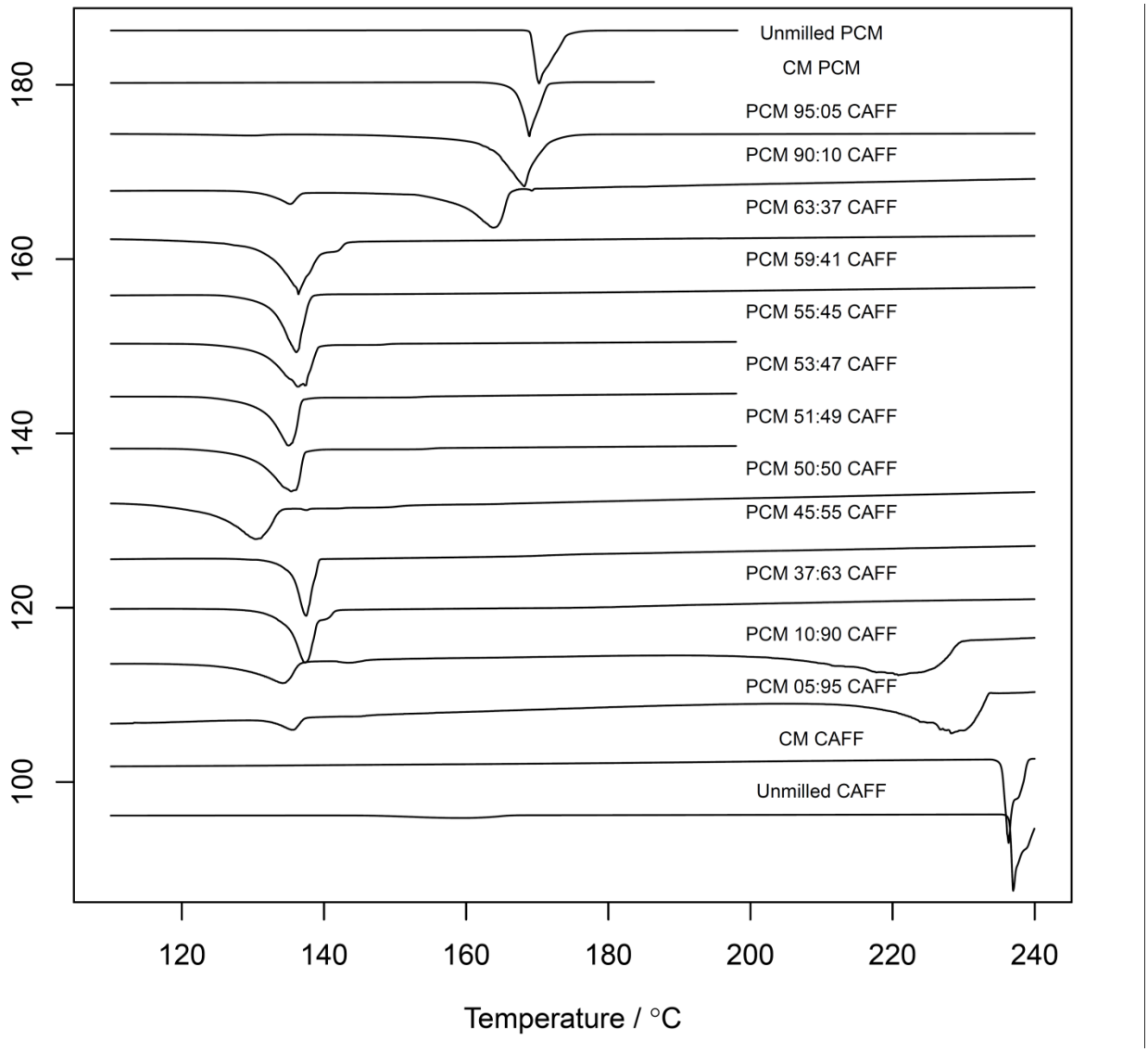


Figure 41: DSC overlays for screening the eutectic composition of different ratios of cryomilled (CM) paracetamol : caffeine (PCM:CAFF %, w/w).

With the mixture being milled at room temperature, the eutectic melting point lied at 133.68 °C with a single sharp endothermic peak of a mixture containing 55:45% w/w of PCM and CAFF respectively. DSC thermogram for RT milled paracetamol-caffeine mixtures are shown in Figure 42.

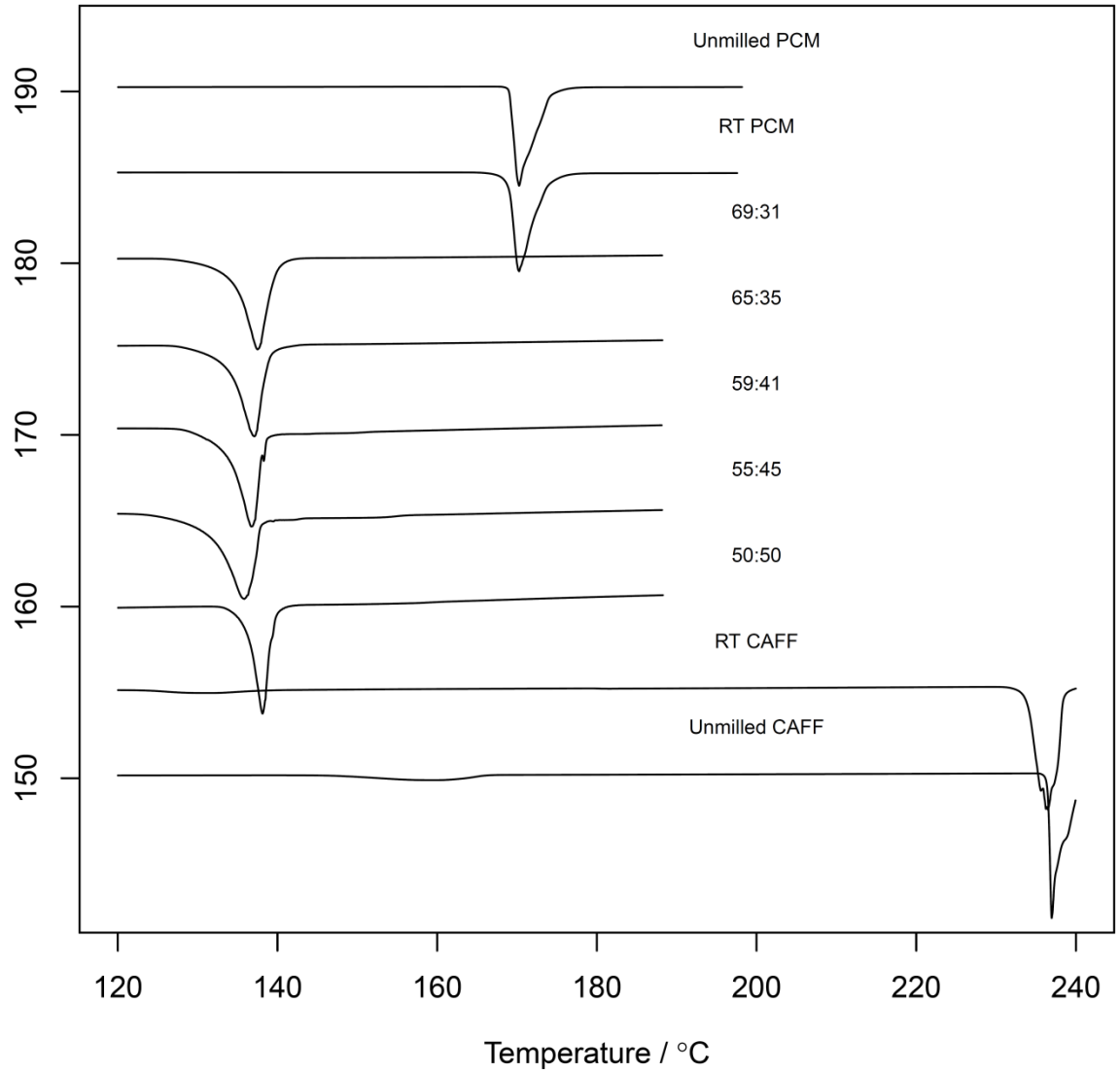


Figure 42: DSC overlays for screening the eutectic composition of different ratios of room temperature milled (RT) paracetamol: caffeine (PCM:CAFF %, w/w)

3.3.2.4. Hot stage microscopy results

Hot stage images were captured for all three systems after cryomilling and milling at room temperature was performed at different ratios in order to visually detect the solidus to liquidus transformation and to confirm the DSC results. All images are displayed in Figure 43.

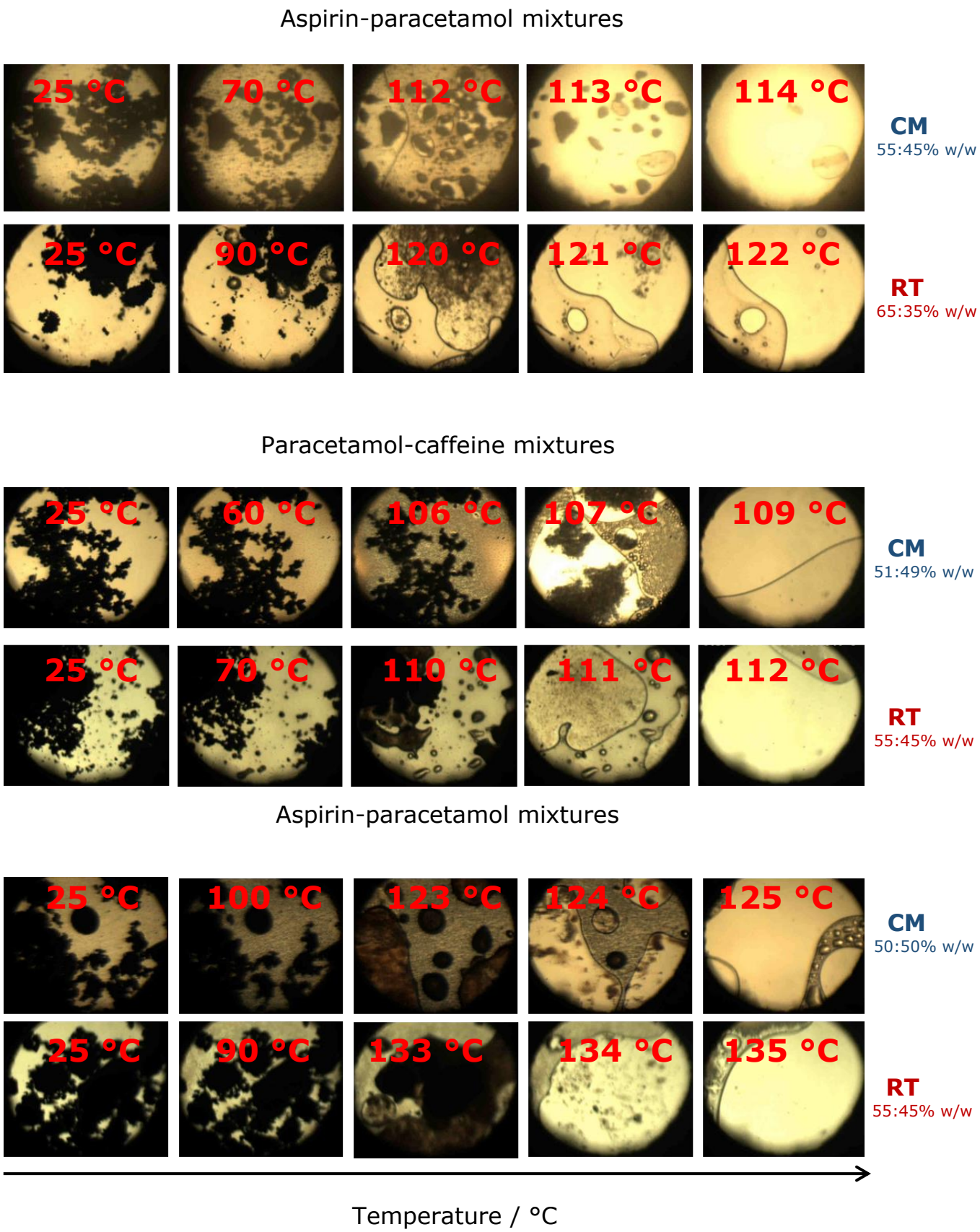


Figure 43: Hot stage microscope images for three binary mixtures of cryomilled (CM) and room temperature milled (RT) ASP-PCM, ASP-CAFF and PCM-CAFF at different molar ratios.

Single component systems	Aspirin	Paracetamol	Caffeine
Unmilled			
• **DSC**	T_m 141°C	T_m 169 °C	T_m 147 ◦C T_m 235 ◦C
• **XRPD**	Sharp peaks	Sharp peaks	Sharp peaks Two peaks detected at 26°
• **Scherrer estimate of Crystallite Size (nm)**	50 nm	80 nm	29 nm
• **HSM**	/	/	Needle like shaped formed at 147 °C (form II)
RT			
• **DSC**	T_m 132°C	T_m 168°C	T_m 124 ◦C T_m 234 ◦C
CM			
• **DSC**	T_m 142°C	T_m 165°C	T_m 235 ◦C
• **XRPD**	Relatively sharp peaks	Relatively sharp peaks	Sharp peaks one peak detected at ~ 26°
• **Scherrer estimate of Crystallite Size (nm)**	39 nm	33 nm	21 nm

Multi-component systems	Aspirin-paracetamol	Paracetamol-caffeine	Aspirin-caffeine
RT			
• **DSC**	Single melting peak at: 120.73 °C 65:35% w/w	Single melting peak at: 120.89 °C 45:55% w/w	Single melting peak at: 133.68 °C 55:45% w/w
• **HSM**	Miscible liquids at ~ 110 °C	Miscible liquids at ~ 110 °C	Miscible liquids at ~ 110 °C
CM			
• **DSC**	Single melting peak at: 112.70 °C 55:45% w/w	Single melting peak at: 105.67 °C 51:49% w/w	Single melting peak at: 123.8 °C 50:50% w/w
• **HSM**	Miscible liquids at ~ 110 °C	Miscible liquids at ~ 100 °C	Miscible liquids at ~ 115 °C

Table 16: Summary table of research work in Chapter 3.

3.5. Discussion

3.5.1. Milling temperature

The temperature at which milling is performed is considered to be a significant parameter that has a substantial effect on the outcome of the milling process. All the experiments reported in this chapter were carried out in two extremely different conditions; the first under liquid nitrogen (-196 °C) and the second at room temperature. Cryogenic milling has an advantage over milling at room temperature in terms of minimizing the sample degradation especially when dealing with thermolabile APIs. Aspirin, for instance, showed a significant reduction in the melting point as a result of milling at room temperature. This reduction was suspected to be due to chemical degradation of the sample rather than just particle size reduction because it was only detected in the sample milled at room temperature while the cryomilled sample shows a single sharp melting endotherm similar to the unmilled aspirin sample. However, FTIR and NMR showed no evidence of degradation. The potential reason for the reduction of melting point of the aspirin sample milled at room temperate is discussed in Section 3.5.2.

Researchers have reported that the temperature of milling with respect of the T_g value of the subjected sample is a key element in the crystal to amorphous transformation (181). In general, milling below the T_g results in the formation of amorphous material, whereas milling above the T_g can lead to a reduction in the particle size or polymorphic conversion from one form to another. Throughout the cryomilling process presented in this thesis all the samples were certainly being milled at a temperature lower than their actual T_g values. However, amorphous formation was not observed in all materials used in this chapter. Unlike aspirin and paracetamol, there are no reports revealing the T_g value of caffeine.

Caffeine exhibited polymorphic transformation from Form II to Form I, this transformation was observed with the unmilled sample and when caffeine was milled at room temperature. This lead to the assumption that the T_g value of caffeine might be quite low that an amorphous material is possibly formed inside the cryomilling vial but as a result of taking the vial out of the cryomill in order for the analysing process to take place at the room temperature a recrystallization might have took place. The same phenomenon might have happened in case of aspirin and paracetamol since their reported T_g values are -29 °C and 25 °C respectively. Kinetically trapping the amorphous phase of the studied materials is possible by using another component in the mixture which will hinder the process of nucleation and thus recrystallisation. This will be studied in more detail in the next chapter.

3.5.2. Melting point reduction

A reduction in the melting point of aspirin was observed as result of milling at room temperature. Chemical decomposition of the material was the first option considered, since this depression in the melting point was not detected with the cryomilled samples. However, the NMR results for the all aspirin samples, as received, room temperature milled and the cryomilled samples were identical. Other reasons that might have caused the reduction in the melting point are crystal defect and particle size reduction. Figure 44 shows the Gibbs energy and the chemical potential curve of a melting system.

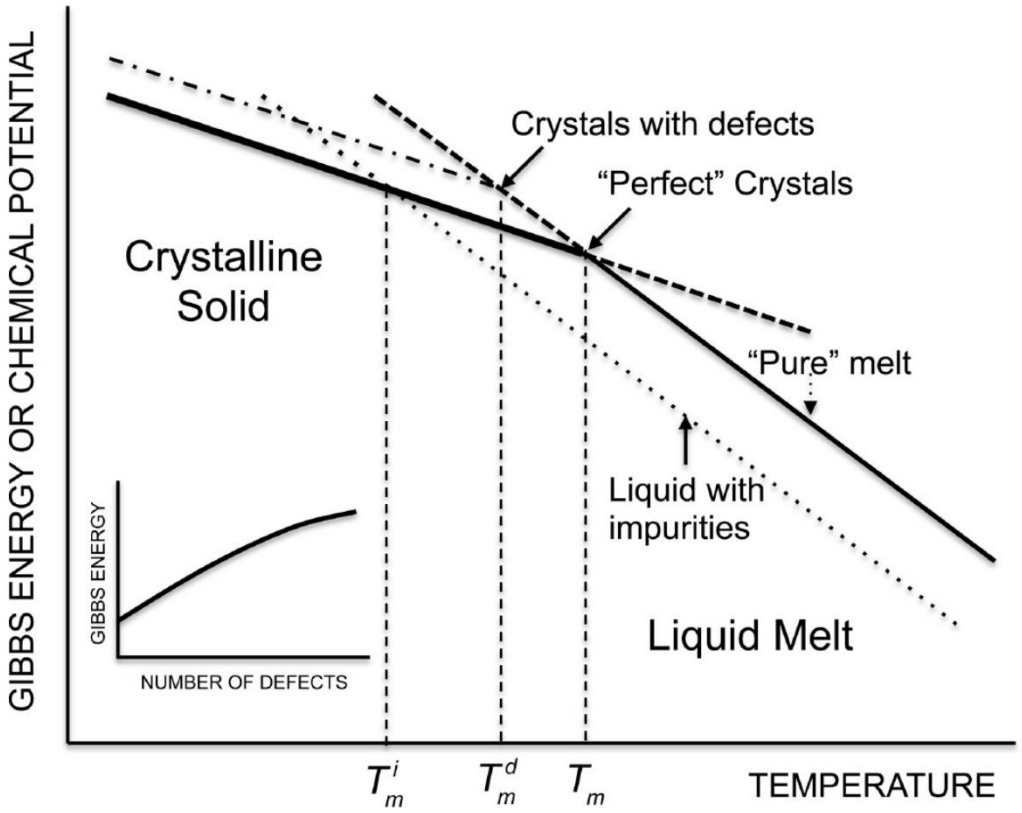


Figure 44: Gibbs energy and chemical potential of a melting system (182).

At the melting temperature of pure molecular crystals (T_m), the solid and liquid states have the same Gibbs energies. A liquid with impurities exhibits a lower Gibbs energy and a respective lower melting temperature of the crystals (T^i_m) (melting point depression). Crystals with defects have a higher Gibbs energy than "ideal" crystals, and their melting can occur at a lower temperature (T^d_m). In a dynamic heating process, crystals with impurities and defects melt at a lower temperature, and they may also show chemical degradation with a consequent increase in impurities and defects (182).

As per the multi-component systems studied in this chapter, significant reduction in the melting points was observed by DSC and confirmed by hot stage microscopy for all the multi-component mixtures. Single sharp endothermic events were detected at specific ratios indicating eutectic

mixture formation. The theoretical maximum reduction prediction in the melting point for each material was predicted using the Schroeder-van Laar equation (Equation 1) mentioned previously in chapter 1 Section 3.4.1. Figures 45-47 show the calculated binary phase diagrams of all three systems.

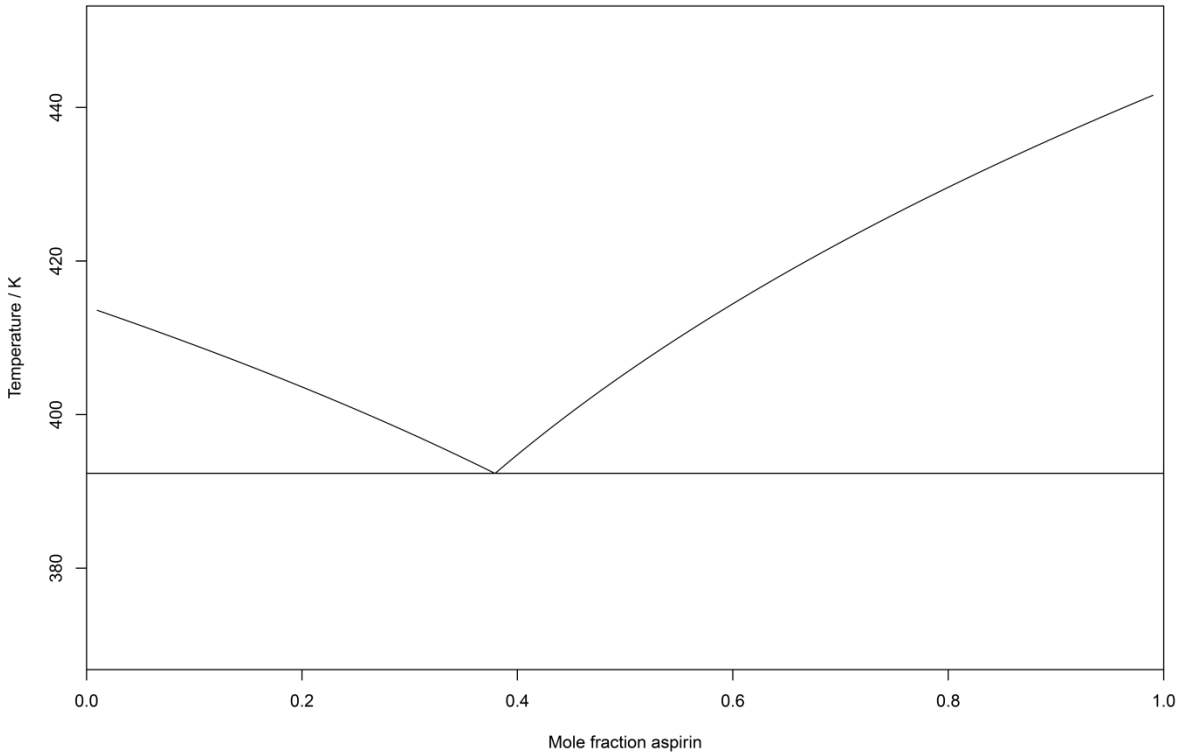


Figure 45: Calculated binary phase diagram of the system aspirin (ASP) - paracetamol (PCM)

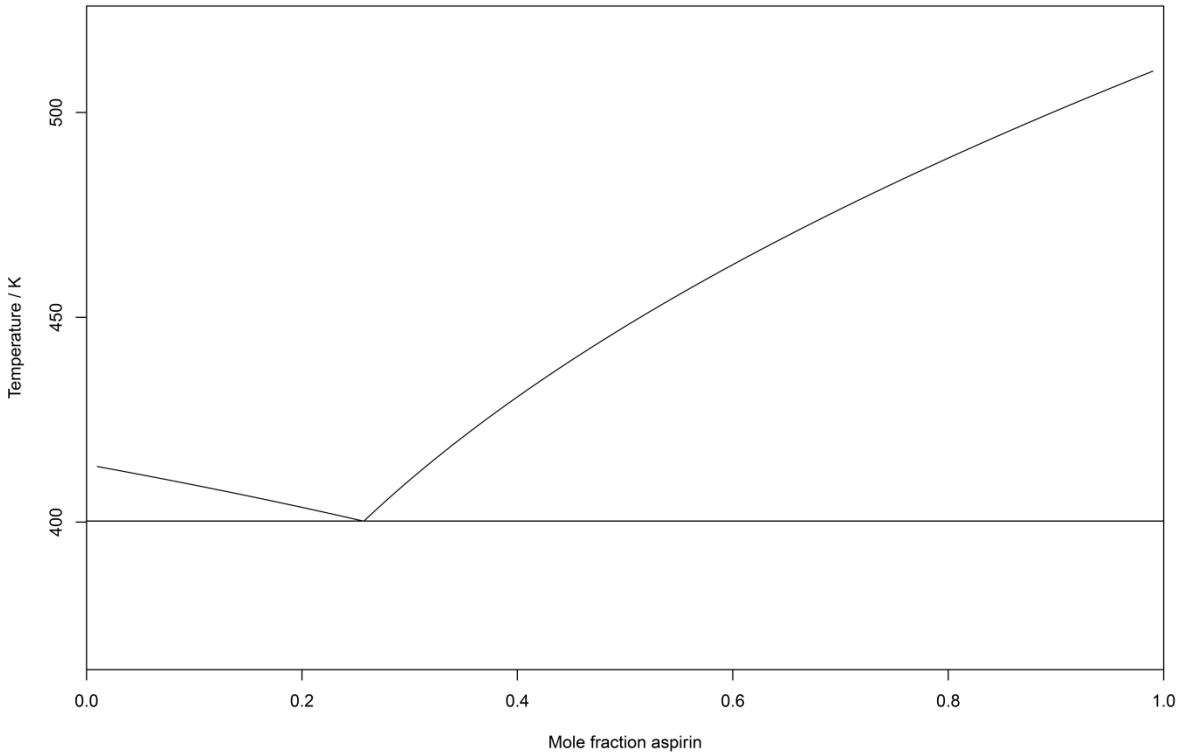


Figure 46: Calculated binary phase diagram of the system aspirin (ASP) - caffeine (CAFF).

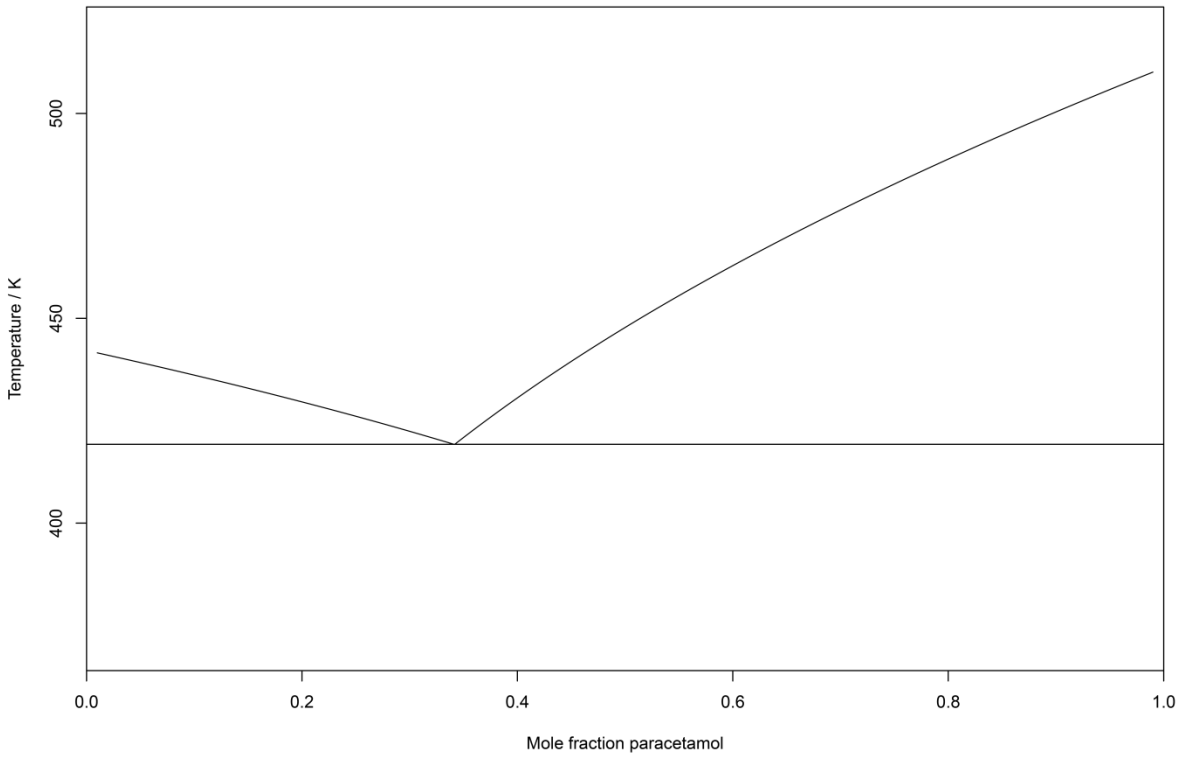


Figure 47: Calculated binary phase diagram of the system paracetamol (PCM) - caffeine (CAFF).

The reduction in melting points is explained as the colligative properties of melted solid substance (material 1) preferably depend on changes in the entropy of the solution as a result of dissolving a solute (material 2), which is determined by the concentration of the solute molecules or ions but does not depend on their structure. The motivation for these colligative properties is the increase in entropy on mixing solutes with the already melted material causing melting to occur at a lower temperature (183).

3.5.3. Summary discussion

With the main benefit of cryomilling compared to other processing methods is likely to be particle size reduction, but that this was not the main aim of this Chapter. The preparation of aspirin with crystal defects was interesting, and that further work outside the scope of this thesis could involve determining whether this wold enhance the solubility of the drug (although the solubility of aspirin is already high enough so there is no pressing need to investigate this). It is interesting that room temperature milling and cryomilling produce different outcomes in terms of DSC traces, and that this suggests that cryomilling may offer better mixing of components than conventional milling. Other potential co-processing methods might include freeze-drying and hot-melt extrusion (as noted in the previous Chapter, Section 2.5), and that these would not be universally applicable here as aspirin is prone to hydrolysis in freeze-drying (184), and caffeine does not melt but sublimes instead so hot-melt extrusion would not be suitable (174). Cryo-milling therefore seems to offer some unique capabilities for processing these pharmaceutical materials.

The appearance of eutectics is unexpected when compared with the results obtained in the previous Chapter given the reasons for the chemical nature of the materials but is not unreasonable as reported in literature reports of room temperature milling producing eutectics (68, 185). At this stage it appears that there is no clear way to predict cryo-milling outcomes, with the di-carboxylic acids undergoing some reduction in crystallinity, but these more drug-like samples showing formation of eutectics. Both of these outcomes again do not seem to be represented in the literature as noted in the previous Chapter.

3.5. Conclusion

In conclusion, DSC and XRPD studies for single component systems have shown that one hour cryomilling run was not enough to achieve crystal-to-amorphous transformation for all three materials. Low T_g values for paracetamol and aspirin could have caused materials to become amorphous inside the mill then to recrystallize immediately once taken out of the cryomill for the analysis. Milling of aspirin at room temperature caused a reduction in the melting point which was attributed to particle size reduction and crystal defect.

DSC and hot-stage microscope studies for cryomilled and ball milled ASP-PCM, ASP-CAFF and PCM-CAFF systems have shown that all materials are immiscible in the solid state. The phase diagrams of the three systems simply a eutectic type one. The addition of a second material in each system caused a significant reduction of the melting temperature of aspirin, paracetamol and caffeine until reaching to the eutectic temperature at which single endothermic event was noticed at lower temperature than the usual melting temperature off all three materials.

Chapter 4

4.1. Introduction

In Chapter 3, the effect of both cryomilling and milling at room temperature was studied on single and multiple component systems of three chosen APIs. As a result of pair mixing different ratios of aspirin-paracetamol, paracetamol-caffeine and aspirin-caffeine, a significant reduction in the melting points were detected. Since all the pharmaceutical formulations are usually formed by mixing one pharmaceutical ingredient or more with excipients, therefore, here, the effect of cryomilling of the previously used APIs with selected and widely used excipients will be investigated. Xylitol is a sweetening agent used in pharmaceutical and food production. It is a sugar alcohol just like sorbitol and mannitol. Xylitol may be found in throat lozenges, cough syrups, children's chewable multivitamins, toothpastes and mouthwashes. In the United States, xylitol is approved to be used as a food additive to suit special dietary requirements, such as diabetes (186). Lactose is a disaccharide composed of one galactose and one glucose molecule. In the pharmaceutical industry, lactose is used to help form tablets because it has excellent compressibility properties. It is also used to form a diluent powder for dry-powder inhalations. Lactose may be listed as lactose hydrous, lactose anhydrous, lactose monohydrate, or lactose spray-dried (187). Sucrose is often referred to as table sugar or saccharose. Sucrose has been used as a sweetener for decades. It is frequently used in pharmaceutical formulations to add a more acceptable taste to often

unpleasant drugs. Sucrose can be found in many medical dosage forms such as chewable tablets, syrups, lozenges, or gums. While sugar is basically non-toxic, it can be associated with several health problems such as, dental caries, exacerbation of diabetes, and weight gain (188). Finally, trehalose is a non-reducing disaccharide consisting of two glucose molecules linked by an α,α-1,1 bond. Trehalose can mask unpleasant tastes and odors, thus improving the quality and acceptability of finished pharmaceuticals such as, dry syrups, liquid preparations, tablets and chewables. Trehalose enhances the stability of minerals mostly magnesium and calcium, and increases their solubility. Trehalose stability is mainly attributed to its non-reducing end, which prevent its reaction with amino acids.

Most formulations (~70%-80%) contain excipients at a higher concentration than the active drug (189). Subsequently, the excipients can significantly have an impact on the formulation's performance and processability (190). Excipients are generally added to protect, support or enhance the stability of the formulation, to mask any unacceptable taste of some APIs, thus, improving the patience compliance, to enhance the bulkiness of the formulation in case of potent drug and to improve the bioavailability of certain active drugs (191). Milling different excipients with APIs allows us to determine drug excipients interactions which can be either prevented or can be adjusted to operate in an efficient way which helps in reducing the risk combined with the excipients. Generally drug excipient interactions are further categorised as, physical, chemical and biopharmaceutical interactions. Cryomilling excipients with several types of APIs have received less attention in the literature. However, milling of the individual excipients was reported before with sucrose (192), lactose monohydrate and trehalose dihydrate

The present chapter aims to study four binary systems of paracetamol, aspirin and caffeine with sucrose, lactose monohydrate, xylitol and

trehalose dihydrate respectively using DSC and XRPD and hot-stage microscope on the cryomilled samples.

4.2. Materials and Methods

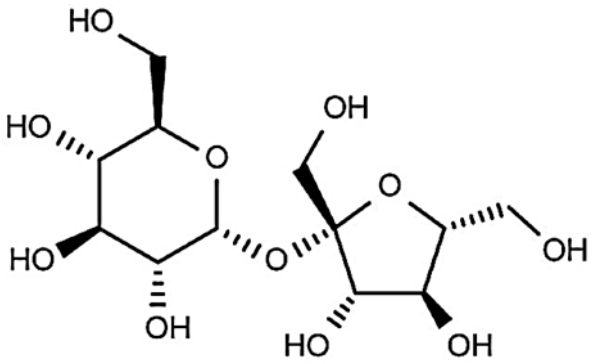
4.2.1. Materials

4.2.1.1. Active Pharmaceutical ingredients APIs

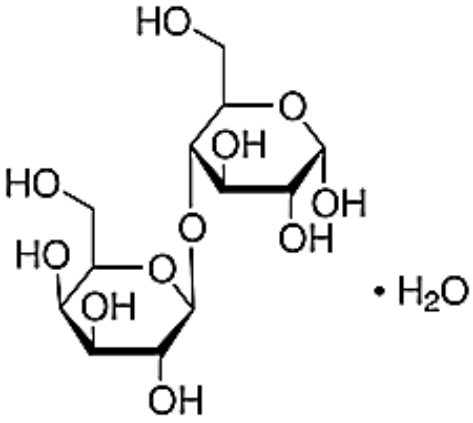
The APIs which were used in the current chapter were listed in the previous chapter (Chapter 3, Section 2.1).

4.2.1.2. Excipients

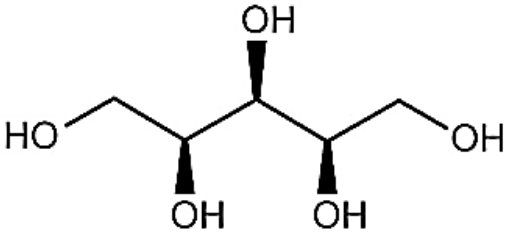
The chemical structures of all excipients used in this study are shown in Figure 48.



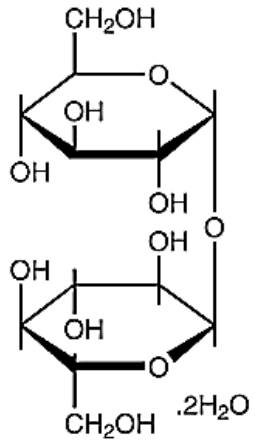
a. Sucrose



b. Lactose monohydrate



c. Xylitol



d. Trehalose dihydrate

Figure 48: Model compounds with range of physical properties (Table 17), used to study the effect of cryomilling on binary mixtures of excipients and APIs

Material	Molecular Mass (g/mol)	Melting Point (°C)	T_g (°C)
Sucrose	342.29	186 (193)	71 (4)
Lactose monohydrate	342.30	210 (194)	50 (195)
Xylitol	152.15	92 (196)	-26 (196) -29 (197)
Trehalose dehydrate	378.32	110 (198)	20 (195)

Table 17: Key physical properties of the selected excipients

i. Sucrose

Sucrose (S9378, ≥99.5%) was purchased from Sigma and used as received. The melting point onset was detected by DSC with a heating rate of 10 °C / minute and it was 189.3 °C. The XRPD was very similar to the pattern from the crystal structure from the Cambridge Structural Database (171), with no extra peaks were detected, which confirms the purity of the material within the instrument detection limits.

ii. Lactose

Lactose (17814, lot no.-BCBH2071V) was purchased from Sigma and used as received. A confirmation of the starting material purity was carried out

using DSC (heating rate 10 °C /minutes) and XRPD. DSC thermogram shows a melting onset of 210 °C while the XRPD was very similar to the pattern from the crystal structure presented at the Cambridge Structural Database (171), with no extra peaks were detected, which confirms the purity of the material within the instrument detection limits.

iii. Xylitol

Xylitol (X3375, ≥99%) was purchased from Sigma and used as received. The melting point was measured using DSC with an onset of 93.4 °C. The XRPD was very similar to the pattern from the crystal structure from the Cambridge Structural Database (171), with no extra peaks were detected, which confirms the purity of the material within the instrument detection limits.

iv. D-(+)-Trehalose dihydrate

D-(+)-Trehalose dihydrate (T9531, ≥99%) was purchased from Sigma and used as received. a confirmation of the starting material purity was carried out using DSC (heating rate 10 °C /minutes) and XRPD. DSC thermogram shows a melting onset of 96.3 °C while the XRPD was very similar to the pattern from the crystal structure presented at the Cambridge Structural Database (171), with no extra peaks were detected, which confirms the purity of the material within the instrument detection limits.

4.2.2. Methods

4.2.2.1. Preparation method

i. **Cryomilling:**

As in Chapter 3, Section 3.2.2.1, Pages 83-84.

4.2.2.2. Characterisation methods

i. **DSC:**

As in Chapter 2, Section 2.2.3, Pages 35-36.

ii. **XRPD:**

As in Chapter 2, Section 2.2.3, Page 36.

iii. **HSM:**

As in Chapter 3, Section 3.2.2.2, Pages 84-85.

4.3. Results

4.3.1. Xylitol

4.3.1.1. Xylitol and aspirin

DSC thermogram shown in Figure 49 represents aspirin and xylitol before and immediately after cryomilling along with 50:50% w/w mixture of aspirin and xylitol cryomilled together for 60 minutes. DSC results for aspirin were previously discussed in Chapter 3 (Section 3.1.2) which showed only a melting endotherm with an onset of 141 °C and an enthalpy of fusion of 167 J/g for the unmilled sample and after cryomilling the melting onset was detected at 142 °C with an enthalpy of fusion of 160 J/g. With regards to the xylitol sample, the unmilled sample shows a single endothermic peak with a melting onset at 93 °C and an enthalpy of fusion of 235 J/g. As a result of cryomilling a slight reduction in melting onset was noticed by 4 °C, which could probably be caused by particle size reduction. The cryomilled xylitol showed a melting onset at 89 °C with an enthalpy of fusion of 222 J/g. Co-cryomilling of aspirin and xylitol for 60 minutes with 50:50% w/w mixing ratio was displayed on the DSC data. The DSC thermogram shows two melting peaks, with the first corresponding to xylitol with an onset of 89 °C and an enthalpy of fusion of 121 J/g.

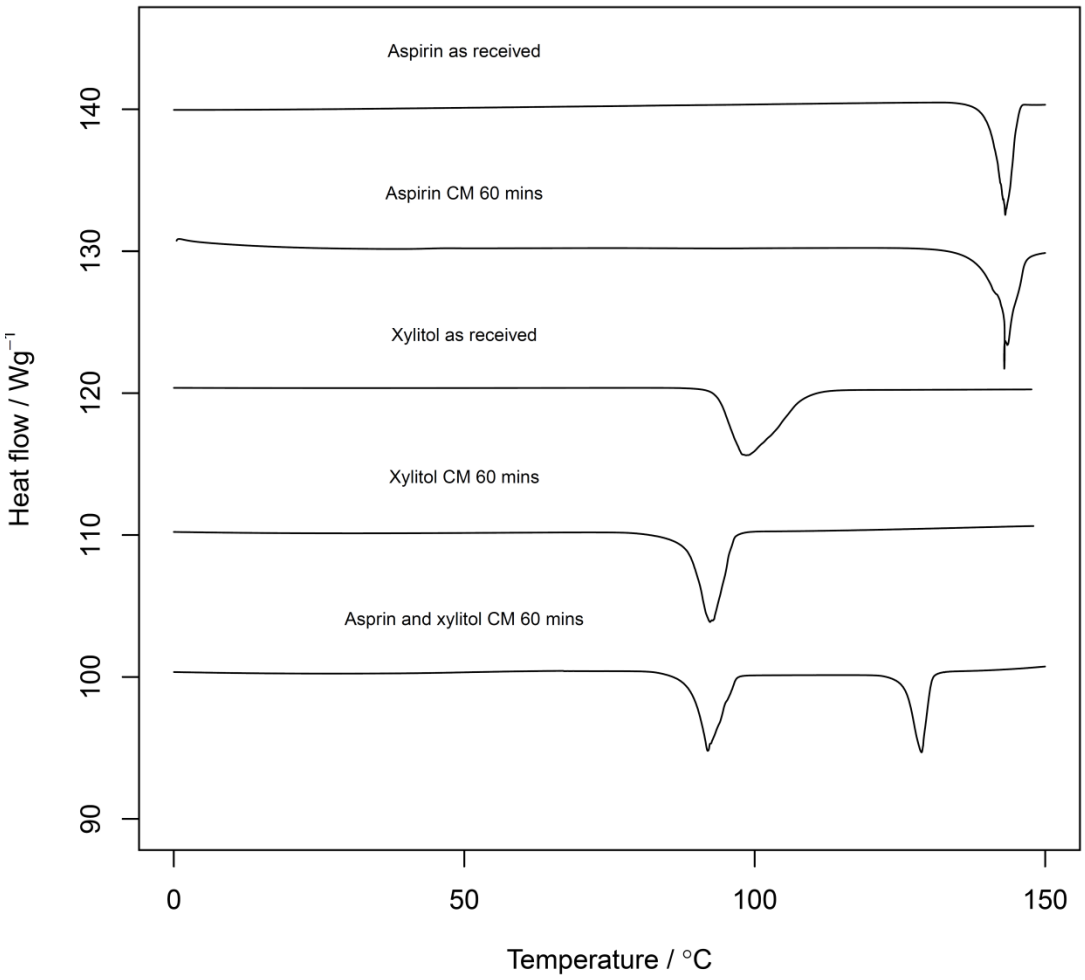
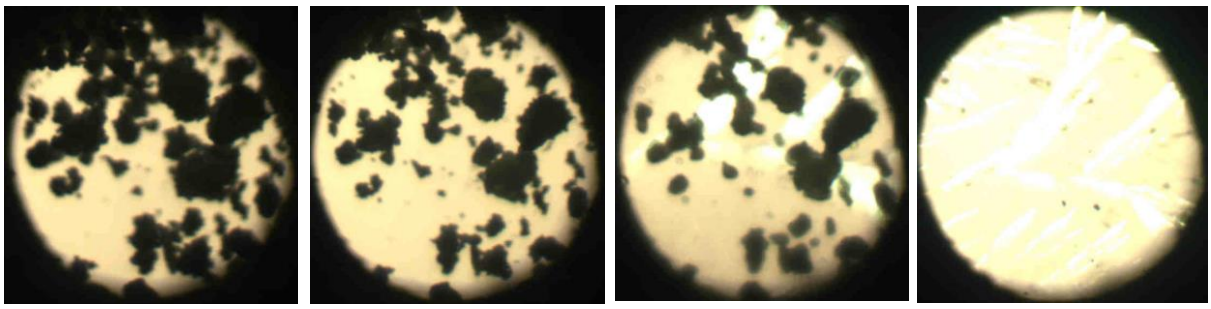


Figure 49: DSC thermograms of aspirin and xylitol before and immediately after cryomilling and a 50:50% w/w mixture of aspirin and xylitol cryomilled together for 60 minutes. Data have been offset by 10 Wg^{-1} for presentational purposes.

On the other hand, the second peak which supposed to represent the aspirin part of the mixture was detected in a lower region as compared with the pure cryomilled aspirin, the melting onset was 125 °C with an enthalpy of fusion of 84 J/g. Xylitol was reported to act as a carrier to many pharmaceutical dispersions for poorly water soluble compounds (199) such as systems containing ibuprofen (IB) and xylitol (XYL) in varying proportions (200). Xylitol can be used as a carrier in tablets for solid dispersions, when a fast drug release is desired, this was achieved when griseofulvin was used as a model drug (201). Co-cryomilling xylitol with aspirin might have produced dispersion with xylitol acting as a solubilizing media for aspirin leading to the reduction in aspirin's melting point when

50:50% w/w ratio was applied. Or the obvious reduction in the melting reduction of aspirin could be attributed to that the two substances are physically separate as solids after cryomilling, but when xylitol melts an eutectic mixture of aspirin/xylitol plus un-melted aspirin. Therefore, hot-stage microscope images were captured for the cryomilled mixture shown in Figure 50 which confirms that this pair mixture is considered to be co-soluble as liquids.



25 °C 86 °C 120 °C 130 °C

Figure 50: Hot-stage microscope images of cryomilled 50:50% w/w mixture of aspirin and xylitol.

The XRPD patterns collected at room temperature for aspirin, xylitol before and after cryomilling and a cryomilled 50:50% w/w mixture of aspirin and xylitol are shown in Figure 51. It is immediately apparent that all samples exhibit Bragg peaks, albeit which vary somewhat in width between samples, which suggests some level of crystallinity is present in all materials. The XRPD trace for unmilled and cryomilled aspirin was shown earlier in Chapter 3 (Section 3.1.2). Bragg peaks for aspirin and xylitol cryomilled separately show different shapes and widths when compared to the unmilled and the cryomilled samples. A marked change in the relative peak intensities was noticed especially in the case of xylitol is resulted from the static fluctuation of atomic positions along the normal of xylitol layers which is reported to have a strong influence on the peak intensities (202). This fluctuation factor may cause the large and regular crystals of the unmilled sample to be in the most preferred orientation. The peaks of the

cryomilled sample appear broader compared with the unmilled samples which exhibit somewhat sharp peaks.

.

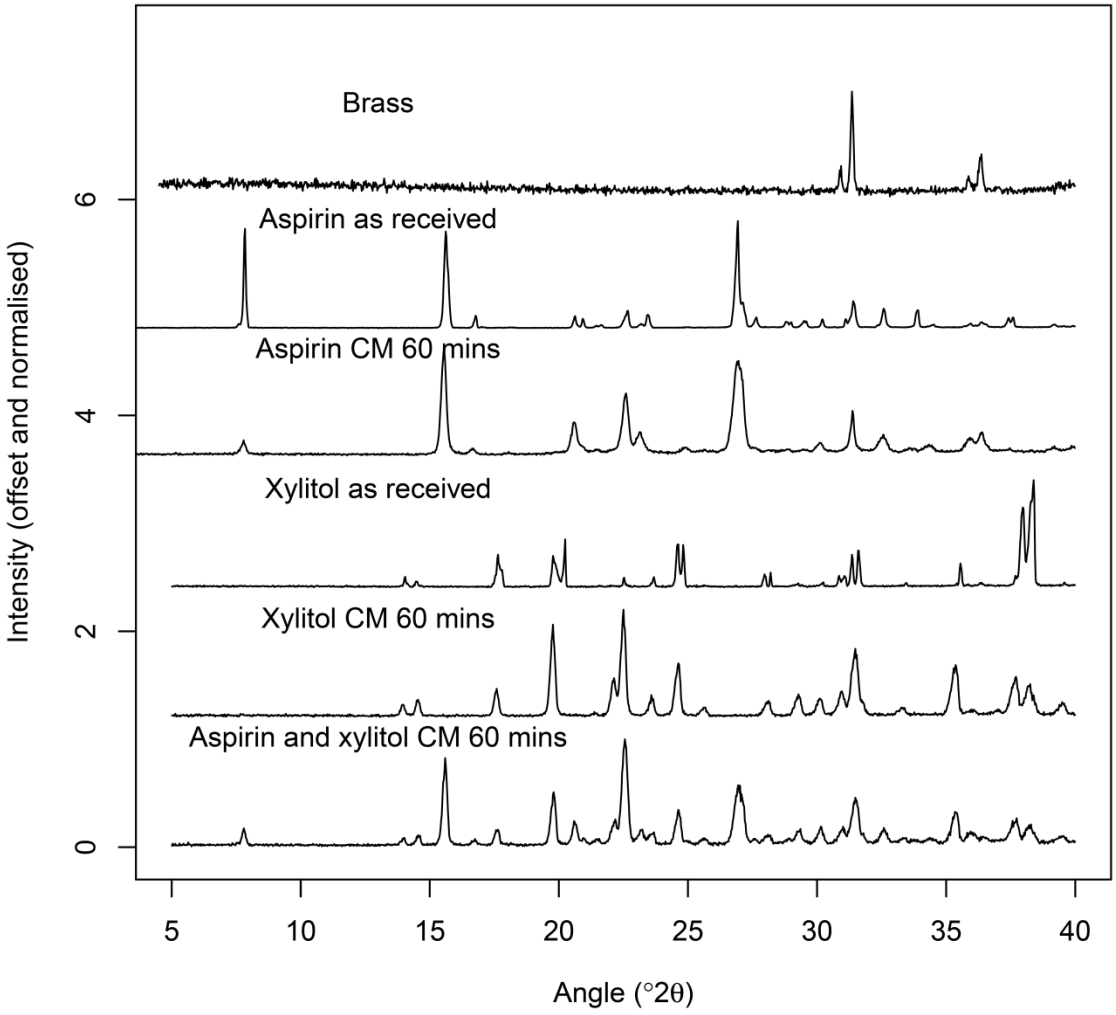


Figure 51: XRPD patterns collected at room temperature for aspirin, xylitol before and after cryomilling and a cryomilled 50:50% w/w mixture of aspirin and xylitol. The data have been scaled and offset for clarity.

The aspirin and xylitol cryomilled together patterns show the presence of somewhat sharp peaks corresponding to aspirin and xylitol. Taken together, the data indicate that cryomilling aspirin and xylitol together does not show any synergistic effect and no clear indications of amorphous material formation in our XRPD data. It therefore appears that co-cryomilling aspirin and xylitol producing a XRPD trace that can be easily

described in terms of a linear combination of both materials, albeit with an increase in peak widths compared to the un-milled materials which likely arises from crystallite size reduction upon milling.

4.3.1.2. Xylitol and paracetamol

Figure 52 shows the DSC thermogram of paracetamol and xylitol before and immediately after cryomilling along with 50:50% w/w mixture of paracetamol and xylitol cryomilled together for 60 minutes. DSC data resulted from individually cryomilling paracetamol were previously discussed in Chapter 3 (Section 3.1.1) with no significant difference between the unmilled and the cryomilled sample shown in the DSC data. Moreover, xylitol DSC theromogram was covered in the previous section with xylitol showing a slight decrease of the melting onset as a result of milling. DSC data for both materials were added in order to make the comparison process more clear. Co-cryomilling of paracetamol and xylitol for 60 minutes with 50:50% w/w ratio displayed two melting endotherms, with the first peak which represents xylitol with an onset of 86 °C and an enthalpy of fusion of 113 J/g. However, the second peak which was assumed to signify the paracetamol portion of the mixture was significantly noticed at a lower region as compared with the pure cryomilled paracetamol sample. The melting onset for paracetamol in the paracetamol-xylitol mixture was 146 °C with an enthalpy of fusion of 95 J/g, while with pure paracetamol a melting peak with an onset of 167 °C and an enthalpy of fusion of 184 J/g, which makes a reduction in melting point by 21 °C.

Taken together, the DSC data indicated that as a result of co-cryomilling xylitol with paracetamol with 50:50% w/w mixing ratio might have been the start of some form of solid dispersion which leads to the reduction of the melting point of paracetamol as the binary systems comprising paracetamol using techniques other than cryomiling were reported (148,

149, 159, 162, 163). The solvent evaporation technique was stated to being the most frequently used strategy (68, 147).

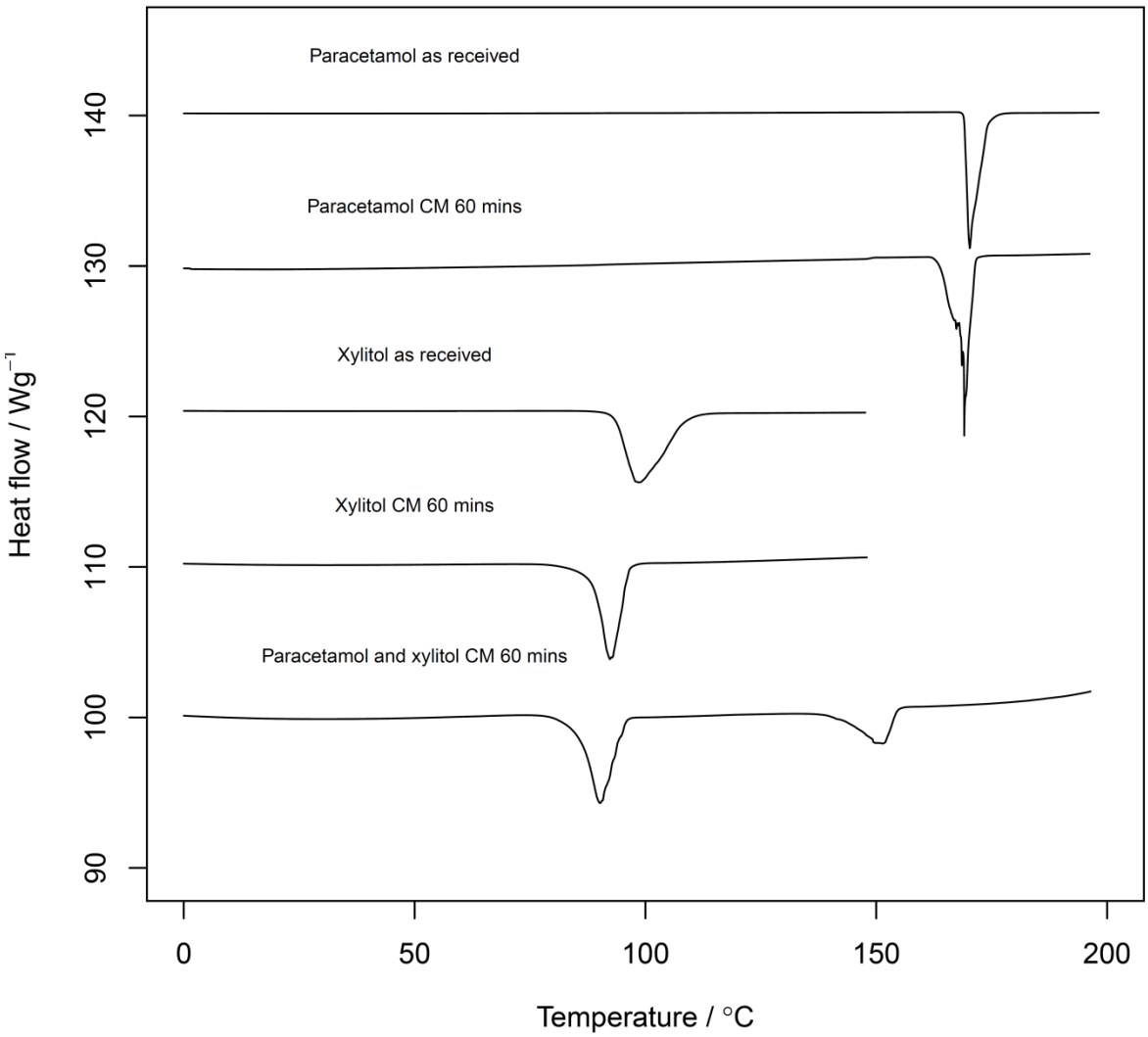


Figure 52: DSC thermograms of paracetamol and xylitol before and immediately after cryomilling and a 50:50% w/w mixture of paracetamol and xylitol cryomilled together for 60 minutes. Data have been offset by 10 Wg^{-1} for presentational purposes.

It was evident that all samples exhibit Bragg peaks which indicate some degree of crystallinity is present in all materials. The XRPD trace for unmilled and cryomilled paracetamol was presented earlier in Chapter 3 (Section 4.3.1.1) as well as the XRPD trace for unmilled and cryomilled xylitol, which were shown in the previous section. Bragg peaks for paracetamol and xylitol cryomilled together does not show any clear difference in shapes and widths when compared with the cryomilled pure

separate materials as shown in Figure 53. The data showed that co-cryomilling paracetamol and xylitol together would produce a XRPD trace of the same two materials combined, no exact evidence was shown leading to co-crystal formation resulting from cryomilling paracetamol and xylitol together. Furthermore, there is no significant indications of amorphous material are apparent in the XRPD data.

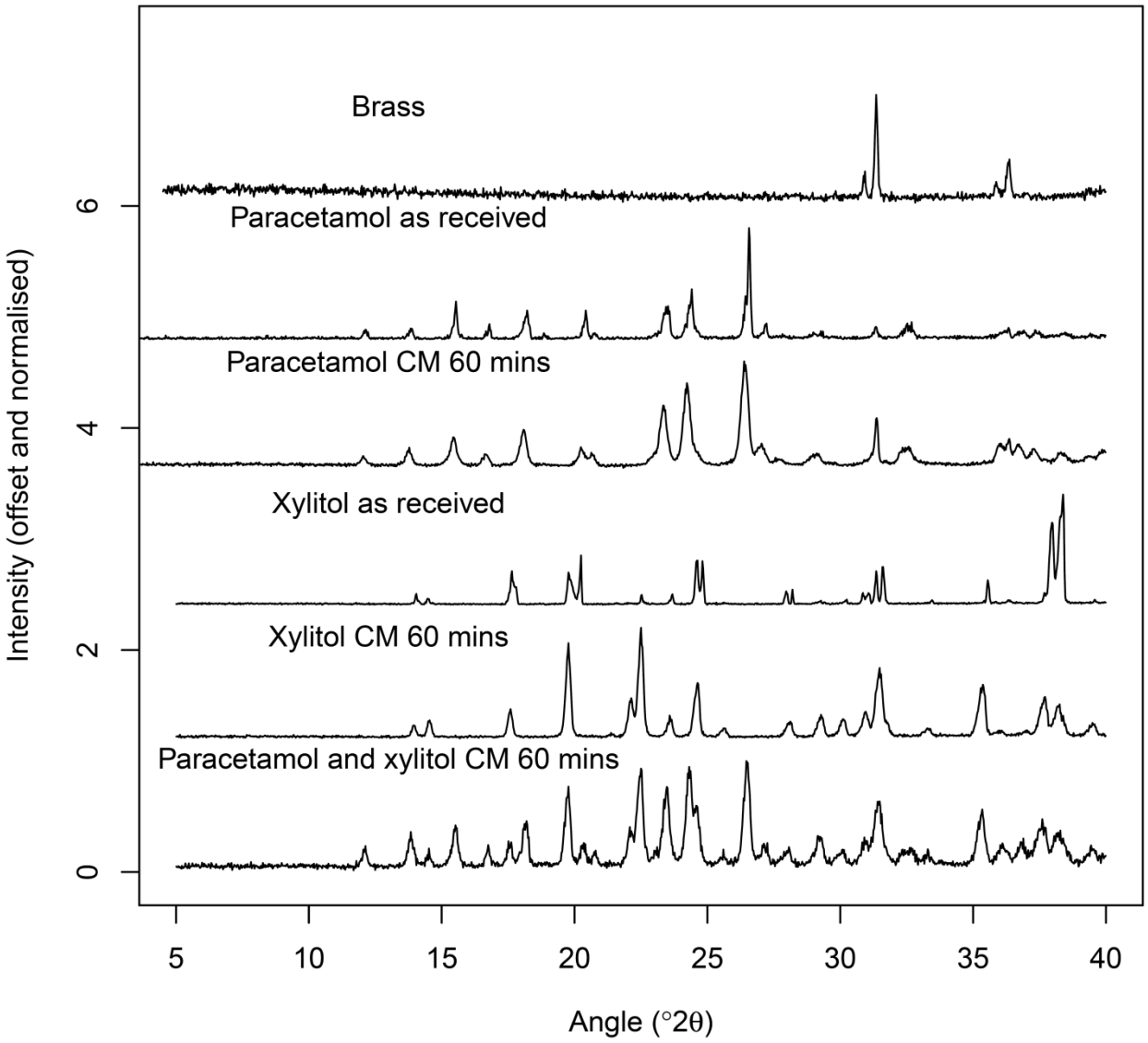


Figure 53: XRPD patterns collected at room temperature for paracetamol, xylitol before and after cryomilling and a cryomilled 50:50% w/w mixture of paracetamol and xylitol. The data have been scaled and offset for clarity.

It therefore appears that co-cryomilling paracetamol and xylitol leads to an obvious reduction in crystallinity for both reagents by producing a trace with broader peaks compared with the unmilled samples rustling from the reduction in crystallite size. However, co-cryomilling produces a XRPD trace that can be described in terms of a linear combination of the individual pure materials.

4.3.1.3. Xylitol and caffeine

The DSC thermogram results for xylitol and caffeine co-cryomilled mixture are seen in Figure 54. The data show no difference from the data resulted from co-cryomilling xylitol with aspirin and paracetamol respectively for 60 minutes. It was highlighted in the previous chapter (Chapter 3, Section 3.1.3) that caffeine is subjected to polymorphic change as a result of cryomilling. Only a single melting endotherm was detected after cryomilling with an onset of 235 °C and an enthalpy of fusion of 102 J/g which is reported to present Form I (176).

As result of co-cryomilling caffeine and xylitol together, xylitol melting peak was clearly detected with an onset of 84 °C with an enthalpy of fusion of 95 J/g. However, as was noticed in case of aspirin and paracetamol a significant reduction in the melting point was seen with caffeine as well. Moreover, the endothermic peak was not as sharp as the peaks resulted from melting purely cryomilled sample. The melting onset was 179 °C with an enthalpy of fusion of 20 J/g. As a result of milling a material, a change in the melting peak is often expected as a result of particle size reduction. In case of caffeine there is not enough literature available discussing this area, and the current work thought to be novel in terms of cryomilling caffeine with xylitol.

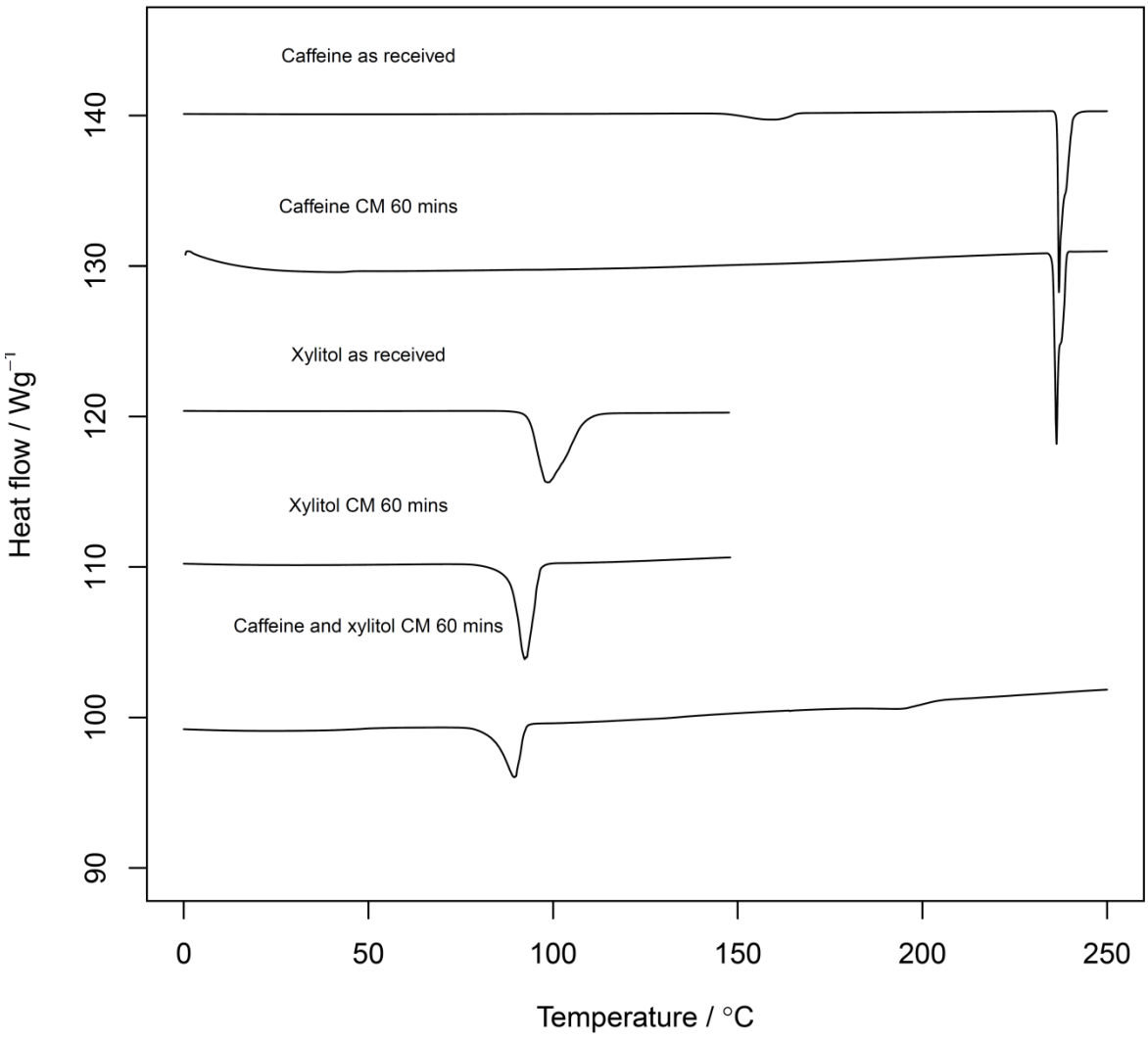


Figure 54: DSC thermograms of caffeine and xylitol before and immediately after cryomilling and a 50:50% w/w mixture of caffeine and xylitol cryomilled together for 60 minutes. The data have been offset by 10 Wg^{-1} for presentational purposes.

The XRPD trace of caffeine and xylitol cryomilled together presented in Figure 55 show merged Bragg peaks of both xylitol and caffeine Form I. The peaks appear to be broader when compared with the unmilled samples. However, co-cryomilling of both materials together produces a XRPD trace that can be described in terms of a linear combination of the individual pure materials.

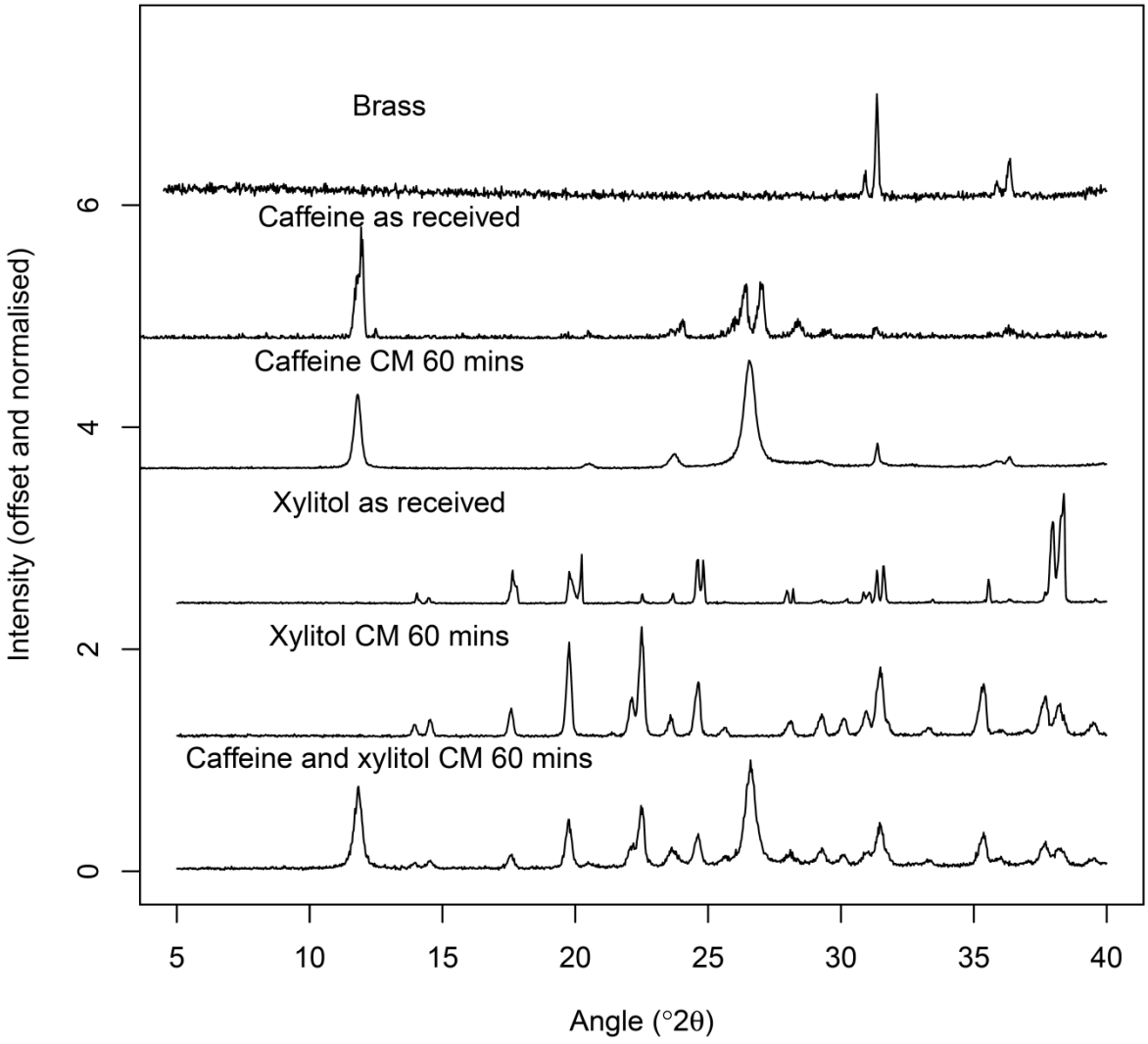


Figure 55: XRPD patterns collected at room temperature for caffeine, xylitol before and after cryomilling and a cryomilled 50:50% w/w mixture of caffeine and xylitol. The data have been scaled and offset for clarity.

4.3.2. Lactose monohydrate

4.3.2.1. Lactose monohydrate and aspirin

DSC measurements of unmilled and cryomilled aspirin, lactose monohydrate and a cryomilled mixture of both materials are presented in Figure 56. The DSC diagram of unmilled lactose monohydrate has an endothermic event at 138 °C, which represents the loss of crystalline water,

followed by two melts of α and β forms combined at 217 °C 241 °C. DSC curve for the cryomilled sample show the amorphous form of the lactose, it was identified by the presence of an exothermic peak at 122°C, which represents the transformation of amorphous to crystalline form. Two endothermic peaks were seen one at 210 and the other at 237°C.

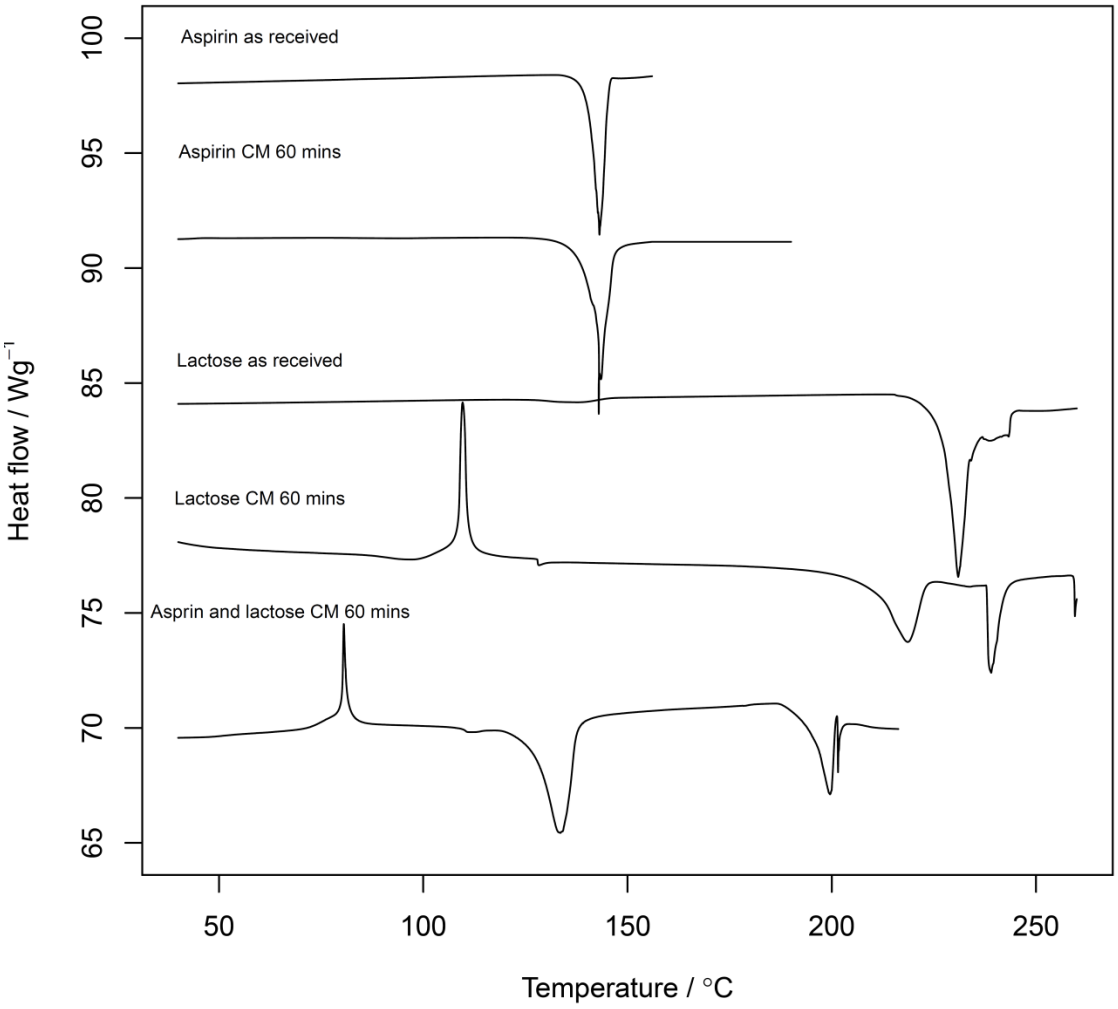


Figure 56: DSC thermograms of aspirin and lactose before and immediately after cryomilling and a 50:50% w/w mixture of aspirin and lactose cryomilled together for 60 minutes. Data have been offset by 7 Wg^{-1} for presentational purposes.

These melting peaks belong to α- and β-lactose respectively, confirming the transformation of the amorphous form of lactose to the two types of crystalline form as a result of heating, agreeing with the previously reported

values (203). The transitions noticed in the as received lactose are slightly higher than the reported values (194). For the amorphous lactose obtained by milling at room temperature, a T_g was detected at 40 °C. Co-cryomilled aspirin and lactose sample showed an exotherm with a small shoulder peak at 80 °C, which might be resulting from that different parts of the sample recrystallizes at different temperatures, followed by two endothermic events representing aspirin and lactose at 127 °C and 195 °C respectively.

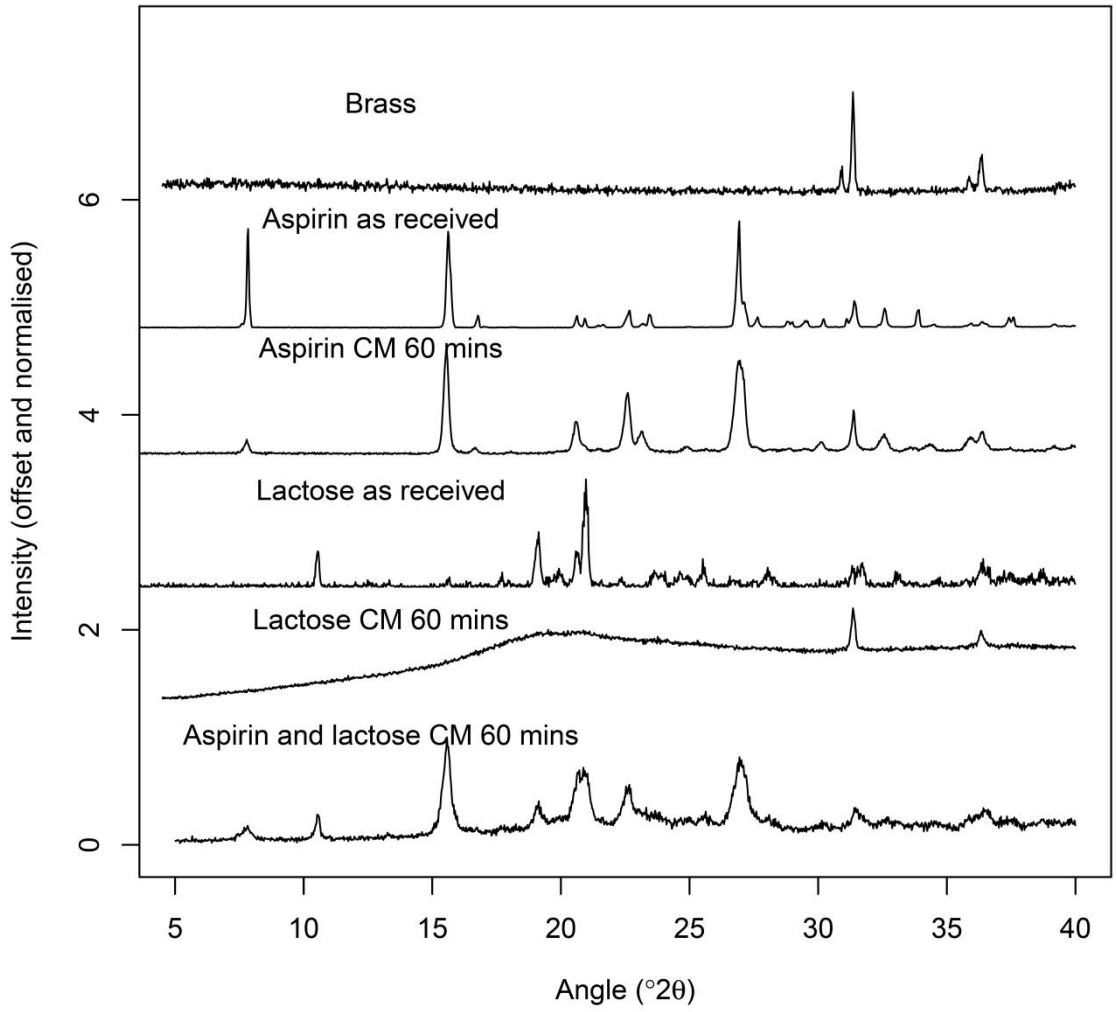


Figure 57: XRPD patterns collected at room temperature for aspirin, lactose before and after cryomilling and a cryomilled 50:50% w/w mixture of aspirin and lactose. The data have been scaled and offset for clarity.

XRPD experiment was conducted to confirm the crystal to amorphous transformation of lactose as a result of cryogenic milling, see Figure 57. The pattern collected show a broad amorphous halo assigned for

amorphous lactose. Several Bragg peaks seen in the XRPD trace for the cryomilled mixture, which are broader than the individually cryomilled reagents. The obtained peaks could easily be visually detected as a combination of lactose and aspirin peaks with no extra peaks detected.

4.3.2.2. Lactose and paracetamol

In Chapter 4 the cryomilling of paracetamol was studied. It was seen in agreement with literature (4), that paracetamol retains its crystalline properties on cryomilling. DSC data of paracetamol and lactose are shown in Figure 58. There is apparent difference in the physical form of paracetamol when comparing between the cryomilled alone and the co-cryomilled sample with lactose. DSC thermogram for paracetamol alone shows an endothermic peak at 168 °C. After cryomilling, there were no obvious events until the melting point at 167 °C, suggesting the presence of a crystalline material even on milling. Cryomilled mixture of paracetamol and lactose displayed two exothermic events one at 48 °C and the second at 92 °C and followed by two melts at 159 °C and 204 °C. The first observed recrystallization peak agrees with the reported value for quench cooled paracetamol (165). And since lactose has no thermal events in this region, we can define the observed crystallisation peak is due to the presence of amorphous paracetamol.

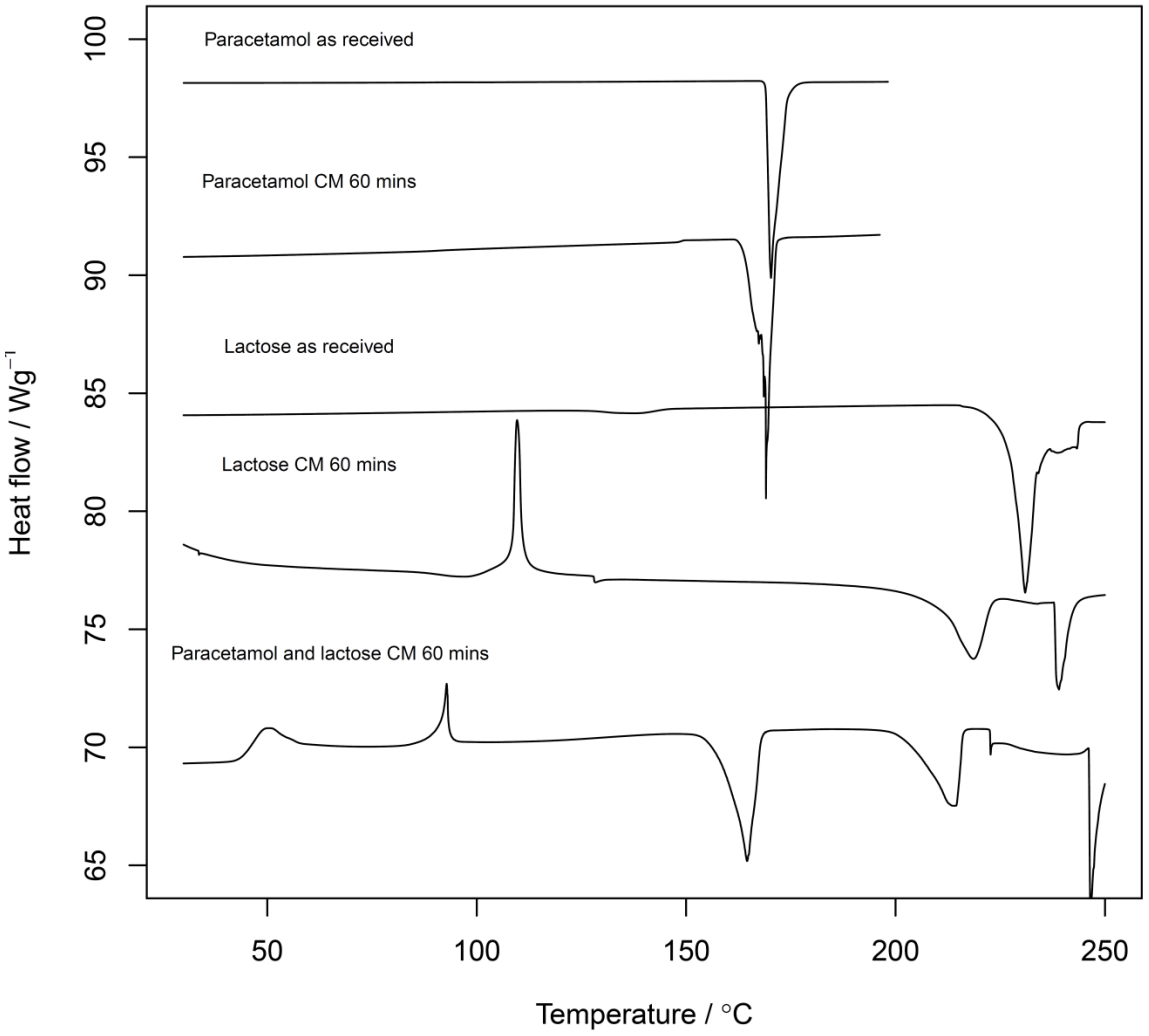


Figure 58: DSC thermograms of paracetamol and lactose before and immediately after cryomilling and a 50:50% w/w mixture of paracetamol and lactose cryomilled together for 60 minutes. Data have been offset by 7 Wg^{-1} for presentational purposes.

Hot-stage microscope images shown in figure 59 were in agreement with the results obtained from the DSC thermogram. The paracetamol/lactose co-cryomilled mixture had went through three melting events started at 160 °C, at 180 °C the image clearly showed liquid and un-melted solid part of the mixture. As the temperature increases co-soluble liquids are formed.

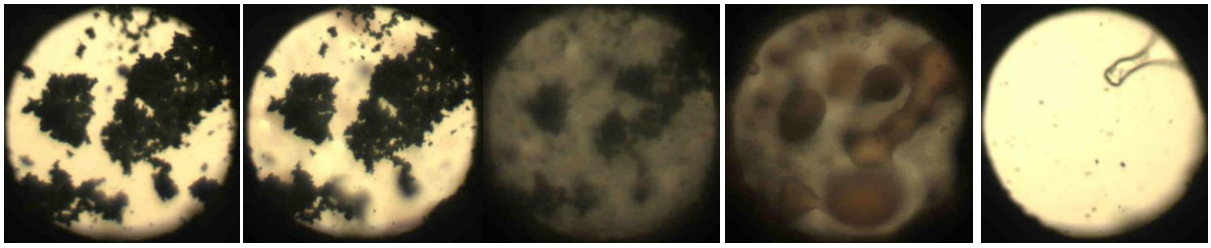


Figure 59: Hot-stage microscope images of cryomilled 50:50% w/w mixture of paracetamol and lactose.

XRPD patterns for unmilled and cryomilled paracetamol, lactose and cryomilled mixture of paracetamol and lactose are shown in Figure 60. It can be seen that unmilled paracetamol contains multiple sharp Bragg peaks indicating pure crystalline material. After cryomilling with lactose there was a broad halo detected, with few peaks indicating partially crystalline paracetamol and also some peaks of lactose seem to reappear after co-cryomilling with paracetamol. It looks as if paracetamol has destabilised the amorphous lactose and caused it to recrystallize.

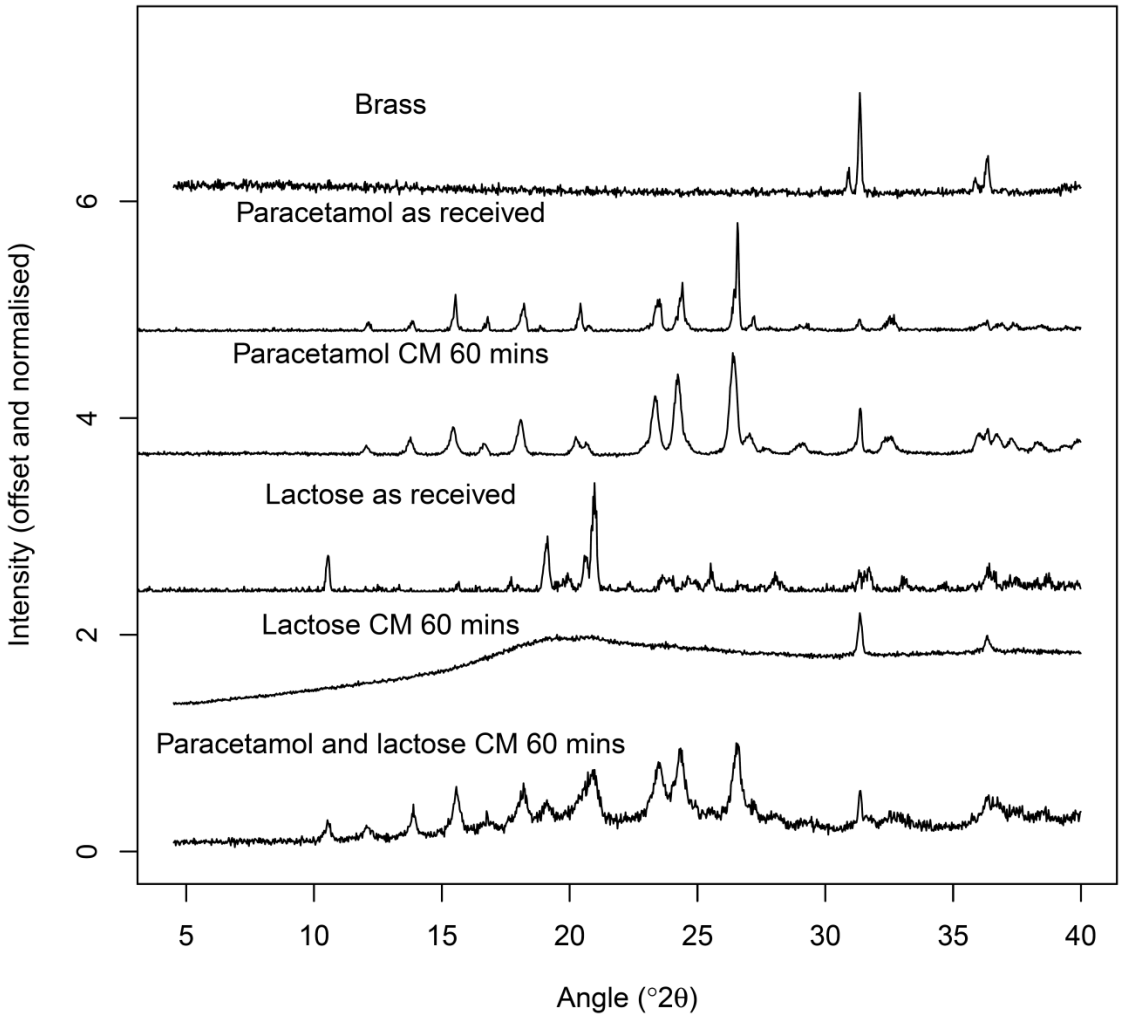


Figure 60: XRPD patterns collected at room temperature for paracetamol, lactose before and after cryomilling and a cryomilled 50:50% w/w mixture of paracetamol and lactose. The data have been scaled and offset for clarity.

4.3.2.3. Lactose monohydrate and caffeine

Cryomilling of caffeine and lactose monohydrate produced a DSC thermogram which was difficult to interpret, see Figure 61. As investigated in chapter 4 the polymorphic transformation of caffeine as a result of heat and this kind of transformation is not accomplished as a result of cryomilling. Cryomilling of caffeine with lactose produced a new DSC thermogram, which

display three endothermic events at 75 °C 147 °C and 219 °C. The region around 147 °C is the area in which unmilled caffeine transforms from Form II to Form I and in which lactose loses its crystalline water content. Cryomilling of these two materials individually displays no endothermic events in this region. Mechanical mixing of the substances might result in homogeneous mixture formation, which tends to behave as eutectic mixture. These melting DSC peaks observed with the first one seen at a lower temperature, could be attributed to the melting of eutectic, while the second, at a higher temperature, corresponded to the melting of the mixture which was not included in the eutectic mixture formation process.

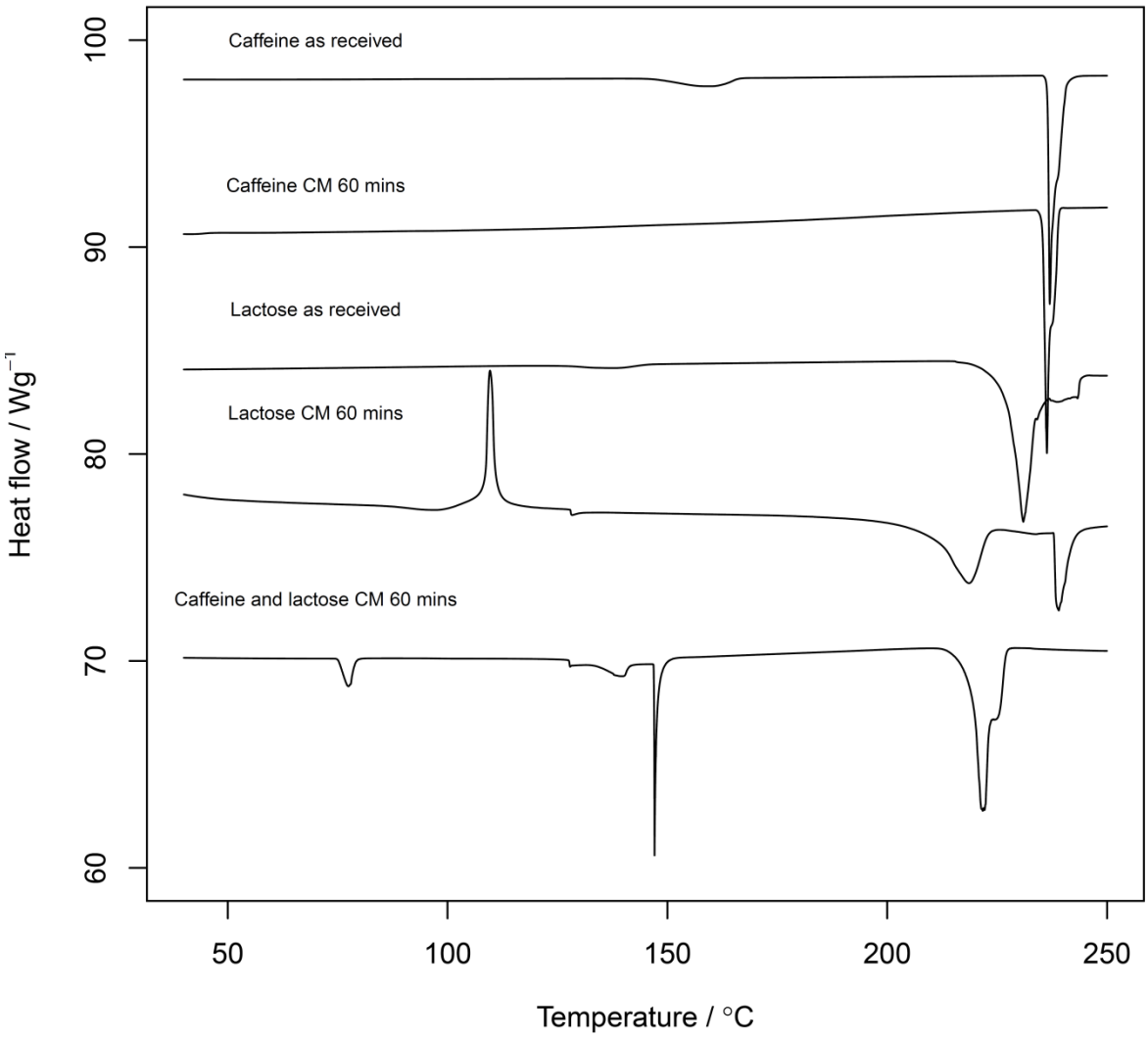
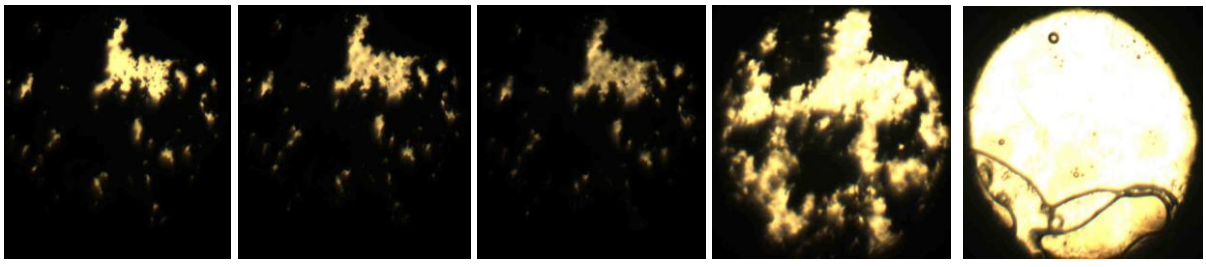


Figure 61: DSC thermograms of caffeine and lactose before and immediately after cryomilling and a 50:50% w/w mixture of caffeine and lactose cryomilled together for 60 minutes. Data have been offset by 7 Wg^{-1} for presentational purposes.



25 °C 150 °C 160 °C 220 °C 230 °C

Figure 62: Hot-stage microscope images of cryomilled 50:50% w/w mixture of caffeine and lactose.

XRPD pattern of caffeine and lactose seen in Figure 63 shows a reasonably wider Bragg peaks than the ones noticed for the cryomilled pure caffeine sample. New additional peaks were identified in the region between 15°-25° indicating that co-cryomilling of caffeine and lactose together produces a synergistic effect. It therefore shows that cryogenic milling of both materials leads to a reduction in crystallinity for both reagents, as well as producing a new XRPD trace that cannot be justified in terms of a linear mixture of lactose and caffeine. A new material appears to have been formed which might be nano-sized co-crystal of lactose and caffeine. As a result, co-cryomilling has produced a very significant effect on the crystal structure of lactose and caffeine mixture that has not been reported before.

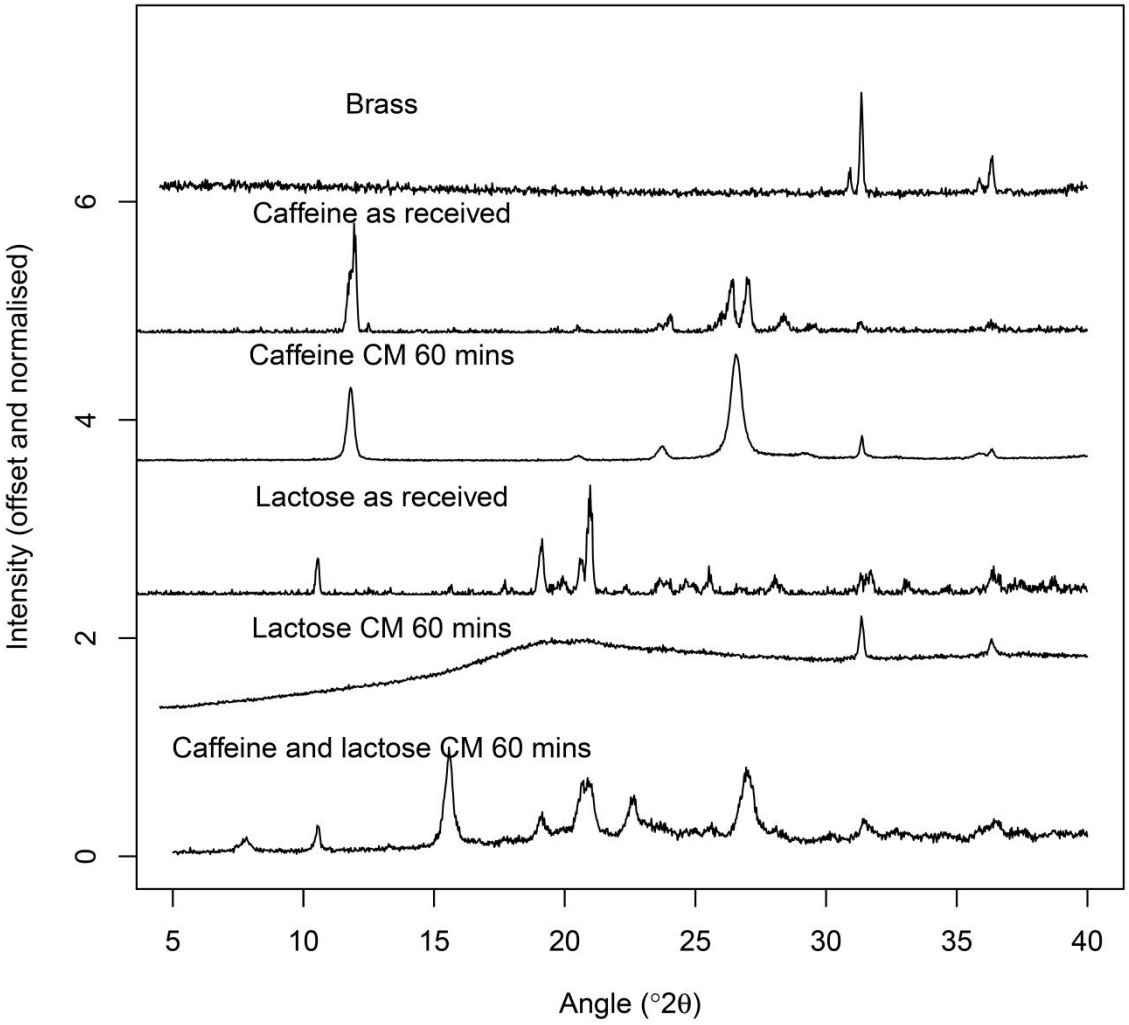


Figure 63: XRPD patterns collected at room temperature for caffeine, lactose before and after cryomilling and a cryomilled 50:50% w/w mixture of caffeine and lactose. The data have been scaled and offset for clarity.

4.3.3. Sucrose

4.3.3.1. Sucrose and aspirin

DSC thermograms for sucrose and aspirin before and immediately after cryomilling, along with the cryomilled mixture of both materials are shown in Figure 64. It is clearly apparent from a visual review that milling of sucrose under cryogenic conditions changes the solid state of the material.

Unmilled sucrose shows a melting onset of 188 °C and an enthalpy of fusion of 109 J/g which is considered to be higher by only by 2 °C than the onset values reported by Hurtta and co-workers (186 °C) (193), who used the same heating rate used in the current work. As a result of cryomilling, a T_g was observed at 71°C followed by a significantly sharp recrystallization exotherm at 98 °C and a broad melting points divided in to two steps with peak maxima at 111 °C and 130 °C. Cryomilling of sucrose has been reported to produce a T_g on the DSC thermogram at 71 °C (4, 204). Furthermore, the obvious reduction in sucrose melting point is possibly attributed to either particle size reduction or decomposition. It has been reported that losing the crystal structure of sucrose leads to its decomposition even before its melting point (205). In a previous study, the difference between the melted and cryomilled sucrose was investigated and it was concluded that amorphous sucrose produced by cryomilling did not go through a melting step and a direct crystal to amorphous transformation was presented (204).

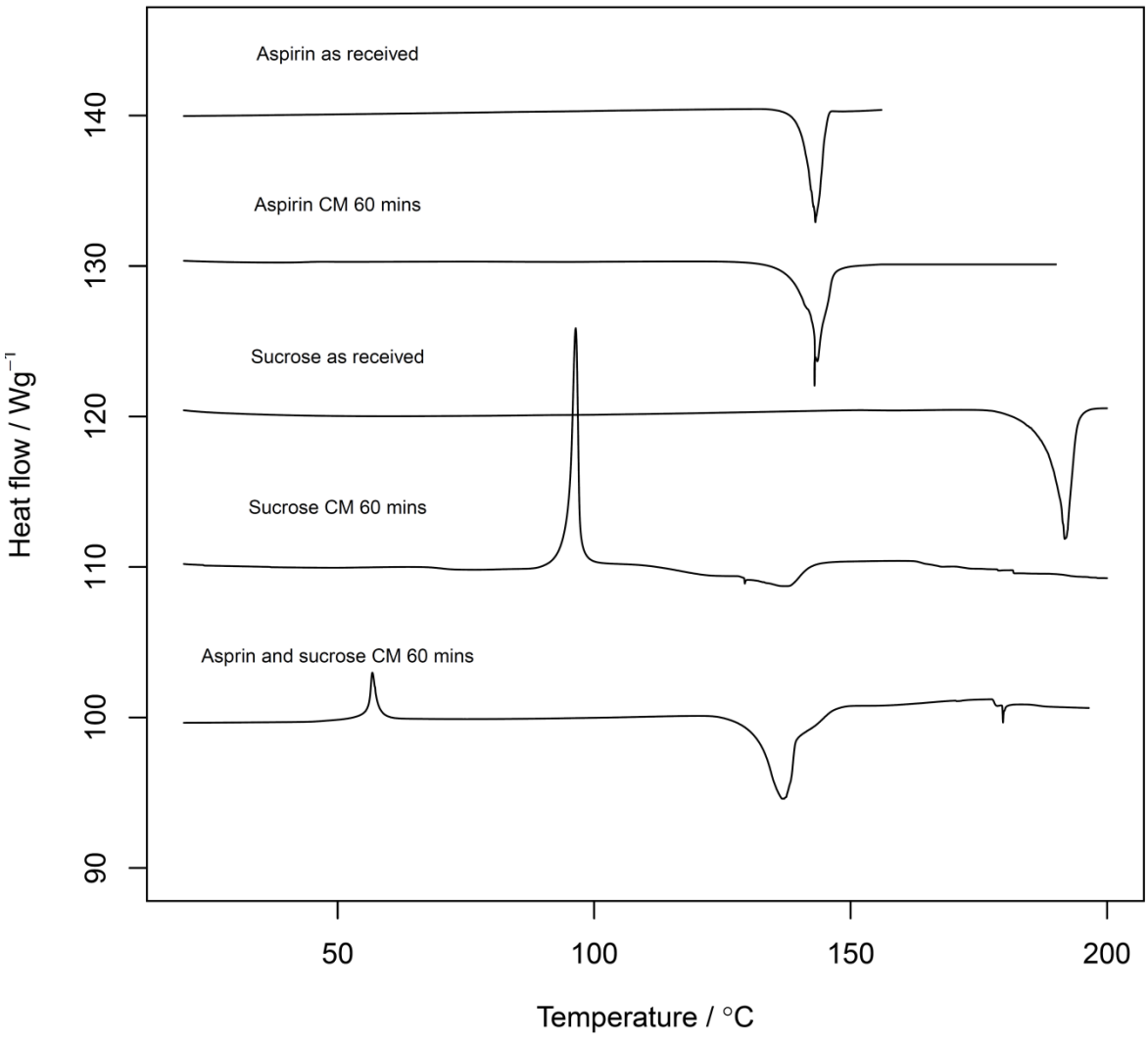


Figure 64: DSC thermograms of aspirin and sucrose before and immediately after cryomilling and a 50:50% w/w mixture of aspirin and sucrose cryomilled together for 60 minutes. Data have been offset by 10 Wg^{-1} for presentational purposes.

As per the cryomilled mixture of aspirin and sucrose, recrystallization was noticed with peak maxima at 57 °C followed by a melting peak with an onset of 131 °C and an enthalpy of fusion of 130 J/g. another small melting peak was detected at 179 °C. The appearance of a recrystallization peak indicates amorphous transformation which the data in Figure 64 presents.

XRPD patterns for unmilled, cryomilled aspirin, sucrose, recrystallised cryomilled sucrose, and 50:50 w/w mixture of aspirin and sucrose cryomilled together for 60 minutes are shown in Figure 65. The as received material was found to match the recrystallized sample which confirmed that

cryomilling does not cause any decomposition to the sample. Co-cryomilling of aspirin and sucrose produced relatively broad Bragg peaks multiple peaks which represent the individually cryomilled aspirin and sucrose and a couple of small new peaks which might suggest that co-cryomilling of aspirin with sucrose would generate some kind of nano-sized co-crystals that is presented in this current work for the first time.

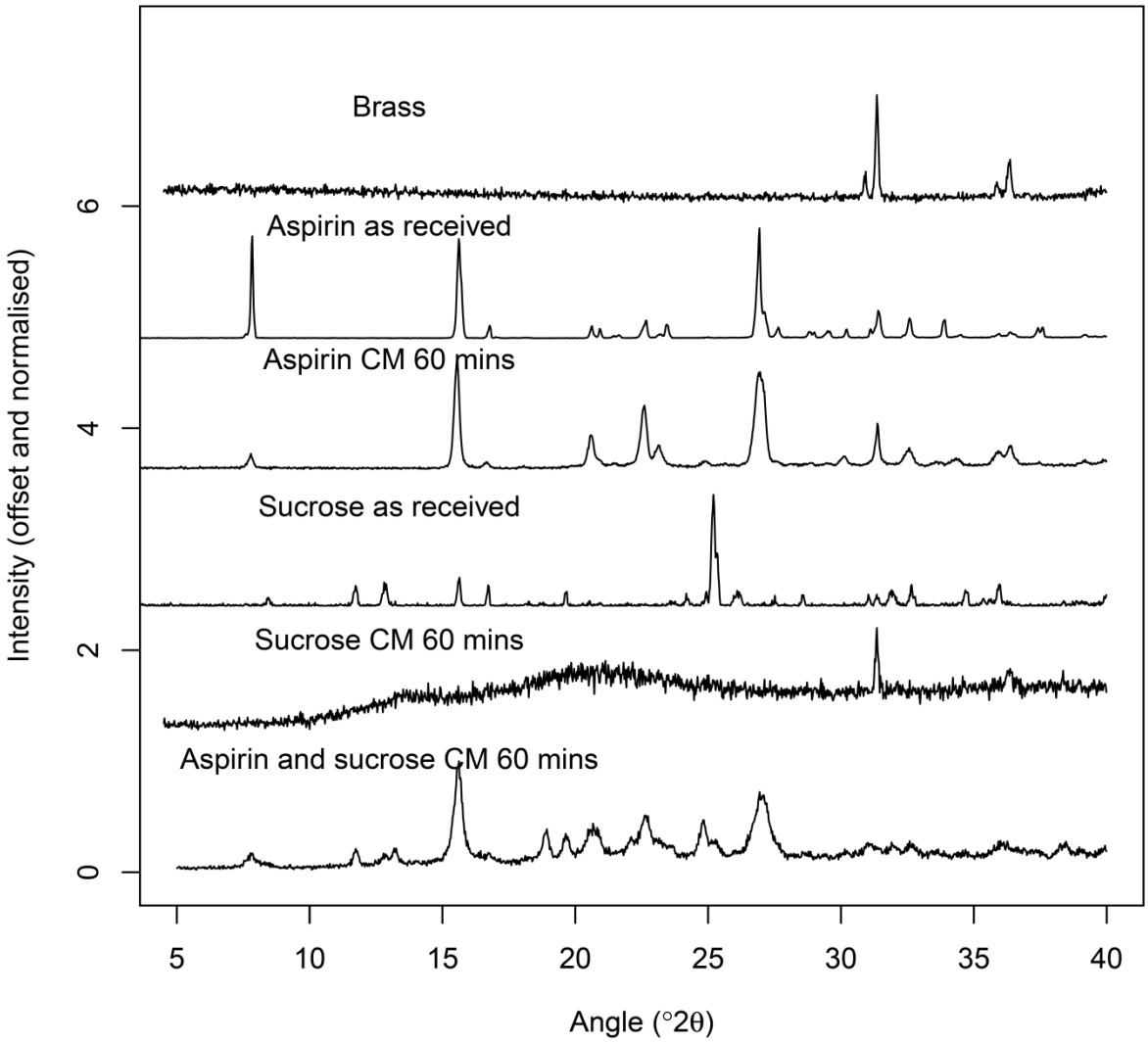


Figure 65: XRPD patterns collected at room temperature for aspirin, sucrose before and after cryomilling and a cryomilled 50:50% w/w mixture of aspirin and sucrose. The data have been scaled and offset for clarity.

FTIR was employed to investigate the possibility of sample sucrose degradation as a result of cryomilling. Spectra for unmilled and cryomilled sucrose are shown in Figure 66. It can clearly be seen that the spectra of the as received material and the cryomilled material are relatively identical it terms of peak positions. The reduction in the peaks sharpness indicates the amorphous transformation (206). The FTIR spectra suggest that sucrose went through crystal to amorphous transformation and no chemical decomposition took place.

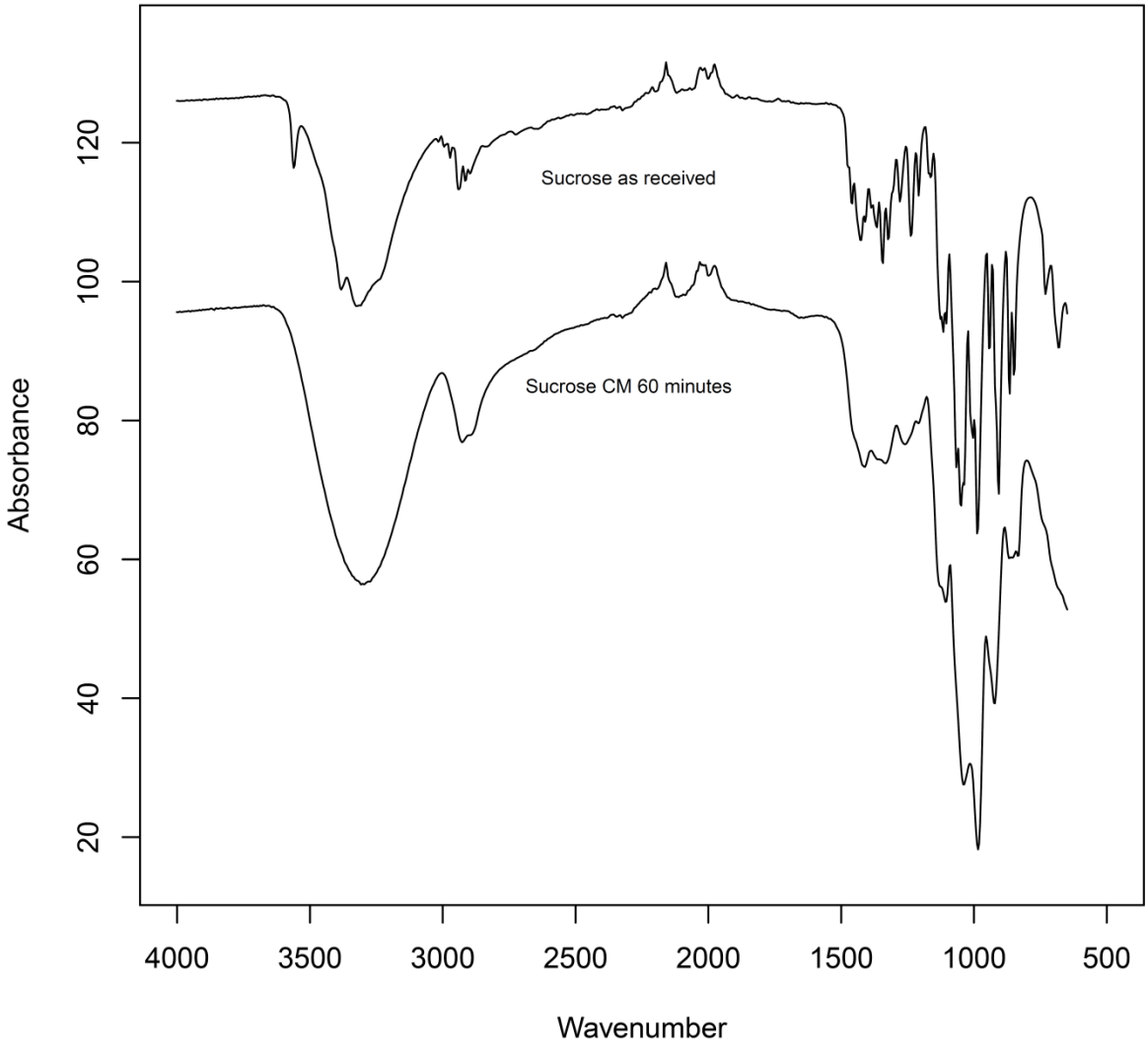


Figure 66: The FTIR spectra of sucrose as received and immediately after cryomilling for 60 minutes.

Furthermore, it can be seen from a visual inspection of the images shown in Figure 67, that melting of sucrose leads to a noticeable and clear colour change which is not detected on the cryomilled sample. On melting and cooling, sucrose changes from white solid to a brown solid.



Unmilled sucrose | Cryomilled sucrose | Melt-quenched sucrose

Figure 67: Images of unmilled sucrose, after cryomilling and after melt-quenching.

4.3.3.2. Sucrose and paracetamol

The DSC thermogram resulted from co-cryomilling paracetamol with sucrose is shown in Figure 68, along with individually milled and unmilled sucrose and paracetamol samples. As mentioned earlier, cryomilling of sucrose results in changing the solid state of the material and causes an amorphous transformation which is confirmed by the appearance of a T_g and a recrystallisation peak. On the other hand, cryomilling of paracetamol produced only a melting peak with an onset of 167 °C and an enthalpy of fusion of 184 J/g. Co-cryomilling both materials together leads to two sharp crystallisation peaks with maxima at 46 °C and 74 °C followed by a single melting peak with a melting onset of 159 °C and an enthalpy of fusion of 142 J/g.

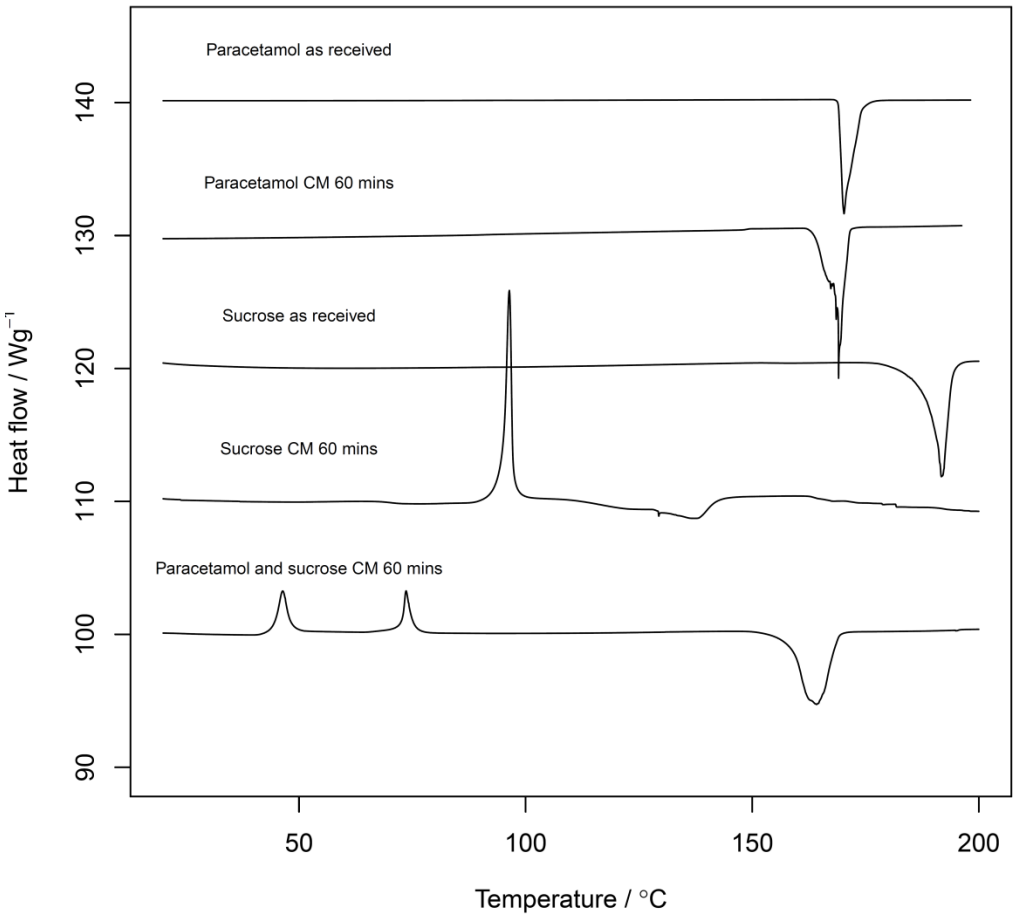


Figure 68: DSC thermograms of paracetamol and sucrose before and immediately after cryomilling and a 50:50% w/w mixture of paracetamol and sucrose cryomilled together for 60 minutes. Data have been offset by 10 Wg^{-1} for presentational purposes.

XRPD trace of paracetamol and sucrose is shown in Figure 69. Multiple Bragg peaks were obtained suggesting some degree of crystallinity. Peaks noticed in the mixture trace are considered to be lower in intensity when compared with the individually cryomilled paracetamol. New peaks were detected signifying the synergistic effect as a result of co-cryomilling both materials together and the formation of a new material.

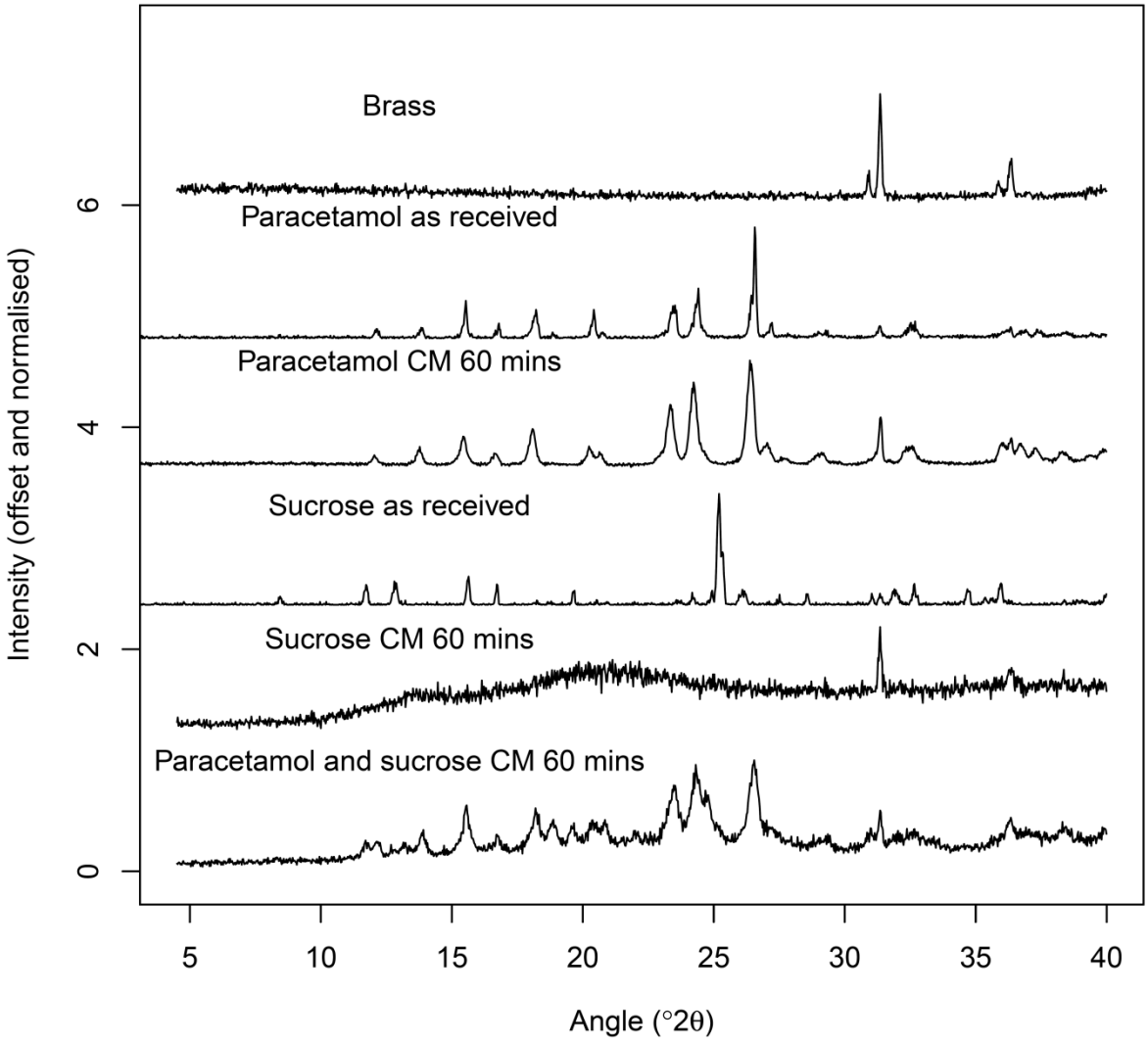


Figure 69: XRPD patterns collected at room temperature for paracetamol, sucrose before and after cryomilling and a cryomilled 50:50% w/w mixture of paracetamol and sucrose. The data have been scaled and offset for clarity.

4.3.3.3. Sucrose and caffeine

DSC overlays of unmilled and cryomilled caffeine, sucrose and a cryomilled mixture containing 50:50% w/w of caffeine and sucrose are shown in Figure 70. All unmilled and individually cryomilled samples showed a single endothermic event except for unmilled caffeine which went through a

polymorphic transformation from Form II to Form I as a result of an increase in temperature. The co-cryomilled mixture showed two endothermic events that were detected at a lower temperature than the pure sucrose and caffeine. This observation suggests that 50:50% w/w mixing ratio could be considered as starting step toward an eutectic mixture formation.

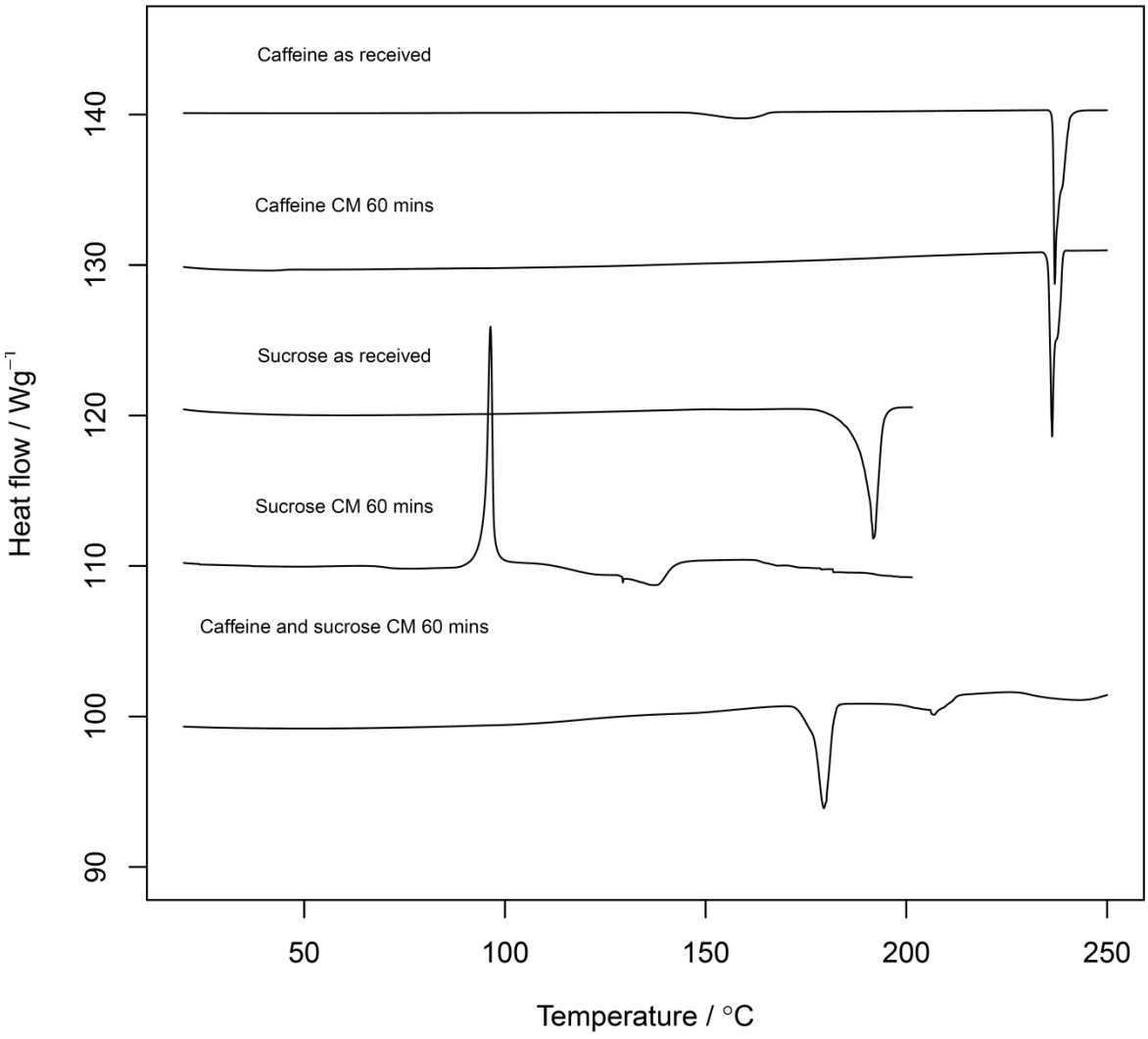


Figure 70: DSC thermograms of caffeine and sucrose before and immediately after cryomilling and a 50:50% w/w mixture of caffeine and sucrose cryomilled together for 60 minutes. Data have been offset by 10 Wg^{-1} for presentational purposes.

XRPD trace of caffeine and sucrose seen in Figure 71 showed relatively wider Bragg peaks than the ones detected for the cryomilled pure caffeine

sample. Extra peaks were detected in the region between 18° to 24° suggesting that cryomilling of caffeine and sucrose together produces a synergistic effect. It therefore appears that co-cryomilling of both materials led to an obvious reduction in crystallinity for both reagents, as well as producing a new XRPD trace that cannot be described in terms of a linear combination of sucrose and caffeine. A new material appears to have been produced. This material could be sucrose and caffeine nano-sized co-crystal. As a result, co-cryomilling produced a very significant effect on the crystal structure of sucrose and caffeine mixture that has not been reported before.

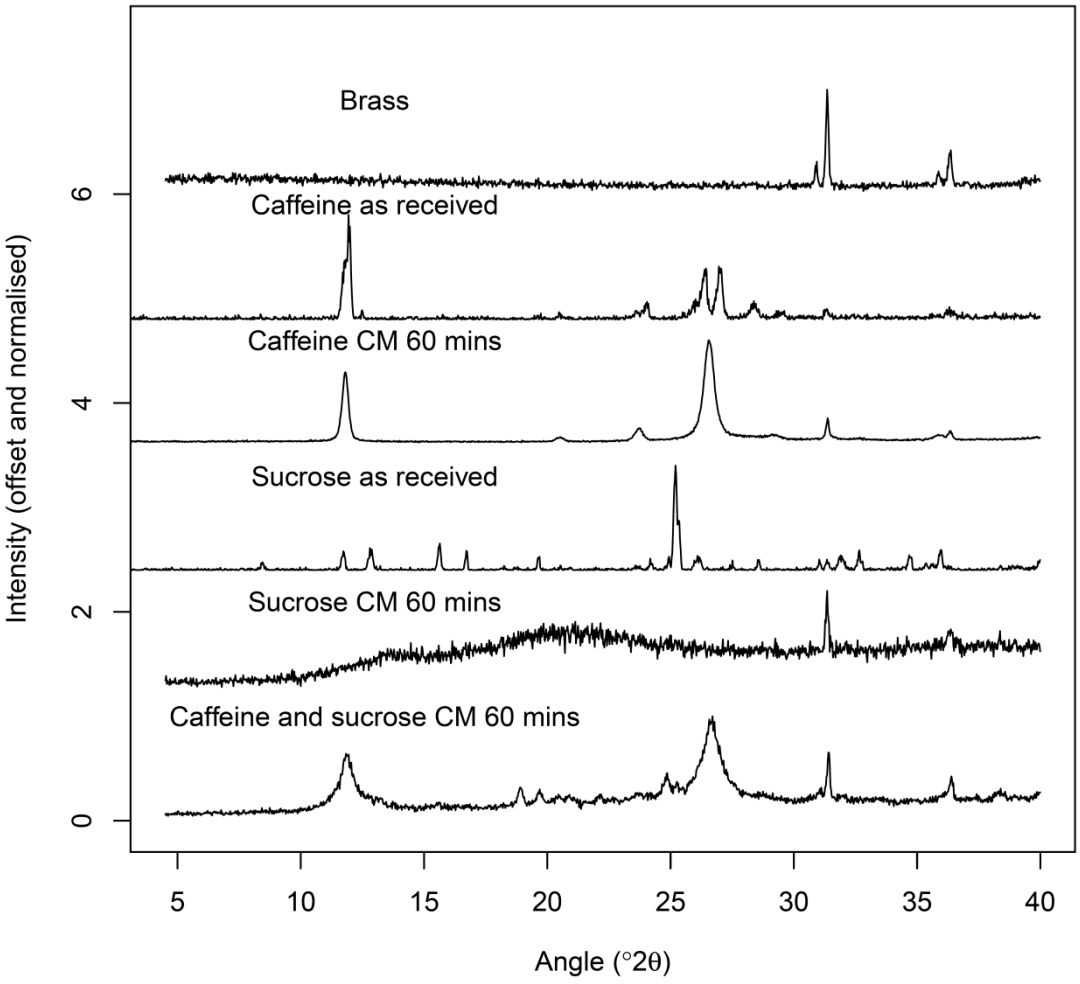


Figure 71: XRPD patterns collected at room temperature for caffeine, sucrose before and after cryomilling and a cryomilled 50:50% w/w mixture of caffeine and sucrose. The data have been scaled and offset for clarity.

4.3.4. D-(+)-Trehalose dihydrate

4.3.4.1. D-(+)-Trehalose dihydrate and aspirin

DSC thermograms for unmilled and cryomilled trehalose dihydrate, aspirin and a mixture of both materials are shown in Figure 72. It is clearly obvious from visual examination of these data that cryomilling transformed the solid state of trehalose dihydrate. Before cryomilling, the thermogram for the crystalline material showed a single endothermic peak at 96 °C, which agrees with the reported values (198). Other researches have reported a second endothermic event before the actual melting point (93 °C), which was attributed to water loss (198). After cryomilling of the pure trehalose dihydrate for 60 minutes, the DSC thermogram showed a T_g with mid-point at 26 °C, an exothermic peak which was attributed to recrystallization of liquid trehalose dihydrate at 53 °C followed by an endotherm with an onset at 89 °C. The position of the T_g was slightly higher than the value reported with a T_g detected at 20 °C achieved by quench-cooling the crystalline material (195). The detection of a single T_g is a clear sign of amorphous transformation.

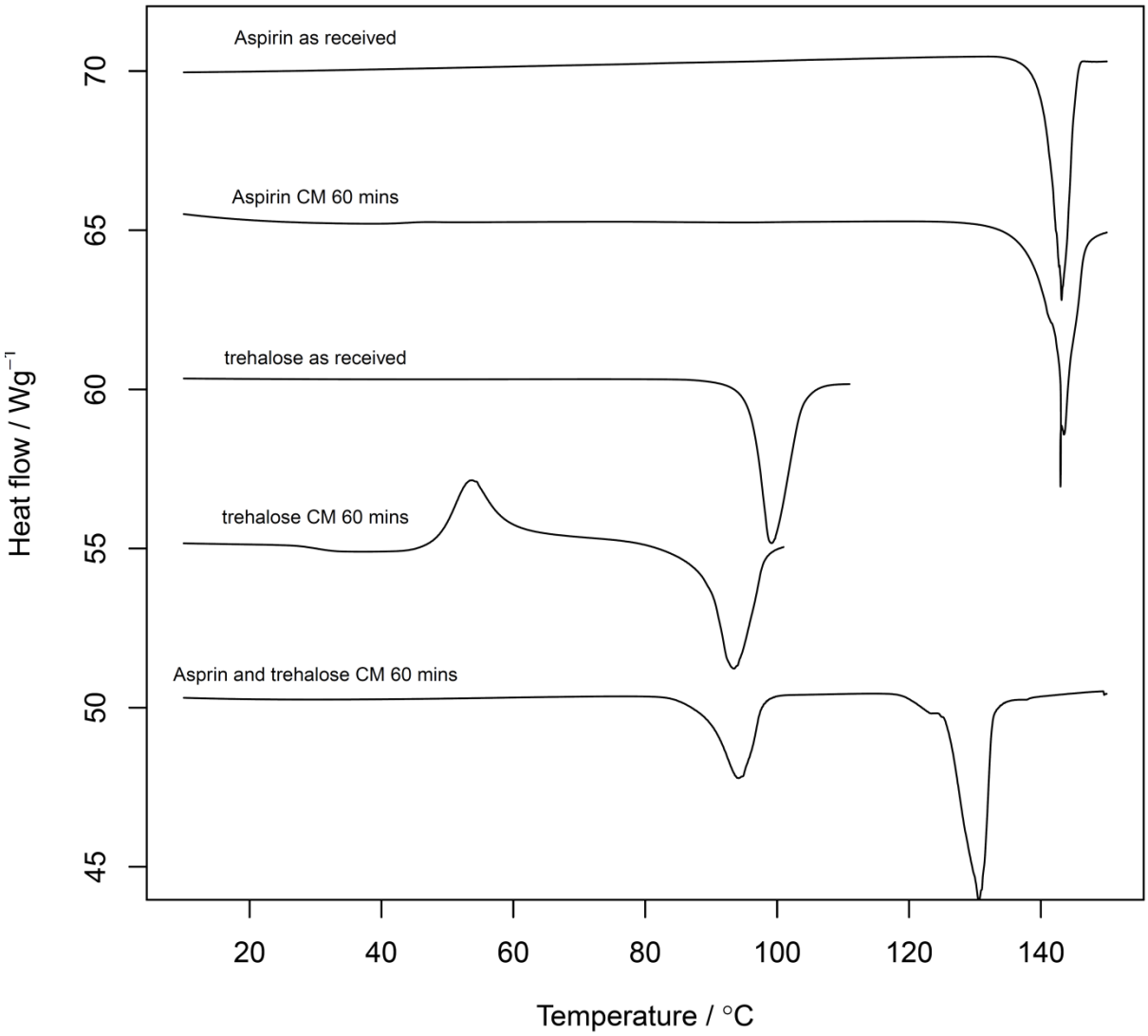


Figure 72: DSC thermograms of aspirin and trehalose dihydrate before and immediately after cryomilling and a 50:50% w/w mixture of aspirin and trehalose dihydrate cryomilled together for 60 minutes. Data have been offset by 5 Wg^{-1} for presentational purposes.

DSC data resulted from co-cryomilling aspirin and trehalose dihydrate showed two endothermic events with the absence of T_g and recrystallization peak. The two melting peaks represent trahalose dihydrate and aspirin, suggesting that cryomilling of aspirin with trehalose would hinder amorphous transformation of the latter reagent. A reduction in the melting point of aspirin by 15 °C was also noticed.

The XRPD data collected for trehalose dihydrate, aspirin and cryomilled mixture of both materials are shown in Figure 73. Concerning the unmilled trehalose dihydrate sample, the XRPD pattern showed multiple sharp Bragg peaks confirming the crystalline nature of the material.

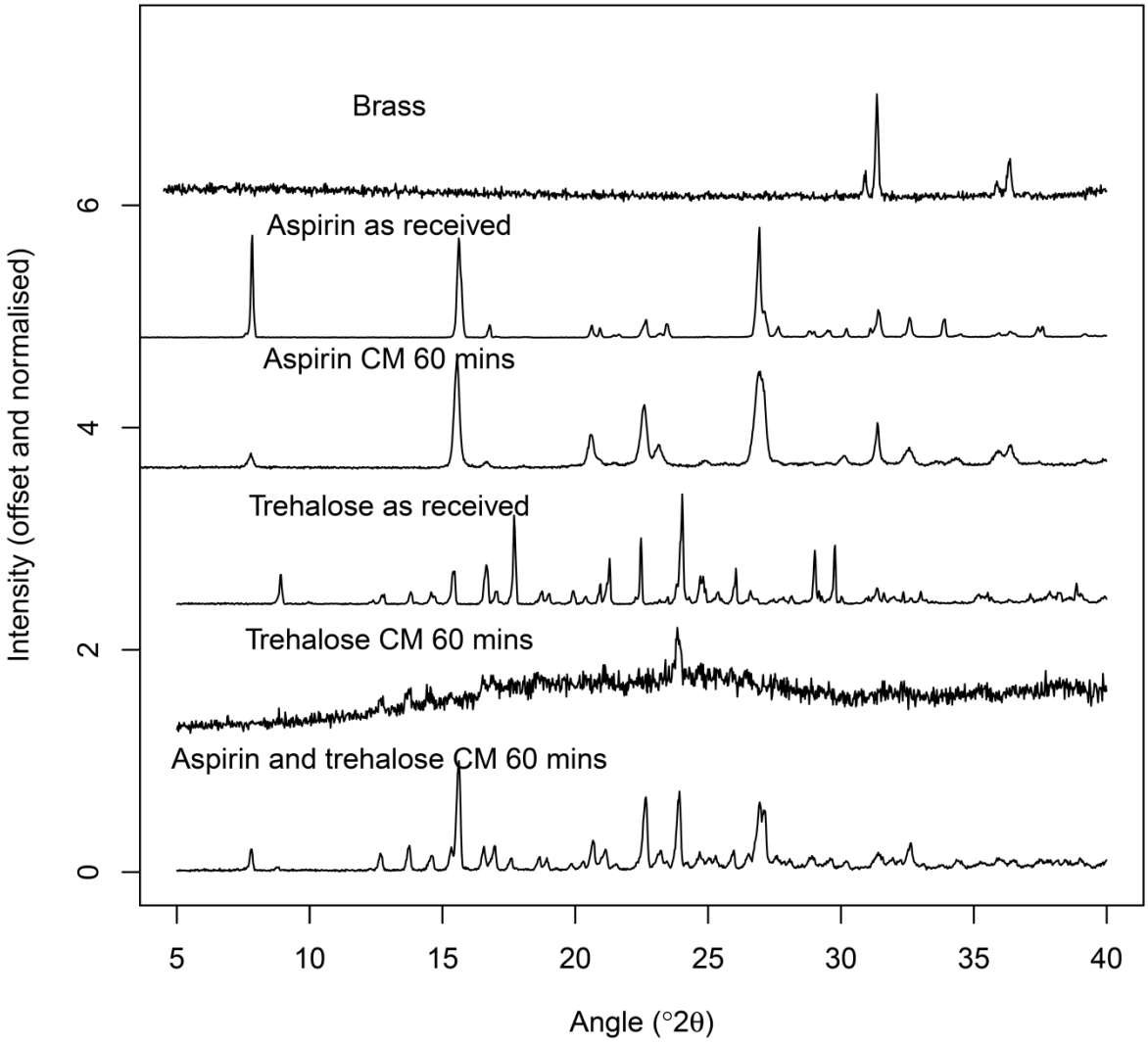


Figure 73: XRPD patterns collected at room temperature for aspirin, trehalose dihydrate before and after cryomilling and a cryomilled 50:50% w/w mixture of aspirin and trehalose dihydrate. The data have been scaled and offset for clarity.

After cryomilling for 60 minutes, the XRPD diffuses to an amorphous halo, confirming a crystalline to amorphous transformation as a result of cryogenic grinding. Furthermore, the mixture of aspirin with trehalose

dihydrate XRPD trace showed multiple Bragg peaks which differ in sharpness and width suggesting that crystalline aspirin along with crystalline trehalose dehydrate were detected. This agrees with the results obtained from DSC data of the same mixture suggesting that aspirin suppressed the crystal to amorphous transformation of trehalose dihydrate leading to the production of XRPD trace which closely matched the unmilled materials.

4.3.4.2. D-(+)-Trehalose dihydrate and paracetamol

DSC thermograms for unmilled and cryomilled trehalose dihydrate, paracetamol and a mixture of both materials are shown in Figure 74. Focusing directly on the cryomilled mixture, the absence of T_g was noticed with the appearance of three endothermic peaks with melting onsets of 81 °C, 143 °C, and 169 °C. However, a wide exothermic event was noticed around the region at 63 °C signifying amorphous material in the mixture. It has been reported that trehalose dihydrate can be crystallized to the anhydrate as a result of heating (198). Crystallization behaviour is primarily dependent on the particle size of the crystals.

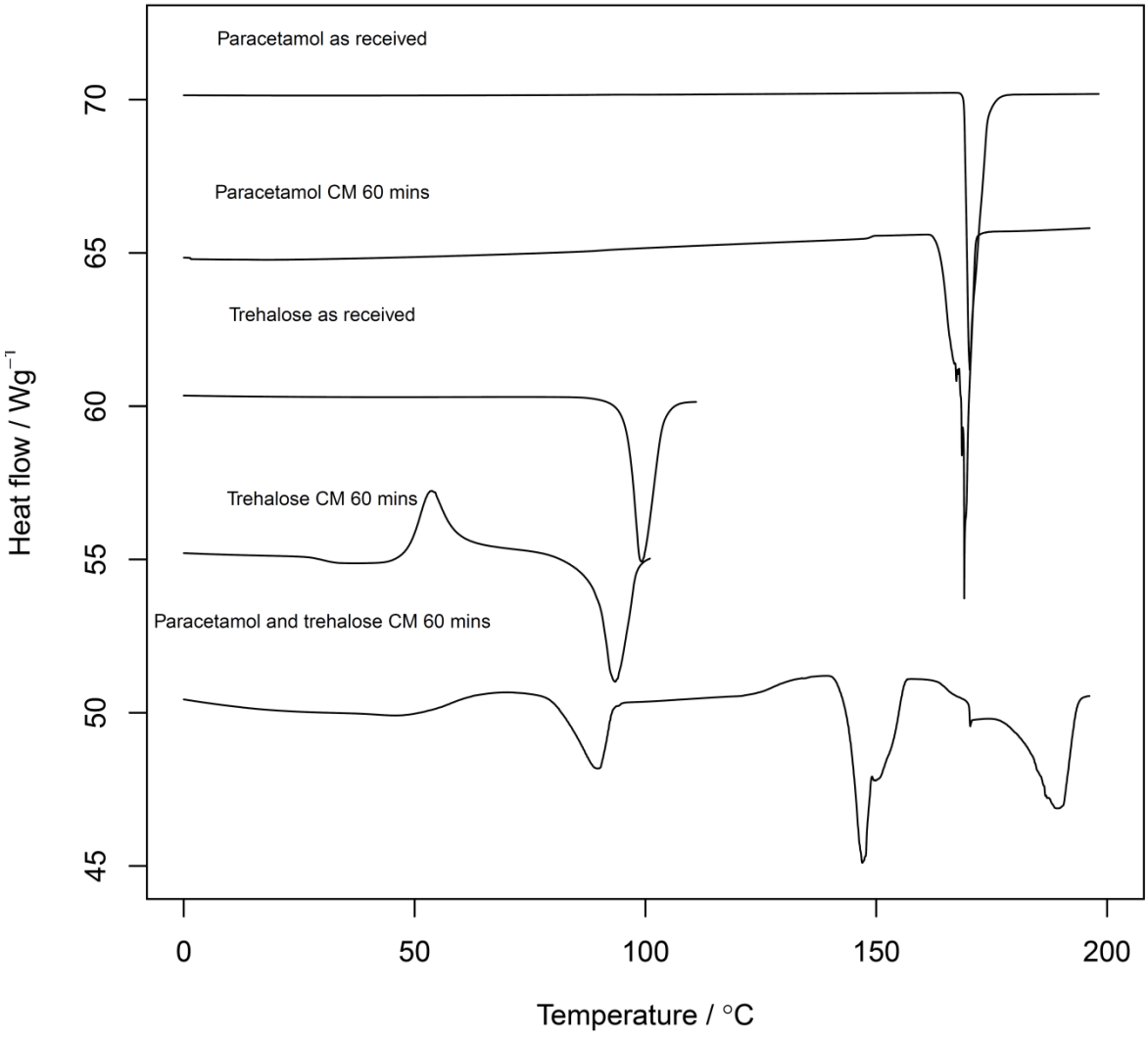


Figure 74: DSC thermograms of paracetamol and trehalose dihydrate before and immediately after cryomilling and a 50:50% w/w mixture of paracetamol and trehalose dihydrate cryomilled together for 60 minutes. Data have been offset by 5 Wg^{-1} for presentational purposes.

As a result of co-cryomilling paracetamol and trehalose dihydrate for 60 minutes the XRPD data seen in Figure 75 showed multiple Bragg peaks which were somewhat broad and less sharp when compared with the unmilled individual materials. The most intense detectable peaks matched the pure cryomilled paracetamol while trehalose dihydrate remained amorphous. It therefore, unlike aspirin, co-cryomilling paracetamol with trehalose dihydrate seems to retain the amorphous properties of the latter material.

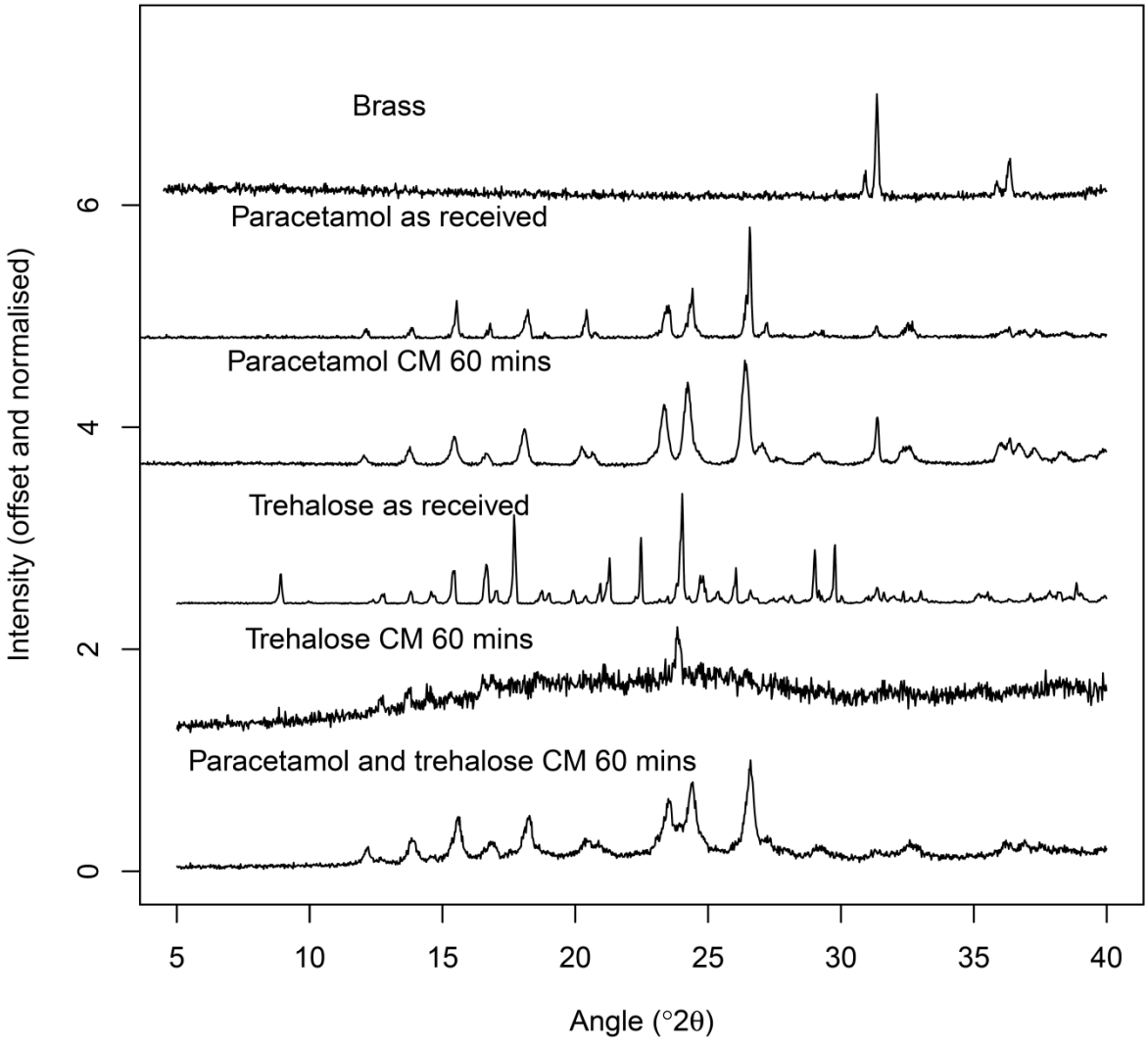


Figure 75: XRPD patterns collected at room temperature for paracetamol, trehalose dihydrate before and after cryomilling and a cryomilled 50:50% w/w mixture of paracetamol and trehalose dihydrate. The data have been scaled and offset for clarity.

4.3.4.3. D-(+)-Trehalose dihydrate and caffeine

DSC thermograms for unmilled and cryomilled trehalose dihydrate, caffeine and a mixture of both materials are shown in Figure 76. Focusing directly on the cryomilled mixture, T_g was not detected and just like with paracetamol, three endothermic peaks with melting onsets of 83 °C 160 °C 209 °C. A small exothermic event is noticed around the region at 63 °C which could be attributed to amorphous material presence in the mixture.

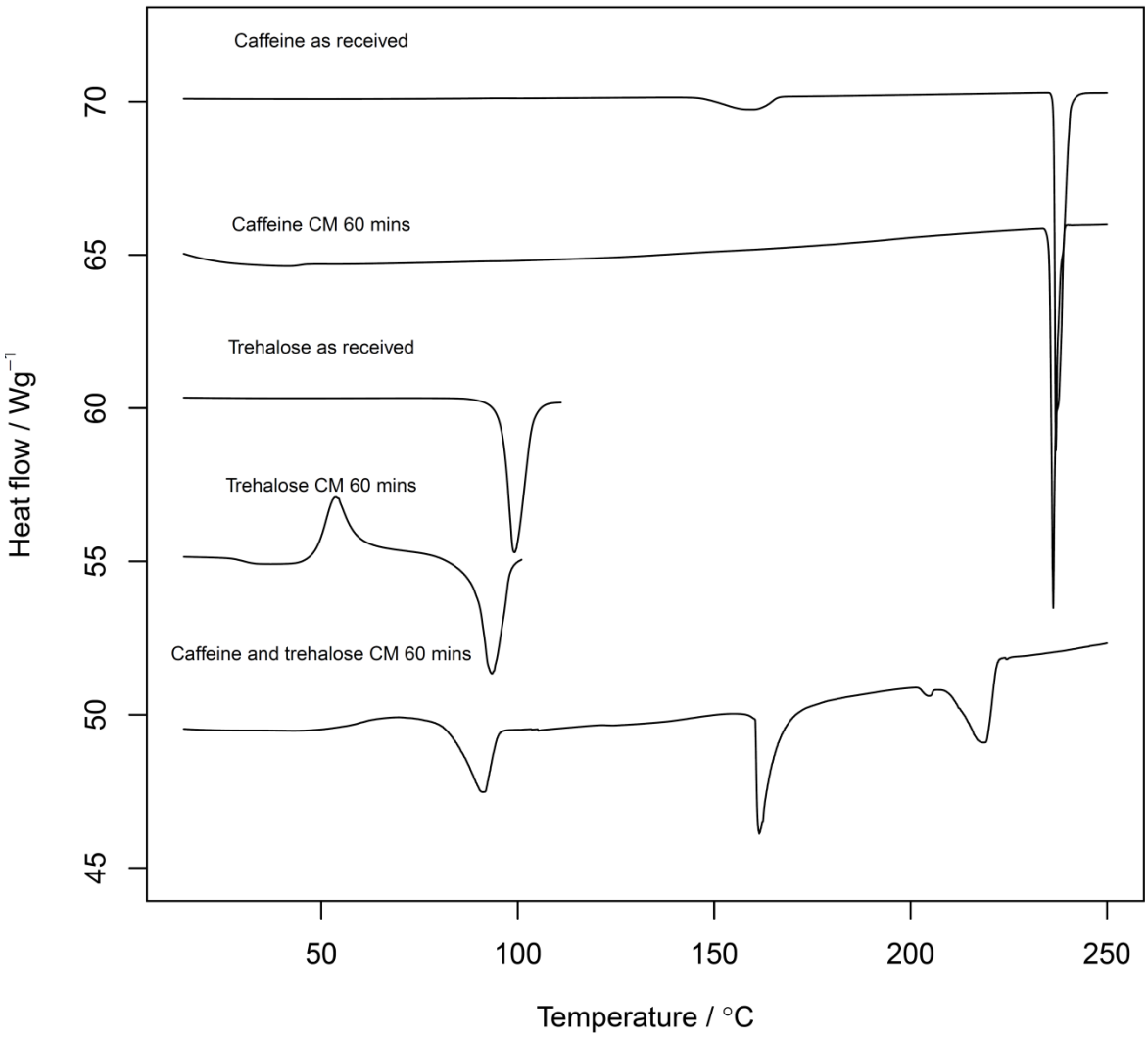


Figure 76: DSC thermograms of caffeine and trehalose dihydrate before and immediately after cryomilling and a 50:50% w/w mixture of caffeine and trehalose dihydrate cryomilled together for 60 minutes. Data have been offset by 5 Wg^{-1} for presentational purposes.

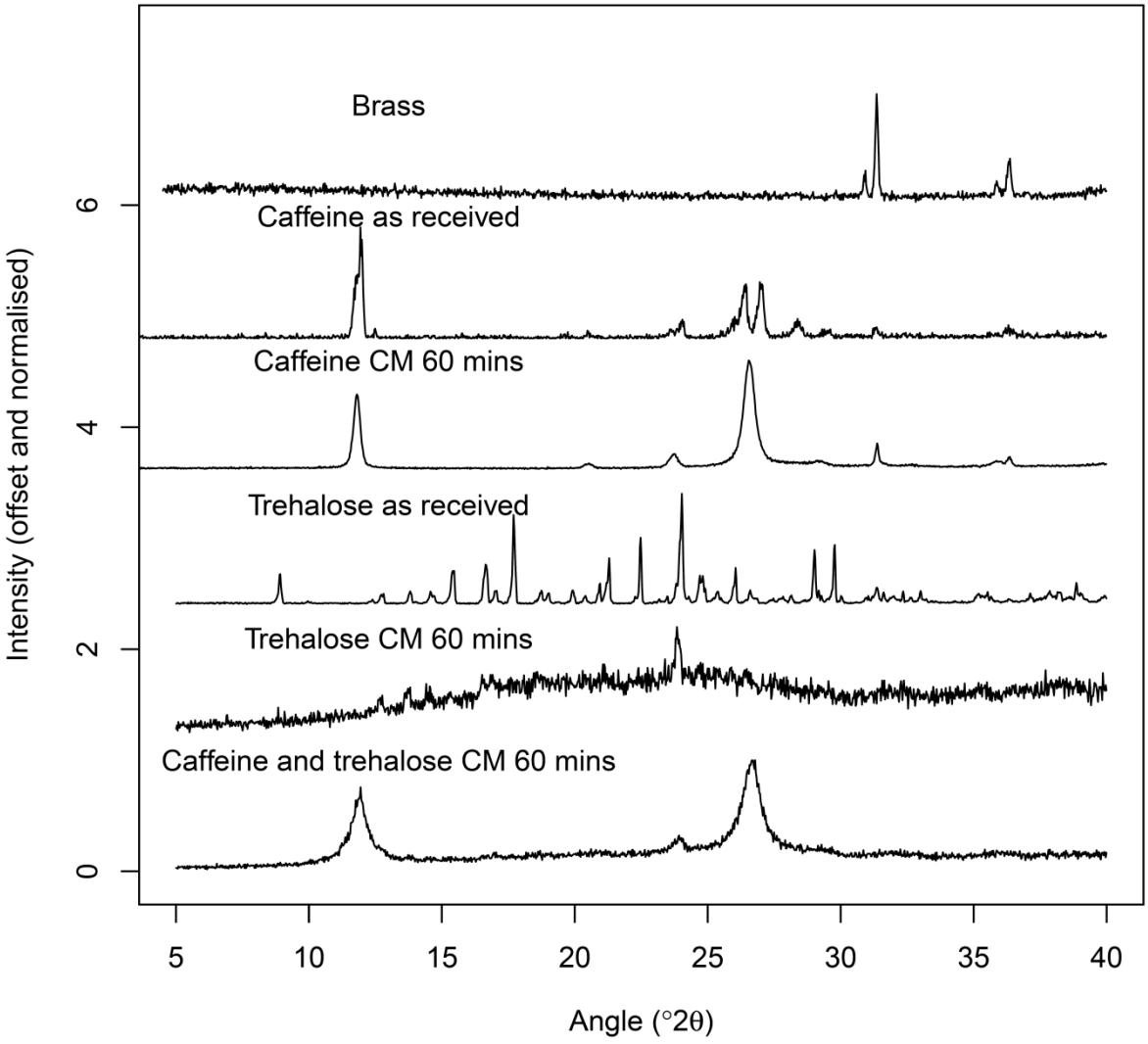


Figure 77: XRPD patterns collected at room temperature for caffeine, trehalose dihydrate before and after cryomilling and a cryomilled 50:50% w/w mixture of caffeine and trehalose dihydrate. The data have been scaled and offset for clarity.

As noticed in the XRPD trace shown in Figure 77 resulted from co-cryomilling trehalose dihydrate with paracetamol. Cryomilling with caffeine produces a trace showing two caffeine peaks with one small peak representing trehalose. The sharp peaks which represented the unmilled excipient are clearly absent from the XRPD trace. All peaks ere considered to be quite broad and few in number. Caffeine seems to not suppress the amorphous transformation of trehalose dihydrate.

4.4. Summary table

	Xylitol	**Lactose monohydrate**	**Sucrose**	**Trehalose dehydrate**
Unmilled				
• **DSC**	T_m 93 °C	Water loss at: 138 °C T_m of α and β at: 217 °C 241 °C	T_m 188 °C	T_m 96 °C
• **XRPD**	Small sharp peaks	Sharp peaks	Sharp peaks	Sharp peaks
Cryomilled				
• **DSC**	T_m 89 °C	T_c 167°C T_m of α and β at: 210 °C 237 °C	T_g 71°C T_c 98 °C T_m 111 °C 130 °C	T_g 26°C T_c 53 °C T_m 89 °C

• **XRPD**	Intense sharp peaks	Amorphous halo	Amorphous halo	Amorphous halo
Aspirin • **DSC**	Two melting peaks: T_m 89 °C T_m 125 °C	T_c 80 °C T_m 127 °C T_m 195 °C	T_c 57 °C T_m 131 °C T_m 179 °C	T_m 88 °C T_m 125 °C
• **XRPD**	➢ No synergistic effect observed ➢ Sharp peaks of xylitol and aspirin ➢ No new peaks detected	➢ No synergistic effect observed ➢ Sharp peaks of lactose and aspirin ➢ No new peaks detected	➢ synergistic effect observed ➢ Broad peaks of sucrose and aspirin ➢ New peaks detected at ~ 18°-25°	➢ No synergistic effect observed ➢ Sharp peaks of trehalose dihydrate and aspirin ➢ No new peaks detected

• **HSM**	Eutectic mixture formation	/	/	/
Paracetamol • **DSC**	Two melting peaks: T_m 86 °C T_m 146 °C	T_c 48 °C T_c 92 °C T_m 159 °C T_m 204 °C	T_c 46 °C T_c 74 °C T_m 159 °C	T_m 81 °C T_m 143 °C T_m 169 °C
• **XRPD**	➢ No synergistic effect observed ➢ Relatively sharp peaks of xylitol and paracetamol	➢ Broad halo, with few peaks indicating partially crystalline ➢ paracetamol	➢ synergistic effect observed ➢ Broad peaks of sucrose and paracetamol ➢ New peaks detected at	➢ No synergistic effect observed ➢ Broad peaks of only paracetamol, trehalose dihydrate

• **HSM**	➢ No new peaks detected /	co-soluble liquids are formed at ~ 220 °C	~ 12°-18°-19° /	remains amorphous ➢ No new peaks seen /
Caffeine • **DSC**	Two melting peaks: T_m 84 °C T_m 179 °C	T_m 75 °C T_m 147 °C T_m 219 °C	T_m 176 °C T_m 205 °C	T_c 63 °C T_m 83 °C T_m 160 °C T_m 209 °C

• **XRPD**	➢ No synergistic effect observed ➢ Broad peaks of xylitol and caffeine ➢ No new peaks detected	➢ synergistic effect observed ➢ Broad peaks of lactose and caffeine ➢ New peaks detected at ~ 15°-25°	➢ synergistic effect observed ➢ Broad peaks of sucrose and caffeine ➢ New peaks detected at ~ 18°-24°	➢ No synergistic effect observed ➢ Broad peaks of caffeine, trehalose dihydrate remains amorphous ➢ No new peaks detected
• **HSM**	/	co-soluble liquids are formed at ~ 230 °C	/	/

Table 18: Summary table of research work in Chapter 4.

4.5. Discussion

4.5.1. Milling temperature

Dehydration is one of the possible strategies adopted in order to produce an amorphous material. In this chapter, two forms of hydrates were studied, trehalose dihydrate and lactose monohydrate. A rapid removal of water from trehalose dihydrate has been shown to produce a glassy amorphous anhydrous phase (207). In the current work, amorphous trehalose dihydrate was successfully produced as a result of particle size reduction induced by cryomilling. Furthermore, T_g detected was in good agreement was previous literature indicating the presence of pure trehalose dihydrate (195), since the T_g value for anhydrated form is 116.9 °C (208), and if the sample went through a dehydration process, than the T_g value is probably expected to be detected at an intermediate region between both forms. Similarly, amorphous material was formed when alpha lactose monohydrate was milled at room temperature. This transformation was achieved in the current work as well when lactose was cryomilled for 60 minutes. The common factor between trehalose dihydrate and lactose monohydrate is in the position of T_g. Researchers have reported that the temperature of milling relative to the T_g is critical to the crystal to amorphous transformation process (200). Therefore, The T_g values for both materials are higher than room temperature which makes it possible to form an amorphous material on room temperature milling.

In the current work, all the experiments were conducted under extremely low temperature during cryogenic milling to establish the suitable

atmosphere for crystal to amorphous transformation. All materials were milled at a temperature lower than their actual T_g values (T_g range -26 °C, 20 °C,50 °C ,71 °C). Amorphous material was observed with sucrose, trehalose dehydrate and lactose. Xylitol is believed to have fairly low T_g Value (-26 °C) which make it possible to form an amorphous material inside the vial during the cryomilling process, and because the sample characterisations usually are carried out at room temperature, allowing the sample to recrystallize rapidly.

A reduction in melting points was observed in this chapter as well and it has been discussed in the previous chapter by studying the binary mixtures of aspirin-paracetamol, paracetamol-caffeine and aspirin-caffeine. One of the most crucial reasons for melting point reduction, especially with thermolabile substances is chemical decomposition. From the list of the four excipients investigated in this chapter, sucrose is considered to be the most thermally sensitive substance. According to the XRPD and FTIR results, sucrose did not undergo any degradation resulting from cryomilling process.

4.5.2. Melting point reduction

A noticeable reduction in the melting points of aspirin, paracetamol and caffeine as a result of co-cryomilling with xylitol, lactose monohydrate, sucrose and trehalose dihydrate. In general, the reduction in the melting points was possibly attributed to several reasons such as, chemical decomposition, polymorphism, impurities, lattice defects, particle size reduction or even could potentially was caused by a mix of both particle size reduction and defects. No evidence of chemical decomposition or polymorphism was observed in the XRPD traces for all mixtures, so both reasons can be certainly ruled out.

The Shroeder-van Laar equation (Equation 1), introduced in Chapter 1 and discussed in Chapter 3, can be employed to predict the melting point of these mixtures. As the hot-stage microscope images for few of the mixtures confirmed that all components are completely miscible in the liquid state and immiscible in the solid state, a phase diagrams of all mixtures calculated using the Shroeder-van Laar equation are shown in figures 78-81.

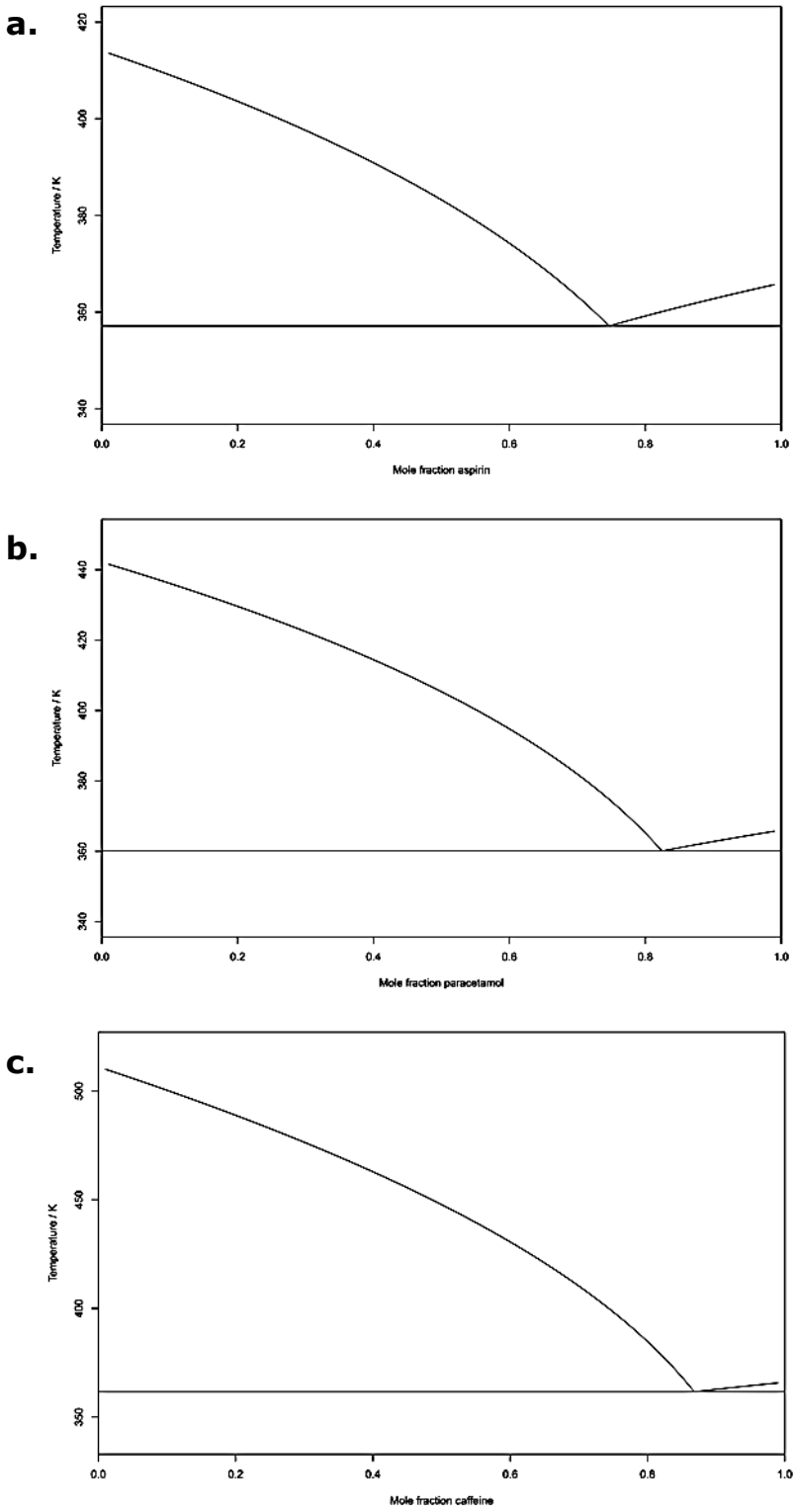


Figure 78: Phase diagrams of xylitol with a. aspirin, b. paracetamol and c. caffeine.

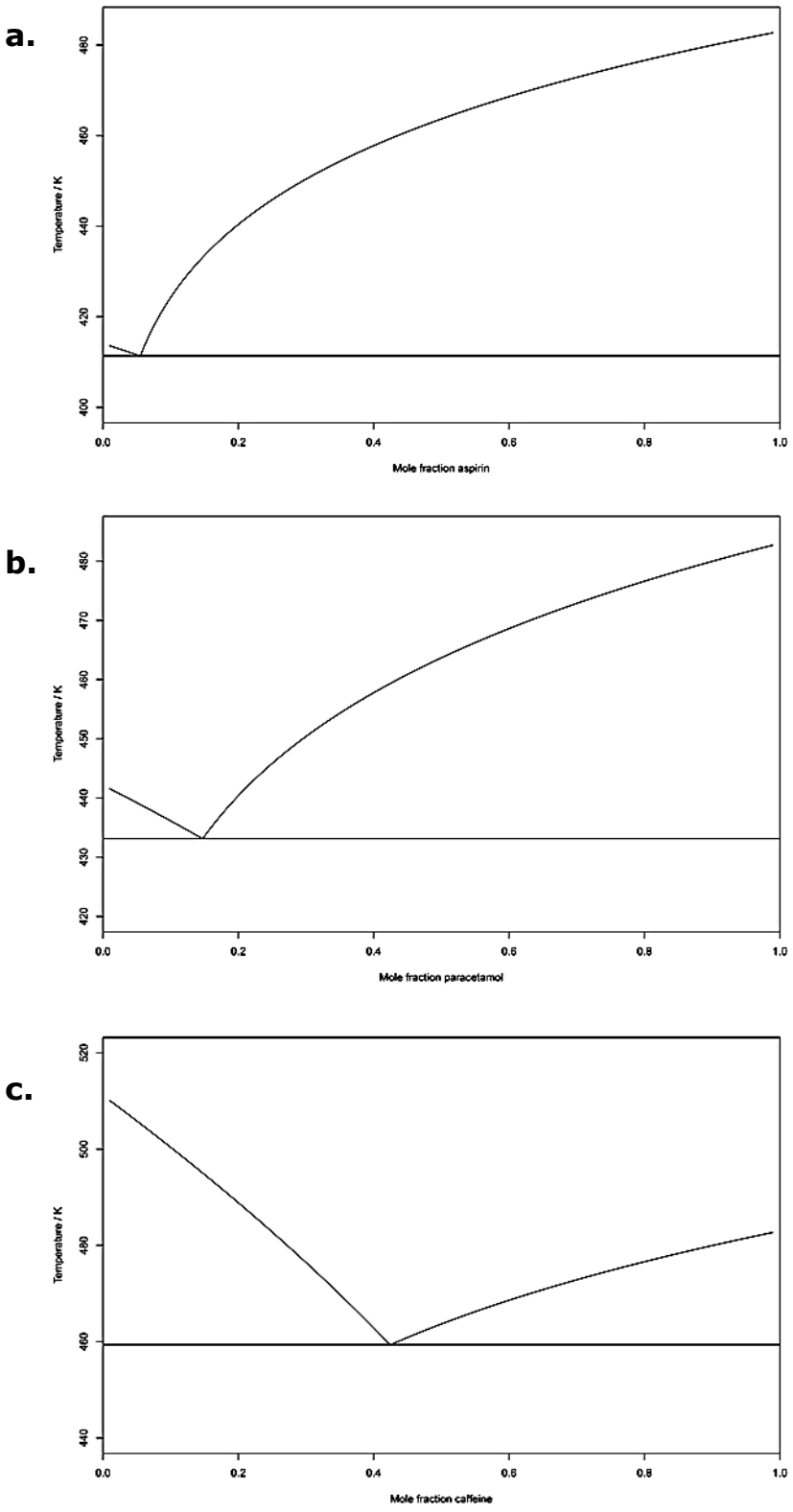


Figure 79: Phase diagrams of lactose monohydrate with a. aspirin, b. paracetamol and c. caffeine.

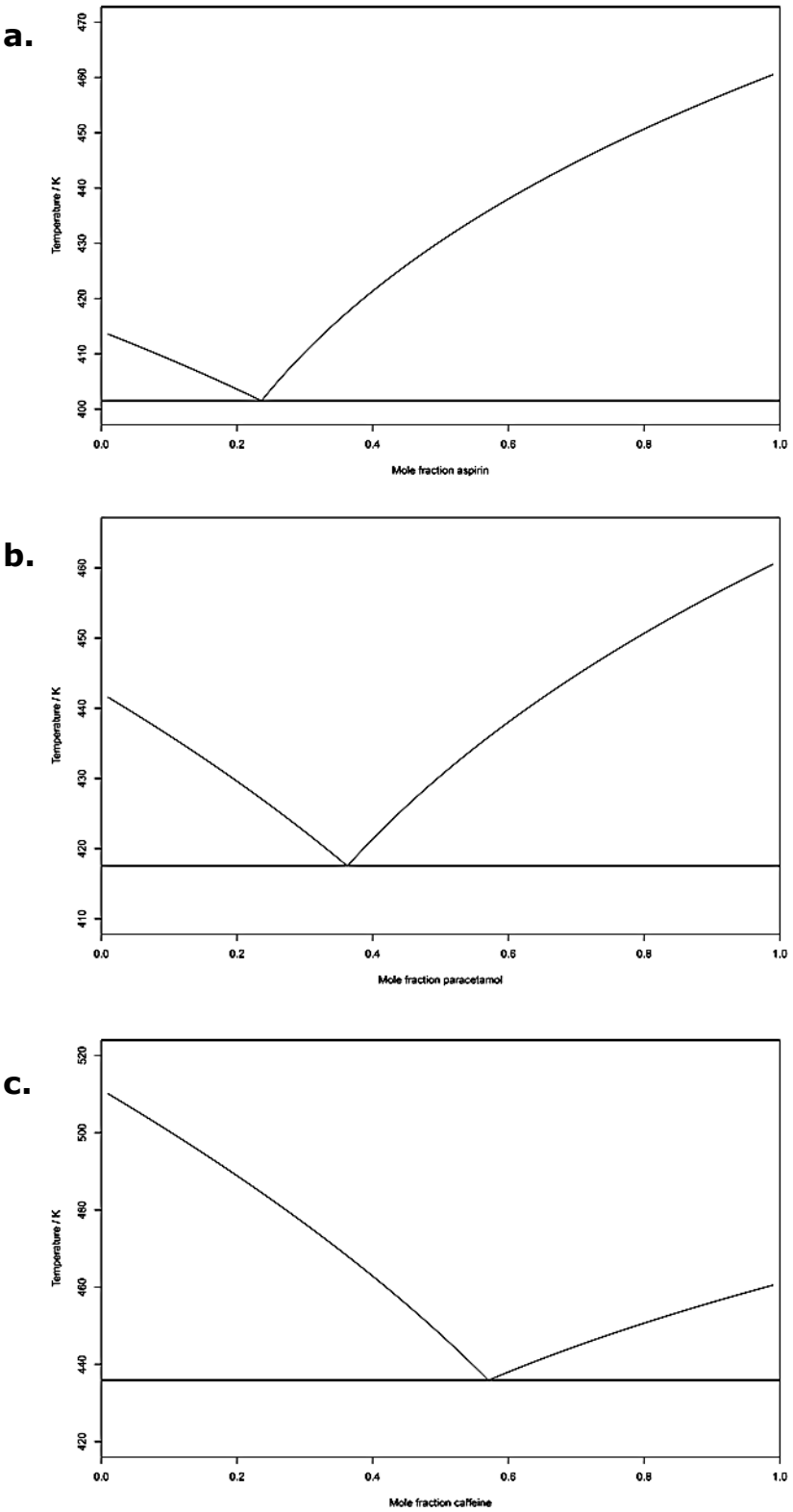


Figure 80: Phase diagrams of sucrose with a. aspirin, b. paracetamol and c. caffeine.

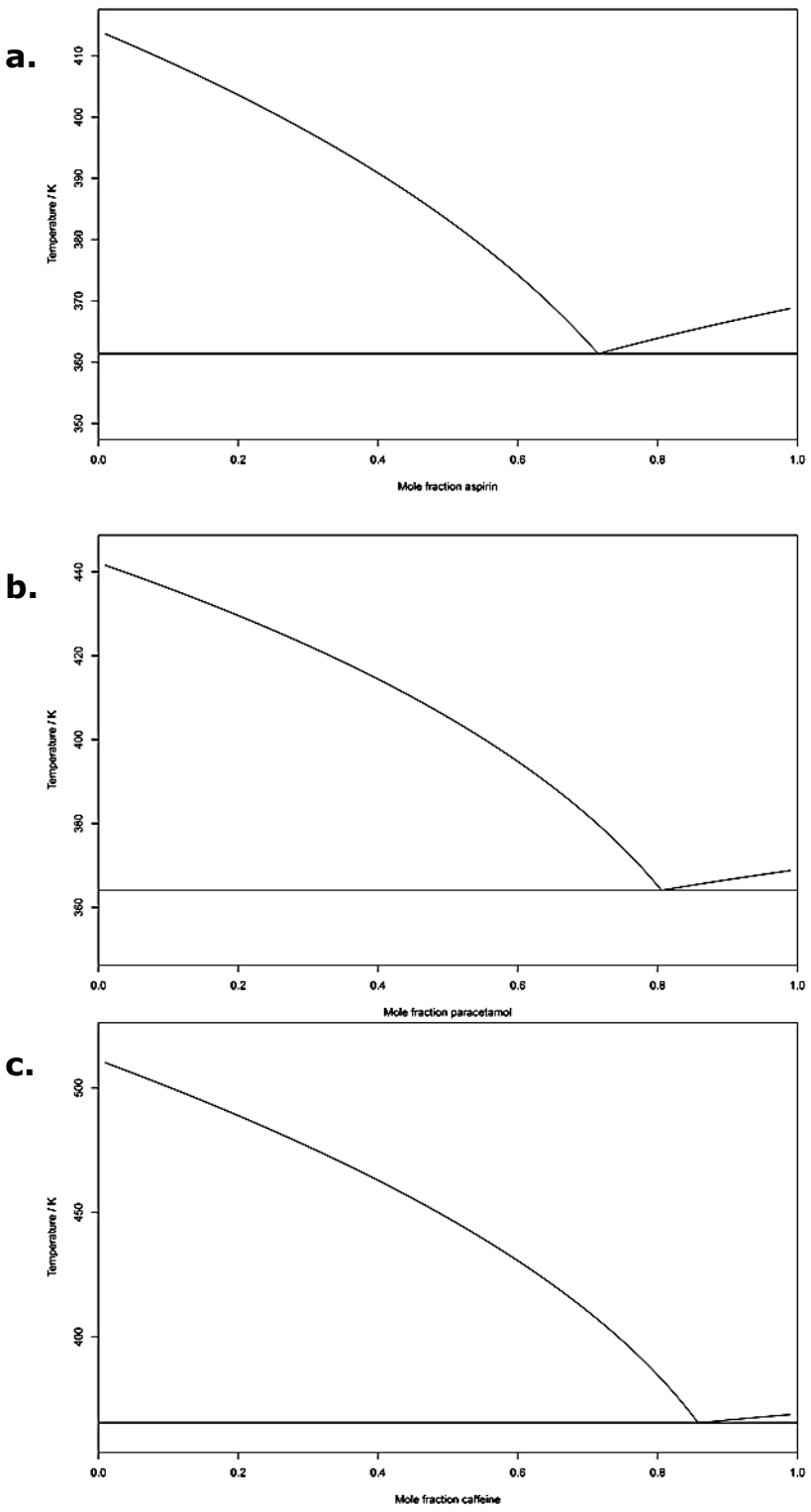


Figure 81: Phase diagrams of trehalose dihydrate with a. aspirin, b. paracetamol and c. caffeine.

The predicted eutectic points of all mixtures at which the two components are forming miscible liquids are found to be estimated at a composition either higher or lower than 50:50% w/w that was used in the current study.

4.6. Conclusion

The preparation of single and multi-component systems by cryomilling has been studied by DSC, XRPD, hot-stage microscope and FTIR. It was found that for the single component systems, a T_g was observed with sucrose, trehalose dihydrate and a recrystallization peak was found in the DSC thermograms for sucrose, lactose and trehalose dehydrate, indicating crystal to amorphous transformation was achieved as a result of cryomilling. As per the multi-component systems recrystallization peaks was only observed when milling sucrose and lactose with the three different APIs under investigation. Surprisingly, co-cryomilling of paracetamol with sucrose and lactose respectively lead to the formation of amorphous or partially amorphous lactose, sucrose and paracetamol. These results suggest that due to an increase in the molecular mobility when the sample was brought at room temperature to be analysed, causing recrystallization to be occurred giving the reason for crystalline to partially crystalline nature of these mixtures.

Chapter 5

Conclusions and future prospects

5.1. Conclusions

In Chapter 2 a range of analytical techniques was used to study the crystal-to-amorphous transformation and a potential recrystallisation of crystalline dicarboxylic acids which has not been investigated before. It was demonstrated that phthalic acid, isophthalic acid and terephthalic acid all undergo crystal to amorphous transformation, with the terephthalic acid remains amorphous even after storing the cryomilled samples for three weeks. The XRPD results for the pair mixtures prepared by physically mixing the individually cryomilled materials or by co-cryomilling together confirms that the mixtures which were prepared by co-cryomilling the components seem to recrystallize at a slower rate, especially the ones containing terephthalic acid. These mixtures show a potential signs of forming a new material with the suggestion of being some kind of nano-sized co-crystal.

In Chapter 3 the effect of milling at room temperature and cryomilling was investigated on single and multi-component systems of more realistic crystalline medicinal substances. As per the single component systems, amorphous material was not observed for aspirin, paracetamol and caffeine. The significance of milling temperature relative to T_g and the temperature at which the samples analysis takes place relative to the T_g value has been highlighted. Reduction in melting points has been observed for aspirin milled at room temperature and has been attributed to crystal defects. The multi-component systems of aspirin-paracetamol, aspirin-caffeine and paracetamol-caffeine were studied at different ratios and

theoretical eutectic points of each system were calculated using the Shroeder-van Laar equation and a first attempt of comparing the results with the experimental results obtained from ball milling and cryomiling was reported.

The observation that can be extracted from Chapters 2 and 3 that materials of different chemical nature when milled together showed a significant reduction in the melting points than that attained by each separately. However, materials of similar chemical nature did not show such behaviour. This finding is a unique one that has never been addressed for cryomilled materials before. Certainly it is worth further investigation to find out any useful implementation.

In Chapter 4 the preparation of a selected number of APIs co-cryomilled with different widely used excipients was studied. It was confirmed that sucrose, lactose monohydrate and trehalose dihydrate all undergo a crystal to amorphous transformation when each material was cryomilled individually. Cryomilling of sucrose and lactose monohydrate gave the first instance of amorphous or partially amorphous paracetamol. Aspirin has been observed to suppress the amorphous transformation of trehalose dihydrate, and it has been assigned to the significantly low T_g value of aspirin compared to paracetamol and caffeine. The XRPD traces for the systems containing aspirin-sucrose, paracetamol-sucrose, caffeine-sucrose and caffeine-lactose has been reported for the first time to produce new peaks indicating that the components were mixed on a molecular level. Melting points depression has been observed on cryomilling of all systems and the results were compared with the theoretical reduction in melting points values obtained from the Shroeder-van Laar equation.

In fact co-cryomilling does not appear to be as predictable as milling single components. Cryomilling of multi-component systems have been showed

to either produce eutectic, amorphous, sometimes simple physical mixtures or co-crystals.

In general, cryomilling is a technique which has the potential of producing an amorphous material without the use of heat or solvents. This is specifically considered to be an appealing strategy for pharmaceutical formulations. Cryomilling offers a number of advantages over other formulation strategies, reducing the risk of chemical instability of amorphous materials produced and offering an access to new amorphous materials. The preparation of single and multi-component systems of amorphous materials without the use of solvents and heat would definitely reduce the risks of chemical instability and provides the opportunity of producing formulations with increased solubility and dissolution rate and consequently bioavailability.

5.2. Future prospects

5.2.1. In situ-XRPD

In situ-XRPD provides an extra information in terms of changes in the crystal structure, crystal phase transformations, transitions from amorphous to crystalline state and vice versa as well as crystallite growth. The work described in this thesis involved milling, followed by ex-situ characterisation of the samples. A recent work by Decamps (209) on beta-trehalose employed an elegant combination of ex-situ and in-situ X-ray diffraction and PDF analysis using a synchroton source, which allowed development of a core/shell model to describe the milling-induced amorphisation. It would be interesting to apply the same approach to the systems studied in Chapter 2 to help determine whether the new materials formed are structurally related to the unmilled materials, along with the mechanism by which the new ,materials are created during the milling process (e.g. two-phase process similar to that observed by Descamps).

5.2.2. Solid-State NMR

Applying NMR to all cryomilled samples would possibly give an extended idea about the mechanism by which amorphisation occurs. It was reported that when crystalline lactose was subjected to various forms of pharmaceutical processing including cryogrinding, solid-state NMR relaxation times become shorter (210). Shorter relaxation times is often detected for the high-energy mixtures indicating the formation of amorphous material. In agreement with our finding cryogrinding often produces mixtures of crystalline and amorphous material, with the amount of amorphous material increasing as the grinding time increases. Furthermore, sixty minutes of grinding time produced mostly amorphous material, with some crystalline material remaining. This led to the

assumption that relaxation measurements when performed on dosage forms could potentially predict the stability of pharmaceutical formulations. Therefore, it would be interesting to apply this technique to the systems studied in Chapters 3 and 4 in order to investigate the stability of amorphous materials formed by cryomilling. It would be interesting to compare relaxation times for cryomilled vs melt-quenched samples which would provide a new knowledge to the field.

5.2.3. Accelerated stability studies

The standard stability performance of drug formulations is a basic requirement for pharmaceutical development and commercialization. The stability of co-milled mixture of polyvinyl pyrrolidone (PVP) and salbutamol sulphate (SS) using a planetary ball mill was studied before and after storage under ambient and elevated humidity conditions (211). The obtained results showed stability against re-crystallization was achieved on storing the co-milled mixtures with a minimum PVP content of 80 wt%. Therefore accelerated stability studies on some of the multi-component systems reported in Chapter 4 would provide a valuable information regarding the mechanism by which crystallisation takes place in order to assess cryomilling as a potential formulation strategy.

5.2.4. Implementation to real-world formulations

It would be valuable to study the effect of cryomilling on samples of molecular alloys involving more than two components that mimic real pharmaceutical formulations. The significant reduction in the materials melting points that was observed in the systems investigated in Chapter 3 and Chapter 4 could be implemented in pharmaceutical formulations that are aimed to possess a rapid dissolution rate to enhance their

bioavailability, such the case of oro-dispersible tablets and local anaesthetic preparations.

Future studies, therefore, could usefully aim at:

- In-situ work to probe the milling process and also the recrystallisation processes for organic small-molecule materials.

- SS-NMR and stability studies to clarify the mechanism by which amorphisation occurs.

- Developing a model to predict milling outcomes in mixed systems (e.g. amorphisation, nano-crystal formation, eutectic formation or no real change)

Appendix I

Experimental

Preparation Methods

Cryomilling

As mentioned in Chapter 1, cryomilling was carried out in this study as it will offer a suitable atmosphere to pharmaceuticals without the downsides accompanying the subjection to heat and solvents adopted in other amorphisation strategies. The aim of milling is typically reducing the particle size of a material by mechanochemical activation (118). According to the Nernst-Brunner equation reducing the surface area may theoretically have a significant effect on the dissolution rate since surface area is dependent on particle size. This is considered to be an essentially important step in pharmaceutical industry to improve the dissolution rate of poorly water soluble active pharmaceutical ingredients. On the other hand a crystalline to amorphous transformation has been reported upon milling several APIs (13). During the past few decades the importance of the amorphous state was widely accepted by the pharmaceutical community (10). Formulation with their API in the amorphous state shows a great potential to overcome the limited bioavailability problems (212). Cryomilling was considered to offer an environment for potentially facilitate direct crystalline to amorphous transformation (169), which is referred to the high milling intensity subjected to the materials under study at low temperature.

A detailed description of several milling strategies was provided by Suryanarayana who has carried out an extensive review on mechanical

alloying and milling (132). The cryomill used in this thesis is a SamplePrep 6870 Freezer/Mill (SPEX, Metuchen, NJ, United States) shown in Figure 82. It is supplied with an electromagnetic coil which can shuttle the impactor back and forward inside the sample vial in order to be grinded against the end cap (Figure 83).



Figure 82: SamplePrep 6870 Freezer/Mill (SPEX, Metuchen, NJ, United States).

The liquid nitrogen submerges the coil and vial to keep sample temperature to a minimum throughout the milling process. Liquid nitrogen boiling point is ~-196 °C which should maintain most APIs below their T_g, supporting the crystalline to amorphous transformation reported and shown by the Martin and Bellon equation (169). 1 g of each sample was weighed and placed in the vial. The vials holder in the cryomill has the capacity of cryomilling four samples each run. Cryomilling time was 60 minutes for all samples, with pre-cooling the instrument for 5 minutes then milling for 2 minutes at frequency 15 cycles per second. Throughout the grinding process, there is a pause of 1 minute between cycles to prevent the temperature rising. In order to avoid condensation of atmospheric moisture on the sample vial and probably on the sample, cryomilling vials were transferred immediately into an argon purged dry-box in which the sample was sealed and protected against the exposure to water before the physical characterisation.

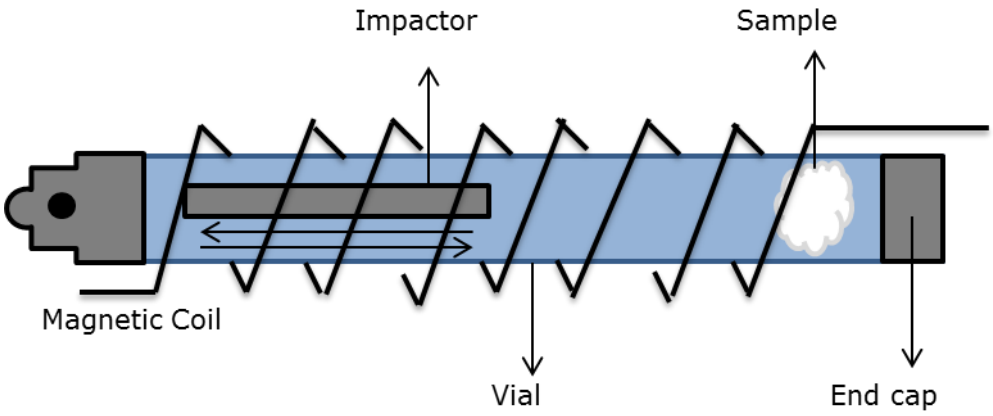


Figure 83: Schematic diagram of electromagnetic impactor back, sample vial and end cap.

Room Temperature Milling (Ball Mill)

A RETSCH Mixer Mill MM400 (Retsch GmbH, 42781 Haan, Rheinische Str.36, Germany) shown in Figure 84, was used to mill the samples at room temperature. The grinding jars, within the mixer mill, perform oscillations in a horizontal position and the inactive surface of the grinding balls causes them to impact with high energy on the sample at the rounded ends of the grinding jars and crushes it. Also, the movement of the grinding jars combined with the movement of the balls result in the intensive mixing of the sample. The degree of mixing can be controlled by the size of the grinding balls.

The grinding jars were filled with 200 mg of the starting materials used, and sense the mixer mill is provided with two grinding stations, two samples were used at each run. All the samples were milled for 60 minutes.

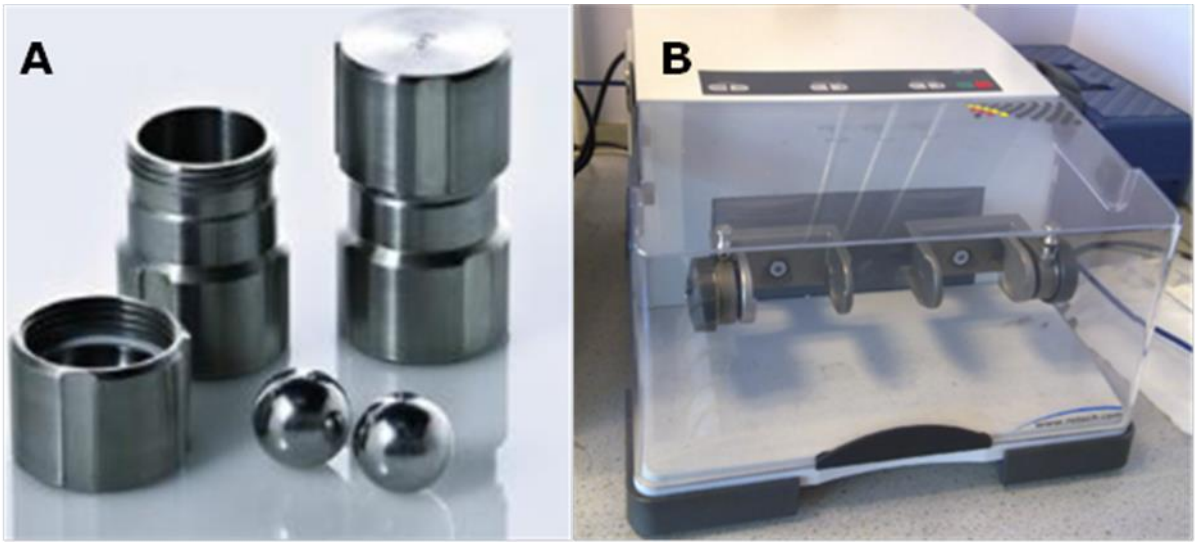


Figure 84: A. Stainless steel jars with two balls B. RETSCH ball mill (Mixer Mill MM400).

Characterisation Techniques

Differential Scanning Calorimetry (DSC)

In definition (213), DSC "means the measurement of the change of the difference in the heat flow rate to the sample and to a reference sample while they are subjected **to** a controlled temperature program'' . Depending on mechanism of operation DSC can be classified into two types:

Heat Flux DSC

In heat flux DSC, both the sample and reference material are heated together by the same heating source. The heat is then transferred to both sample and reference pans via a thermoelectric disk. The existent difference in temperature detected between the sample and the reference is attributed to the difference in heat capacity between both pans.

Power Compensated DSC

In power compensated DSC, the sample and reference pan are heated by separate heaters. Both the sample and reference are maintained at the same temperature and the difference in thermal energy required to maintain them at the same temperature is measured and plotted as a function of temperature or time. A sketched diagram showing the working principle of power compensated DSC is shown in Figure 85.

This kind of measurement would be significant in order to study the thermal transition of samples under study (213). It is typically used in the analysis

of amorphous pharmaceutical solids (30). Heat flow is simply the amount of heat supplied (q) to the sample at given time (t) (Equation 3).

$$heat\ flow = \frac{q}{t} \tag{3}$$

In order to maintain the sample and the reference pan at the same temperature, more heat will be supplied to the sample during an endothermic transition and less heat during an exothermic transition. Heat capacity (Cp) is identified as the amount of heat required to increase the temperature of a sample by a given amount. It can be calculated as shown in Equation 4:

$$Cp = \frac{q}{\Delta T} = \frac{q}{\alpha t} \tag{4}$$

Where Cp is the heat capacity, q is the heat supplied, ΔT is the change in temperature, α is the heating rate and t is the time.

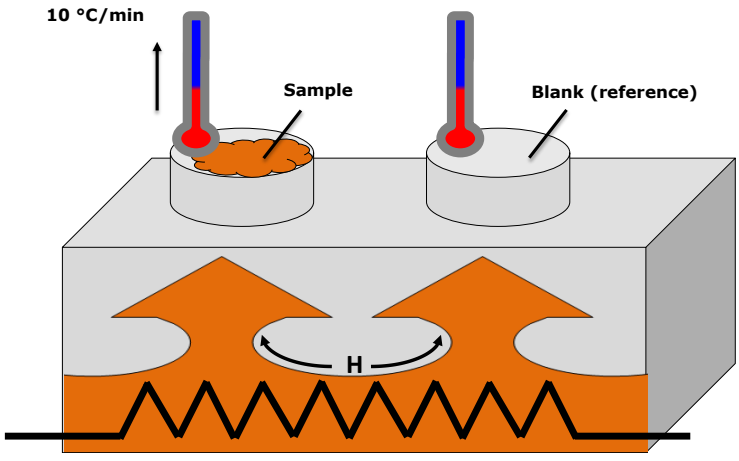


Figure 85: Sketched diagram showing the principle of power compensated DSC.

A typical thermogram of a material subjected to heat could reveal its melting temperature, crystallisation temperature and glass transition temperature; this makes DSC an ideal strategy for the detection of amorphous solids. DSC provides a convenient and moderately accurate method of measuring enthalpy changes. The area under a curve between any two temperature limits yields an enthalpy change and can be calculated using equation 5:

$$\Delta H = \int_{T1}^{T2} CpdT \tag{5}$$

Where ΔH is the change in enthalpy, T1 is the temperature at the beginning of the transition, T2 is the temperature at the end of the transition, Cp is the heat capacity and dT is the change in temperature. The DSC thermogram could be useful in providing information on the amount of the amorphous and crystalline content of the sample, which could be quantified using the equation 6 proposed by Lefort *et al* (214).

$$\tau_{DSC} = \frac{\Delta H_{cr}}{\Delta H_m^*} \frac{1}{1 - \alpha_{frac}} \tag{6}$$

Where τ_{DSC} represent the samples' amorphous fraction, ΔH_{cr} is the enthalpy of the samples' crystallisation at specific temperature known as the crystallisation temperature, ΔH_m^* is the enthalpy of fusion of the crystalline material and α_{frac} is the fraction of amorphous material which on heating

does not undergo recrystallization. This has been applied in the study of the structural disorder in milled indomethacin by Planinsek *et al* (215). The shapes and the number of peaks on the DSC thermogram can be useful to identify the presence of impurities and particle size reduction (216). It has been reported that heating rate can have an effect on the sample stability (217), DSC was utilised to determine the stability of acetylsalicylic acid ASA , both as pure samples and in ASA-containing pharmaceuticals. Two broad endothermic peaks were detected to be attributed to the two decomposition steps of ASA. This phenomenon was found to be prominent as the heating rate was increased.

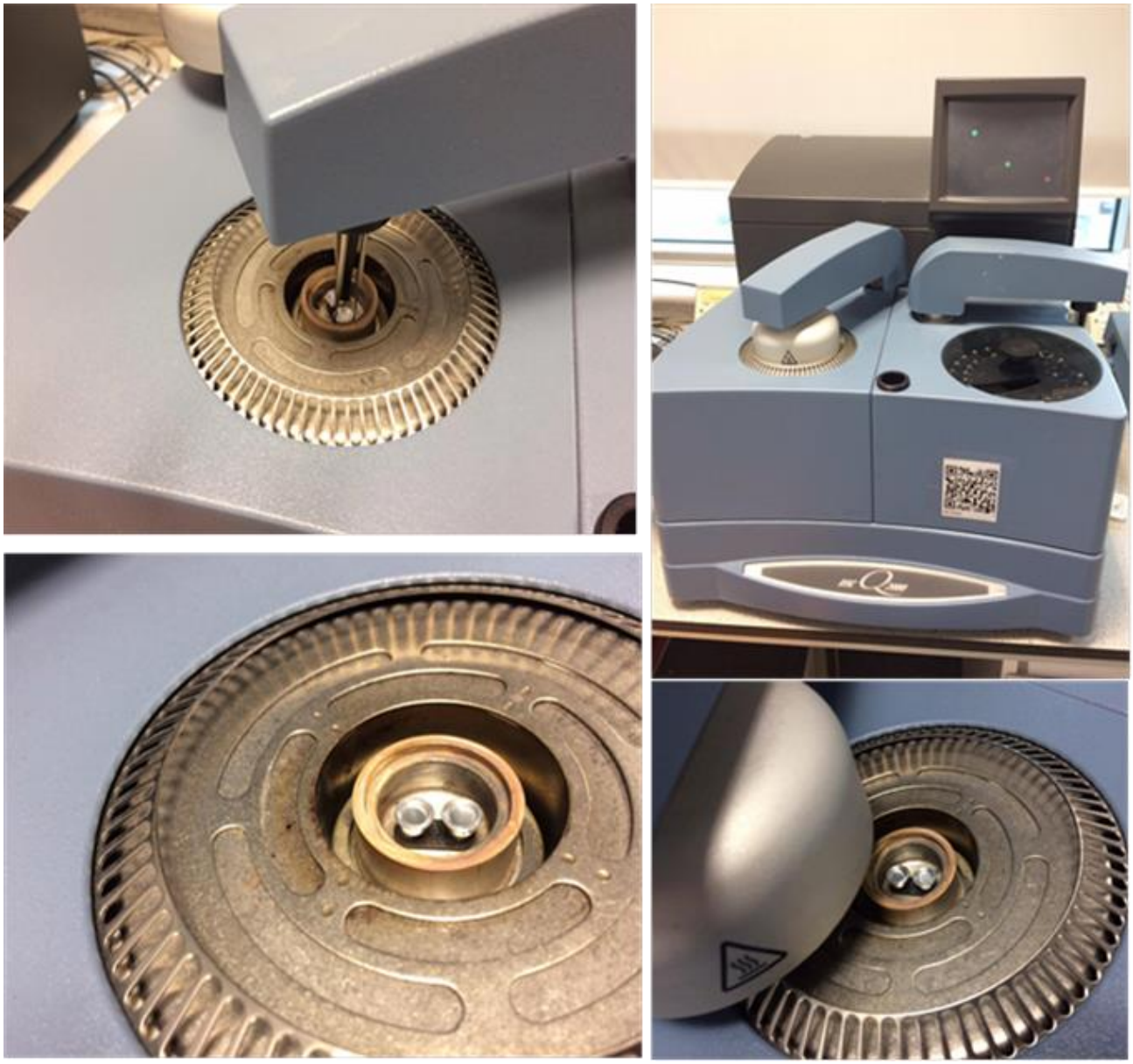


Figure 86: TA Q2000 Differential Scanning Calorimeter (TA Instruments, NewCastle, DE, USA).

The type of DSC used in this investigation is a TA Q2000 Differential Scanning Calorimeter (TA Instruments, NewCastle, DE, USA) shown in Figure 86. Supplied by constant purge of nitrogen gas of 50ml per minute. Tzero (TA Instruments, New Castle, DE, USA) aluminium hermetic pans and lids were used to contain the samples with a sample size range of ~5 mg. These pans were sealed in an argon purged dry-box and tapped lightly to spread out the sample evenly within the pans. The instrument was calibrated for temperature and enthalpy using indium. The standard or

conventional DSC mode was adopted to measure Tg, melting points, recrystallization and enthalpy. Measurements were run from -40°C to specific temperatures above each component's melting temperature with heating rates of 10°C/min. Analysis is carried out through the Universal Analysis Software (TA Analysis) to estimate the enthalpy, onset and peak of thermal events such as the glass transition, melting and recrystallization. Experiments were carried out in triplicate (n=3).

Hot Stage Polarised Microscopy

Hot-stage polarised microscopy is considered to be one of the several techniques that can be used to characterise the physical properties of pharmaceutical solids (218). Microscopic observation offers a rapid, adaptable and often non-destructive method for investigating samples. This characterisation provides information regarding the physicochemical properties (219), such as crystal morphology, crystal optics, crystallisation and thermal behaviour when microscopy is connected to a hot stage compartment (220).

A detailed description of the basics of hot-stage polarising microscopy is described in Figure 87. During this work the thermoscopic behaviour of pharmaceutical samples under study was investigated using PriorLux Pol advanced polarised light microscope (PriorLux Pol, Prior Scientific, Fulbourn, Cambridge, UK) (Figure 88).

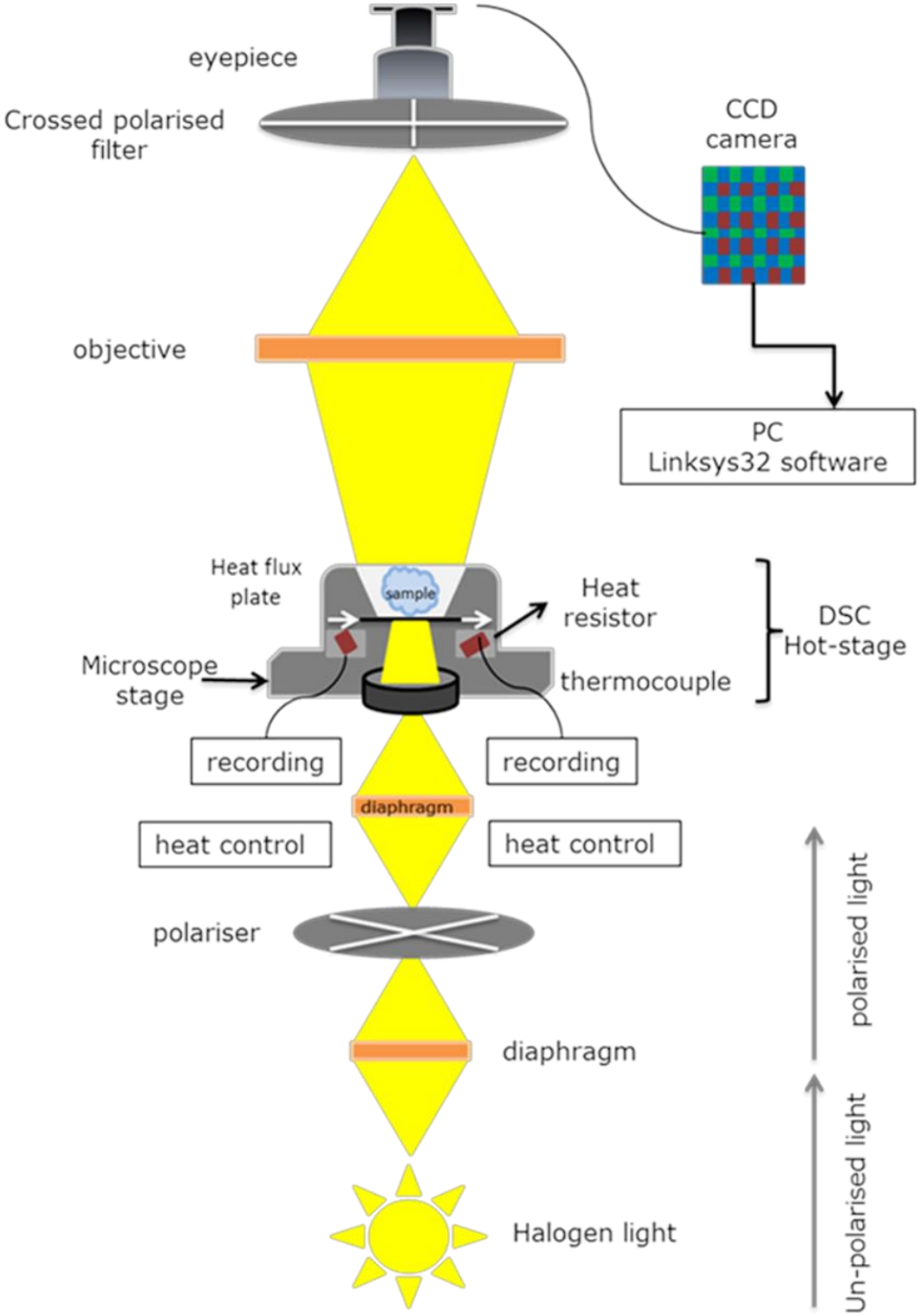


Figure 87: Sketched diagram showing the principle of polarised thermoscopy.

The samples are placed on a 360 degree rotational mechanical stage and focused through several focusing eyepieces of 10x magnification and 20

mm view field, and PriorLux Pol is equipped with free objectives of either 4x, 10x, 20x, 40x and 60x magnification. A halogen lamp is conducted with variable brightness control to provide illumination to the subjected samples by a 12 V and 30 V.



Figure 88: PriorLux Pol advanced polarised light microscope (PriorLux Pol, Prior Scientific, Fulbourn, Cambridge, UK).

CCD camera is attached to the microscope that can be either used in its still mode for basic image capture, or for more advanced imaging mode for moving pictures. There is an image capturing software build within Linksys32 package that could be into video generation using different pictures captured at desired time intervals. The PriorLux Pol is supported with a Linkam dsc600 heating-freezing stage, which is controlled by T95-Linksys temperature programmer and Linksys32 software (Linkam Scientific Instruments Ltd., Tadworth, Surry, UK). The latter is programmed to control the hot-stage temperature.

X-Ray Powder Diffraction (XRPD)

X-ray crystallographic techniques have been regarded as the most definitive methods for quantifying molecular order (8), characterising the structural conformation of materials (221) and they are frequently employed in pharmaceutical analysis (222). As a result of the fingerprint-like features of diffractograms of each distinctive material whether it is to be confirmed for being identified or to be determined in the case of new solid forms, can be characterised using XRPD (223). X-ray diffraction (Bragg diffraction) occurs when radiation with wavelength comparable to atomic spacings is scattered in a specular fashion by the atoms of a crystalline system, and undergoes constructive interference (224). When an interaction between the x-ray and the sample is achieved, each atom in its unit cell interacts with the incident beam resulted in x-ray diffraction (225). Moreover, an interference similar to that detected between electrons occurred between scattered x-rays. The x-ray diffraction does not occur until Bragg`s law is satisfied. Bragg diffraction from a set of crystal planes separated by a distance d is shown in Figure 89.

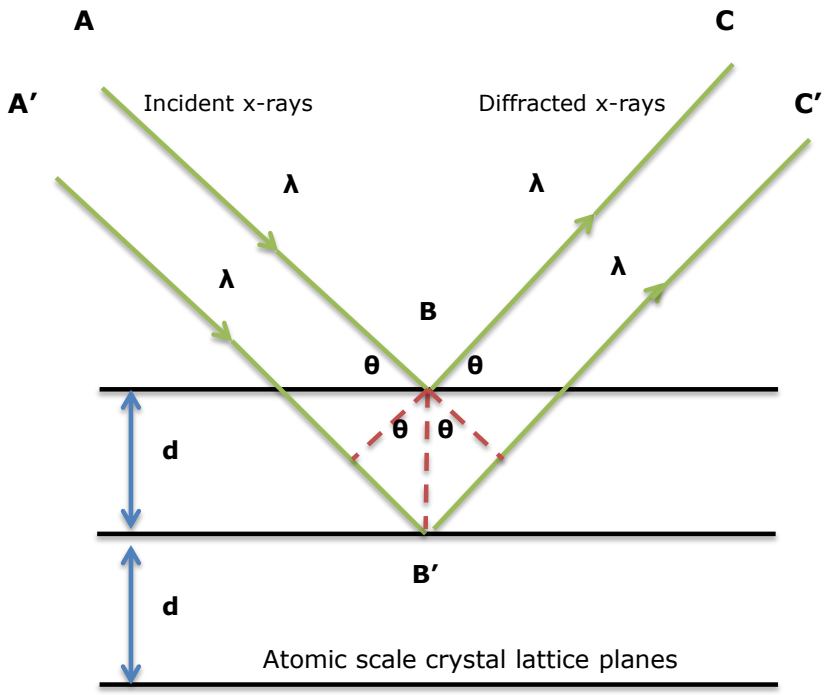


Figure 89: Diagram of Bragg diffraction from a set of crystal planes with a spacing of d.

Bragg's Law was introduced by Sir W.H. Bragg and his son Sir W.L. Bragg. The law states that when the x-ray is incident onto a crystal surface, its angle of incidence *θ* will reflect back with a same angle of scattering *θ*. When the path difference d is equal to a whole number *n* of wavelength. Bragg expressed this in Equation 7.

$$n\lambda = 2\,\mathrm{d}\sin\,(\theta) \qquad (7)$$

Where λ is the wave length of the rays, *θ is* the between the incident rays and the surface of the crystal, d is the spacing between layers of atoms when **n** is an integer (1, 2, 3 etc.). XRPD can clearly distinguish amorphous from crystalline material (13). The long-range translational order which

molecules exhibit in their crystalline state but not in the amorphous state. As a result, amorphous solids fail to diffract X-rays constructively (8). Therefore, characteristic patterns of amorphous materials produce broad, diffused haloes without distinctive sharp peaks (226). The XRPD was measured in this work by using flat-plate diffractometer, the X'Pert PRO(PANalytical, Almelo, Netherlands) shown in Figure 90. Reflection mode was set up using Cu Kα1 (λ = 1.54 Å) operating in Bragg-Brentano geometry.

0.0260 2 θ /° was used as a step size with a total collection time of 5 minutes. The Voltage of the generator was sat to 40 kV and the current to 40 mA. Brass was used as a holder for the samples. The XRPD could be utilised into determining the crystallinity of nanocrystalline samples with the limit of detection been approximated around 5% (222). There is a number of milled APIs has been characterised using XRPD, such as indomethacin (227), griseofulvin (228), paracetamol and sucrose (4).



Figure 90: the X'Pert PRO(PANalytical, Almelo, Netherlands).

Fourier Transform Infrared Spectroscopy (FTIR)

Infrared spectroscopy has been considered as a significant procedure for materials examination in the research facility and it has been gaining acceptance as a reliable analytical tool for over seventy years (229). An infrared spectrum represents a fingerprint of a sample with absorption peaks which correspond to the frequencies of vibrations between the bonds of the atoms making up the material (230). Because each different material is a unique combination of atoms, no two compounds produce the exact same infrared spectrum. Therefore, infrared spectroscopy can result in a positive identification (qualitative analysis) of every different kind of

material. In addition, the size of the peaks in the spectrum is a direct indication of the amount of material present. With modern software algorithms, infrared is an excellent tool for quantitative analysis.

FTIR spectrometers are further more effective than the original dispersive techniques which were used in the past with grating-type or prism instruments (231) because all the IR radiation reaches the detector at the same time after passing through the sample (232). Measurement of a single spectrum is faster for the FTIR technique because the information at all frequencies is collected simultaneously. This allows multiple samples to be collected and averaged together resulting in an improvement in sensitivity.

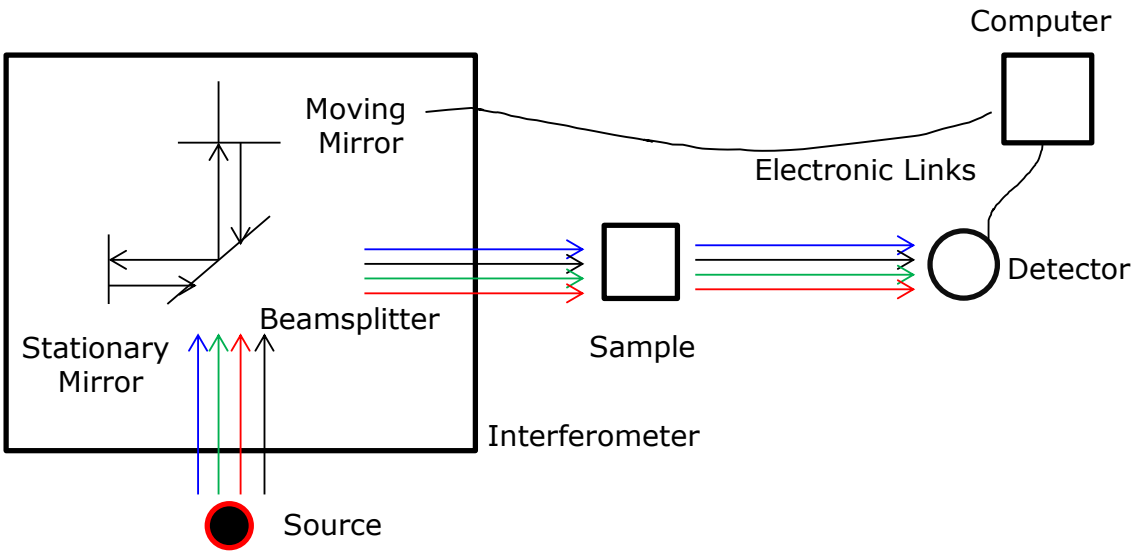


Figure 91: Sketched diagram showing the principle of FTIR

In an FT-IR instrument, a Michelson interferometer replaces the monochromator of a conventional infrared spectrometer which splits the infrared beam using a semi-permeable beamsplitter (233). The infrared beam is taken from the source by the interferometer to a beam splitter

which is designed to transmit part of the light towards a fixed mirror, and the other part is reflected towards a moving mirror (234). When the two lights is reflected back from the mirrors, they return to the beam splitter where they are recombined, and directed to a sample holder (234). As the infrared light interacts with the sample, a fraction of the radiation is absorbed while the rest passes through towards a detector (234).

The intensity of the signal from the detector, as a function of the change in optical pathlength corrected by a constant component, is called an interferogram (229). This interferogram showing intensity versus pathlength is converted by a mathematical algorithm, called a Fourier transform, into an IR spectrum giving absorbance versus frequency (235). Figure 91 shows a simple diagram of fourier transform spectrometer working mechanism.



Figure 92: Agilent/Cary630/FTIR, United States.

The IR spectra of all the samples in this study were collected using Agilent / Cary630 / FTIR, United States shown in Figure 92. The attenuated total

reflectance (ATR) is widely used to obtain spectra of solids, liquid, semisolids and thin films. Samples were applied to the plate of Diamond ATR type II crystal which is considered to be the most common sample interface used in spectroscopy, because diamond provides high-quality spectra with no sample preparation required.

The diamond`s extreme strength which enables it to withstand the applied pressure for proper contact especially with solid samples and it is highly resistant to the chemical changes. The signal-reflection diamond has a 1 mm diameter sampling surface with 200 µm active area and provides approximately 2 µm depth of penetration for infrared energy at 1700 cm^{-1}. The samples were analysed by Agilent MicroLab PC software. The spectral range was taken between 4000-500 cm^{-1}. Figure 93 shows the working principle of attenuated total reflectance (ATR).

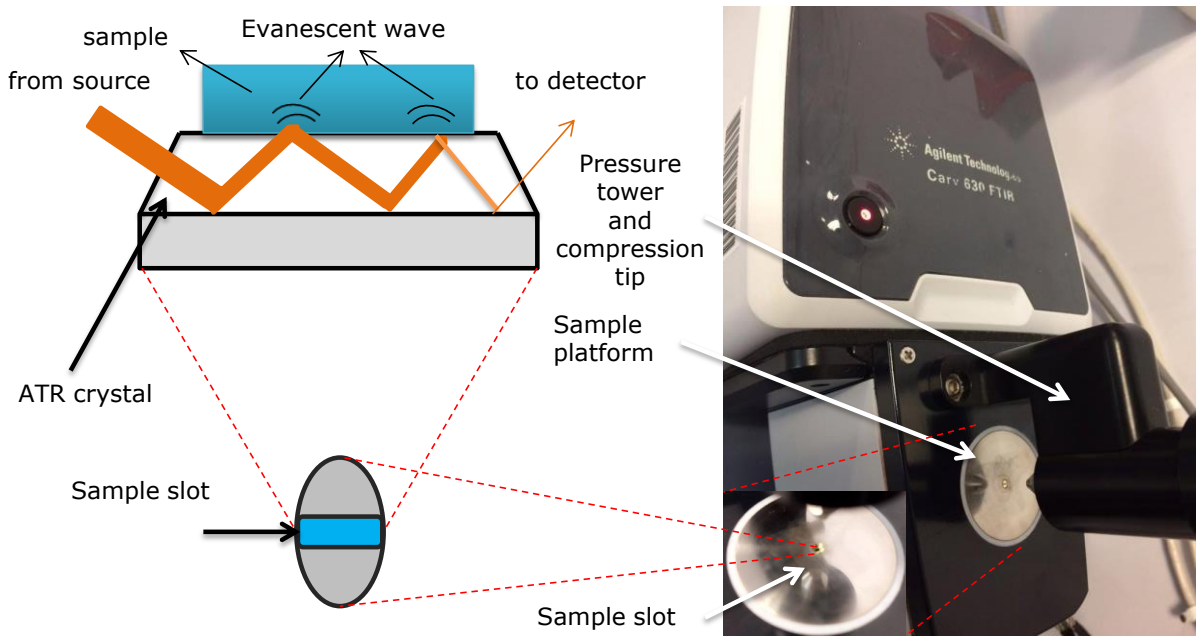


Figure 93: Sketched diagram showing the principle of attenuated total reflectance (ATR).

Bibliography

1. Amidon GL, Lennernäs H, Shah VP, & Crison JR (1995) A theoretical basis for a biopharmaceutic drug classification: the correlation of in vitro drug product dissolution and in vivo bioavailability. *Pharmaceutical research* 12(3):413-420.
2. Cook J, Addicks W, & Wu YH (2008) Application of the biopharmaceutical classification system in clinical drug development—an industrial view. *The AAPS journal* 10(2):306-310.
3. Kawabata Y, Wada K, Nakatani M, Yamada S, & Onoue S (2011) Formulation design for poorly water-soluble drugs based on biopharmaceutics classification system: basic approaches and practical applications. *International journal of pharmaceutics* 420(1):1-10.
4. Wildfong PL, Hancock BC, Moore MD, & Morris KR (2006) Towards an understanding of the structurally based potential for mechanically activated disordering of small molecule organic crystals. *Journal of pharmaceutical sciences* 95(12):2645-2656.
5. Food & Administration D (2000) Guidance for industry: waiver of in vivo bioavailability and bioequivalence studies for immediate-release solid oral dosage forms based on a biopharmaceutics classification system. *Food and Drug Administration, Rockville, MD*.
6. Baghel S, Cathcart H, & O'Reilly NJ (2016) Polymeric Amorphous Solid Dispersions: A Review of Amorphization, Crystallization, Stabilization, Solid-State Characterization, and Aqueous Solubilization of Biopharmaceutical Classification System Class II Drugs. *Journal of pharmaceutical sciences*.
7. Einfalt T, Planinšek O, & Hrovat K (2013) Methods of amorphization and investigation of the amorphous state. *Acta pharmaceutica* 63(3):305-334.
8. Hancock BC & Zografi G (1997) Characteristics and significance of the amorphous state in pharmaceutical systems. *Journal of pharmaceutical sciences* 86(1):1-12.
9. Sareen S, Mathew G, & Joseph L (2012) Improvement in solubility of poor water-soluble drugs by solid dispersion. *International journal of pharmaceutical investigation* 2(1):12.
10. Guo Y, Shalaev E, & Smith S (2013) Physical stability of pharmaceutical formulations: solid-state characterization of amorphous dispersions. *TrAC Trends in Analytical Chemistry* 49:137-144.
11. Nanubolu JB & Burley JC (2012) Investigating the recrystallization behavior of amorphous paracetamol by variable temperature Raman studies and surface Raman mapping. *Molecular pharmaceutics* 9(6):1544-1558.
12. Karmwar P, Graeser K, Gordon KC, Strachan CJ, & Rades T (2011) Investigation of properties and recrystallisation behaviour of amorphous indomethacin samples prepared by different methods. *International journal of pharmaceutics* 417(1):94-100.
13. Willart J & Descamps M (2008) Solid state amorphization of pharmaceuticals. *Molecular Pharmaceutics* 5(6):905-920.
14. Trasi NS & Taylor LS (2012) Effect of polymers on nucleation and crystal growth of amorphous acetaminophen. *CrystEngComm* 14(16):5188-5197.
15. Kawakami K & Pikal MJ (2005) Calorimetric investigation of the structural relaxation of amorphous materials: Evaluating validity of the methodologies. *Journal of pharmaceutical sciences* 94(5):948-965.
16. Kawakami K (2012) Modification of physicochemical characteristics of active pharmaceutical ingredients and application of supersaturatable dosage forms for improving bioavailability of poorly absorbed drugs. *Advanced drug delivery reviews* 64(6):480-495.
17. Meste ML, Champion D, Roudaut G, Blond G, & Simatos D (2002) Glass transition and food technology: a critical appraisal. *Journal of Food Science* 67(7):2444-2458.

18. Hilden LR & Morris KR (2004) Physics of amorphous solids. *Journal of pharmaceutical sciences* 93(1):3-12.

19. Hu Y*, et al.* (2013) Formation, physical stability, and quantification of process-induced disorder in cryomilled samples of a model polymorphic drug. *Journal of pharmaceutical sciences* 102(1):93-103.

20. Pikal M, Lukes A, & Lang J (1977) Thermal decomposition of amorphous β-lactam antibacterials. *Journal of pharmaceutical sciences* 66(9):1312-1316.

21. Shamblin SL, Hancock BC, & Pikal MJ (2006) Coupling between chemical reactivity and structural relaxation in pharmaceutical glasses. *Pharmaceutical research* 23(10):2254-2268.

22. Descamps M, Willart J, Dudognon E, & Caron V (2007) Transformation of pharmaceutical compounds upon milling and comilling: The role of Tg. *Journal of pharmaceutical sciences* 96(5):1398-1407.

23. Marsac PJ, Konno H, & Taylor LS (2006) A comparison of the physical stability of amorphous felodipine and nifedipine systems. *Pharmaceutical research* 23(10):2306-2316.

24. Chokshi RJ, Shah NH, Sandhu HK, Malick AW, & Zia H (2008) Stabilization of low glass transition temperature indomethacin formulations: Impact of polymer-type and its concentration. *Journal of pharmaceutical sciences* 97(6):2286-2298.

25. Karmwar P, Graeser K, Gordon KC, Strachan CJ, & Rades T (2012) Effect of different preparation methods on the dissolution behaviour of amorphous indomethacin. *European Journal of Pharmaceutics and Biopharmaceutics* 80(2):459-464.

26. Duong A, Steinmaus C, McHale CM, Vaughan CP, & Zhang L (2011) Reproductive and developmental toxicity of formaldehyde: a systematic review. *Mutation Research/Reviews in Mutation Research* 728(3):118-138.

27. Löbmann K*, et al.* (2012) Co-amorphous simvastatin and glipizide combinations show improved physical stability without evidence of intermolecular interactions. *European Journal of Pharmaceutics and Biopharmaceutics* 81(1):159-169.

28. Löbmann K, Grohganz H, Laitinen R, Strachan C, & Rades T (2013) Amino acids as co-amorphous stabilizers for poorly water soluble drugs–Part 1: Preparation, stability and dissolution enhancement. *European Journal of Pharmaceutics and Biopharmaceutics* 85(3):873-881.

29. Murdande SB, Pikal MJ, Shanker RM, & Bogner RH (2010) Solubility advantage of amorphous pharmaceuticals: II. Application of quantitative thermodynamic relationships for prediction of solubility enhancement in structurally diverse insoluble pharmaceuticals. *Pharmaceutical research* 27(12):2704-2714.

30. Baird JA & Taylor LS (2012) Evaluation of amorphous solid dispersion properties using thermal analysis techniques. *Advanced drug delivery reviews* 64(5):396-421.

31. Mahlin D, Ponnambalam S, Heidarian Hőckerfelt M, & Bergstrőm CA (2011) Toward in silico prediction of glass-forming ability from molecular structure alone: a screening tool in early drug development. *Molecular pharmaceutics* 8(2):498-506.

32. Ilevbare GA, Liu H, Edgar KJ, & Taylor LS (2013) Impact of polymers on crystal growth rate of structurally diverse compounds from aqueous solution. *Molecular pharmaceutics* 10(6):2381-2393.

33. Vogt M, Kunath K, & Dressman JB (2008) Dissolution improvement of four poorly water soluble drugs by cogrinding with commonly used excipients. *European journal of pharmaceutics and biopharmaceutics* 68(2):330-337.

34. Feng T, Stanciu L, & Carvajal M (Making Sense of Milling: the Role of Water on the Micro-Structural Relaxation-Like of Cryo-Milled Griseofulvin.

35. Adrjanowicz K*, et al.* (2011) Comprehensive studies on physical and chemical stability in liquid and glassy states of telmisartan (TEL): solubility advantages given by cryomilled and quenched material. *Philosophical Magazine* 91(13-15):1926-1948.

36. Roos Y & Karel M (1991) Water and molecular weight effects on glass transitions in amorphous carbohydrates and carbohydrate solutions. *Journal of Food Science* 56(6):1676-1681.

37. Guzmán HR*, et al.* (2007) Combined use of crystalline salt forms and precipitation inhibitors to improve oral absorption of celecoxib from solid oral formulations. *Journal of pharmaceutical sciences* 96(10):2686-2702.

38. Loftsson T, Hreinsdóttir D, & Másson M (2005) Evaluation of cyclodextrin solubilization of drugs. *International journal of pharmaceutics* 302(1):18-28.

39. Stella VJ & Nti-Addae KW (2007) Prodrug strategies to overcome poor water solubility. *Advanced drug delivery reviews* 59(7):677-694.

40. Thakuria R*, et al.* (2013) Pharmaceutical cocrystals and poorly soluble drugs. *International journal of pharmaceutics* 453(1):101-125.

41. Sekhon BS (2012) Nutraceutical cocrystals: an overview. *RGUHS J. Pharm. Sci.* 2:16-25.

42. Merisko-Liversidge E, Liversidge GG, & Cooper ER (2003) Nanosizing: a formulation approach for poorly-water-soluble compounds. *European Journal of Pharmaceutical Sciences* 18(2):113-120.

43. Pudipeddi M & Serajuddin A (2005) Trends in solubility of polymorphs. *Journal of pharmaceutical sciences* 94(5):929-939.

44. Serajuddin A (1999) Solid dispersion of poorly water-soluble drugs: Early promises, subsequent problems, and recent breakthroughs. *Journal of pharmaceutical sciences* 88(10):1058-1066.

45. Elder DP*, et al.* (2010) The utility of sulfonate salts in drug development. *Journal of pharmaceutical sciences* 99(7):2948-2961.

46. Serajuddin AT (2007) Salt formation to improve drug solubility. *Advanced drug delivery reviews* 59(7):603-616.

47. Dokoumetzidis A & Macheras P (2006) A century of dissolution research: from Noyes and Whitney to the biopharmaceutics classification system. *International journal of pharmaceutics* 321(1):1-11.

48. Desiraju GR (2003) Crystal and co-crystal. *CrystEngComm* 5(82):466-467.

49. Dunitz JD (2003) Crystal and co-crystal: a second opinion. *CrystEngComm* 5(91):506-506.

50. Aakeröy CB (1997) Crystal engineering: strategies and architectures. *Acta Crystallographica Section B: Structural Science* 53(4):569-586.

51. Trask AV, Motherwell WS, & Jones W (2005) Pharmaceutical cocrystallization: Engineering a remedy for caffeine hydration. *Crystal Growth & Design* 5(3):1013-1021.

52. Remenar JF*, et al.* (2003) Crystal engineering of novel cocrystals of a triazole drug with 1, 4-dicarboxylic acids. *Journal of the American Chemical Society* 125(28):8456-8457.

53. McNamara DP*, et al.* (2006) Use of a glutaric acid cocrystal to improve oral bioavailability of a low solubility API. *Pharmaceutical research* 23(8):1888-1897.

54. Basavoju S, Boström D, & Velaga SP (2008) Indomethacin–saccharin cocrystal: design, synthesis and preliminary pharmaceutical characterization. *Pharmaceutical research* 25(3):530-541.

55. Hickey MB*, et al.* (2007) Performance comparison of a co-crystal of carbamazepine with marketed product. *European journal of pharmaceutics and biopharmaceutics* 67(1):112-119.

56. Atkinson R, Bedford C, Child K, & Tomich E (1962) The effect of griseofulvin particle size on blood levels in man. *Antibiotics & Chemotherapy* 12(4):232-238.

57. Hilfiker R (2006) *Polymorphism: in the pharmaceutical industry* (John Wiley & Sons).

58. Rodŕiguez-Spong B, Price CP, Jayasankar A, Matzger AJ, & Rodŕiguez-Hornedo Nr (2004) General principles of pharmaceutical solid polymorphism: a supramolecular perspective. *Advanced drug delivery reviews* 56(3):241-274.

59. Singhal D & Curatolo W (2004) Drug polymorphism and dosage form design: a practical perspective. *Advanced drug delivery reviews* 56(3):335-347.

60. Bauer J*, et al.* (2001) Ritonavir: an extraordinary example of conformational polymorphism. *Pharmaceutical research* 18(6):859-866.

61. Salole E & Al-Sarraj F (1985) Spironolactone crystal forms. *Drug Development and Industrial Pharmacy* 11(4):855-864.

62. Blagden N, De Matas M, Gavan P, & York P (2007) Crystal engineering of active pharmaceutical ingredients to improve solubility and dissolution rates. *Advanced drug delivery reviews* 59(7):617-630.

63. Liu R (2008) *Water-insoluble drug formulation* (CRC Press).

64. Vasconcelos T, Sarmento B, & Costa P (2007) Solid dispersions as strategy to improve oral bioavailability of poor water soluble drugs. *Drug discovery today* 12(23):1068-1075.

65. Craig DQ (2002) The mechanisms of drug release from solid dispersions in water-soluble polymers. *International journal of pharmaceutics* 231(2):131-144.

66. Janssens S & Van den Mooter G (2009) Review: physical chemistry of solid dispersions. *Journal of Pharmacy and Pharmacology* 61(12):1571-1586.

67. Leuner C & Dressman J (2000) Improving drug solubility for oral delivery using solid dispersions. *European journal of Pharmaceutics and Biopharmaceutics* 50(1):47-60.

68. Jain H, Khomane KS, & Bansal AK (2014) Implication of microstructure on the mechanical behaviour of an aspirin–paracetamol eutectic mixture. *CrystEngComm* 16(36):8471-8478.

69. Matsuoka M & Ozawa R (1989) Determination of solid-liquid phase equilibria of binary organic systems by differential scanning calorimetry. *Journal of Crystal Growth* 96(3):596-604.

70. Chow K, Tong HH, Lum S, & Chow AH (2008) Engineering of pharmaceutical materials: An industrial perspective. *Journal of pharmaceutical sciences* 97(8):2855-2877.

71. Rastogi R & Rastogi V (1969) Mechanism of eutectic crystallization. II. *Journal of Crystal Growth* 5(5):345-353.

72. Boumrah Y, Bouzahia I, Bouanani S, Khimeche K, & Dahmani A (2016) Thermodynamic and analytical studies of drugs binary systems of paracetamol mixed with pseudoephedrine. HCl, dextropropoxyphene. HCl and tramadol. HCl. *Thermochimica Acta* 634:48-56.

73. Huang C-C & Chen Y-P (2000) Measurements and model prediction of the solid–liquid equilibria of organic binary mixtures. *Chemical Engineering Science* 55(16):3175-3185.

74. Takiyama H, Suzuki H, Uchida H, & Matsuoka M (2002) Determination of solid–liquid phase equilibria by using measured DSC curves. *Fluid phase equilibria* 194:1107-1117.

75. Kozma D, Pokol G, & Ács M (1992) Calculation of the efficiency of optical resolutions on the basis of the binary phase diagram for the diastereoisomeric salts. *Journal of the Chemical Society, Perkin Transactions 2* (3):435-439.

76. Demus D, Fietkau C, Schubrt R, & Kehlen H (1974) Calculation and experimental verification of eutectic systems with nematic phases. *Molecular Crystals and Liquid Crystals* 25(3-4):215-232.

77. Hsu EC & Johnson JF (1973) Phase diagrams of binary nematic mesophase systems. *Molecular Crystals and Liquid Crystals* 20(2):177-190.

78. Gala U, Pham H, & Chauhan H (2013) Pharmaceutical applications of eutectic mixtures. *Journal of Developing Drugs* 2013.

79. Florence A, Attwood D, Florence A, & Attwood D (2011) Solids. *Physicochemical principles of pharmacy, 5th edn. Pharmaceutical Press, London*:7-42.

80. Goud NR, Suresh K, Sanphui P, & Nangia A (2012) Fast dissolving eutectic compositions of curcumin. *International journal of pharmaceutics* 439(1):63-72.

81. Stott PW, Williams AC, & Barry BW (1998) Transdermal delivery from eutectic systems: enhanced permeation of a model drug, ibuprofen. *Journal of controlled release* 50(1):297-308.

82. Buddhiranon S & Kyu T (2012) Solubilization of genistein in poly (oxyethylene) through eutectic crystal melting. *The Journal of Physical Chemistry B* 116(27):7795-7802.

83. Li F, Feng J, Cheng Q, Zhu W, & Jin Y (2007) Delivery of 125 I-cobrotoxin after intranasal administration to the brain: a microdialysis study in freely moving rats. *International journal of pharmaceutics* 328(2):161-167.

84. Yong CS*, et al.* (2004) Preparation of ibuprofen-loaded liquid suppository using eutectic mixture system with menthol. *European journal of pharmaceutical sciences* 23(4):347-353.

85. Sharma D, Soni M, Kumar S, & Gupta G (2009) Solubility enhancement–Eminent role in poorly soluble drugs. *Research Journal of Pharmacy and Technology* 2(2):220-224.

86. Savjani KT, Gajjar AK, & Savjani JK (2012) Drug solubility: importance and enhancement techniques. *ISRN pharmaceutics* 2012.

87. Aulton ME (2002) *Pharmaceutics: The science of dosage form design* (Churchill livingstone).

88. Stegemann S, Leveiller F, Franchi D, De Jong H, & Lindén H (2007) When poor solubility becomes an issue: from early stage to proof of concept. *European journal of pharmaceutical sciences* 31(5):249-261.

89. Wang J & Hou T (2011) Recent advances on aqueous solubility prediction. *Combinatorial chemistry & high throughput screening* 14(5):328-338.

90. Takagi T*, et al.* (2006) A provisional biopharmaceutical classification of the top 200 oral drug products in the United States, Great Britain, Spain, and Japan. *Molecular pharmaceutics* 3(6):631-643.

91. Loftsson T & Hreinsdôttir D (2006) Determination of aqueous solubility by heating and equilibration: a technical note. *Aaps Pharmscitech* 7(1):E29-E32.

92. Llinas A, Glen RC, & Goodman JM (2008) Solubility challenge: can you predict solubilities of 32 molecules using a database of 100 reliable measurements? *Journal of chemical information and modeling* 48(7):1289-1303.

93. Persson LC, Porter CJ, Charman WN, & Bergström CA (2013) Computational prediction of drug solubility in lipid based formulation excipients. *Pharmaceutical research* 30(12):3225-3237.

94. Stark AN, Jackson G, Carey PJ, Arfeen S, & Proctor SJ (1989) Severe renal toxicity due to intermediate-dose methotrexate. *Cancer chemotherapy and pharmacology* 24(4):243-245.

95. Gardner CR, Walsh CT, & Almarsson Ö (2004) Drugs as materials: valuing physical form in drug discovery. *Nature Reviews Drug Discovery* 3(11):926-934.

96. Lipinski CA (2000) Drug-like properties and the causes of poor solubility and poor permeability. *Journal of pharmacological and toxicological methods* 44(1):235-249.

97. Leeson P (2012) Drug discovery: Chemical beauty contest. *Nature* 481(7382):455-456.

98. Lipinski CA, Lombardo F, Dominy BW, & Feeney PJ (2012) Experimental and computational approaches to estimate solubility and permeability in drug discovery and development settings. *Advanced drug delivery reviews* 64:4-17.

99. Butler JM & Dressman JB (2010) The developability classification system: application of biopharmaceutics concepts to formulation development. *Journal of pharmaceutical sciences* 99(12):4940-4954.

100. Fridgeirsdottir GA, Harris R, Fischer PM, & Roberts CJ (2016) Support Tools in Formulation Development for Poorly Soluble Drugs. *Journal of Pharmaceutical Sciences* 105(8):2260-2269.

101. Hancock BC & Parks M (2000) What is the true solubility advantage for amorphous pharmaceuticals? *Pharmaceutical research* 17(4):397-404.

102. Bahl D & Bogner RH (2008) Amorphization alone does not account for the enhancement of solubility of drug co-ground with silicate: the case of indomethacin. *AAPS PharmSciTech* 9(1):146-153.

103. Hellrup J & Mahlin D (2011) Pharmaceutical micro-particles give amorphous sucrose higher physical stability. *International journal of pharmaceutics* 409(1):96-103.

104. Vincent S & Huot J (2011) Effect of air contamination on ball milling and cold rolling of magnesium hydride. *Journal of Alloys and Compounds* 509(19):L175-L179.

105. Sheth AR, Lubach JW, Munson EJ, Muller FX, & Grant DJ (2005) Mechanochromism of piroxicam accompanied by intermolecular proton transfer probed by spectroscopic methods and solid-phase changes. *Journal of the American Chemical Society* 127(18):6641-6651.

106. Williams III RO, Watts AB, & Miller DA (2012) *Formulating poorly water soluble drugs* (Springer).

107. Sugimoto S, Niwa T, Nakanishi Y, & Danjo K (2012) Development of a novel ultra cryo-milling technique for a poorly water-soluble drug using dry ice beads and liquid nitrogen. *International journal of pharmaceutics* 426(1):162-169.

108. Kawashima Y, Saito M, & Takenaka H (1975) Improvement of solubility and dissolution rate of poorly water-soluble salicylic acid by a spray-drying technique. *Journal of Pharmacy and Pharmacology* 27(1):1-5.

109. Jung J-Y*, et al.* (1999) Enhanced solubility and dissolution rate of itraconazole by a solid dispersion technique. *International journal of pharmaceutics* 187(2):209-218.

110. AG BL (2002) Training papers spray drying. *Buchi Corporation*.

111. Cal K & Sollohub K (2010) Spray drying technique. I: Hardware and process parameters. *Journal of pharmaceutical sciences* 99(2):575-586.

112. Ahmed I, Nafadi M, & Fatahalla F (2006) Formulation of a fast-dissolving ketoprofen tablet using freeze-drying in blisters technique. *Drug development and industrial pharmacy* 32(4):437-442.

113. Hu J*, et al.* (2002) Improvement of dissolution rates of poorly water soluble APIs using novel spray freezing into liquid technology. *Pharmaceutical research* 19(9):1278-1284.

114. Leuenberger H (2002) Spray freeze-drying–the process of choice for low water soluble drugs? *Journal of Nanoparticle Research* 4(1-2):111-119.

115. Konno H & Taylor LS (2008) Ability of different polymers to inhibit the crystallization of amorphous felodipine in the presence of moisture. *Pharmaceutical research* 25(4):969-978.

116. Willart J, Descamps M, & Caron V (2008) Direct crystal to glass transformations of trehalose induced by milling, dehydration and annealing. *COMPLEX SYSTEMS: 5th International Workshop on Complex Systems*, (AIP Publishing), pp 108-113.

117. Crowley MM*, et al.* (2007) Pharmaceutical applications of hot-melt extrusion: part I. *Drug development and industrial pharmacy* 33(9):909-926.

118. Colombo I, Grassi G, & Grassi M (2009) Drug mechanochemical activation. *Journal of pharmaceutical sciences* 98(11):3961-3986.

119. Sugimoto S, Niwa T, Nakanishi Y, & Danjo K (2012) Novel ultra-cryo milling and co-grinding technique in liquid nitrogen to produce dissolution-enhanced nanoparticles for poorly water-soluble drugs. *Chemical and Pharmaceutical Bulletin* 60(3):325-333.

120. Ye J & Schoenung JM (2004) Technical cost modeling for the mechanical milling at cryogenic temperature (cryomilling). *Advanced engineering materials* 6(8):656-664.

121. Sheth AR, Bates S, Muller FX, & Grant DJ (2004) Polymorphism in piroxicam. *Crystal growth & design* 4(6):1091-1098.

122. Chieng N, Zujovic Z, Bowmaker G, Rades T, & Saville D (2006) Effect of milling conditions on the solid-state conversion of ranitidine hydrochloride form 1. *International journal of pharmaceutics* 327(1):36-44.

123. Adrjanowicz K*, et al.* (2011) Effect of cryogrinding on chemical stability of the sparingly water-soluble drug furosemide. *Pharmaceutical research* 28(12):3220-3236.

124. Niwa T, Nakanishi Y, & Danjo K (2010) One-step preparation of pharmaceutical nanocrystals using ultra cryo-milling technique in liquid nitrogen. *European Journal of Pharmaceutical Sciences* 41(1):78-85.

125. Crowley KJ & Zografi G (2002) Cryogenic grinding of indomethacin polymorphs and solvates: assessment of amorphous phase formation and amorphous phase physical stability. *Journal of pharmaceutical sciences* 91(2):492-507.

126. Shakhtshneider T*, et al.* (2007) Grinding of drugs with pharmaceutical excipients at cryogenic temperatures. *Journal of Thermal Analysis and Calorimetry* 89(3):699-707.

127. Chung KH, He J, Shin DH, & Schoenung JM (2003) Mechanisms of microstructure evolution during cryomilling in the presence of hard particles. *Materials Science and Engineering: A* 356(1):23-31.

128. Suryanarayana C (2004) *Mechanical alloying and milling* (CRC Press).

129. Lee J, Zhou F, Chung K, Lavernia E, & Kim N (2001) Grain growth of nanocrystalline Ni powders prepared by cryomilling. *Metallurgical and Materials Transactions A* 32(12):3109-3115.

130. Zhang X, Wang H, Narayan J, & Koch C (2001) Evidence for the formation mechanism of nanoscale microstructures in cryomilled Zn powder. *Acta materialia* 49(8):1319-1326.

131. Birringer R (1989) Nanocrystalline materials. *Materials Science and Engineering: A* 117:33-43.

132. Suryanarayana C (2001) Mechanical alloying and milling. *Progress in materials science* 46(1):1-184.

133. Koch C (1997) Synthesis of nanostructured materials by mechanical milling: problems and opportunities. *Nanostructured Materials* 9(1):13-22.

134. Chung KH, Rodriguez R, Lavernia EJ, & Lee J (2002) Grain growth behavior of cryomilled INCONEL 625 powder during isothermal heat treatment. *Metallurgical and Materials Transactions A* 33(1):125-134.

135. Zhou F, Lee J, & Lavernia E (2001) Grain growth kinetics of a mechanically milled nanocrystalline Al. *Scripta materialia* 44(8):2013-2017.

136. Mahasukhonthachat K, Sopade P, & Gidley M (2010) Kinetics of starch digestion in sorghum as affected by particle size. *Journal of Food Engineering* 96(1):18-28.

137. Lepek P*, et al.* (2013) Effect of amorphization method on telmisartan solubility and the tableting process. *European Journal of Pharmaceutics and Biopharmaceutics* 83(1):114-121.

138. Feng T, Bates S, & Carvajal MT (2009) Toward understanding the evolution of griseofulvin crystal structure to a mesophase after cryogenic milling. *International journal of pharmaceutics* 367(1):16-19.

139. Teissier P (2007) L'émergence de la chimie du solide en France (1950-2000): de la formation d'une communauté à sa dispersion. (Paris 10).

140. Howard M (1998) *Introduction to crystallography and mineral crystal systems* (Bob's Rock Shop).

141. Andronis V & Zografi G (1998) The molecular mobility of supercooled amorphous indomethacin as a function of temperature and relative humidity. *Pharm Res* 15(6):835-842.

142. Qi S*, et al.* (2010) An investigation into the crystallisation behaviour of an amorphous cryomilled pharmaceutical material above and below the glass transition temperature. *J. Pharm. Sci.* 99(1):196-208.

143. Descamps M, Willart JF, Dudognon E, & Caron V (2007) Transformation of pharmaceutical compounds upon milling and comilling: the role of T(g). *J. Pharm. Sci.* 96(5):1398-1407.

144. Willart JF, Carpentier L, Danede F, & Descamps M (2012) Solid-state vitrification of crystalline griseofulvin by mechanical milling. *J. Pharm. Sci.* 101(4):1570-1577.

145. Craig DQ, Royall PG, Kett VL, & Hopton ML (1999) The relevance of the amorphous state to pharmaceutical dosage forms: glassy drugs and freeze dried systems. *International journal of pharmaceutics* 179(2):179-207.

146. Feng X*, et al.* (2016) The Effects of Polymer Carrier, Hot Melt Extrusion Process and Downstream Processing Parameters on the Moisture Sorption Properties of Amorphous Solid Dispersions. *The Journal of pharmacy and pharmacology* 68(5):692-704.

147. Klimova K & Leitner J (2012) DSC study and phase diagrams calculation of binary systems of paracetamol. *Thermochimica acta* 550:59-64.

148. Bi M, Hwang S-J, & Morris KR (2003) Mechanism of eutectic formation upon compaction and its effects on tablet properties. *Thermochimica acta* 404(1):213-226.

149. Zalac S*, et al.* (1999) Paracetamol-propyphenazone interaction and formulation difficulties associated with eutectic formation in combination solid dosage forms. *Chemical and pharmaceutical bulletin* 47(3):302-307.

150. Chiarella RA, Davey RJ, & Peterson ML (2007) Making co-crystals the utility of ternary phase diagrams. *Crystal growth & design* 7(7):1223-1226.

151. Chadwick K, Davey R, Sadiq G, Cross W, & Pritchard R (2009) The utility of a ternary phase diagram in the discovery of new co-crystal forms. *CrystEngComm* 11(3):412-414.

152. Ribeiro Y, De Oliveira J, Leles M, Juiz S, & Ionashiro M (1996) Thermal decomposition of some analgesic agents. *Journal of Thermal Analysis and Calorimetry* 46(6):1645-1655.

153. Sacchetti M (2000) Thermodynamic analysis of DSC data for acetaminophen polymorphs. *Journal of thermal analysis and calorimetry* 63(2):345-350.

154. Di Martino P, Conflant P, Drache M, Huvenne J-P, & Guyot-Hermann A-M (1997) Preparation and physical characterization of forms II and III of paracetamol. *Journal of Thermal Analysis and Calorimetry* 48(3):447-458.

155. Boldyreva E, Shakhtshneider T, Ahsbahs H, Sowa H, & Uchtmann H (2002) Effect of high pressure on the polymorphs of paracetamol. *Journal of thermal analysis and calorimetry* 68(2):437-452.

156. Boldyreva EV, Drebushchak V, Paukov I, Kovalevskaya YA, & Drebushchak TN (2004) DSC and adiabatic calorimetry study of the polymorphs of paracetamol. *Journal of thermal analysis and calorimetry* 77(2):607-623.

157. Espeau P*, et al.* (2005) Polymorphism of paracetamol: Relative stabilities of the monoclinic and orthorhombic phases inferred from topological pressure-temperature and temperature-volume phase diagrams. *Journal of pharmaceutical sciences* 94(3):524-539.

158. Xu F, Sun L, Tan Z, Liang J, & Zhang T (2005) Adiabatic calorimetry and thermal analysis on acetaminophen. *Journal of thermal analysis and calorimetry* 83(1):187-191.

159. Guillory JK, Hwang SC, & Lach JL (1969) Interactions between pharmaceutical compounds by thermal methods. *Journal of pharmaceutical sciences* 58(3):301-308.

160. Myrick ML, Baranowski M, & Profeta LT (2010) An experiment in physical chemistry: polymorphism and phase stability in acetaminophen (paracetamol). *Journal of chemical education* 87(8):842-844.

161. Perlovich G, Volkova T, & Bauer-Brandl A (2007) Polymorphism of paracetamol: Relative stability of the monoclinic and orthorhombic phase revisited by sublimation and solution calorimetry. *Journal of Thermal Analysis and Calorimetry* 89(3):767-774.

162. Jeanjean B, Alberola S, Terol A, & Sabon F (1978) Contribution to the study of paracetamol-theophylline and paracetamol-caffeine associations (author's transl). *Annales pharmaceutiques francaises*, pp 95-100.

163. Grant D, Jacobson H, Fairbrother J, & Patel C (1980) Phases in the paracetamol-phenazone system. *International Journal of Pharmaceutics* 5(2):109-116.

164. Granberg RA & Rasmuson ÅC (1999) Solubility of paracetamol in pure solvents. *Journal of Chemical & Engineering Data* 44(6):1391-1395.

165. Qi S, Avalle P, Saklatvala R, & Craig DQ (2008) An investigation into the effects of thermal history on the crystallisation behaviour of amorphous paracetamol. *European Journal of Pharmaceutics and Biopharmaceutics* 69(1):364-371.

166. Yalkowsky SH & Dannenfelser RM (1992) Aquasol database of aqueous solubility. *College of Pharmacy, University of Arizona, Tucson, AZ*.

167. Neil MJ (2006) The Merck Index: An Encyclopedia of chemicals, drugs and biologicals. Whitehouse station, New Jersey: Published by Merck Research Laboratories, Division of Merck and Co. (Inc).

168. Huang Z, Sun G-B, Chiew YC, & Kawi S (2005) Formation of ultrafine aspirin particles through rapid expansion of supercritical solutions (RESS). *Powder Technology* 160(2):127-134.

169. Seidell A (1919) *Solubilities of inorganic and organic compounds c. 2* (D. Van Nostrand Company).

170. Johannsen M & Brunner G (1994) Solubilities of the xanthines caffeine, theophylline and theobromine in supercritical carbon dioxide. *Fluid Phase Equilibria* 95:215-226.

171. Allen FH (2002) The Cambridge Structural Database: a quarter of a million crystal structures and rising. *Acta Crystallographica Section B: Structural Science* 58(3):380-388.

172. Motan G & Puia A (2014) Studies of different types of aspirin by spectrophotometric methods. *Acta Chemica Iasi* 22(2):155-164.

173. Nehlig A, Daval J-L, & Debry G (1992) Caffeine and the central nervous system: mechanisms of action, biochemical, metabolic and psychostimulant effects. *Brain Research Reviews* 17(2):139-170.

174. Cesaro A & Starec G (1980) Thermodynamic properties of caffeine crystal forms. *The Journal of Physical Chemistry* 84(11):1345-1346.

175. Epple M, Cammenga H, Sarge S, Diedrich R, & Balek V (1995) The phase transformation of caffeine: investigation by dynamic X-ray diffraction and emanation thermal analysis. *Thermochimica acta* 250(1):29-39.

176. Pinto SS & Diogo HP (2006) Thermochemical study of two anhydrous polymorphs of caffeine. *The Journal of Chemical Thermodynamics* 38(12):1515-1522.

177. Brittain HG (2002) Effects of mechanical processing on phase composition. *Journal of pharmaceutical sciences* 91(7):1573-1580.

178. Hubert S*, et al.* (2011) Process induced transformations during tablet manufacturing: Phase transition analysis of caffeine using DSC and low frequency micro-Raman spectroscopy. *International journal of pharmaceutics* 420(1):76-83.

179. Pirttimäki J, Lehto V, & Laine E (1993) The determination of relative amounts of phases in binary mixtures with quantitative X-ray diffraction. *Drug development and industrial pharmacy* 19(19):2561-2577.

180. Brittain HG (1994) *Analytical profiles of drug substances and excipients* (Academic Press).

181. Hancock BC, Shamblin SL, & Zografi G (1995) Molecular mobility of amorphous pharmaceutical solids below their glass transition temperatures. *Pharmaceutical research* 12(6):799-806.

182. Roos YH*, et al.* (2013) Melting and crystallization of sugars in high-solids systems. *Journal of agricultural and food chemistry* 61(13):3167-3178.

183. Alexandrowicz Z & Katchalsky A (1963) Colligative properties of polyelectrolyte solutions in excess of salt. *Journal of Polymer Science Part A: General Papers* 1(10):3231-3260.

184. Chaudhary A, Wang J, & Prabhu S (2010) Development and validation of a high-performance liquid chromatography method for the simultaneous determination of aspirin and folic acid from nano-particulate systems. *Biomedical chromatography : BMC* 24(9):919-925.

185. Klímová K & Leitner J (2012) DSC study and phase diagrams calculation of binary systems of paracetamol. *Thermochimica Acta* 550:59-64.

186. Warshaw HS & Powers MA (1999) A search for answers about foods with polyols (sugar alcohols). *The Diabetes Educator* 25(3):307-321.

187. Dave RH (2008) Overview of pharmaceutical excipients used in tablets and capsules. *Drug Topics, Oct* 24.

188. Coulston AM & Johnson RK (2002) Sugar and sugars: myths and realities. *Journal of the Academy of Nutrition and Dietetics* 102(3):351.

189. York P (1992) Crystal engineering and particle design for the powder compaction process. *Drug development and industrial pharmacy* 18(6-7):677-721.

190. Nachaegari SK & Bansal AK (2004) Coprocessed excipients for solid dosage forms. *Pharmaceutical technology* 28(1):52-65.

191. Chaudhari SP & Patil PS (2012) Pharmaceutical excipients: a review. *Int J Adv Pharmacy Biol Chem* 1(1):21-34.

192. Yang W, Kwan C, Ding Y, Ghadiri M, & Roberts K (2007) Milling of sucrose. *Powder technology* 174(1):14-17.

193. Hurtta M, Pitkänen I, & Knuutinen J (2004) Melting behaviour of D-sucrose, D-glucose and D-fructose. *Carbohydrate research* 339(13):2267-2273.

194. Gombas A, Szabó-Révész P, Kata M, Regdon G, & Erős I (2002) Quantitative determination of crystallinity of α-lactose monohydrate by DSC. *Journal of Thermal Analysis and Calorimetry* 68(2):503-510.

195. Willart J, Dujardin N, Dudognon E, Danède F, & Descamps M (2010) Amorphization of sugar hydrates upon milling. *Carbohydrate research* 345(11):1613-1616.

196. Roos Y (1993) Melting and glass transitions of low molecular weight carbohydrates. *Carbohydrate research* 238:39-48.

197. Hartel RW, Ergun R, & Vogel S (2011) Phase/state transitions of confectionery sweeteners: thermodynamic and kinetic aspects. *Comprehensive Reviews in Food Science and Food Safety* 10(1):17-32.

198. Taylor LS & York P (1998) Characterization of the phase transitions of trehalose dihydrate on heating and subsequent dehydration. *Journal of pharmaceutical sciences* 87(3):347-355.

199. Franson NM, Guillot MA, Laughlin SM, & Rocco WL (2001) Pharmaceutical formulations containing poorly soluble drug substances. (Google Patents).

200. Greenhalgh DJ, Williams AC, Timmins P, & York P (1999) Solubility parameters as predictors of miscibility in solid dispersions. *Journal of pharmaceutical sciences* 88(11):1182-1190.

201. Sjökvist E & Nyström C (1991) Physicochemical aspects of drug release. XI. Tableting properties of solid dispersions, using xylitol as carrier material. *International journal of pharmaceutics* 67(2):139-153.

202. Li Z, Lu C, Xia Z, Zhou Y, & Luo Z (2007) X-ray diffraction patterns of graphite and turbostratic carbon. *Carbon* 45(8):1686-1695.

203. Angberg M (1995) Lactose and thermal analysis with special emphasis on microcalorimetry. *Thermochimica acta* 248:161-176.

204. Megarry AJ, Booth J, & Burley J (2014) Sucrose/Glucose Molecular Alloys by Cryomilling. *Journal of pharmaceutical sciences* 103(7):2098-2106.

205. Lee JW, Thomas LC, & Schmidt SJ (2010) Investigation of the heating rate dependency associated with the loss of crystalline structure in sucrose, glucose, and fructose using a thermal analysis approach (part I). *Journal of agricultural and food chemistry* 59(2):684-701.

206. Tajber L, Corrigan OI, & Healy AM (2005) Physicochemical evaluation of PVP–thiazide diuretic interactions in co-spray-dried composites—analysis of glass transition composition relationships. *European journal of pharmaceutical sciences* 24(5):553-563.

207. Willart J*, et al.* (2002) Vitrification and polymorphism of trehalose induced by dehydration of trehalose dihydrate. *The Journal of Physical Chemistry B* 106(13):3365-3370.

208. Miller DP & de Pablo JJ (2000) Calorimetric solution properties of simple saccharides and their significance for the stabilization of biological structure and function. *The Journal of Physical Chemistry B* 104(37):8876-8883.

209. Bordet P*, et al.* (2016) Solid State Amorphization of β-Trehalose: A Structural Investigation Using Synchrotron Powder Diffraction and PDF Analysis. *Crystal Growth & Design* 16(8):4547-4558.

210. Lubach JW, Xu D, Segmuller BE, & Munson EJ (2007) Investigation of the effects of pharmaceutical processing upon solid-state NMR relaxation times and implications to solid-state formulation stability. *J Pharm Sci* 96(4):777-787.

211. Balani PN*, et al.* (2010) Influence of polymer content on stabilizing milled amorphous salbutamol sulphate. *Int J Pharm* 391(1-2):125-136.

212. Gupta MK, Vanwert A, & Bogner RH (2003) Formation of physically stable amorphous drugs by milling with Neusilin. *Journal of pharmaceutical sciences* 92(3):536-551.

213. Höhne G, Hemminger W, & Flammersheim H-J (2003) Calibration of Differential Scanning Calorimeters. *Differential Scanning Calorimetry*, (Springer), pp 65-114.

214. Lefort R, De Gusseme A, Willart J-F, Danede F, & Descamps M (2004) Solid state NMR and DSC methods for quantifying the amorphous content in solid dosage forms: an application to ball-milling of trehalose. *International journal of pharmaceutics* 280(1):209-219.

215. Planinsek O, Zadnik J, Kunaver M, Srcic S, & Godec A (2010) Structural evolution of indomethacin particles upon milling: Time-resolved quantification and localization of disordered structure studied by IGC and DSC. *Journal of pharmaceutical sciences* 99(4):1968-1981.

216. Tip T (Interpreting DSC curves Part 1: Dynamic measurements.

217. Campanella L, Micieli V, Tomassetti M, & Vecchio S (2011) Kinetic investigation and predictive model for the isothermal degradation time in two commercial acetylsalicylic acid-based pharmaceutical tablet formulations. *Thermochimica acta* 526(1):151-156.

218. Vitez IM, Newman AW, Davidovich M, & Kiesnowski C (1998) The evolution of hot-stage microscopy to aid solid-state characterizations of pharmaceutical solids. *Thermochimica Acta* 324(1):187-196.

219. McCrone WC, McCrone LB, & Delly JG (1978) *Polarized light microscopy* (Ann Arbor Science Publishers Inc. and McCrone Research Institute).

220. Storey RA & Ymen I (2011) *Solid state characterization of pharmaceuticals* (John Wiley & Sons).

221. Harris KD, Tremayne M, & Kariuki BM (2001) Contemporary advances in the use of powder X-ray diffraction for structure determination. *Angewandte Chemie International Edition* 40(9):1626-1651.

222. Shah B, Kakumanu VK, & Bansal AK (2006) Analytical techniques for quantification of amorphous/crystalline phases in pharmaceutical solids. *Journal of pharmaceutical sciences* 95(8):1641-1665.

223. Bond AD (2012) Pharmaceutical crystallography: is there a devil in the details? *CrystEngComm* 14(7):2363-2366.

224. Meyers H & Myers H (1997) *Introductory solid state physics* (CRC press).

225. Birkholz M (2006) *Thin film analysis by X-ray scattering* (John Wiley & Sons).

226. Chieng N, Rades T, & Saville D (2008) Formation and physical stability of the amorphous phase of ranitidine hydrochloride polymorphs prepared by cryo-milling. *European Journal of Pharmaceutics and Biopharmaceutics* 68(3):771-780.

227. Desprez S & Descamps M (2006) Transformations of glassy indomethacin induced by ball-milling. *Journal of non-crystalline solids* 352(42):4480-4485.

228. Willart JF, Carpentier L, Danède F, & Descamps M (2012) Solid-state vitrification of crystalline griseofulvin by mechanical milling. *Journal of pharmaceutical sciences* 101(4):1570-1577.

229. Ismail AA, van de Voort FR, & Sedman J (1997) Fourier transform infrared spectroscopy: principles and applications. *Techniques and instrumentation in analytical chemistry* 18:93-139.

230. Markovich RJ & Pidgeon C (1991) Introduction to Fourier transform infrared spectroscopy and applications in the pharmaceutical sciences. *Pharmaceutical research* 8(6):663-675.

231. Faix O (1992) Fourier transform infrared spectroscopy. *Methods in lignin chemistry*, (Springer), pp 83-109.

232. Santos AM (2010) Handheld Infrared Technology As a Tool for Quantifying and Predicting Quality Attributes of Tomato Products. (The Ohio State University).

233. Günzler H & Gremlich H-U (2002) IR spectroscopy. An introduction.

234. Maurer N (2012) Profiling Lipids for Authentication of High Value Ingredients by Mid-Infrared Spectroscopy Combined with Multivariate Analysis. (The Ohio State University).

235. Wehling RL (2010) Infrared spectroscopy. *Food analysis*, (Springer), pp 407-420.